SYNTHESIS OF AZANAPHTHOQUINONE ANNELATED THIAZOLE AS CYTOSTATIC COMPOUNDS

PRASEAT TUMTONG

A THESIS SUBMITTED IN PARTIAL FULFILLMENT OF THE REQUIREMENTS
FOR THE DEGREE OF MASTER OF SCIENCE
MAJOR IN CHEMISTRY
FACULTY OF SCIENCE
UBON RATCHATHANI UNIVERSITY
ACADEMIC YEAR 2016

UBON RATCHATHANI UNIVERSITY

THESIS APPROVAL

MASTER OF SCIENCE

MAJOR IN CHEMISTRY FACULTY OF SCIENCE

TITLE SYNTHESIS OF AZANAPHTHOQUINONE ANNELATED THIAZOLE AS CYTOSTATIC COMPOUNDS

AUTHOR MR. PRASEAT TUMTONG

EXAMINATION COMMITTEE

DR. THEERACHART LEEPASERT	CHAIRPERSON
ASST. PROF. DR. NIPAWAN PONGPROM	MEMBER
ASST. PROF. DR. RUKKIAT JITCHATI	MEMBER

ADVISOR .....

(ASST. PROF. DR. NIPAWAN PONGPROM)

....

(ASSOC. PROF. DR. UTITH INPRASIT) (ASSOC. PROF. DR. ARIYAPORN PONGRAT)

DEAN, FACULTY OF SCIENCE VICE PRESIDENT FOR ACADEMIC AFFAIRS

ACADEMIC YEAR 2016

ACKNOWLEDGEMENTS

I would like to acknowledge my advisor, Asst. Prof. Dr. Nipawan Pongprom, for allowing me to undertake this project, all the brilliant ideas, her enthusiasm, advice and guiding me throughout the three years. Thank for her support, patience, and encouragement throughout my graduate studies. It is not often that one finds an advisor and colleague that always finds the time for listening to the little problems and roadblocks that unavoidably crop up in the course of performing research. Her technical and editorial advice was essential to the completion of this dissertation She taught me innumerable lessons and insights on the workings of academic research in general and improved my English writing for both publication and thesid in every problem especially. Her advice was most valuable to understand the obtained results and to determine the next steps for the research presented in this thesis. I would like to thank many people who contributed their time and their advice. Thank to Assoc. Prof. Dr. Pronpan Pungpo for advice and support in quantum calculation chemistry and improved my writing to publication in The 19th International Annual Symposium on Computational Science and Engineering (ANSCSE 19th). I would like to thanks Dr. Bancha Yingngam for his advice and support in evaluation of antiproliferative activity with cancer cell and normal cell.

I would like to thank to the Military Explosives Factory (MEF), Defence Industry Department (DID), Defence Industry and Energy Centre (DICEC) for me in graduate of Master of Science. I would like to thank to Faculty of Science, Ubon Ratchathani University for the chemical facilities.

Finally, I must thank my family for their love and personal support during my study.

Praseat Tumtong
Researcher

บทคัดย่อ

เรื่อง : การสังเคราะห์สารออกฤทธิ์ยับยั้งเซลล์มะเร็งที่มีโครงสร้างพื้นฐานเป็นเอซาแนพโธควิโนนที่ต่อยู่กับวงไธเอโซล

ผู้วิจัย : ประเสริฐ ตุ้มทอง

ชื่อปริญญา : วิทยาศาสตรมหาบัณฑิต

สาขาวิชา : เคมี

อาจารย์ที่ปรึกษา : ผู้ช่วยศาสตราจารย์ ดร.นิภาวรรณ พองพรหม

คำสำคัญ : สารต้านมะเร็ง, เอซาแนพโธควิโนน, วงไธเอโซล, ไธโอเซมิคาร์บาไซด์, สารอินเตอร์แคลลาติง

สารออกฤทธิ์ยับยั้งเซลล์มะเร็งที่มีโครงสร้างพื้นฐานเป็นเอซาแนพโธควิโนนที่ต่อยู่กับวงไธเอโซลชนิดใหม่ถูกออกแบบ, สังเคราะห์, พิสูจน์เอกลักษณ์ทางสเปกโตสโคปี, ตรวจวัดการยับยั้งเซลล์มะเร็ง และศึกษาทางเคมีคำนวณเชิงโครงสร้าง โมเลกุลเป้าหมายถูกออกแบบโดยวิธีศึกษาความสัมพันธ์ระหว่างโครงสร้างกับฤทธิ์ทางชีวภาพ พบว่า หมู่แทนที่ตำแหน่งที่ 2 ต้องการหมู่ที่เป็นหมู่ดึงอิเล็กตรอน และหมู่นั้นต้องมีขนาดใหญ่ หมู่แทนที่ตำแหน่งที่ 5 ต้องการหมู่ที่มีขนาดใหญ่ และมีขั้วต่ำ จึงทำการต่อสายโซ่ต่างๆ กับโครงสร้างหลัก และหมู่แทนที่ตำแหน่งที่ 7 ควรจะเป็นอะตอมไนโตรเจน จึงใช้โครงสร้างหลักเป็นไอโซควิโนนลีนเกิดเป็นโมเลกุลเป้าหมายสารยับยั้งเซลล์มะเร็งที่มีโครงสร้างพื้นฐานเป็นเอซาแนพโธควิโนนที่ต่อยู่กับวงไธเอโซล ที่สังเคราะห์ขึ้นภายใต้สภาวะกรด และเบส ผ่าน 3 ขั้นตอน โดยขั้นตอนแรก ทำปฏิกิริยาออซิเดชันของ 5-ไฮดรอกซีไอโซควิโนลีน โดยใช้กรดไนตริกเข้มข้น และกรดไฮโดรคลอริกเข้มข้น ขั้นตอนที่ 2 ทำปฏิกิริยาปิดวงซึ่งเป็นขั้นตอนสำคัญของกระบวนการสังเคราะห์ ในสภาวะกรดใช้กรดไฮโดรคลอริกเข้มข้น ส่วนในสภาวะเบสใช้ โพแทสเซียมคาร์บอนเนต ในตัวทำละลายเอทานอล ขั้นสุดท้าย ทำปฏิกิริยาอัลคิลเลชัน กับสายโซ่อัลคิลเฮไลด์ชนิดต่างๆ ในตัวทำละลายไดเมททิลฟอร์มามายด์ จากนั้นนำสารที่สังเคราะห์ขึ้นทั้งหมด 12 ชนิดไปทดลองฤทธิ์ยับยั้งเซลล์มะเร็งลำไส้ และเซลล์ปกติ พบว่า สารที่สังเคราะห์ขึ้นออกฤทธิ์ยับยั้งเซลล์มะเร็งลำไส้ในระดับปานกลาง และมีความจำเพาะกับเซลล์มะเร็ง จากนั้นศึกษาทางเคมีคำนวณเชิงโครงสร้างในการแทรกสอดระหว่างดีเอ็นเอพบว่า สารที่ปิดวง 3 วงต่อกันหมายเลข 21 มีพลังงานยึดเหนี่ยวต่ำที่สุด และมีอันตรกิริยาที่แข็งแรงมากที่สุด ซึ่งสอดคล้องกับผลการทดสอบฤทธิ์การยับยั้งเซลล์มะเร็ง ดังนั้นสารหมายเลข 21 เป็นสารที่มีศักยภาพในการยับยั้งเซลล์มะเร็งมากที่สุด

CONTENTS (CONTINUED)

LIST OF TABLES

LIST OF FIGURES

LIST OF FIGURES (CONTINUED)

LIST OF FIGURES (CONTINUED)

LIST OF FIGURES (CONTINUED)

LIST OF FIGURES (CONTINUED)

LIST OF FIGURES (CONTINUED)

LIST OF FIGURES (CONTINUED)

LIST OF ABBREVIATIONS

ABBREVIATION	DEFINITION
Ar	Aromatic
br s	Broad singlet
$CDCl_3$	Deuterated chlorofrom
CD_3OD	Deuterated methanol
conc.	Concentrated
CoMSIA	Comparative molecular similarity index analysis
cm^{-1}	Reciprocal centimeter (unit of wavenumber)
^{13}C-NMR	Carbon nuclear magnetic resonance
^{o}C	Degree Celsius
d	Doublet (for NMR spectral data)
DCM	Dichloromethane
DMF	Dimethylformamide
DMSO	Dimethyl sulfoxide
DMSO-D_6	Deuterated dimethyl sulfoxide
DNA	Deoxyribonucleic acid
EtOAc	Ethyl acetate
EtOH	Ethanol
g	Gram
h	Hour
HCl	Hydrochloric acid
HMBC	Heteronuclear multiple bond correlation
HMQC	Heteronuclear multiple quantum correlation
^{1}H-NMR	Proton nuclear magnetic resonance
HNO_3	Nitric acid
HQSAR	Hologram quantitative structure activity relationship
Hz	Hertz
IR	Infrared
J	Coupling constant (for NMR spectral data)

LIST OF ABBREVIATIONS (CONTINUED)

ABBREVIATION	DEFINITION
L	Liter
m	Multriplet (for NMR spectral data)
MHz	Mega hertz
mL	Milliliter
mM	Millimolar
mmol	Millimol
mp	Melting point
NaH	Sodium hydride
QSAR	Quantitative structure activity relationship
s	Singlet (for NMR spectral data)
TLC	Thin layer chromatography
TMS	Tetra methylsilane
t	Triplet (for NMR spectral data)
δ	Chemical shift (for NMR spectral data)
%	Percent
/	Per
>	More than; greater than; above
<	Less than; under; below
µM	Micromolar
V_{max}	Maximum absorption frequency

CHAPTER 1
INTRODUCTION

1.1 Cancer chemotherapy

Chemotherapy is cancer treatment which use drugs to destroy cancer cell. It works by keeping the cancer cells from growing and dividing to make more cells. Because cancer cells usually grow and divide faster than healthy cells, chemotherapy destroys them more quicker than it destroys the healthy cells. Since chemotherapy drugs are powerful, they cause damage to many growing cells, including some healthy cells. This damage causes the side effects of chemotherapy. In this work, we focus on intercalating agent as chemotherapy type. Intercalating agent was developed and modified chemical structure by several research groups. Intercalating agent can be divided in to 4 catagories.

1.1.1 Anthracycline analogues

Anthracyclines are anticancer drug, discovered in 1960 in the fungus *Streptomyces* species. They were used to treat metastatic cancer of various types, for example, lung cancer, cervical cancer, breast cancer, lymphoma etc. The first group of drugs used to treat the disease are doxorubicin and daunorubicin as shown in Figure 1.1 later on the semi synthetic derivative, Epirubicin, was developed and used in cancer chemotherapy [1].

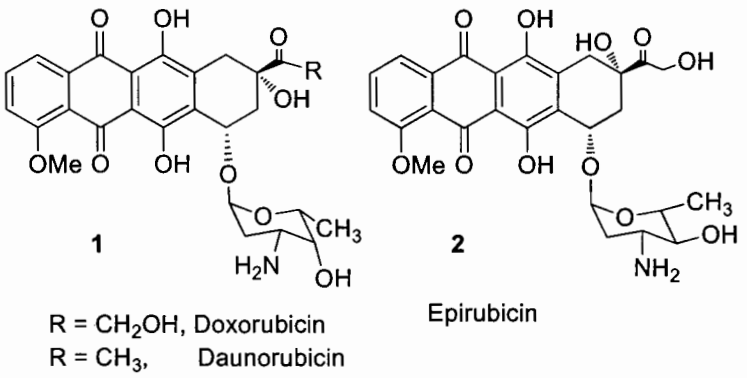

Figure 1.1 The structure of the drugs in anthracycline analogues

Although the anthracycline analogue is the most effective drug in the past but there is a risk of toxicity to the heart muscle cells caused toxicity by free radicals (Reactive oxygen species; ROS) and the mechanism of inhibition of enzyme Topoisomerase II beta (TOP2B). When TOP2B can not work, causes heart failure. Therefore the patient must get control of this medication. Many attempts have been made in order to develop new drugs for anthracycline with lower toxicity. The action of drugs in this group has mechanisms uncertain [2], to consolidate, the mechanism of action has four types as follows:

1.1.1.1 DNA-RNA Binding

The drug interacts with bases in the DNA strands. Causing DNA strands twisted. The activates body's self-defense system to be classified as damaged DNA and ordered to kill itself or not allow cell division.

1.1.1.2 Creation complex with topoisomerase enzyme leads to the break of DNA strands. Topoisomerase enzyme type 2 (Topo II) called DNA gyrase, functions in loosening super spiral coil of DNA, which was created by DNA replication. So if there is a drug to binding with Topo II enzyme then it does not work normally and can not loosen super coil spiral. This make the DNA strands are too tight or the DNA strands are torn.

1.1.1.3 Binding of anthracyclines to cell membranes

Anthracyclines drugs often to bind with cell membranes well, causes the chemical and physical properties changes such as viscosity, distribution of ions in membrane cell. In the cell division process, mother cells need to receive external signals that they are suitable of conditions for cell division, if the cell membrane is abnormal, it will not receive the signal. Therefore, the synthesis of DNA process will not occur and inhibit cancer cell division.

1.1.1.4 The formation of semiquinones radicals

Anthracyclines are mild oxidants, when into the body, cause the reduction reaction by receiving a single electron and giving semiquinone radical. Then semiquinone radical transforms to superoxide radical. This is a poisonous particle that binds to DNA and breaks the strands of DNA. This resulted in killing cancer.

1.1.2 Anthracene analogue

Anthracene is medicine, composed of three aromatic rings. It was first discovered in hydrocarbon compounds to produce dyeing color. Afterwards, there have been developed as a widely used cancer drug that is Mitoxantrone as shown in Figure 1.2. It is used to treat breast cancer, leukemia cancer, ovarian cancer and liver cancer.

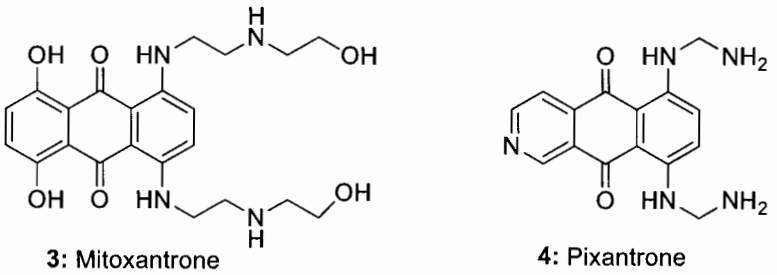

3: Mitoxantrone **4**: Pixantrone

Figure 1.2 Structure of anthracene groups

Mitoxantrone active by reversible binding with strands of DNA by inserting between strands of DNA and into the area of major groove in strands DNA. However, The mechanism of action of mitoxantrone is also to inhibit the activity of topoisomerase II enzyme. Using of Mitoxantrone, still shows side effects to myocardial, although slightly lower compared to medicine in anthracyclines groups. By eliminating of the hydroxyl groups in positions 2, 5 and adding nitrogen into the ring, it is expected that the drug will be less bioreduced to generate semiquinone radical. This will make the drug low toxicity on cadiotoxicity and the trial found that the drug gives good treatment results. Pixantrone show a lowering effect on the cardiac muscle compared to Mitoxantrone [3, 4].

1.1.3 Anthrapyrazole and azaanthrapyrazole analogues

The development in structure of quinones to increase the effectiveness of medicine and reduce the side effects from the medicine. A. P. Kracho's research group introduced nitrogen atom into the anthrapyrazole ring and eliminated hydroxyl groups. It was found that azaanthrapyrazoles gave a good biological activity and no side effects to cardiac muscle such as BBR 3409 and BBR 3438 substance. For the

medicine in anthrapyrazoles groups, the medicine giving good result is Losoxantron (Figure 1.3) [5].

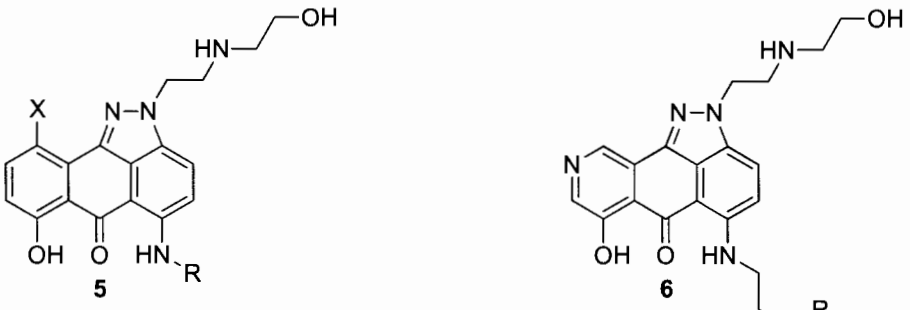

X = OH, R = $(CH_2)_2NHCH_3$, Teloxantrone
X = H, R = $(CH_2)_2NH(CH_2)_2OH$, Losoxantrone
X = OH, R = $(CH_2)_3NH_2$, Piroxantrone

R = CH_3, BBR 3409
R = H, BBR 3438

Figure 1.3 The structure of medicine in anthrapyrazole and azaanthrapyrazole analogues

1.1.4 Azanaphthoquinone annelated pyrrole analogue

Intercalating substance had basic structure of azanaphthoquinone attached to pyrroles ring. It is a new basic structure that has been developed by Spreitzer's group at the University of Vienna. It has been synthesized core structure with nitrogen atom inserted in different positions in structure of types **11**, **12** and **13** as shown in Figure 1.4 [6].

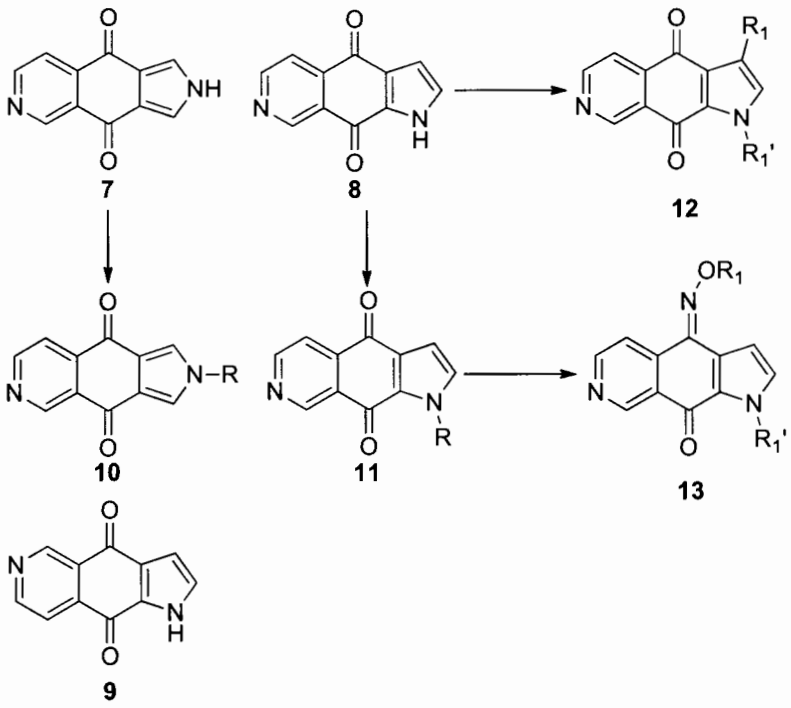

Figure 1.4 Structure of azanaphthoquinone fused to pyrrole

In the previour, our group has developed the target molecule from azanaphthoquinone annelated pyrrole series. The first series of azanaphthoquinone annelated pyrroles was added nitrogen atom in molecule for hydrogen bonding interaction and reduce side effect of quinolone system of core structure by synthesize oxime and hydrazone derivatives. The synthesized compounds were evaluated cytotoxic activity against KB/HeLa cell line. The results showed that this series of compounds exhibited promising cytotoxicity. The mono-substituted product with 2-(pyrrolidin-1-yl)ethyl group **14** showed very good activity with IC_{50} of 0.008 μM. While, the longer side chains exhibited lower activity. Hydrazone **15** showed lower activity than mono-substituted derivatives. Therefore, the modification of the target molecules needs to be investigated by introducing of 2 and 3-carbon side chains with cyclic amine group [7].

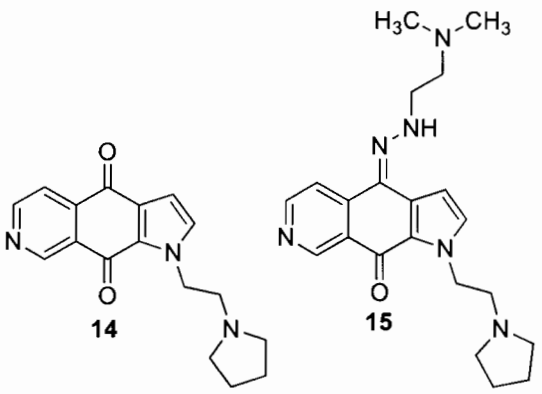

Figure 1.5 Structure of azanaphthoquinone annelated pyrrole mono-substituted product (14) and hydrazone derivative (15)

The later series of azanaphthoquinone annelated pyrrole was thiosemicarbazone series obtained from condensation of thiosemicarbazide with carbonyl moiety. The antiproliferative activity of thiosemicarbazone series was evaluated with HeLa cell line. The results showed that compound **16** exhibited higher cytotoxicity than hydrazone series with IC_{50} value of compound **16** is 10.850 μM. From the previous work of thiosemicarbazone analogue suggested that adding of sulfur atom into quinone ring was the important role of the cytotoxic activity [8].

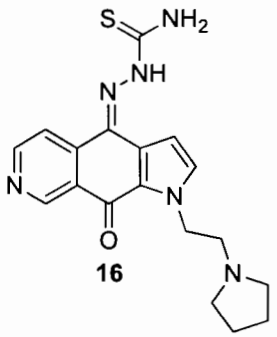

Figure 1.6 Structure of azanaphthoquinone annelated pyrrole thiosemicabazone series

In this work, we design the target molecule from molecular calculation quantitative structure analysis relationship (QSAR). We study the synthesis of azanaphthoquinone annelated thiazole derivative as antiproliferative agents. The target molecules were designed to replace carbonyl moiety with thiosemicarbazide under acidic conditions and basic conditions. We modified core skeleton by condensation with thiosemicarbazide to give thiazole ring. We added nitrogen atom and sulfur atom in molecule for hydrogen bonding interaction between the target molecule and DNA of cancer cell. Increase hydrogen donor at the side chain position and reduce cardiotoxic from quinone moiety. Finally, mono-substituted side chains will be introduced into core skeleton. Side chains with that 2-carbon linker with amino group will be used to give final compounds. We expected the target molecules of acid and basic conditions have potential biological activity, less side effect and suitable solubility. The synthesized compounds were evaluated biological activity with cancer cell and normal cell. Finally, the synthesized compounds were studied interaction, binding energy and arrangement in DNA cancer cell with molecular docking calculation.

1.2 Objectives

In this study, we focuse on synthesis of azanaphthoquinone annelated thiazole derivatives as antiproliferative agents. We introduced sulfur atom such as thiosemicarbazide in to core structure to avoid quinone system. The core skeleton consisting of different basic side chains linker. The aims of this study are:

1.2.1 To design the target molecules by quantitative structure activity relationship (QSAR).

1.2.2 To study the synthesis of azanaphthoquinone annelated thiazole derivatives under acidic conditions and basic conditions as shown in Figure 1.7.

1.2.3 To purify the synthesized molecules by chromatography techniques and characterize the synthesized compounds by spectroscopic techniques including ^{1}H-NMR, ^{13}C-NMR, IR and Mass spectrometry.

1.2.4 To evaluated the antiproliferative activity of the synthesized compounds with human colorectal cancer cells (HT-29), human normal mouse subcutaneous connective tissue cells (L929).

1.2.5 To study computational calculation chemistry of azanaphthoquinone annelated thiazole derivative using molecular docking of azanaphthoquinone annelated thiazole derivatives.

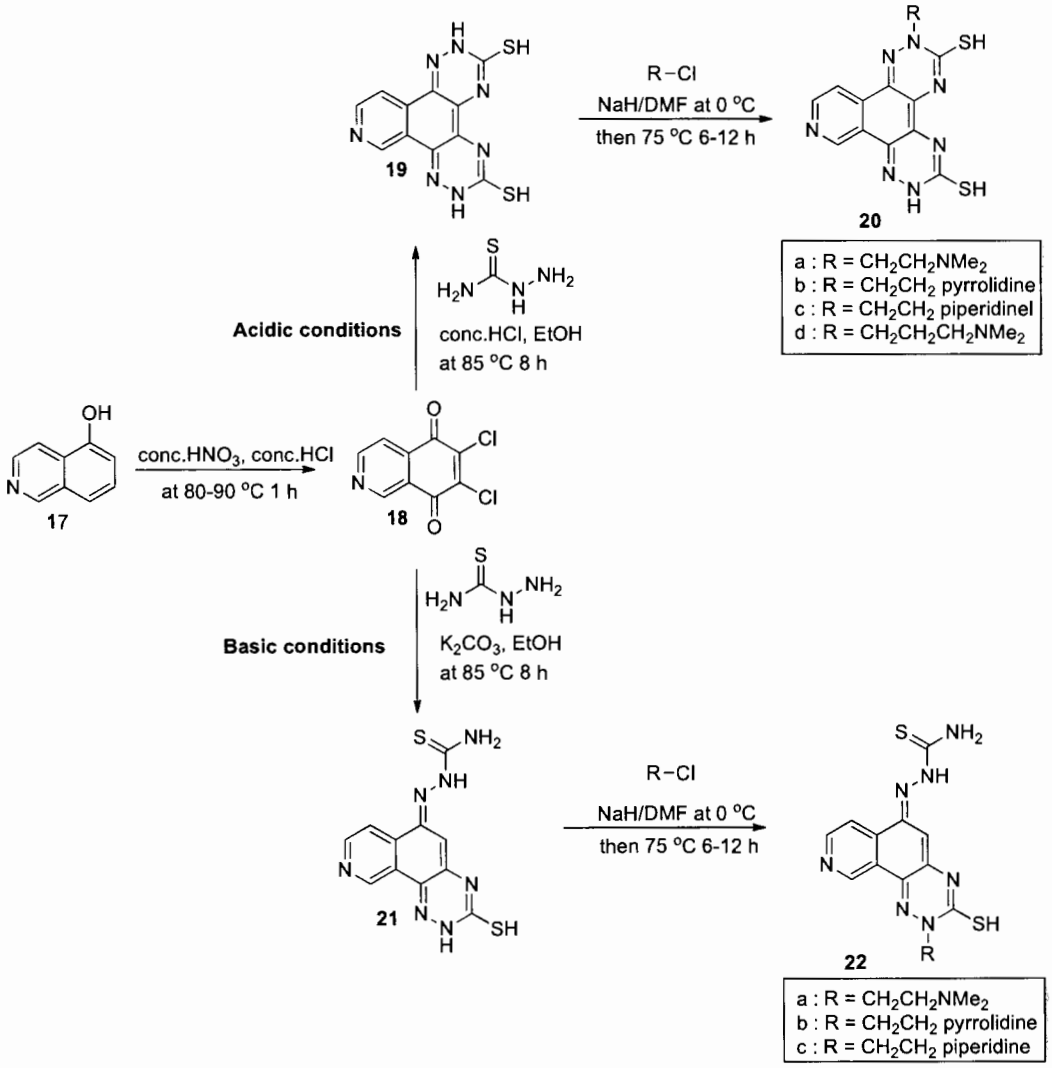

Figure 1.7 The synthetic pathway of azanaphthoquinone annelated thiazole derivatives under acidic and basic conditions

1.3 Scope of research

This research was interested on the synthesis and characterized of azanaphthoquinone annelated thiazole derivatives under acidic conditions and basic conditions. The synthesized compounds were characterized by spectroscopic techniques such as ^{1}H-NMR, ^{13}C-NMR, IR and Mass spectrometry. The antiproliferative activity of synthesized compounds was evaluated with human colorectal cancer cells (HT-29), mouse subcutaneous connective tissue cells (L929). The studies on computational calculation chemistry of azanaphthoquinone pyrrolo-annelated derivative was performed by using quantitative structure activity relationship (QSAR) and molecular docking of azanaphthoquinone annelated thiazole derivatives.

CHAPTER 2
LITERATURE REVIEWS

2.1 Cancer

Cancer is a class of diseases characterized by out-of-control cell growth. According to World Health Organization (WHO), common risk factors for cancer including tobacco, alcohol, overweight and obesity, physical inactivity and chronic infections from helicobacter pylori hepatitis B, C and P virus (HBV, HCV, HPV) [9].

2.2 Cell cycle and regulation

The cell cycle is pictorially represented in Figure 2.1, divided into four main parts. The G_1 or Gap 1 phase is the period when a newly created cell is born. The period of time a cell remains in the G_1 phase depends on the tissue type and whether it is a normal cell or a tumor cell. If the cell is proliferating cell, it will quickly move into the S or synthesis phase. It is during this period that DNA is replicated, and at the end of the S phase, two copies of DNA are presented in the cell. The next phase is the G_2 or Gap 2 period and this phase is largely a time during which preparations are made for the final cell cycle phase. The M or mitosis phase the time between mitoses is the cell cycle time, although this time can vary depending mainly on duration of G_1 phase. The cancer cells divide indefinitely uncontrolled the mechanisms that control cell division disorders. Typically, the genes that control cell division is divided into two groups [9].

2.1.1 Tumour suppressor genes

Tumour suppressor genes are normal genes that slow down cell division, repair DNA mistakes, or tell cells when to die (a process known as apoptosis or programmed cell death). When tumour suppressor genes don't work property, cells can grow out of control, which can lead to cancers.

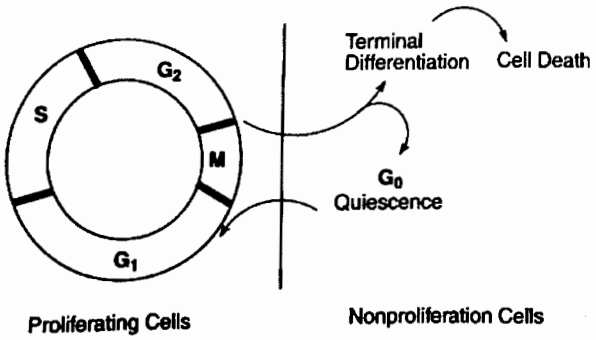

Figure 2.1 The life cycle of cells

From the Figure 2.1, G_1 phase is the initial step with the cell growth. S phase is the process that created the DNA, Deoxyribonucleic acid, a new set-up. G_2 is the step of the cell prepares to divide it up for M phase, which is the term that is cell division controlled growth and division of cells to replace dead cells called oncogenes. Tumor suppressor genes can inhibit and slow down the proliferative of cell at G_1 phase into S phase. Control, cell and cell growth can lead to mutation of tumor suppression genes. Which can allow cells grew more abnormal, then spread to neighboring areas, the bloodstream, lymph nodes and other organs away [10].

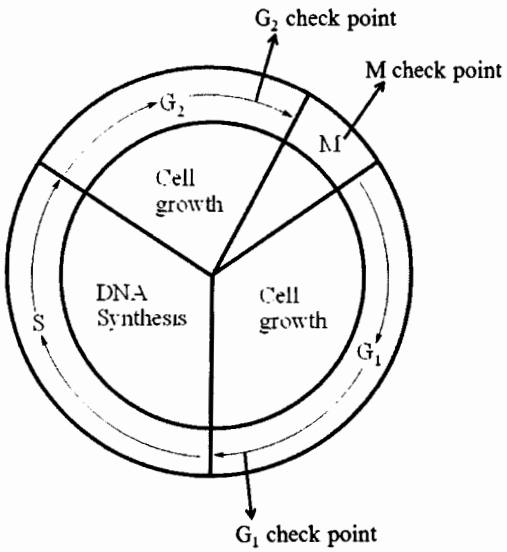

Figure 2.2 Check point in the process of cell division

As shown in Figure 2.2, at G_1 checkpoint, a main cell must receive mitogenic signal from neighboring cells that the cell has a complete and ready to DNA synthesis. If the main cell does not receive mitogenic signal that means cell's DNA is abnormal. Then, it is ordered to kill cells by sending back to the G_0 phase. There is no cell division occurs.

At G_2 checkpoint, cell checks that DNA replication is complete without the disorder. For example, if abnormalities of DNA at this point, cells are ordered to kill itself by apoptosis process.

At M checkpoint, accuracy of chromosome are ordered correctly. If a chromosome abnormality, it can lead to apoptosis process. It has been found the normal cell division will be regulated properly and no cause abnormal cell. However, if there is something interfering with the mechanism of this complex. Causing malfunctions the aforementioned error in the control of cell division, and let these abnormal cells divide indefinitely lead to cause cancer cell [11, 12].

2.2.2 Proto oncogenes[13]

Proto oncogenes behave contrary to the tumour suppression genes. In other words, Proto oncogen is expression for cell division and whenever stopping gene expression, cells division will be stopped.

There are two major control points in the cell cycle. One of these is at G_1/S when cell commit to replicate. The second is at G_2/M when cells commit to divide. Of these two major point in the cell cycle, the G_1/S is of major importance in understanding cancer and cancer treatment. During the G_1 phase a cell can take one of three routes. First, the cell may enter the S phase. Second, a cell in the G_1 phase may enter into a fifth phase called G_0 or Gap 0. Cell in G_0 are termed quiescent. Third, the cell may terminally differentiate and die. In normal cell populations, cell may be proliferating quiescent, or terminally differentiating such that there is on net change in the number of cell. However, in tumors, the fraction of cells proliferating increases at the expense of quiescent or terminally differentiating cell such that there is a net increase in the number of cells.

2.3 Cancer treatment [14]

For the treatments of cancer, doctors will diagnose the disease. By examination of the cancer cells spread in some areas of the body. So that, the doctor will treat the symptoms followed the type of cancer, Cancer treatment can be divided into 5 catagoeies as follows.

2.3.1 Surgery

Surgery means cutting out of some organs. For patients with liver cancer, surgery improved chances of a treatment from the disease or survive longer and a way to ensure that the cancer can be eliminated completely and prevent the cancer spread to other parts of the body. The remaining liver can continue to function even after being cut off some part. If the patients can surgery, the doctor will surgery first. To eliminated of the tumor in the body off but this method can not treated with any type of cancer and if the surgery is still uncertain whether cured 100 % or not because cancer cells may also remains or hidden in the body, doctors can not know or notice. For a while, it will return to original appearance, cancer cells began to grow up and needed to surgery again. Almost, the doctor usually recommend chemotherapy or chemotherapy in combination with surgery, to increase the chances that the cancer will be cured.

2.3.2 Radiotherapy

Radiotherapy is the use radiation to the cancer cells in the body, to destroy cancer cells. For this exposure treatment maintain a specific position based on the type of cancer. The patient will be exposed to light around 2-10 minutes to make radiation 5 days per week for about 5-8 weeks, depending on the doctor's diagnosis. Radiation therapy treatment can cause side effects such as dry skin, itching and red spots or dark, sore throat, dry mouth, tongue can not taste and very fatigue.

2.3.3 Immunotherapy and vaccinees

Immune therapy called Combined Immunotherapy for Cancer (CIC). It became interested in researcher group about cancer in the last 10 years, starting with education and understand more about the mechanism for destroying the cancer cell. Immunotherapy which focuses on increase immunity was fruitful as well.

Fuda cancer research center success in treating cancer by surgery, cryosurgery. It is the world leader in surgery this way. Many medical professionals used this surgery

procedure and treatment in successful including the International Society used this surgery procedure. Fuda research center proposed CIC combined with surgery with a cold, so the first immunotherapy with surgery and cryosurgery. it is a symbol of the Fuda cancer research center. Since the year 1991, 1,000 cancer patients were treated with CIC combined with normal treatment. Patients receiving treatment with CIC were found to live longer, reduce the spread and disease recurrence.

2.3.4 Photodynamic therapy (PDT)

Photodynamic therapy (PDT) is treatment that uses special drugs, celled photosensitizing agents, along with light to kill cancer cell. The drugs only work after they have been activated or "turn on" by certain kinds of light. PDT has been used in the treatment of esophageal cancer at an early stage. Photodynamic therapy treatment can cure metastatic esophageal cancer symptoms.

2.3.5 Chemotherapy

Cancer chemotherapeutic agents are used for a wide range of purposes. The intent of their administration may be to cure, reduce the size of a tumor prior to surgery, sensitize tumors to radiation therapy or to destroy microscopic metastases after tumors are surgically removed. Chemotherapeutic agents are complementary to either surgery or radiation therapy in that they are effective against metastasized tumors or residual tumors after surgery or radiation therapy. Chemotherapy are useful for eliminating tumors that are small in size. The reason that they are less useful for larger tumor is that large tumors are not well perfused by blood and thus the inner reaches of a tumor are not accessible to cancer chemotherapeutic agents [9].

The use of chemotherapy means giving medications to control or destroy cancer cells by inhibiting growth and proliferation of cancer cells. Directly destroy cancer cells is a solution that directly causes because it is administered to destroy all cancer cells within the body including the spread to the lymph nodes or the bloodstream. The doctor will perform a physical exam appointment and check blood pressure, blood drawing and if the results of a physical examination passed, the doctor will give to chemotherapy, which is the same as give a general saline, just have to wait several hours until the drug is depleted. In during the chemotherapy, patients may have allergic reactions, including dizziness, nausea, or vomiting. Side effects of chemotherapy after about 1-2 weeks, are hair loss, nausea, vomiting, sores in the

mouth and the blood cells volume decrease which make tired, difficulty tired, difficulty breathing, rashes, constipation or fever [14].

2.4 Type of chemotherapy

In the early 1900s, the famous German chemist, Paul Ehrlich set about developing drugs to treat infectious diseases. He is the one who coined the term "chemotherapy" and defined it as the use of chemicals to treat disease [19]. In 1950s, the National Cancer Institute (NCI) began to play a major role in the development of anticancer agents. NCI has been involved in the development of drugs in a variety of ways including screening chemicals for antitumor activity, funding cancer related research at all levels, and conducting basic cancer research. . Drugs in this group can be divided into 6 categories based on the active ingredient of the drug as follows;

2.4.1 Alkylating agent [15]

Alkylating agents represent the oldest class of anticancer agents with the approval of mechlorethmine by the FDA (Food and Drug Administration) in 1949. Alkylating agents were first used as chemical weapons during the First World War. The active ingredient of the drug alkylating agent group inhibit to cancer cell. The structure of the alkyl groups (active alkylating moiety) attached with sulfur, nitrogen, oxygen or phosphorus as a component of DNA. Alkylation between DNA and drug causes breakage of DNA made cell death. It can be divided into two categories: Non-platinum analogue and Platinum analogue as detailed below.

2.4.1.1 Non-platinum analogue

This type of medicine forms covalent bond with electron-rich nucleophile especially in nitrogen position seventh of guanine and other position on the DNA to make DNA formation abnormalities. This drug can alkylate with DNA in two types; inter-strand and intra-strand cross-link. The drugs in this group are Ifosfamide and Cyclofosfamide as shown in Figure 2.3.

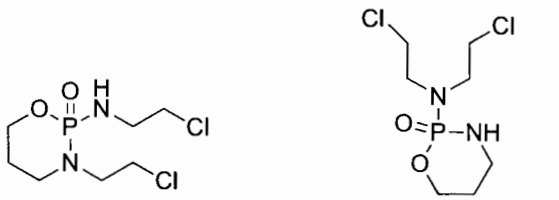

Figure 2.3 The structure of Ifosfamide and Cyclofosfamide

The drugs in this group alkylated with base in DNA strand by generating active inter mediate as aziriniumion as can be seen in Figure 2.4. However, this type of medicine caused many side effects became can occur alkylation with protein or other molecules. Therefore, replacing N-methyl with aromatic ring can reduce the nucleophilic properties of nitrogen and form azirinium ion hardens.

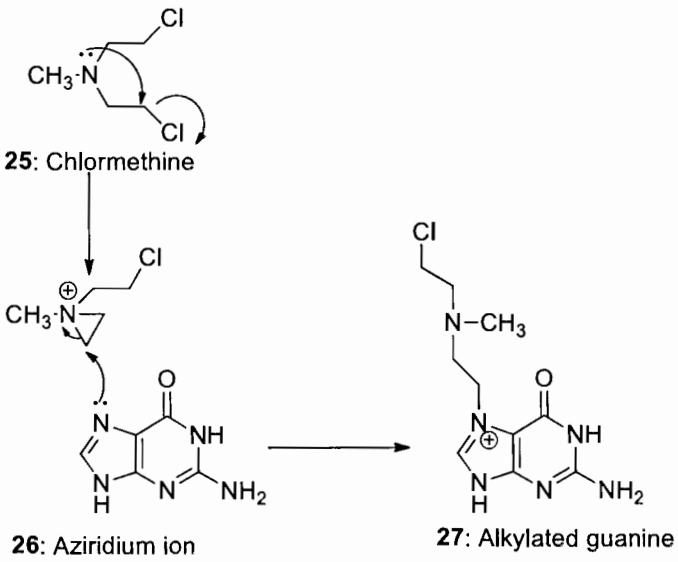

Figure 2.4 The mechanism of action of drugs Non-platinum analogue

2.4.1.2 Platinum analogue

This type of drug composed of platinum atom in the structure, for example cisplatin. Medicine actives by binding to DNA causing the abnormal of DNA structure. However, cisplatin medicine is high polar, thus eliminated a lot pass the kidneys, which is cause kidney toxicity (nephrotoxicity). Later, modification of the

structure to less derivatives, carboplatin can be absorbed better and is less toxic than cisplatin. The structures are shown in Figure 2.5

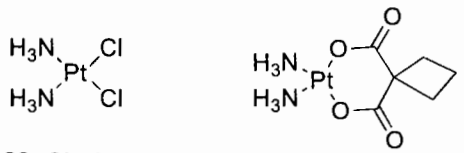

28: Cisplatin **29:** Carboplatin

Figure 2.5 The structure of cisplatin and carboplatin

2.4.2 Intercalating agent [7]

Intercalation is the insertion of molecules between the planar bases of DNA. This process is used as a method for analyzing DNA and it is also the basis of certain kinds of poisoning. Drug and substances in intercalating group are bioactive substances on the DNA by block and inserting between the base pairs of DNA strands as shown in Figure 2.6. Because this structure of substances is a three aromatic ring planar then occur interact to cause distortion of the DNA of cancer cells, so the cells can not divide further. Drugs in this group can be classified into five groups based on the structure.

A number of antibiotics such as anthracyclines, dactinomycin, bleomycin, adriamycin, mithramycin, bind to DNA and inactivate it. Thus the synthesis of RNA is prevented. General properties of these drugs include: interaction with DNA in a variety of different ways including intercalation (squeezing between the base pairs), DNA strand breakage and inhibition with the enzyme topoisomerase II. Most of these compounds have been isolated from natural sources and antibiotics. However, they lack the specificity of the antimicrobial antibiotics and thus produce significant toxicity.

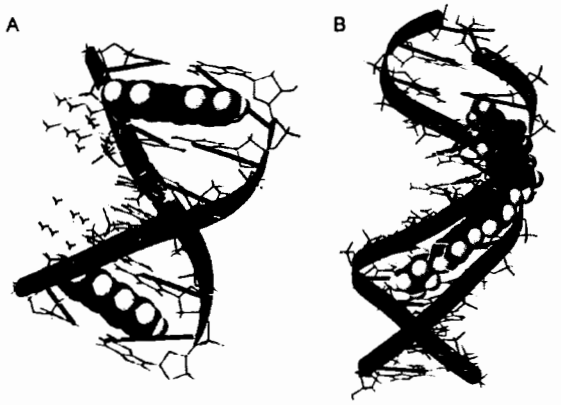

Figure 2.6 Insertion of drug into laterally between the base pairs of DNA a) major groove binder and b) minor groove binder

The anthracyclines are among the most important antitumor drugs available. Doxorubicin is widely used for the treatment of several solid tumors while daunorubicin and idarubicin are used exclusively for the treatment of leukemia. These agents have a number of important effects including: intercalating (squeezing between the base pairs) with DNA affecting many functions of the DNA including DNA and RNA synthesis. Breakage of the DNA strand can also occur by inhibition of the enzyme topoisomerase II [16].

2.4.3 Topoisomerase inhibitor

Topoisomerases are enzymes that participate in the overwinding or underwinding of DNA. The winding problem of DNA arises due to the intertwined nature of its double helical structure. During DNA replication and transcription, DNA becomes overwound ahead of a replication fork. Topoisomerase inhibitor is a newly developed drug that inhibits enzyme activity Topoisomerase I and II are enzymes that regulate changes within the DNA structure that play a key role in the cell division process. Medications in this group include amsacrine and asulacrine [17] as shown in Figure 2.7.

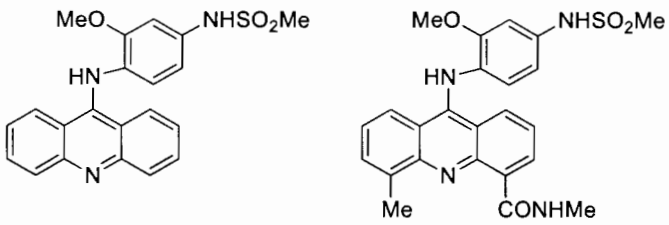

30: Amsacrine **31**: Asulacrine

Figure 2.7 The structure of amsacrine and asulacrine

The development of innovative chemotherapeutic treatments for cancer has made great strides within the last few decades. DNA, which is the genetic material, and the enzymes responsible for all the reactions in the body are major targets of interest for medical researchers looking for new cancer treatments.

Because DNA is the blueprint for humans and all other life forms, any damage to the DNA can result in cancer. Enzymes are proteins that facilitate and regulate many processes in the cells, several of which are necessary for the well being and the survival of every individual. Vitally important enzymes are often researched to figure out how they can be used in new cancer treatments.

DNA is normally a coiled double helix of two strands and is periodically uncoiled in the process of replication during cell division or in the process of reading the code to make new proteins. Two enzymes that play the biggest role in this uncoiling and recoiling process are topoisomerase I and topoisomerase II. They also play a significant role in fixing DNA damage that occurs as a result of exposure to harmful chemicals or UV rays.

There is a distinct difference in way the two enzymes work. Topoisomerase I cuts a single strand of the DNA double helix while topoisomerase II cuts both strands of DNA, using ATP for fuel. The rest of the process by which the two enzymes work is very similar. The process entails the relaxation of the coil of the two DNA strands, and then after the cuts are made and replication or repair is complete, the strands are paired back together and reform a coil.

The topoisomerase enzymes have been researched as targets for the generation of new cancer treatments because when they are inhibited in a cell, the result is that the cell dies. Therefore inhibitors of the topoisomerase enzymes have the

ability to kill all cells undergoing DNA replication, reading of the DNA for protein production or experiencing repair of DNA damage. Since cancer cells divide much more rapidly than normal cells, the cancer cells will be killed by the topoisomerase inhibitors, though some normal cells with topoisomerase activity will also be killed.

The typical way that both topoisomerase I and II inhibitors work is that the inhibitor binds to the topoisomerase molecule. This makes the enzyme nonfunctional by blocking the ability of the topoisomerase to bind the DNA back together after it has been cut. Therefore cuts are made to either one or both strands of the DNA molecule which are never repaired, ultimately leading to death of the cell. To name some recognizable drugs, the topoisomerase I inhibitors are camptothecin and its derivatives. Topoisomerase II inhibitors include doxorubicin, etoposides and mitoxantrone. Here is just one example of the reported effectiveness of a commonly used topoisomerase inhibitor. Studies have looked at the cancer-killing efficiency of Irinotecan (CPT-11), which is a derivative of camptothecin that is FDA approved for use in colorectal cancer. Results show that, it has a 13% to 32% response rate when used by itself or in combination with other chemotherapy drugs. That means 13 to 32% of cancer patients were used it have had their tumor shrink or disappear completely [18-20].

Advances have made it possible to treat cancer on a cellular level with more precision and effectiveness than ever before. Inhibiting the topoisomerase enzymes lead to cell death, especially in the cancer cells since they are rapidly dividing. Therefore topoisomerase inhibitors can eradicate certain forms of rapidly growing cancers [21].

2.4.4 Antimetabolites

Another way of treating cancers is by inhibiting the metabolism process, in the synthesized step and DNA replication, because cell division of cancer cell is always cell division more than normal cells. So when giving drugs in antimetabolites group to treatment will interfere the synthesis of DNA by three types of mechanisms as follows [23];

2.4.4.1 Antifolate agent

In our body, there is a process of producing folate and maintaining the body's cells, especially during the fast cell division in infants and pregnant women.

This folate is an anion of folic acid and will be used in DNA replication. So inhibiting the action of folate acids sent effect to inhibition of DNA synthesis and cell division. The most commonly of medicine used antifolate groups is methotrexate that inhibits activity of dihydrofolate reductase (DHFR) or thymidilate synthase (TS) enzyme. It is used to treat many cancers, but also found side effects including drug resistance, gastric ulcer and intestinal, harmful to the liver and kidneys and destroy leukocytes [22]. The structures are shown in Figure 2.8.

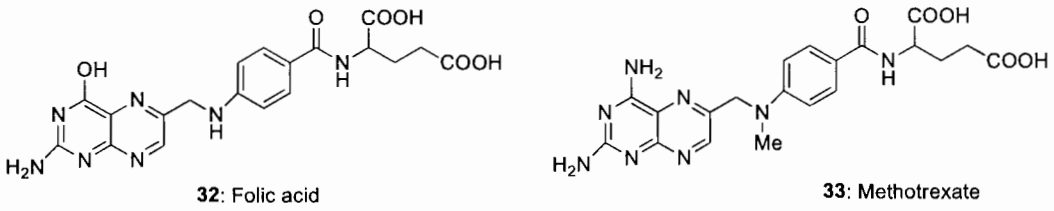

32: Folic acid **33**: Methotrexate

Figure 2.8 The structure of Folic acid and Methotrexate

2.4.4.2 Pyrimidine antimetabolites

Pyrimidine antimetabolites is medicine in antimetabolites groups. The structure is a derivative of the pyridine base with fluorine substitute in position 5. The size of fluorine and hydrogen are similar. Make the enzymes target not distinguish the difference. The medicine in this group is 5-Fluorouracil (5-FU), when entering the body will be changed to fluorodeoxyuridylate (FdUMP) and will interfere doing work of thymidilate synthase (TS). 5-FU can also be changed to fluorouridylate (FUMP) causes abnormalities DNA synthesis in the cell [9, 23]. The structure of substance is shown in Figure 2.9.

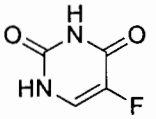

34: 5-Fluorouracil

Figure 2.9 The structure of 5-Fluorouracil

2.4.4.3 Purine antagonists

Purine base is a base important to life. There are also derivatives of purpurin which acts as a prodrug, such as 6-mercaptopurine and 6-tioquanine. When entering to the body, it will be transformed into monophosphates derivative which inhibit the synthesis of purines. Both of drugs are used to treat acute leukemia. Another derivative is fludarabine, when entering to the body will transformed to triphosphate derivative and activate by transcription or attached to strand of RNA [9, 23]. The structures of purine base medicine are shown in Figure 2.10.

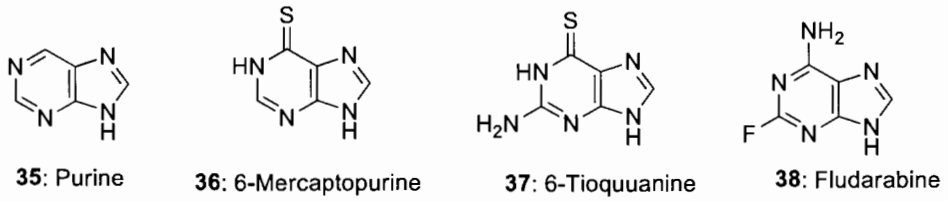

Figure 2.10 The structure of purine derivatives

2.4.5 Antitobuline agents

Microtubule can be found in cytoplasm of eukaryote cell. It is a type of cytoskeleton, which in the middle of shape is a hollow tube, the wall of tube is protein cube called tubulins. There are two types that are α-tubulin and β-tubulin. The important medicine in antitobulin groups which widely used is paclitaxel or trade name is Taxol. Taxol is a type of diterpene, the structure has four ring complex. It is a natural product that is isolated from the bark of a tree from China, named is *Taxus brevifolia*. The action of drug is by blinding with β-subunit of tubulins in microtubule. This will increase the polymerization of tubulins to be more stable and inhibit depolymerization process make tubulins not ready to used with other cells anymore. It is another process that inhibits cancer cell division [24, 25]. The structure of medicine paclitaxel (Taxol) is shown in Figure 2.11.

Taxol was isolate from the Pacific yew tree in the early 1960s. Although its use as an anticancer agent for ovarian cancer was not approved until the mid-1990s.

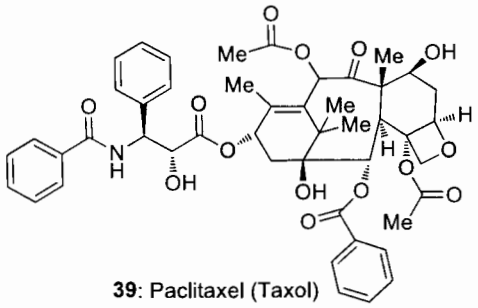

39: Paclitaxel (Taxol)

Figure 2.11 The structure of medicine paclitaxel (taxol)

Paclitaxel acts by binding to tubulin. However, unlike the vinca alkaloids, paclitaxel does not cause depolymerization. Paclitaxel causes microtubules to arrange themselves in a parallel array rather than the required arrangement of the mitotic spindle [9].

2.4.6 Antihormonal agent

Hormone is a good helper for cause of cancer. When cancer requires specific hormones to be used for growth, it can give hormones that active on the opposite side of the cell and can inhibit the growth of cancer cells. For example, the breast cancer is based on female hormone levels or estrogen hormone can induce breast cancer and accelerate the growth of cancer. Therefore, giving the medicine in anti-estrogens groups can reduce the synthesis of estrogen hormones. This drug active by binding to the receptor of the estrogen in the cytosol, move into the nucleus and inhibit the synthesis of estrogen. The structure of drugs that inhibit breast cancer, Tamoxifen and Toremifene are shown in Figure 2.12 [26].

Tamoxifen has been a prototype structure for the development of antiestrogens, but while tamoxifen's antiestrogen action appears to play a significant role in its anticancer activity the complete action is more complex than simply estrogen antagonism. Added to the arsenal of estrogen antagonists is the drug Toremifene [9].

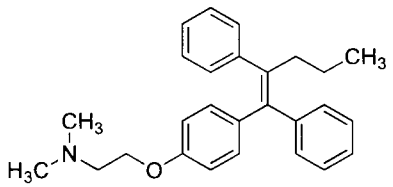

40: Tamoxifen

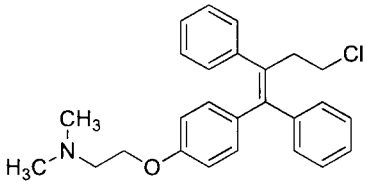

41: Toremifene

Figure 2.12 The structure of medicine anti-estrogen groups

2.4.7 Tumor-activated prodrugs

Prodrugs is chemical substance can be changed to a drug after entering to the body of patient by metabolism process or reaction. Therefore, prodrugs development has been of interest to reduce side effect on normal cells while treatment cancer with chemotherapy method. For example, Tirapazamine (SR-4233) is anticancer medicine in during test for treat cancer, when the cells have low oxygen levels, this substance will change to a drug when it enters to cells with low oxygen levels. Using of Tirapazamine in combination with the general treatment of cancer gives in good therapeutic results. The structure of Tirapazamine is shown in Figure 2.13.

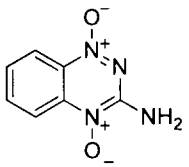

42: Tirapazamine

Figure 2.13 Structure of prodrug in tumor-activated prodrug groups

2.5 Drug design

Drug design, often referred to as rational drug design or simply rational design, is the inventive process of finding new medications based on the knowledge of a biological target as can been seen in figure 2.14. The drug is most commonly an organic small molecule that activates or inhibits the function of a biomolecule such as a protein, which in turn results in a therapeutic benefit to the patient. In the most basic sense, drug design involves the design of molecules that are complementary in shape

and charge to the biomolecular target with which they interact and therefore will bind to it. Drug design frequently but not necessarily relies on computer modeling techniques. This type of modeling is sometimes referred to as computer-aided drug design. Finally, drug design that relies on the knowledge of the three-dimensional structure of the biomolecular target is known as structure-based drug design. In addition to small molecules, biopharmaceuticals and especially therapeutic antibodies are an increasingly important class of drugs and computational methods for improving the affinity, selectivity, and stability of these protein-based therapeutics have also been developed [27].

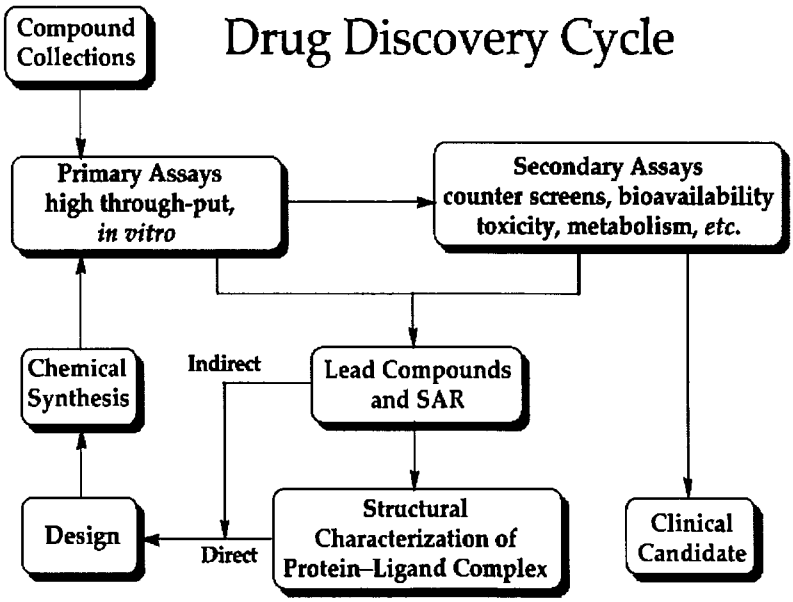

Figure 2.14 The pathway of drug discovery cycle [27]

The phrase "drug design" is to some extent a misnomer. A more accurate term is ligand design. Although design techniques for prediction of binding affinity are reasonably successful. There are many other properties that first must be optimized before a ligand can become a safe and efficacious drug. These other characteristics are often difficult to predict with rational design techniques. Nevertheless, due to high attrition rates, especially during clinical phases of drug development, more attention is being focused early in the drug design process on selecting candidate drugs whose physicochemical properties are predicted to result in fewer complications during

development and hence more likely to lead to an approved, marketed drug. Furthermore, in vitro experiments complemented with computation methods are increasingly used in early drug discovery to select compounds with more favorable ADME (absorption, distribution, metabolism, and excretion) and toxicological profiles.

2.5.1 Type of drug design

There are two major types of drug design. The first is referred to as ligand-based drug design and the second, structure-based drug design.

2.5.1.1 Ligand-based drug design

Ligand-based drug design (or indirect drug design) relies on knowledge of other molecules that bind to the biological target of interest. These other molecules may be used to derive a pharmacophore model that defines the minimum necessary structural characteristics a molecule must possess in order to bind to the target. In other words, a model of the biological target may be built based on the knowledge of what binds to it, and this model in turn may be used to design new molecular entities that interact with the target. Alternatively, a quantitative structure-activity relationship (QSAR), in which a correlation between calculated properties of molecules and their experimentally determined biological activity, may be derived. These QSAR relationships in turn may be used to predict the activity of new analogs [28].

2.5.1.2 Structure-based drug design

Structure-based drug design (or direct drug design) relies on knowledge of the three dimensional structure of the biological target obtained through methods such as x-ray crystallography or NMR spectroscopy. If an experimental structure of a target is not available, it may be possible to create a homology model of the target based on the experimental structure of a related protein. Using the structure of the biological target, candidate drugs that are predicted to bind with high affinity and selectivity to the target may be designed using interactive graphics and the intuition of a medicinal chemist. Alternatively various automated computational procedures may be used to suggest new drug candidates [29].

Current methods for structure-based drug design can be divided roughly into three main categories. The first method is identification of new ligands for a given receptor by searching large databases of 3D structures of small molecules

to find those fitting the binding pocket of the receptor using fast approximate docking programs. This method is known as virtual screening. A second category is de novo design of new ligands. In this method, ligand molecules are built up within the constraints of the binding pocket by assembling small pieces in a stepwise manner. These pieces can be either individual atoms or molecular fragments. The key advantage of such a method is that novel structures, not contained in any database, can be suggested A third method is the optimization of known ligands by evaluating proposed analogs within the binding cavity [27].

2.6 Anthracene and anthraquinone derivatives

In 2015, Yongseok Kwon et al. designed, synthesized, and evaluated biological activity of the methanesulfonamide analogues of natural alkaloids. The antiproliferative activity and unique mode of action phenanthroindolizidine and phenanthroquinolizidine alkaloids showed by antofine and cryptopleurine, have attracted attention recently as potential therapeutic agents. The derivative indicated enhanced growth inhibition of human cancer cells compared with the parent natural products. In particular, a methanesulfonamide analogue of cryptopleurine (**43**) showed improved bioavailability and significant antitumor activity, which suggests that compound **44** is a promising novel anticancer agent. They suggested that the inhibition of cancer cell growth by **44** was associated with the induction of G_0/G_1 cell cycle arrest via nicotinamide N-methyltransferase-dependent JNK activation in Caki-1 renal cancer cells. Moreover, compound **44** significantly inhibited the migration and invasion of Caki-1 cancer cells by modulating the p38 MAPK signaling pathway [30].

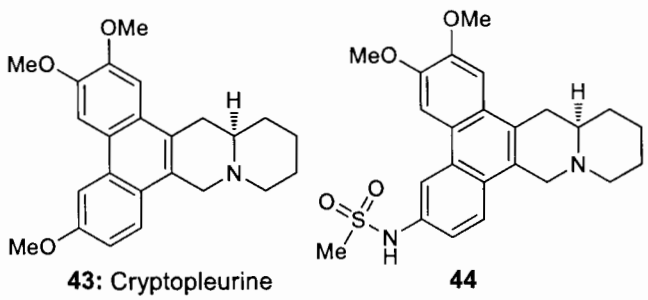

43: Cryptopleurine **44**

Figure 2.15 The chemical structure Cryptopleurine (43) and compound 44

In 2015, Jian-Sung Wu et al. studied the structure-based virtual screening strategy, comprising homology modeling, ligand support binding site optimization and virtual screening. Structure clustering analysis was developed and used to identify new tryptophan-2,3-dioxygenase (TDO) inhibitors (IC_{50} = 711 nM), selected by virtual screening, indicated inhibitory activity toward TDO and was subjected to structural modifications and molecular docking studies. The resultes indicate the potent TDO as selective inhibitor (**45**, IC_{50} = 30 nM), making it a potential compound for further investigation as a anticancer agent and other TDO-related targeted treatment [31].

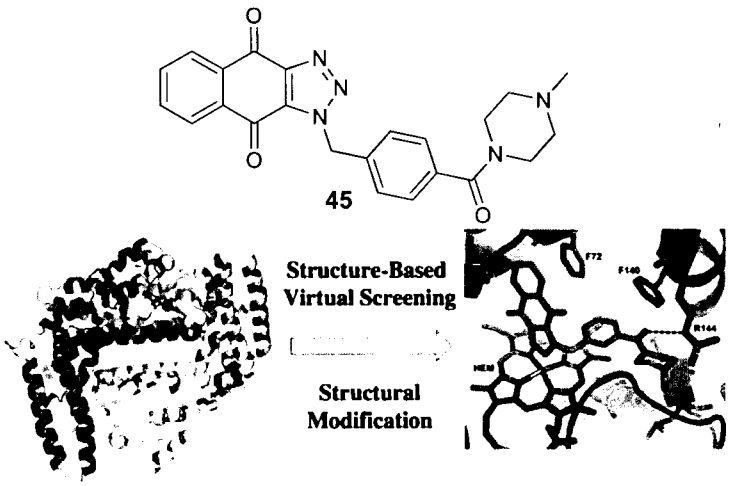

Figure 2.16 The chemical structure of compound 45 and virtual screening of compound 45

In 2015, Susanna Cogoi et al. found that two neighboring G-quadruplexes behave as a molecular switch controlling the expression of HRAS. They designed anthrathiophenediones with two chloroacetamidine-containing side chains (CATDs) as G-quadruplex binders and have examined their anticancer activity in T24 bladder cancer cells bearing mutant HRAS and in T24 xenografts. The designed CATDs five compounds, bearing alkyl side chains of different length, penetrated T24 cancer cells more than their analogues with guanidine-containing side chains. The lead compounds **46a** and **46c** inhibited HRAS expression, metabolic activity, and colony formation in T24 cancer cells. Compounds **46a** and **46c** also activated a strong apoptotic response, as indicated by PARP-1, caspases 3/7, and annexin V/propidium iodide assays.

Apoptosis occurs under conditions where cyclin D1 is down-regulated and block the cells in the G_2 phase. Finally, compound **46a** inhibited the growth of T24 xenografts and suggested that increases the median survival time of nude mice and chloroacetamidine-containing anthrathiophenediones may have potential in the treatment of human bladder cancer [32].

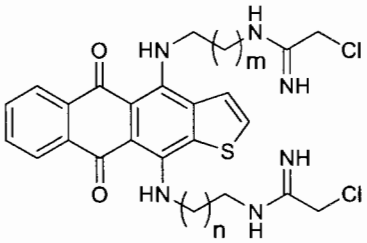

46 a-e m,n = 1,2,3

Figure 2.17 Structure of anthrathiophenediones with two chloroacetamidine-containing side chains (CATDs) 46a-e

In 2016, Katarzyna Gach et al. reported that an efficient and general synthesis of substituted 3-diethoxyphosphorylnaphtho [2,3-*b*]furan-4,9-diones and 3-diethoxyphosphorylbenzo [*f*]indole-4,9-diones were integrated the natural 1,4-naphtalenedione scaffold. The synthesized compounds were evaluated cytotoxicity with HL-60 and NALM-6 and against a breast adenocarcinoma MCF-7 cell line. Compound **47a-f** showed high cytotoxic activity with the IC_{50} values below 10 μM, much higher cytotoxic activity than benzoindole-4,9-diones. The synthesized compounds were tested on inhibition of HL-60 and MCF-7 cells. The mechanism of action of synthesized compounds was generating DNA damage and inducing apoptosis. The suggested mechanism of its cytotoxic activity was the generation of intracellular reactive oxygen species (ROS) and the induction of mitochondrial membrane potential dissipation [33].

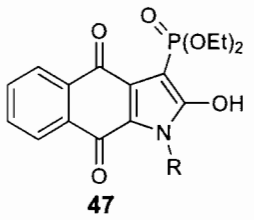

47

Compound 47	R
a	Me
b	n-Pr
c	c-Pr
d	n-Hex
e	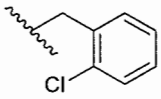

Figure 2.18 Structure of compound 3-diethoxyphosphorylbenzo [*f*]indole-4,9-diones 47a-e

2.7 Thiosemicarbazide derivatives

In 2003, Zahra Afrasiabi et al. synthesized and characterized Copper(II), Nickel(II), Palladium(II) and Platinum(II) complexes of ortho-naphthaquinone thiosemicarbazone. In both solution (NMR) and solid state (IR, single-crystal X-ray diffraction determination) the free ligand NQTS exists as the thione form. The Pd complex (X-ray) crystallizes as the H-bonded dimer, $[Pd(NQTS)Cl]_2 \cdot 2DMSO$, where Palladium(II) coordinated in a square planar configuration to the monodeprotonated, tridentate thiosemicarbazone ligand. The Nickel(II) complex showed 1:2 metal to ligand stoichiometry while the other complexes exhibit 1:1 metal–ligand compositions. In *vitro* anticancer studies on MCF7 human breast cancer cells revealed that adding a thiosemicarbazone pharmacophore to the parent quinone carbonyl considerably enhanced its antiproliferative activity. Among the metal complexes, the nickel compound exhibited the low IC_{50} value (2.25 μM) suggesting a different mechanism of action involving inhibition of topoisomerase II activity [34].

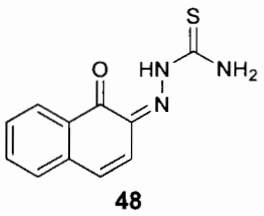

48

Figure 2.19 The chemical structure of 1,2-naphthaquinone thiosemicarbazone (NQTS) (48)

In 2006, Ana Cristina Lima Leite et al. synthesized novel thiosemicarbazones, aminoacyl-thiosemicarbazides and aminoacyl-thiazolidones by using accessible methodologies. Compounds **49** and **50** exhibit significant in *vitro* activity against epimastigote *T. cruzi*, particularly. Docking studies were carried out in order to investigate the binding pattern of these compounds for the *T. cruzi* cruzain (TCC) protein, and these showed a significant correlation with experimental data [35].

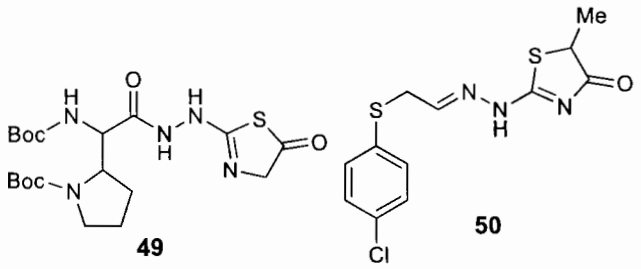

49 50

Figure 2.20 Structure of thiosemicarbazones 49 and aminoacyl-thiazolidones 50

In 2014, Rajesh A. Rane et al. reported the synthesis and screening of forty novel 4-nitropyrrole-semicarbazide conjugates inspired from the reported bio-potential of bromopyrrole alkaloids and semicarbazide derivatives for antimicrobial activity. Herein, hybrids **51k–51o**, **51r**, **51s** and **51t** displayed four-fold increased activity (MIC = 0.39 µg/mL) against *Escherichia coli* compared to standard ciprofloxacin. Eight hybrids, **51k–51o** and **51r–51t** displayed equal antibacterial activity (MIC = 1.56 µg/mL) against *Klebsiella pneumonia* compared to standard ciprofloxacin. Hybrid, **51k–51o** (MIC = 0.195 µg/mL) displayed highly potent antibacterial activity against MSSA as compared to standard ciprofloxacin. Eight-fold superior activity was observed for four hybrids **51k–51m** and **51o** (MIC = 0.39 µg/mL) against MRSA.

Further, nine hybrids displayed four-fold superior antifungal activity (MIC = 0.78 µg/mL) compared to standard Amphotericin B. Encouraging MICs of these hybrids recognize them as promising leads for development of potential antimicrobial drugs [36].

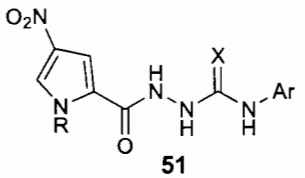

51

51(a-j) : R=H, X=S

51(k-t) : R=CH3, X=S

51a : Ar = 4-nitrophenyl	**51k** : Ar = 4-nitrophenyl
51b : Ar = 4-methoxyphenyl	**51l** : Ar = 4-methoxyphenyl
51c : Ar = 4-fluorophenyl	**51m** : Ar = 4-fluorophenyl
51d : Ar = 2-fluorophenyl	**51n** : Ar = 2-fluorophenyl
51e : Ar = 4-chlorophenyl	**51o** : Ar = 4-chlorophenyl
51f : Ar = pheneth-2-yl	**51p** : Ar = pheneth-2-yl
51g : Ar = benzyl	**51q** : Ar = benzyl
51h : Ar = cyclohexyl	**51r** : Ar = cyclohexyl
51i : Ar = o-tolyl	**51s** : Ar = o-tolyl
51j : Ar = 3,4,5-trimethoxyphenyl	**51t** : Ar = 3,4,5-trimethoxyphenyl

Figure 2.21 Structure of 4-nitropyrrole-semicarbazide derivatives 51a-t

In 2014, Poornachandran Mahalingam et al. reported that the 4EGI-1 is the prototypic inhibitor of eIF4E/eIF4G interaction (**52**), a potent anticancer of translation initiation in *vitro* and in *vivo* and an evaluated anticancer agent in animal models of human cancers. They designed, synthesized, and in *vitro* characterized a series of rigidified mimetic of this prototypic inhibitor. The bridge consisted one of the following: ethylene, methylene oxide, methylenesulfide, methylenesulfoxide, and methylenesulfone. The phenyl moiety in the 2-(4-(3,4-dichlorophenyl)thiazol-2-yl) moiety was bridged into a tricyclic system. Numerous analogues in this series were found to be markedly more potent than the parent prototypic inhibitor in the inhibition

of eIF4E/ eIF4G interaction (**52**). Thus they prevented the eIF4F complex formation, a rate limiting step in the translation initiation cascade in eukaryotes, and inhibition of human cancer cell proliferation [37].

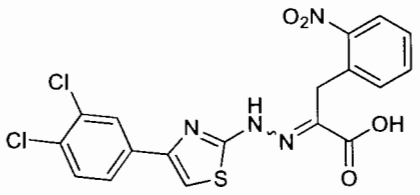

52

Figure 2.22 The chemical structure of eIF4E/eIF4G inhibitor-1 compound 52

In 2016, Jose Ignacio Manzano et al. synthesized thiosemicarbazone derivative as potential antileishmanial agents. The 32 compounds were synthesized and their efficacy was evaluated against the clinically relevant intracellular amastigotes of Leishmania donovani. Found that, 22 compounds showed EC_{50} values below 10 μM. Compound **53** showed potent cytotoxic activity with EC_{50} of 0.8 μM with very low toxicity on two different mammalian cell lines. The most relevant structural elements required for higher activity indicated the presence of a fused bicyclic aromatic ring. This series is easy synthesis, high activity and low toxicity, the most active compounds could be considered as a lead for further development [38].

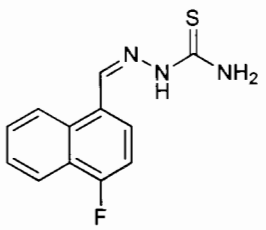

53

Figure 2.23 The chemical structure of Arylthiosemicarbazones 53

2.8 Azanaphthoquinone derivatives

In 1999, Chung-Kyu Ryn et al. studied the synthesis of 6-chloro-7-arylamino-5,8-isoquinolinediones. The compounds are potent cytotoxic agents against HCT-15 and SK-MEL-2. 6-Chloro-7-arylamino-5,8-isoquinolinediones were newly synthesized and evaluated for in *vitro* cytotoxic activities against five human solid tumor cell lines. Among them, **54**, **55** and **56** showed potent activities against the cell lines HCT-15 and SK-MEL-2 [39].

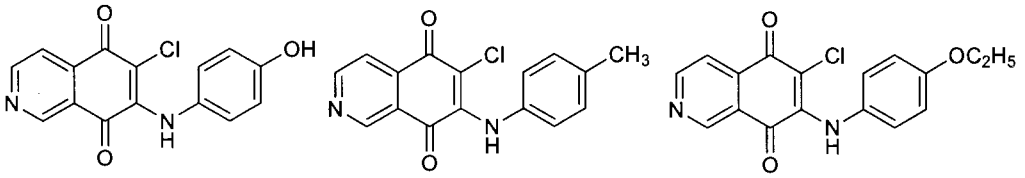

Figure 2.24 Structure of 6-chloro-7-arylamino-5,8-isoquinolinediones derivatives 54, 55 and 56

In 2004, Jin Sung Kim et al. synthesized a series of mono-substituted 2-methyl-1*H*-imidazo[4,5-*g*]phthalazine-4,9-dione derivatives from 6,7-dichlorophthalazine-5,8-dione. All the synthesized compounds indicated more potent cytotoxicity than ellipticine, clinically used agent for the treatment of solid tumor. All three compounds (**57**, **58**, **59**) were more active than doxorubicin, clinically used for the treatment of solid tumor. Most of the tested compounds showed potential cytotoxic activity considerably higher than that of the reference compounds, ellipticine and doxorubicin [40].

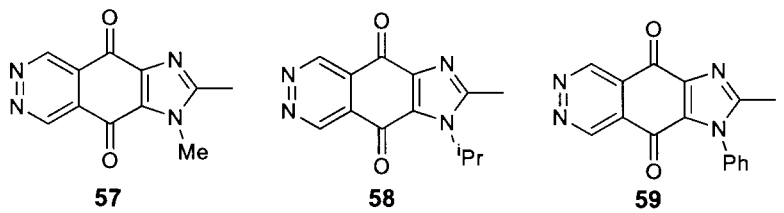

Figure 2.25 Structure of 2-methyl-1*H*-imidazo[4,5-*g*]phthalazine-4,9-dione derivatives 57, 58 and 59

In 2006, Jin Sung Kim et al. studied the synthesis of 6-chloroisoquinoline-5,8-diones and pyrido[3,4-*b*]-phenazine-5,12-diones. The compounds were synthesized and evaluated the cytotoxic activity and topoisomerase II inhibitory activity. The cytotoxicity of the synthesized compounds were evaluated by a SRB (Sulforhodamine B) assay against various cancer cell lines such as A549, SNU-638, Col2, HT1080, and HL-60. The pyrido[3,4-*b*]phenazinediones series showed greater cytotoxic potential than ellipticine (IC_{50} = 1.82–5.97 μM). In general, the cytotoxicity of the pyrido[3,4-*b*]phenazinediones was higher than that of the corresponding chloroisoquinolinediones. The cytotoxic mechanism, the topoisomerase II inhibitory activity of the synthesized compounds was estimated by a plasmid cleavage assay. Most of compounds showed the topoisomerase II inhibitory activity (28–100%) at 200 μM. IC_{50} values for the most active compound **60** were 0.082 μM. However, the compounds were inactive for DNA relaxation by topoisomerase I at 200 μM [41].

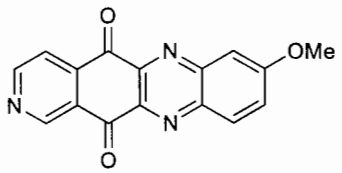

60

Figure 2.26 Structure of pyrido[3,4-*b*]phenazinediones (60)

In 2008, Ippolito Antonini et al. designed and synthesized a series of symmetrical bis derivatives, compounds **61** as anticancer agents. These compounds are dimers of different aza-anthracenedione and aza-anthrapyrazolone monomers connected by the linker found to be the most appropriate among potential bis intercalators. Compound **61**, shows very potent cytostatic and cytocide action and a high capacity for early apoptosis induction, expected a good candidate for in *vivo* preclinical studies. The synthesized compounds were evaluated cytotoxicity with human cancer adenocarcinoma cell line, HT29. Compound **61** showed GI_{50} value of 0.36 nM and two selected compounds have been investigated for their capacity of inducing early apoptosis [42].

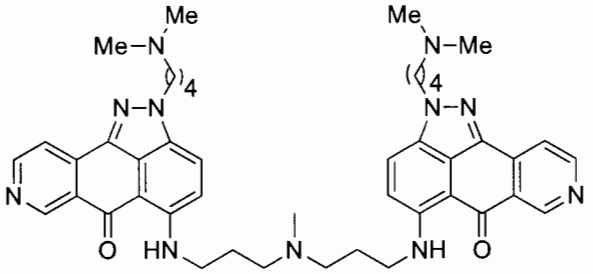

61

Figure 2.27 Structure dimers of aza-anthracenedione (61)

In 2010, Karem Shanab et al. investigated the synthesis of azanaphthoquinone pyrrolo-annelated derivatives as antiproliferative agents. The synthesized compounds were evaluated on cytotoxicity with KB/HeLa, SKOV-3, SF-268, NCI-H460, RKOp27 and RKOp27IND cell line. The results showed that quinazolines **62** exhibited highest inhibition across all cell lines. Compound **62** indicated highest inhibition with EC_{50} of 0.08 µg/mL against NCI-H460 and 0.11 µg/mL and compound **62** showing mean EC_{50} of 0.18 µg/mL in NCI-H460 and 0.2 µg/mL in SF-268 cell lines. The effects on cell cycle and intercalation were investigated [43].

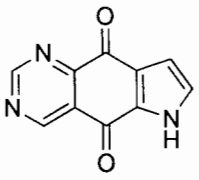

62

Figure 2.28 Structure of quinazolines (62)

In 2011, Karem Shanab et al. synthesized 6-azanaphthoquinone pyrrolo annelated derivatives attached to different basic side chains linker as anticancer agents. The 6-azanaphthoquinone pyrrolo annelated derivatives were evaluated biological activity with various cancer cell line including KB/HeLa, SKOV-3, SF-268, NCI-H460, RKOp27 and RKOp27IND using Mitoxantrone as reference compound. The results showed very good to moderate biological activity of compounds **63** and **64**. For the aziridine series, C4 linker chains revealed the highest activity [44].

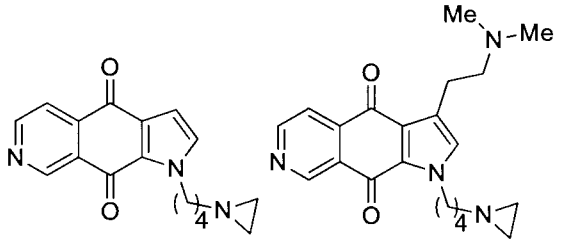

63 64

Figure 2.29 Structure of 6-azanaphthoquinone pyrrolo annelated (63, 64)

In 2013, Manochehr Shahabi et al. synthesized indazolo[4,3-*gh*]isoquinolinones derivatives. This series has been synthesized to decrease cardiotoxic side effects using Mitoxantrone as the reference drug. The synthesized compounds were tested for antiproliferative activity against at least four cancer cell lines cervix, ovarian, CNS, NSCLC (non-small-cell lung cancer) and colon carcinoma. It was found that the compound **65** showing better than reference compound Mitoxantrone. Cell cycle arrest studies gave complex results, including an induction of S-phase arrest with an inversed dose dependency [45].

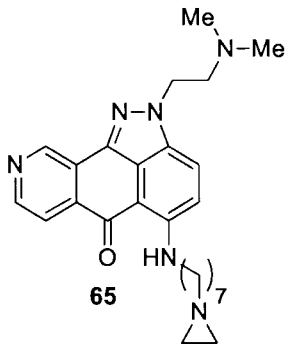

65

Figure 2.30 Structure of indazolo[4,3-*gh*]isoquinolinones (65)

In 2013, Theerachart Leepasert et al. synthesis new series of substituted tri-/tetraazabenzo[3,2-*a*]fluorene-5,6-diones and oxime derivatives. The antiproliferative activities of all compounds were evaluated with KB/HeLa, SKOV-3 and NCI-H460 cell line. The annelated derivatives **66** and **67** were studied compared with

Mitoxantrone and doxorubicin. The result showed that compound **66** and **67** exhibited satisfactory biological activity in three cancer cells line [46].

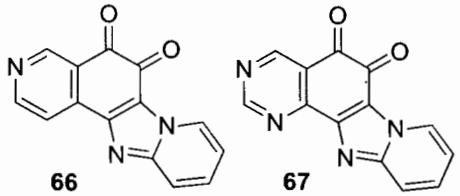

66 **67**

Figure 2.31 Structure of tetraazabenzo[3,2-*a*]fluorene-5,6-dione (66, 67)

In 2014, Veda Prachayasittikul el at. synthesis of 2-substituted amino-3-chloro-1, 4-naphthoquinone derivatives **68** as anticancer agents and evaluated biological activity synthesized compound with four cancer cell lines including HepG2, HuCCA-1, A549 and MOLT-3. The most potent cytotoxic activity against in HepG2, HuCCA-1 and A549 cell lines was found to be macetylphenylamino-1,4-naphthoquinone affording IC_{50} values of 4.758, 2.364 and 12.279 μM, respectively. On the other hand, *p*-acetylphenylamino-1, 4-naphthoquinone **68** exhibited the most potent cytotoxic activity against the MOLT-3 cell line with an IC_{50} of 2.118 μM. Quantitative structure activity relationship (QSAR) investigation provided good predictive performance as observed from cross validated R of 0.9177-0.9753 and RMSE of 0.0614-0.1881. The effects of substituents at the 2-amino position on the naphthoquinone core structure and its corresponding influence on the cytotoxic activity were investigated by virtually constructing additional 1, 4-naphthoquinone compounds for which cytotoxic activities were predicted using equations obtained from the previously constructed QSAR models [47].

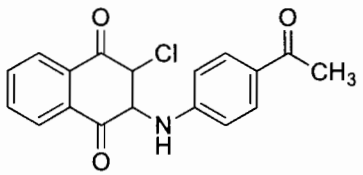

68

Figure 2.32 Structure of *p*-acetylphenylamino-1,4-naphthoquinone (68)

CHAPTER 3
EXPERIMENT

3.1 General procedure and instruments

^{1}H-NMR spectra were recorded on a Bruker AVANCE (300 MHz) spectrometer. The residue of the nondeuterated solvent was used as internal standard which was related to tetramethylsilane with δ = 7.26 ppm for $CHCl_3$, δ = 4.78 and 3.31 ppm for CH_3OH and δ = 2.50 ppm for DMSO. ^{13}C-NMR spectra were recorded on a Bruker AVANCE (75 MHz) with the residue of the non-deuterated solvent peak as the internal standard, δ = 77.0 ppm for $CHCl_3$ δ = 49.15 ppm for CH_3OH and δ = 39.51 ppm for DMSO. The IR spectra were recorded by attenuated total reflectance (ATR) using neat sample on Perkin-Elmer FT-IR Spectrum RX.I. Mass spectra were recorded on a GC-MS Shimadzu GCMS-QP-2010.

All reactions and atmospheric pressure distillations were performed under a positive pressure of nitrogen. Reaction flasks were dried at 120 °C for 2 h and connected with N_2-line when they were still warm. Extracts were dried over anhydrous magnesium sulfate ($MgSO_4$). Solvents were removed by rotary evaporator. A trace amount of solvent was further removed under vacuum pump.

Thin layer chromatography (TLC) was performed with Merck silica gel 60 PF254 plate (Merck-Nr 1.05554: 0.2 mm, 20×20 cm) or Merck aluminium oxide plate (Merck-Nr 1.05550 : 0.2 mm, 20×20 cm). Chromatography was performed using Merck silica gel 60, 70–230 mesh ASTM, Nr 1.07734.

3.2 Chemical and reagents

Table 3.1 Chemical and solvents for synthesis

Chemical	Formula	Grade	Company
Chloroform-D	$CDCl_3$	99.8 %	Cambridge Isotope Laboratories, Inc.
2-chloro-*N,N*-dimethyl ethyl amine hydrochloride	$C_4H_{10}NCl.HCl$	98 %	ACROS Organics
N-(2-chloroethyl)piperidine hydrochloride	$C_8H_{14}NCl.HCl$	98 %	ACROS Organics
2-chloro-*N,N*-dimethyl propyl amine hydrochloride	$C_5H_{12}NCl.HCl$	98 %	ACROS Organics
N-(2-chloroethyl)pyrrolidine hydrochloride	$C_6H_{12}NCl.HCl$	98 %	ACROS Organics
Dichloromethane	CH_2Cl_2	Commercial	Ultima
Dimethylformamide	C_3H_7NO	99.8 %	ACROS Organics
Ethanol	C_2H_6O	Commercial	Ultima
Ethyl acetate	$C_4H_8O_2$	Commercial	Ultima
Hexane	C_6H_{14}	Commercial	Ultima
Hydrochloric acid	HCl	37 %	CARLO ERBA
5-hydroxyisoquinoline	C_9H_7NO	90 %	ACROS Organics
Magnesium sulfate anhydrous	$MgSO_4$	96 %	Panreac
Methanol	CH_4O	Commercial	Ultima
Methanol-D	CD_4O	99.8 %	Cambridge Isotope Laboratories, Inc.
Nitric acid	HNO_3	65 %	Merck
Potassium carbonate			
Silica gel 60	SiO_2	-	CARLO ERBA
Sodium hydride	NaH	60 %	-
Thiosemicarbazide	CH_5N_2S	99 %	ACROS Organics

3.3 Synthesis and characterization

3.3.1 Synthesis of 6,7-dichloroisoquinoline-5,8-dione (18)

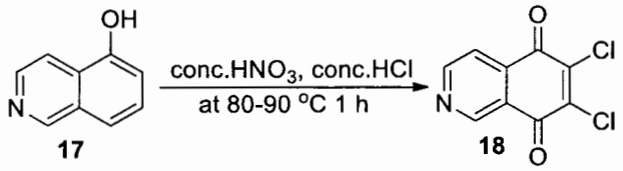

5-Hydroxyisoquinoline **(17)** (0.7586 g, 5.23 mmol) was dissolved in hydrochloric acid (17 mL) and then nitric acid (3 mL) was slowly added. The mixture was stirred 1 h at 80 – 90 °C under nitrogen atmosphere. The mixture was extracted with DCM (5x100 mL). The organic layers were dried over anh. $MgSO_4$. The solvent was removed in rotary evaporator. The residue of **18** was purified by column chromatography (silica gel) eluting with Hexane/EtOAc; 7:3 (v/v) to give product **18** (0.2436 g, 20 %), m.p. > 250 °C as yellow solid.

^{1}H-NMR (300 MHz, $CDCl_3$): δ = 9.42 (s, 1H, H-1), 9.12 (d, J = 4.8 Hz, 1H, H-3), 7.97 (d, J = 4.8 Hz, 1H, H-4) ppm.

^{13}C-NMR (75 MHz, $CDCl_3$): δ = 175.5 (C- 5), 175.3 (C-8), 156.0 (C-3), 149.5 (C-1), 144.0 (C-6), 143.5 (C-7), 136.0 (C-4a), 124.0(C-8a), 119.5 (C-4) ppm.

IR (Neat): V_{max} = 2922 (w), 2852 (w), 1676 (s), 1585 (m), 1555(m), 1416 (w), 1288 (m), 1174 (m), 1124 (m), 1035 (w), 888 (w), 833 (w), 718 (s), 694 (s), 670 (m), 563 (w) cm^{-1}.

MS-EI m/z calcd for $C_9H_3Cl_2NO_2$ (M^++H) 227.9619; found: 227.9533.

3.3.2 Synthesis of cyclized product 2,7-dihydrobis([1,2,4]triazino)[6,5-*f*:5',6'-*h*]isoquinoline-3,6-dithiol (19)

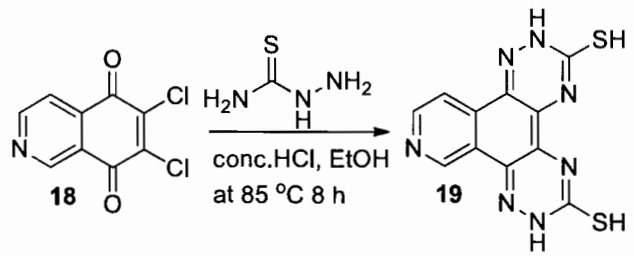

The mixture of compound **18** (0.2416 g, 1.06 mmol) and thiosemicarbazide (0.1158 g, 1.27 mmol) was dissolved in EtOH. After that, 10 drops of hydrochloric acid were added at room temperature into the mixture and then reaction mixture was refluxed at 85 °C for 8 h under nitrogen atmosphere. The crude reaction **19** was removed solvent by rotary evaporator. The crude reaction of **19** was purified by column chromatography (silica gel) eluting with gradient EtOAc to EtOAc/MeOH; 8:2 (v/v) to give product **19** (0.1283 g, 40 %), m.p. > 250 °C as dark brown solid.

^{1}H-NMR (300 MHz, CD_3OD): δ = 9.98 (s, 1H, H-1), 8.59 (d, J = 5.4 Hz, 1H, H-3), 8.34 (d, J = 5.7 Hz, 1H, H-4) ppm.

^{13}C-NMR (75 MHz, CD_3OD): δ = 162.5 (C=N), 162.0 (C=N), 151.5 (C-SH), 151.0 (C-SH), 147.0 (C-1), 146.5 (C-3), 134.5 (C-8a), 132.0 (C-6), 130.0 (C-7) 122.5 (C-4a), 119.0 (C-4) ppm.

IR (Neat): ν_{max} = 3369 (br w), 3171 (br w), 2921 (m), 2850 (m) 1610 (m), 1555 (m), 1455 (m), 1423 (m), 1285 (m), 1241 (m), 1178 (m) cm^{-1}.

MS-EI m/z calcd for $C_{11}H_5N_7S_2$ (M^+-2H) 299.0048; found: 299.2705.

3.3.3 The synthesis of mono-substituted azanaphthoquinone annelated thiazole derivatives of the cyclized product under acid conditions

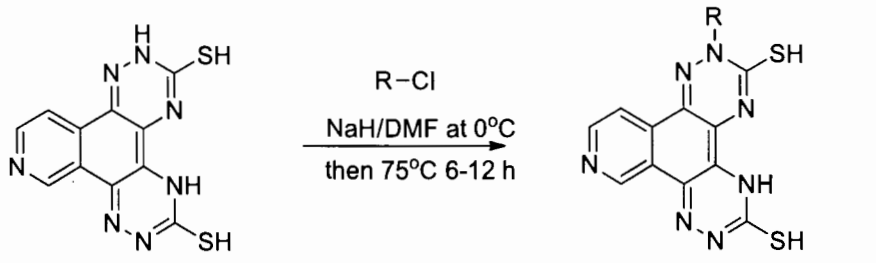

19 **20**

a : R = $CH_2CH_2NMe_2$
b : R = $CH_2CH_2CH_2NMe_2$
c : R = CH_2CH_2 (pyrrolidine)
d : R = CH_2CH_2 (piperidine)

General procedure

60% NaH (2.6 equiv.) was dissolved in DMF and cooled at 0 °C. Then compound **19** (1 equiv.) in DMF was added dropwise and stirred for 30 min under nitrogen atmosphere. The side chain (1.5 equiv.) in DMF was added to the mixture

and refluxed at 75 °C for 8 h. After that, water was added to quench the reaction. The solvent was removed by using rotary evaporator. The crude product was purified by column chromatography to give alkylated product.

3.3.3.1 The synthesis of compound **20a**

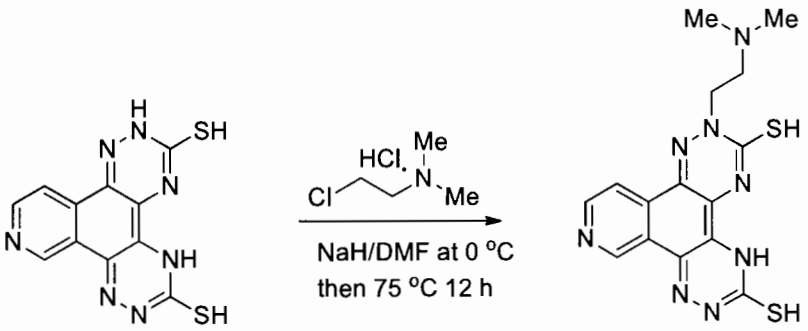

The mixture of NaH (0.0475 g, 1.19 mmol), compound **19** (0.1379 g, 0.46 mmol) and 2-chloro-*N,N*-dimethyl ethylamine hydrochloride (0.0990 g, 0.69 mmol) in DMF (10 mL) was refluxed at 75 °C for 8 h under nitrogen atmosphere. The crude reaction of **20a** was purified by column chromatography (silica gel) eluting with gradient EtOAc to EtOAc/MeOH; 7:3 (v/v) to give product **20a** (0.0298 g, 17 %), m.p. > 250 °C as orange solid.

^{1}H-NMR (300 MHz, $CDCl_3$): δ = 9.92 (s, 1H, H-1), 8.98 (d, J = 6.3 Hz, 1H, H-3), 8.19 (d, J = 6.3 Hz, 1H, H-4), 4.65 (s, 2H, H-1′), 2.96 (s, 2H, H-2′), 2.33 (s, 6H, H-3′) ppm.

IR (Neat): ν_{max} = 3492 (m), 3257 (m), 3061 (m), 2740 (m), 1633 (m), 1598 (m), 1586 (s), 1488 (m), 1451 (w), 1390 (s), 1378 (s), 1250 (m), 1167 (m), 1101 (m), 893 (w), 853 (m), 824 (w) cm^{-1}.

MS-EI m/z calcd for $C_{15}H_{16}KN_8S_2^+$ (M^++K) 441.0576; found: 441.3795.

3.3.3.2 The synthesis of compound **20b**

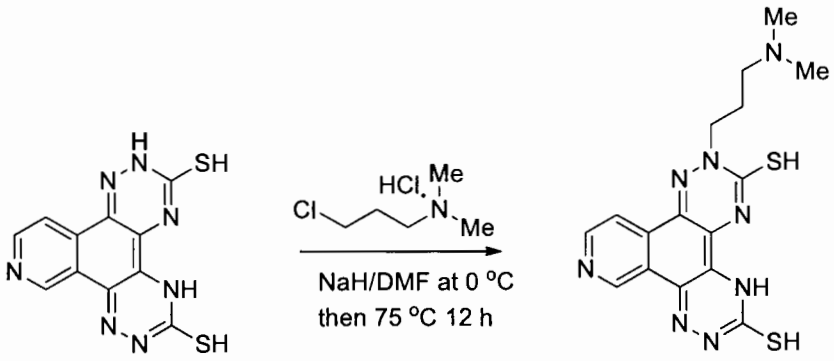

19 **20b**

The mixture of NaH (0.0435 g, 1.08 mmol), compound **19** (0.1093 g, 0.36 mmol) and 2-chloro-*N*,*N*-dimethyl propylamine hydrochloride (0.0593 g, 0.55 mmol) in DMF 10 (mL) was refluxed at 75 °C for 16 h under nitrogen atmosphere. The crude reaction of **20b** was purified by column chromatography (silica gel) eluting with gradient EtOAc to EtOAc/MeOH; 7:3 (v/v) to give product **20b** (0.0304 g, 22 %), m.p. > 250 °C as orange solid

^{1}H-NMR (300 MHz, $CDCl_3$): δ = 10.03 (s, 1H, H-1), 8.98 (d, J = 6.6 Hz, 1H, H-2), 8.22 (d, J = 6.6 Hz, 1H, H-3), 4.79 (brs, 2H, H-1′), 2.49 (s, 2H, H-3′), 1.78 (s, 6H, H-4′), 1.25 (s, 2H, H-2′) ppm.

^{13}C-NMR (75 MHz, $CDCl_3$): δ = 163.0, 143.0, 140.0, 135.0, 133.0, 126.0, 123.0, 60.0, 54.0, 44.0, 31.0 ppm.

IR (Neat): ν_{max} = 3392 (br m), 2923 (s), 2852 (s), 1730 (w), 1574 (s), 1504 (w), 1492 (w), 1459 (m), 1431 (m), 1376 (w), 1296 (w), 1252 (m), 1199 (w), 1160 (w), 923 (w) cm^{-1}.

MS-EI m/z calcd for $C_{15}H_{14}N_8S_2^+$ (M^+-CH_4) 370.0777; found: 369.3379.

3.3.3.2 The synthesis of compound **20c**

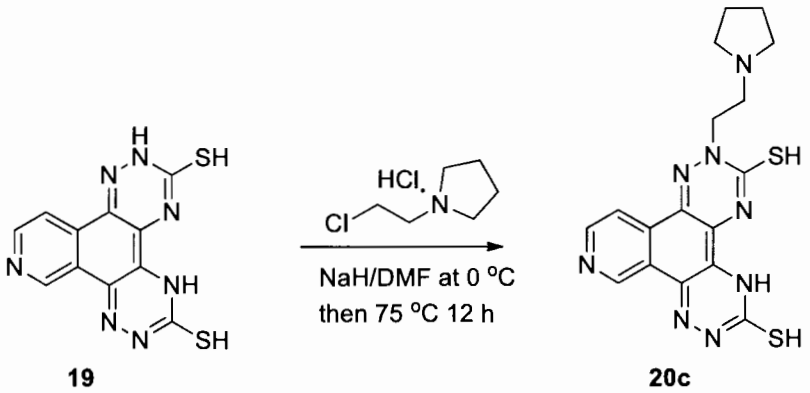

19 **20c**

The mixture of NaH (0.0362 g, 1.50 mmol), compound **19** (0.1048 g, 0.34 mmol) and 1-(2-chloroethyl)pyrrolidine hydrochloride (0.0887 g, 0.52 mmol) in DMF 10 (mL) was refluxed at 75 °C for 8 h under nitrogen atmosphere. The crude reaction of **20c** was purified by column chromatography (silica gel) eluting with gradient EtOAc to EtOAc/MeOH; 7:3 (v/v) to give product **20c** (0.0649 g, 42 %), m.p. > 250 °C as orange solid.

^{1}H-NMR (300 MHz, $CDCl_3$): δ = 9.90 (s, 1H, H-1), 8.91 (d, J = 5.4 Hz, 1H, H-3), 8.25 (d, J = 5.7 Hz, 1H, H-4), 4.44 (s, 2H, H-1′), 2.95 (s, 4H, H-4′), 2.60 (s, 2H, H-2′), 1.24 (s, 4H, H-5′) ppm.

^{13}C-NMR (75 MHz, $CDCl_3$): δ = 166.0, 154.0, 147.0, 140.0, 135.0, 133.0, 128.0, 124.0, 120.0, 114.0, 110.0, 60.0, 56.0, 54.0, 24.0 ppm.

IR (Neat): ν_{max} = 3358 (br w), 3066 (w), 2921 (m), 2851 (m), 2491 (br w), 1925 (w), 1734 (w), 1635 (m), 1609 (m), 1579 (m), 1454 (m), 1221 (s), 1221 (s), 1040 (m), 813 (m), 655 (s) cm^{-1}.

MS-EI m/z calcd for $C_{34}H_{36}KN_{16}S_4^+$ ($2M^+$-K) 835.1823; found: 833.7356.

Table 3.2 NMR data ($CDCl_3$) for alkylated product 20c (^1H 300 MHz, ^{13}C 75 MHz)

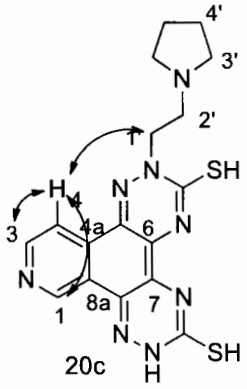

position	Compound 20c		
	δ_C, type	δ_H (J in Hz)	HMBC
1	147.0, CH	9.90, s	8a
2			
3	120.0, CH	8.91, d (5.4)	4, 6, 7, 4a
4	135.0, CH	3.25, d (5.7)	1, 3, 1′
4a	124.0, C		
5	166.0, C		
6	140.0, C		3
7	140.0, C		3
8	166.0, C		
8a	133.0, C		
1′	60.0, CH_2	4.44, s	4,
2′	56.0, CH_2	2.95, s	3′, 4′
3′	54.0, CH_2	2.60, s	2′, 4′
4′	24.0, CH_2	1.24, s	2′, 3′

3.3.3.2 The synthesis of compound **20d**

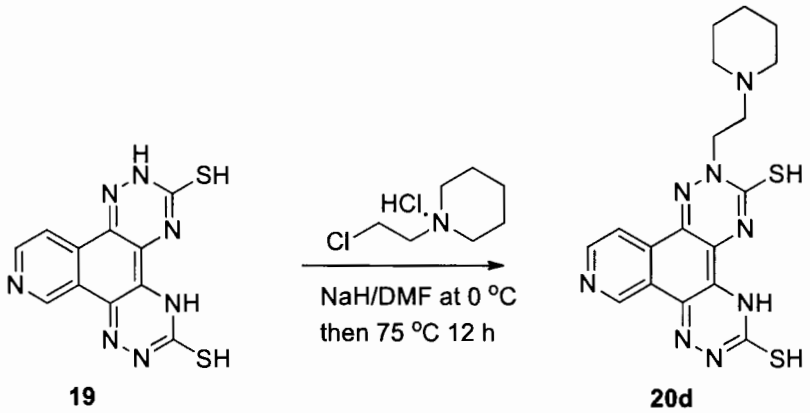

The mixture of NaH (0.0405 g, 1.68 mmol), compound **19** (0.1172 g, 0.39 mmol) 1-(2-chloroethyl)piperidine hydrochloride (0.1074 g, 0.58 mmol) in DMF 10 (mL) was refluxed at 75 °C for 8 h under nitrogen atmosphere. The crude reaction of **20d** was purified by column chromatography (silica gel) eluting with gradient EtOAc to EtOAc/MeOH; 7:3 (v/v) to give product **20d** (0.0428 g, 27 %) m.p. > 250 °C as orange solid.

^{1}H-NMR (300 MHz, $CDCl_3$): δ = 9.90 (s, 1H, H-1), 8.91 (d, *J* = 5.4 Hz, 1H, H-3), 8.25 (d, *J* = 5.7 Hz, 1H, H-4), 4.60-4.9 (m, *J* = 6.6, 2H, 1′), 2.40-2.65 (m, *J* =4.8, 2H, 4′), 2.25-2.40 (m, *J* = 6.6, 2H, 2′), 1.50-1.75 (m, 2H, 5′), 1.35-1.50 (m, 2H, 6′) ppm.

IR (Neat): ν_{max} = 2978 (w), 2927 (w), 2601 (m), 2530 (w), 2496 (m), 1731 (w), 1574 (w), 1474 (s), 1443 (s), 1397 (s), 1383 (m), 1364 (w), 1171 (s), 1072 (w), 1035 (s), 851 (w), 807 (m) cm^{-1}.

MS-EI m/z calcd for $C_{18}H_{19}KN_8S_2^+$ (M^++3H) 415.1487; found: 415.2375.

3.3.4 Synthesis of cyclized (*E*)-2-(3-mercapto-[1,2,4]triazino[5,6-*h*]isoquinolin-6(2*H*)-ylidene)hydrazinecarbothioamide (21)

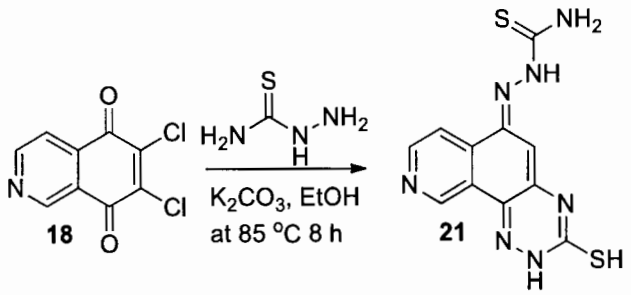

The mixture of compound **18** (0.2034 g, 0.89 mmol), thiosemicarbazide (0.0976 g, 1.07 mmol) and potassium carbonate (0.1479 g, 1.07 mmol) was dissolved in EtOH. The reaction mixture was refluxed at 85 °C for 8 h under nitrogen atmosphere. The crude reaction **21** was removed solvent by rotary evaporator. The crude reaction of **21** was purified by column chromatography (silica gel) eluting with gradient EtOAc to EtOAc/MeOH; 8:2 (v/v) to give product **21** (0.1284 g, 47 %), m.p. > 250 °C as dark brown solid.

^{1}H-NMR (300 MHz, DMSO-D$_6$): δ = 9.97 (s, 1H, H-1), 9.51 (s, 1H, H-7), 8.76 (d, J = 5.1 Hz, 1H, H-3), 8.23 (d, J = 5.7 Hz, 1H, H-4) ppm.

^{13}C-NMR (75 MHz, DMSO-D$_6$): δ = 166.0 (C=N), 165.0 (C-6), 158.0 (C-SH), 157.5 (C-1),155.0 (C-3), 147.0 (C-7), 143.0 (C-8a), 133.5 (C-4a), , 127.0 (C-4) ppm.

IR (Neat): ν_{max} = 3358 (br w), 3066 (w), 2921 (m), 2851 (m), 1734 (w), 1635 (m), 1690 (m), 1579 (s), 1454 (s), 1221 (s), 987 (w), 930 (w), 831 (m), 813 (m), 779 (m) cm^{-1}.

MS-EI m/z calcd for $C_{11}H_{12}N_7S_2$ (M^++Na) 326.0259; found: 327.1894.

3.3.5 The synthesis of mono-substituted azanaphthoquinone annelated thiazole derivatives of the cyclized product under basic conditions

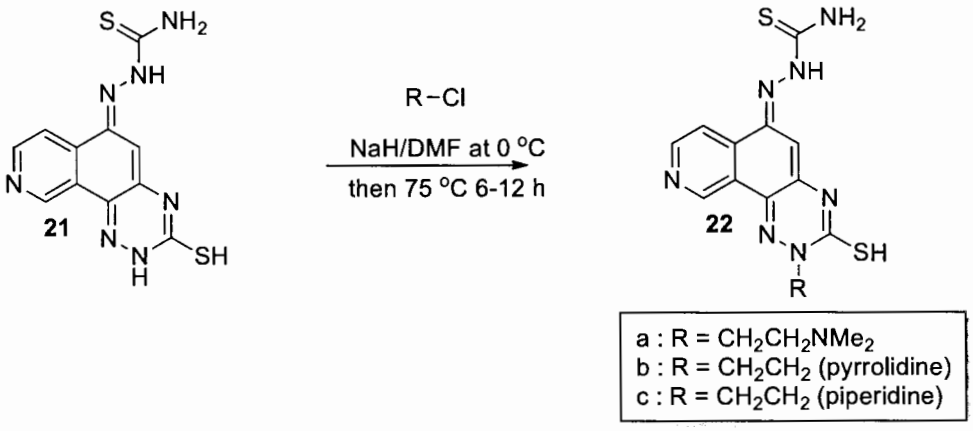

General procedure

60% NaH (2.6 equiv.) was dissolved in DMF and cooled at 0 °C. Then compound **21** (1 equiv.) in DMF was added dropwise and stirred for 30 min under nitrogen atmosphere. The side chain (1.5 equiv.) in DMF was added to the mixture and refluxed at 75 °C for 8 h. After that, water was added to quench the reaction. The solvent was removed by using rotary evaporator. The crude product was purified by column chromatography to give alkylated product.

3.3.5.1 The synthesis of compound **22a**

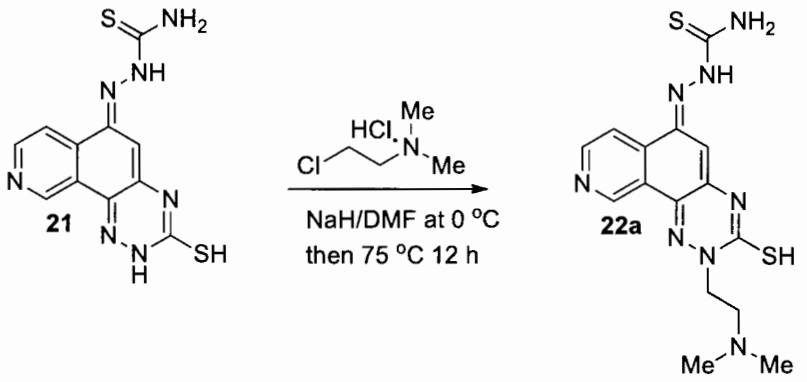

The mixture of NaH (0.0313 g, 1.30 mmol), compound **21** (0.0912 g, 0.30 mmol) and 2-chloro-*N,N*-dimethyl ethylamine hydrochloride (0.0649 g, 0.45 mmol) in DMF 10 (mL) was refluxed at 75 °C for 8 h under nitrogen atmosphere. The crude reaction of **22a** was purified by column chromatography (silica gel) eluting with gradient EtOAc to EtOAc/MeOH; 7:3 (v/v) to give product **22a** (0.0527 g, 46 %), m.p. > 250 °C as orange solid.

^{1}H-NMR (300 MHz, $CDCl_3$): δ = 9.48 (s, 1H, H-1), 8.74 (d, J = 5.7 Hz, 1H, H-3), 8.58 (s, 1H, H-7), 7.98 (d, J = 5.7 Hz, 1H, H-4), 4.43 (s, 2H, H-1′), 2.61 (s, 2H, H-2′), 2.27 (s, 6H, H-3′) ppm.

^{13}C-NMR (75 MHz, $CDCl_3$): δ = 155.0, 149.0, 142.0, 133.0, 125.0, 59.2, 45.0, 29.6 ppm.

IR (Neat): ν_{max} = 2978 (m), 2927 (m), 2601 (s), 2496 (s), 1574 (w), 1474 (s), 1443 (s), 1397 (s), 1383 (m), 1171 (s), 1072 (w), 1035 (s), 851 (w), 807 (m) cm^{-1}.

MS-EI m/z calcd for $C_{15}H_{21}N_8S_2$ (M^++3H) 377.1331; found: 377.1805.

3.3.5.2 The synthesis of compound **22b**

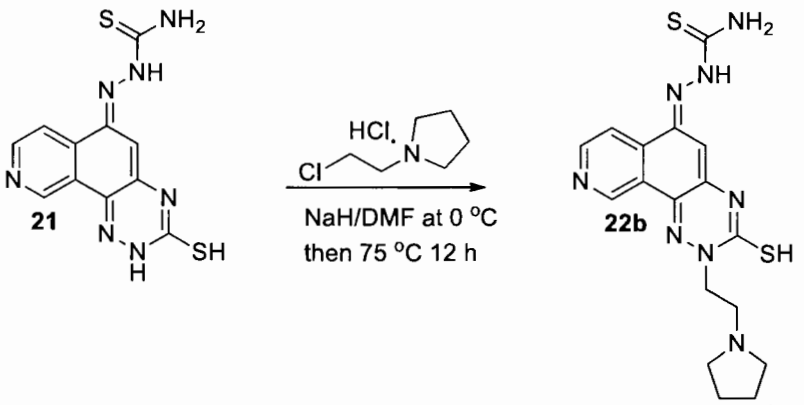

The mixture of NaH (0.0403 g, 1.68 mmol), compound **21** (0.1176 g, 0.38 mmol) and 1-(2-chloroethyl)pyrrolidine hydrochloride (0.0403 g, 1.68 mmol) in DMF 10 (mL) was refluxed at 75 °C for 16 h under nitrogen atmosphere. The crude reaction of **22b** was purified by column chromatography (silica gel) eluting with gradient EtOAc to EtOAc/MeOH; 7:3 (v/v) to give product **22b** (0.0728 g, 47 %), m.p. > 250 °C as orange solid

^{1}H-NMR (300 MHz, $CDCl_3$): δ = 9.65 (s, 1H, H-1), 8.90 (d, J = 5.1 Hz, 1H, H-3), 8.65 (s, 1H, H-7), 7.90 (d, J = 5.7 Hz, 1H, H-4), 4.75 (s, 2H, H-1′), 3.00 (s, 6H, H-2′), 2.50 (s, 4H, H-4′) 1.24 (s, 4H, H-5′) ppm.

^{13}C-NMR (75 MHz, $CDCl_3$): δ = 154, 150, 149, 146, 144, 132, 129, 123, 116, 73, 59, 28, 26 ppm.

IR (Neat): ν_{max} = 2978 (m), 2925 (m), 2601 (m), 2496 (m), 1680 (w), 1577 (m), 1531 (s), 1474 (s), 1443 (s), 1396 (s), 1287 (w), 1171 (s), 1072 (w), 1035 (s), 850 (w), 806 (w) cm^{-1}.

MS-EI m/z calcd for $C_{17}H_{24}N_9S_2$ (M^++NH_4^+) 418.1596; found: 418.3008.

3.3.5.3 The synthesis of compound **22c**

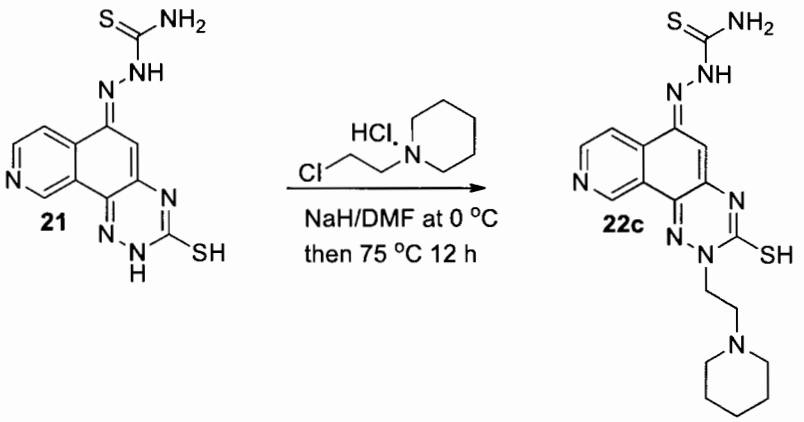

The mixture of NaH (0.0364 g, 1.52 mmol), compound **21** (0.1068 g, 0.35 mmol) and 1-(2-chloroethyl)piperidine hydrochloride (0.0968 g, 0.52 mmol) in DMF 10 (mL) was refluxed at 75 °C for 8 h under nitrogen atmosphere. The crude reaction of **22c** was purified by column chromatography (silica gel) eluting with gradient EtOAc to EtOAc/MeOH; 7:3 (v/v) to give product **22c** (0.0867 g, 59 %), m.p. > 250 °C as orange solid.

^{1}H-NMR (300 MHz, $CDCl_3$): δ = 10.13 (s, 1H, H-1), 9.16 (s, 1H, H-6), 8.75 (d, J = 5.7 Hz, 1H, H-3), 8.20 (d, J = 5.7 Hz, 1H, H-4), 4.34 (t, J = 5.1 Hz, 2H, H-1′), 2.93 (t, J = 5.1 Hz, 2H, H-2′), 2.55 (s, 4H, H-3′), 1.63 (d, J = 4.8 Hz, 4H, H-4′) 1.47 (s, 2H, H-6′) ppm.

^{13}C-NMR (75 MHz, $CDCl_3$): δ = 188.0, 155.0, 149.0, 145.0, 132.0, 123.0, 72.0, 59.0, 55.0, 27.0, 25.0 ppm.

IR (Neat): ν_{max} = 3179 (w), 2163 (br w), 1583 (s), 1542 (s), 1497 (s), 1401 (s), 1309 (s), 1229 (s), 1105 (s), 959 (w), 912 (w), 838 (w), 804 (w), 786 (s), 747 (s), 712 (m) cm^{-1}.

MS-EI m/z of core struture calcd for $C_{10}H_7N_5S^+$ (M^++H) 229.0417; found: 229.2039. m/z of side chain calcd for $C_8H_{19}N_4S$ (M^++H) 203.1330; found: 203.0201.

Table 3.3 NMR data ($CDCl_3$) for alkylated product 22c (^1H 300 MHz, ^{13}C 75 MHz)

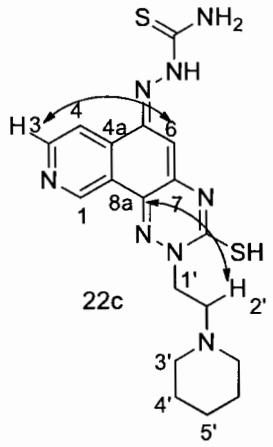

position	Compound 22c		
	δ_C, type	δ_H (J in Hz)	HMBC
1	149.0, CH	10.13, s	3, 6, 8a, 4a
2			
3	145.0, CH	8.74, d (5.7)	1, 4, 6, 8a
4	115.0, CH	8.20, d (5.8)	
4a	123.0, C		
5	188.0, C		
6	155.0, CH	9.16, s	3, 8a
7			1, 4a
8	188.0, C		
8a	132.0, C		2′
1′	72.0, CH_2	4.34, t (5.1)	2′
2′	59.0, CH_2	2.93, t (5.1)	1′
3′	55.0, CH_2	2.55, s	2′, 4′
4′	27.o, CH_2	1.63, s	3′, 4′, 5′
5′	25.0, CH_2	1.47, s	2′, 4′

3.4 Antiproliferative assay

3.4.1 Cell culture and sub-culture cell line

The HT-29 cells and L929 cells were maintained in McCoy's 5A complete growth medium (CGM) supplemented with 10 % fetal bovine serum (FBS) and 1 % antibiotics (penicillin/streptomycin). HT-29 cells and L929 cells were grown in a humidified incubator under an atmosphere of 95 % air and 5 % CO_2 at 37 °C to sub-confluence (90 - 95 %). The culture medium was replaced every 48 h.

3.4.2 Cell treatment

Once the cells reached 90 – 95 % confluency, the medium was aspirated, and the cell monolayer was washed three times with sterile phosphate buffered saline. The cell monolayer was treated with 1 mL of 0.25 % (w/v) trypsin-EDTA and

incubated briefly at 37 °C and visualized microscopically to ensure complete cell detachment. Cells were re-suspended in McCoy's 5A complete growth medium. Cells were also stained with trypan blue (100 µM of cell suspension and 100 µM of 0.4 % trypan blue), incubated for 2 minutes at room temperature, and counted using a hemacytometer. The cells were seeded at a density of 1.5 × 104 cells/well in 96-well microtiter tissue culture plates prior to arsenic trioxide treatment. HT-29 cells and L929 cells were seeded in 96-well plates with 1.5 × 104 cells/well and placed at 37 °C in a 5 % CO_2 humidified incubator until 60 % confluency. The CGM was removed and the cells were serum-starved for 24 h prior to treatment. Cells incubated in culture medium alone served as a control for cell viability (untreated cells).

3.5 Computational design of target molecules

3.5.1 Computational details

3D-QSAR is application in computer-aided drug design or Ligand-Based Drug Design method. It use information of drug in designing of the novel drug in order to increase efficient new drug. In this study, the GaussView 3.07 program was fully optimized using the quantum chemical method 249 (HF/6-31G*) implement in the Gaussian 09 program in the study 2D-QSAR (Conventional and HQSAR) and 3D-QSAR (CoMSIA). HQSAR and 3D-QSAR were performed using Sybyl 8.0.

3.5.2 Data set and biological activity

Structures and biological activities of azanaphthoquinone pyrrolo-annelated derivative were taken from literature [7-8,43-45, 48-49] as shown in Table A.1 and general structure is shown in Figure 3.1. The biological activities of these compounds were used the half maximal inhibitory concentration (IC_{50}) and converted to $\log(1/IC_{50})$ for simple to linear relationship and reducing the long range of biological data.

3.5.3 2D and 3D-QSAR technique

2D-QSAR was using HQSAR (Hologram Quantitative Structure Relationship) and 3D-QSAR was using CoMSIA (Comparative Molecular Similarity Indices Analysis) and performed by Sybyl 8.0. Molecular alignment was used pharmacophore alignment GALAHAD (genetic algorithm with a linear assignment for the hypermolecular alignment of datasets module).

There used to be explained the relationship between the structures and the biological activities of azanaphthoquinone annelated pyrrole derivatives. The descriptors of HQSAR, including atom (At), bond (B), connections (C), chiral (Ch) hydrogen atom (H) and donor and acceptor (DA) fields were calculated. Five CoMSIA similarity index descriptors including steric (S), electrostatic (E), hydrophobic (H), hydrogen donor (D) and hydrogen acceptor (A). Fields were derived with the grid spacing of 2 Å. The statistical method partial least square (PLS) analysis was performed the relationship between molecular descriptors and activities. The cross-validation was performed using the leave-one-out method with a 2.0 kcal/mol column filter to minimize the influence of noisy columns. A final non cross-validated analysis with the optimal number of components was sequentially performed and was then employed to analyze the results. The predictive ability of CoMSIA models used evaluate by r^2 and q^2 values.

3.6 Molecular docking calculations

3.6.1 Computational details

Molecular Docking Calculations is application in computer-aided drug design or Structure-Based Drug Design method. It uses information of drug and receptor in calculation binding energy of drug and receptor. In this study, the GaussView 3.07 program was fully optimized using the quantum chemical method 249 (HF/6-31G*) implement in the Gaussian 09 program. In the study Molecular Docking Calculations were performed using AutoDockTools-1.5.6 and Discovery Studio 25.

3.6.2 DNA binding mode

3.5.2.1 Hydrogen bonding interactions

Hydrogen atom (H) and high electronegativity atom such as sulfur (S), nitrogen (N) and oxygen (O) could form bonds distance not more than 2.5 Å.

3.3.8.2 van der Waals interactions

Sum of van der Waals radius between both atoms were investigated. These interactions will be discussed in the section of results and discussion.

3.6.3 Data set of molecular docking calculations

Structures of azanaphthoquinone annelated thiazole derivatives were synthesized and evaluated with cancer cell and normal cell used to ligand in Molecular Docking Calculations as shown in Figure 3.1. The biological activities of these compounds were used the half maximal inhibitory concentration (IC_{50}) and converted to binding energy of experimental. Compound **69** was obtained from the previous work by condensation of 6,7-dichloroisoquinoline-5,8-dione (**18**) with thiourea and was used as comparative compound.

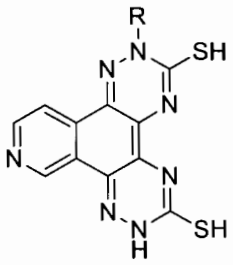

19: R = H

20a: R = $CH_2CH_2NMe_2$

20b: R = $CH_2CH_2CH_2NMe_2$

20c: R = CH_2CH_2(pyrrolidine)

20d: R = CH_2CH_2(piperidine)

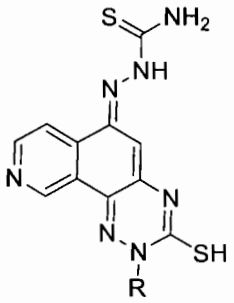

21: R = H

22a: R = $CH_2CH_2NMe_2$

22b: R = CH_2CH_2(pyrrolidine)

22c: R = CH_2CH_2(piperidine)

22d: R = $CH_2CH_2CH_2NMe_2$

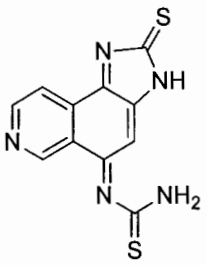

69

Figure 3.1 Structures of azanaphthoquinone thiazole derivatives

3.6.4 Scoring function

The scoring function takes a pose as input and returns a number indicated the possibility that the pose represents a favorable binding interaction. Most scoring functions are physics based molecular mechanics force fields that estimate the energy of the pose. A low energy indicates a stable system and thus a likely binding interaction.

Scoring function in AutoDock

$$\Delta G_{binding} = \Delta G_{vdW} + \Delta G_{H-bond} + \Delta G_{elec} + \Delta G_{desolv} + \Delta G_{tor} \quad (3.1)$$

Molecular Mechanics Terms

Van der Waals $\Delta G_{vdW} = W_{vdW} \sum_{i,j}\left(A_{ij}/r_{ij}^{12} - B_{ij}/r_{ij}^{6}\right)$

Hydrogen bonding $\Delta G_{H-bond} = W_{H-bond} \sum_{i,j} E(t)\left((C_{ij}/r_{ij}^{12} - D_{ij}/r_{ij}^{10}) + E_{H-bond}\right)$

Electrostatics $\Delta G_{elec} = W_{elec} \sum_{i,j}\left(q_i q_j\right) / \left(\varepsilon(r_{ij}) r_{ij}\right)$

Desolvation $\Delta G_{desolv} = W_{desolv} \sum_{i(C),j} \left(S_i V_j exp\left(-r_{ij}^2/2\sigma^2\right)\right)$

Change in torsional free energy when the ligand goes from unbound to radius

Torsional $\Delta G_{tor} = W_{tor} N_{tor}$

CHAPTER 4
RESULTS AND DISCUSSION

4.1 Design of target molecules

4.1.1 CoMSIA and HQSAR models

The results of HQSAR and CoMSIA model showed high correlation and predictive ability base on good statistical parameters as shown in Table 4.1. The best fields of CoMSIA model were included the steric, electrostatic, hydrophobic and H-bond acceptor. The cross-validated correlation coefficient (q^2) was 0.61 and non-cross-validated correlation coefficient (r^2) was 0.99. The contribution of steric, electrostatic, hydrophobic and hydrogen acceptor fields was 18.5%, 27.7%, 31.5% and 22.3%, respectively. The results showed that, the electrostatic and hydrophobic fields have more influence on the activity of azanaphthoquinone pyrrolo-annelated derivative. The best HQSAR model was generated based on the combination of the different fragment types, atom (At), chiral (Ch), connections (C) and bond (B) showing with the q^2 value of 0.62 and with the r^2 value of 0.86.

Table 4.1 Summary of statistical results of CoMSIA and HQSAR models

Models	**Descriptors**	**Statistical parameters**						**Fraction**
		q^2	**r^2**	**N**	**S**	**SEE**	**F**	
CoMSIA	S/E/H/A	0.61	0.99	6	0.84	0.11	585.3	18.5/27.7/31.5/22.3
Models	**Descriptors**	**q^2**	**r^2**	**N**	**S**	**SEE**		**Bond length**
HQSAR	At/Ch/C/B	0.62	0.86	4	0.80	0.49	353	

q^2: Cross-validated correlation coefficient; r^2: Non-cross-validated correlation coefficient; N: Optimal number of components; s: standard error of prediction; SEE: standard error of estimate; F: F-test

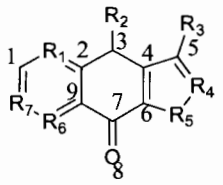

Figure 4.1 General structure of azanaphthoquinone pyrrolo annelated derivative

The data set has 37 compounds are shown in Table A.1 with activity range from 2.26 to 8.10 in log(1/IC_{50}) units and the compound **14** show a high activity value. For evaluate the predictive ability of this CoMSIA model, the activities of the test set compounds were predicted such as compound **81**, **84**, **87** and **108**. The relationship between experimental and predicted activities (log(1/IC_{50}) of CoMSIA and HQSAR for the training set and test set are reported in Figure 4.2. Found that, the best model of HQSAR was not 253 closed to the experimental biological activities. It showed low correlation of the experimental and predicted biological activities. But the CoMSIA indicated linearity of the plot between the experimental biological and predicted biological activities. It has high predictive ability more than HQSAR models to predict the biological activity of azanaphthoquinone annelated pyrrole derivatives.

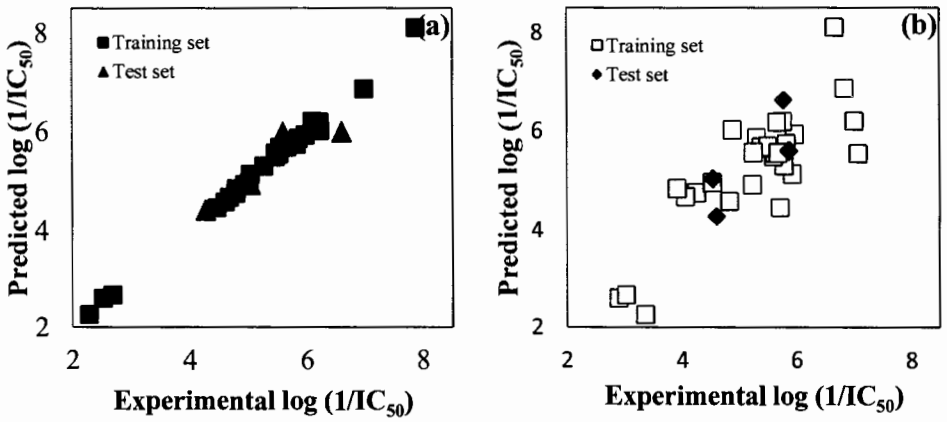

Figure 4.2 Plots between the experimental biological and predicted biological activities from the best CoMSIA (a) and HQSAR (b) models, respectively

4.1.2 CoMSIA contour maps

In the CoMSIA contour maps as shown in Figures 4.3, it had the influence of steric, electrostatic, hydrophobic and hydrogen acceptor fields to the activity of azanaphthoquinone annelated pyrrole derivatives. Favorable and unfavorable steric regions are represented in green and yellow contours, respectively. The electropositive and electronegative regions showed in blue and red contours, respectively. The magenta and white contours implied the favorable and unfavorable hydrophobic regions. The cyan and orange contours indicated regions that favor the hydrogen donor group and unfavor hydrogen donor group, respectively.

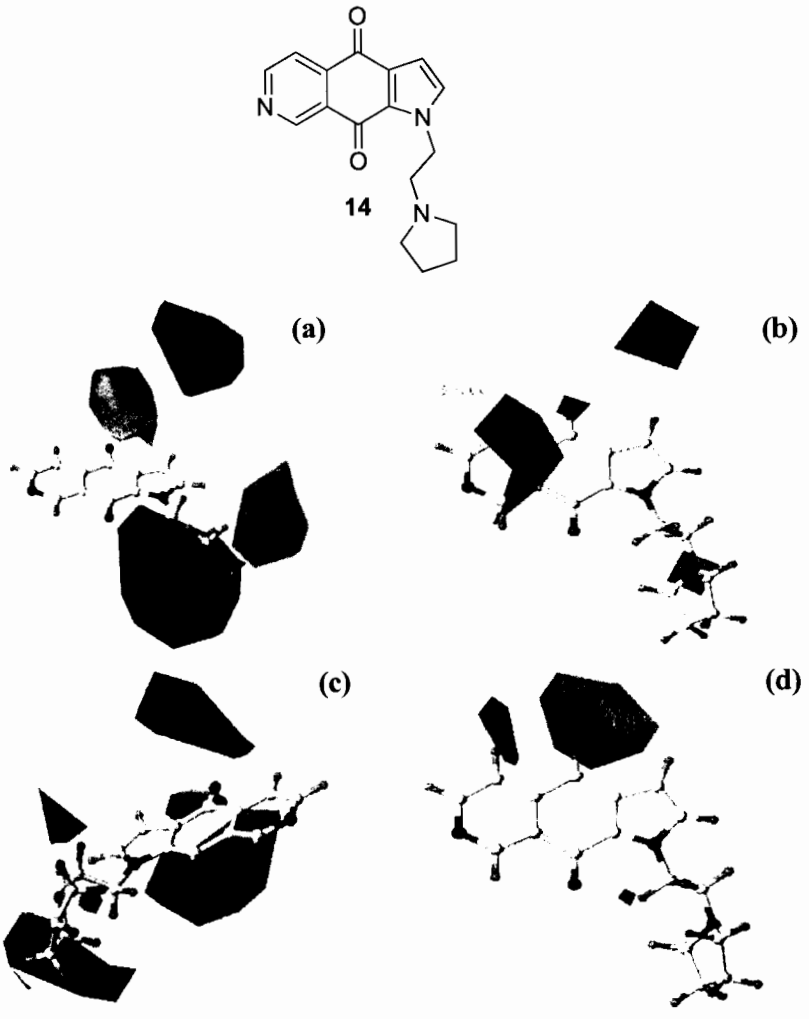

Figure 4.3 Steric (a), Electrostatic (b), Hydrophobic (c) and Hydrogen bond acceptor (d) CoMSIA contours in combination with compound 14

In the R1 Position found blue, a few orange and near yellow contour refering to the small substituent, unfavor hydrogen donor and electropositive atom. The R1 position should be S and N atom. The S and N atoms on the aromatic ring will be less hydrogen, small substituent and positive charge. The orange contour suggested that compound **93** bearing a nitrogen atom at the R1 position exhibit lower potency than compound **86**. The R2 position was a large yellow and cyan, contour overlapping with a blue contour, which suggested to be oxygen of carbonyl group. This result indicated the struture of compound **14**. For that reason, the oxygen carbonyl may be the best substituent in R2 position. R3, R4 and R6 position did not show contour. R5 position showed a large green and magent contours. The contour inserted was red contour. These corresponded to the substituent of compound **14** in R5 position. The red contour showed electronegative atom. It confirmed pyrrolidine group of compound **14** for the best substituent. Which had bulky and lipophilic substituents.

4.1.3 HQSAR contributions

HQSAR showed organge to red contribution represented to negative atom, white contribution represented to neutral atom and yellow to green contribution represented to positive atom. The results of HQSAR pointed to the positive contribution in R1 and R7 position, the carbon near R2 and R3 position, and the substituent at R5 position. HQSAR model corresponded to a substituent of high activity compounds. It can confirm CoMSIA another method.

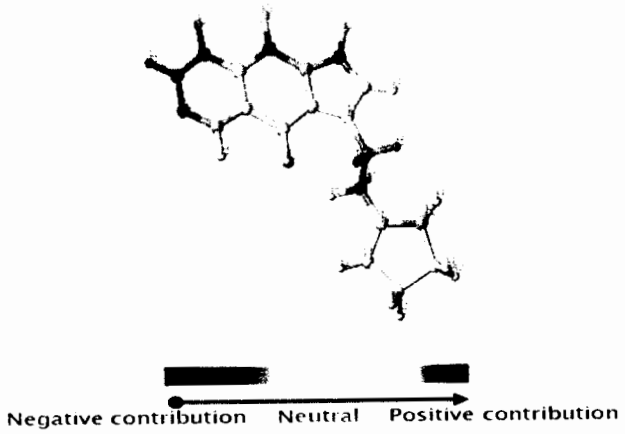

Figure 4.4 The HQSAR contribution map of azanaphthoquinone pyrrolo annelated derivatives compound 14

4.2 Synthesis and characterize

4.2.1 Synthesis of 6,7-dichloroisoquinoline-5,8-dione (18)

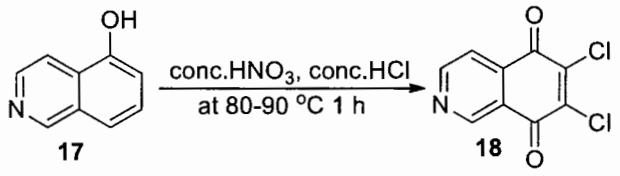

17 18

6,7-dichloroisoquinoline-5,8-dione (**18**) was successfully synthesized by oxidation reaction of 5-hydroxyisoquinoline (**17**). The oxidizing agents were using concentration nitric acid and concentration hydrochloric acid at 80-90 °C for 1 h to obtained 6,7-dichloroisoquinoline-5,8-dione (**18**) in moderate yield (25%) as yellow solid. The strong conditions reaction lead to low yield product without recovered starting material.

The mechanism of oxidation reaction of 6,7-dichloroisoquinoline-5,8-dione (**18**) is shown in Figure 4.5. Initially, the electron of nitric acid reacted with hydrochloric acid to generate nitronium intermediate **A**. The lone pair electrons oxygen of 5-hydroxyisoquinoline attacked nitronium intermediate **A** to give intermediate **B**. The lone pair electrons on oxygen of water abstract proton of intermediate **B** to give the intermediate **C**. The lone pair electrons of nitrogen in intermediate **C** delocalized electron to nitrate moiety to obtain carbonyl moiety of intermediate **D** and gas nitrous was eliminated. The intermediate **D** was unstable molecule then leaded to rearomatization to nitrogen cation to give pyridine ring (intermediate **F**). The lone pair electrons on oxygen of water attacked cation of intermediate **F** to give intermediate **G**. The lone pair electrons of oxygen from water abstracted proton of intermediate **G** to obtain intermediate **H**. The oxidation of the hydroxyl group was occurred repeatly under same mechanism as mentioned above. The chloride ion from hydrochloric acid attacked to intermediate **K** and delocalized electron to carbonyl moiety to give intermediate **L**. The intermediate **L** is unstable molecule then the molecule delocalized electron or annulated to quinone system to obtain intermediate **M**. The substation was occurred at carbon 6 with the same repeated mechanism to obtain 6,7-dichloroisoquinoline-5,8-dione (**18**).

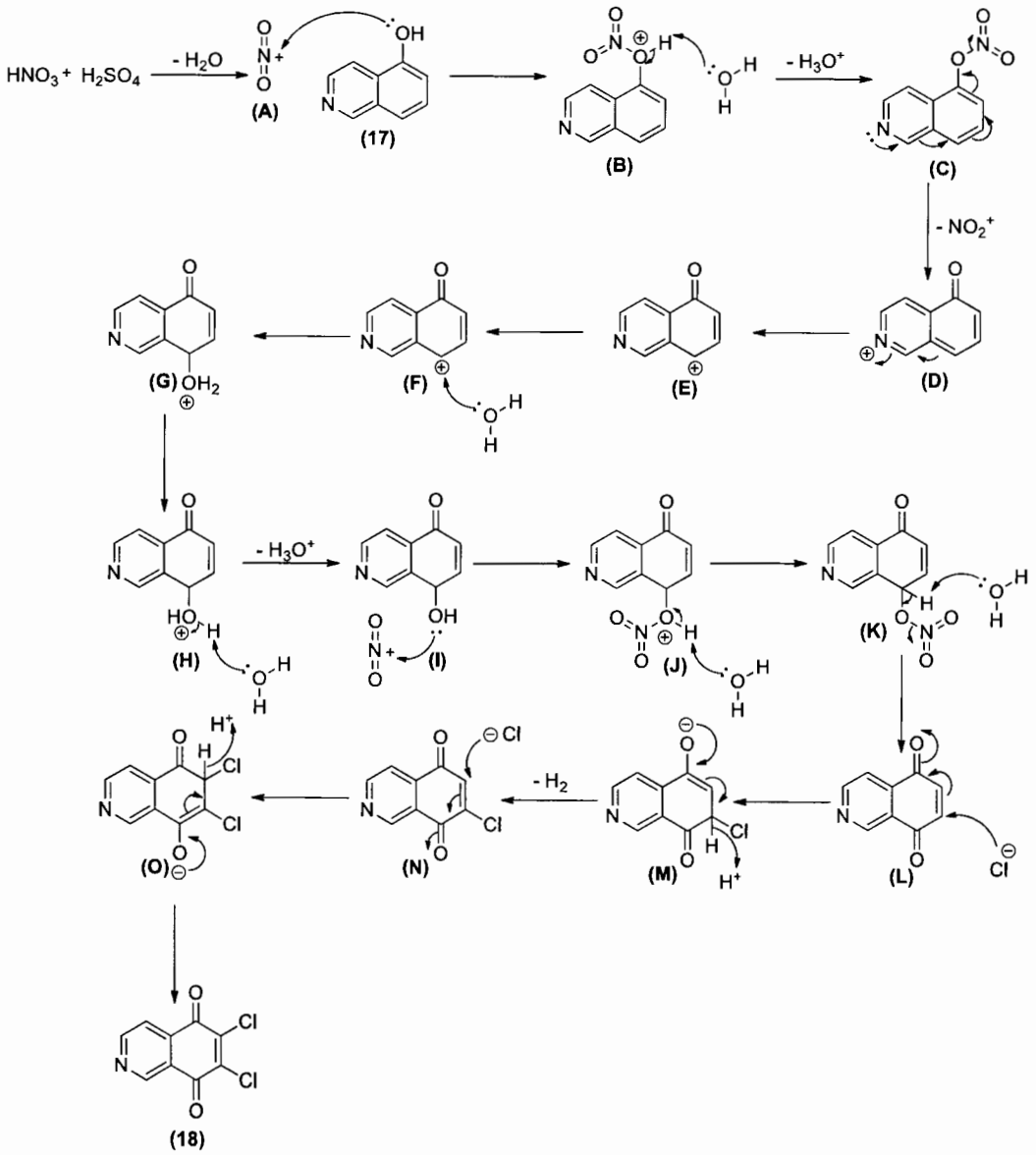

Figure 4.5 The proposed mechanism of the oxidation reaction

^{1}H-NMR spectrum of 6,7-dichloroisoquinoline-5,8-dione (**18**) is showed in Figure 4.6. 5-hydroxyisoquinoline (**17**) are shown six signals of aromatic proton after oxidation reaction the ^{1}H-NMR spectrum showed three signals of aromatic pyridine proton of 6,7-dichloroisoquinoline-5,8-dione (**18**) at 9.42 (H-1), 9.12 (H-3), 7.97 (H-4) ppm, respectively. The proton position 3 and 4 are coupling constant 4.8 Hz indicating proton 3 and 4 near position. Structure of compound **18** can be preliminary confirmed by ^{1}H-NMR

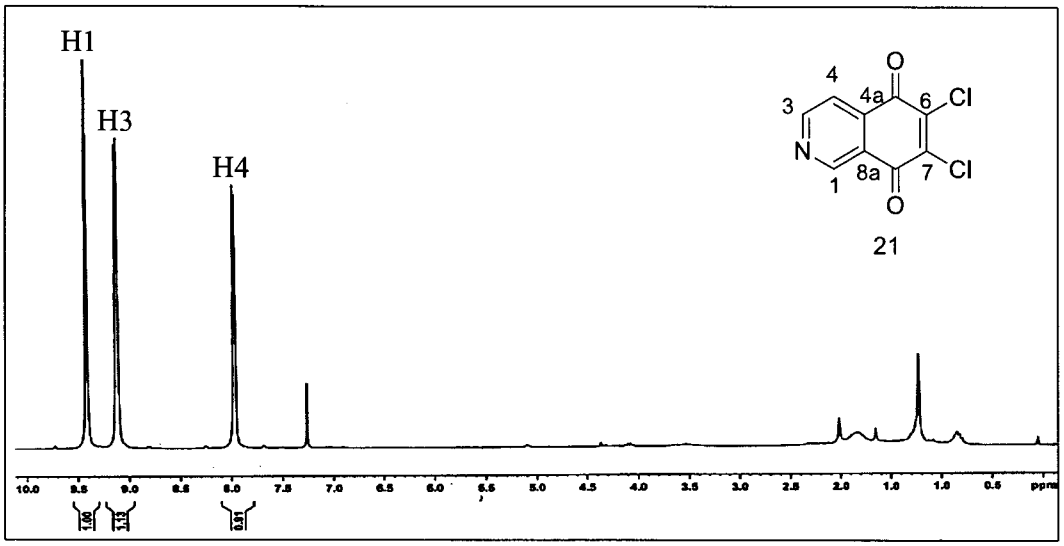

Figure 4.6 ^{1}H-NMR spectrum of 6,7-dichloroisoquinoline-5,8-dione (18) in $CDCl_3$

^{13}C-NMR spectrum of 6,7-dichloroisoquinoline-5,8-dione (**18**) as shown in Figure 4.7 giving nine aromatic carbon of core isoquinoline. The signal of two carbonyl moiety showed at 175.5 and 175.3 ppm. The main carbon C-Cl moiety showed signal at chemical shift 144.0 and 143.5 ppm. There the methine carbon the carbon including C1, C3 and C4 were toward at chemical shift 149.5, 156.0 and 119.5 ppm, respectively. The quaternary carbon 4a and 8a were found that 136.0 and 124.0 ppm, respectively. Structure of 6,7-dichloroisoquinoline-5,8-dione (**18**) can be confirmed by ^{13}C-NMR data.

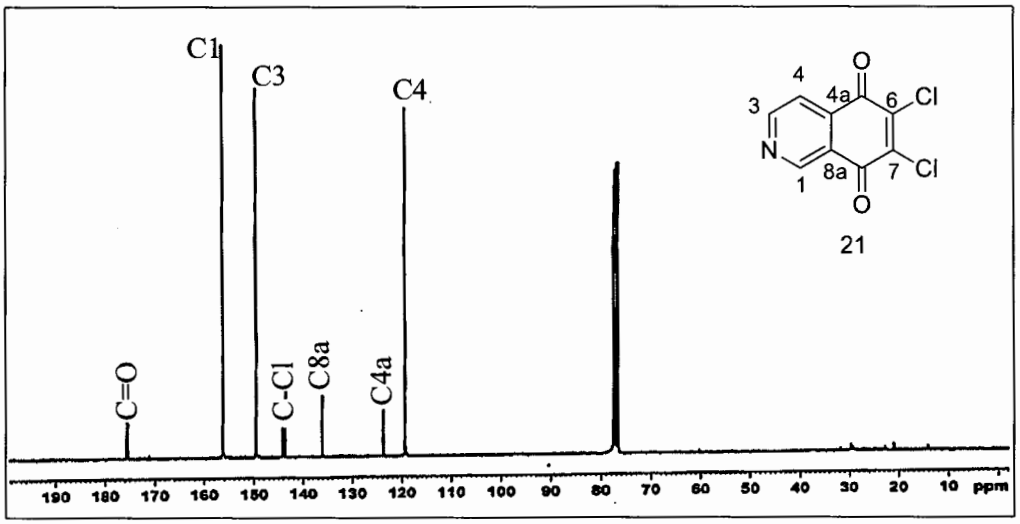

Figure 4.7 ^{13}C-NMR spectrum of 6,7-dichloroisoquinoline-5,8-dione (**18**) in $CDCl_3$

IR spectrum found that important vibrational mode four peak including functional medium signal of C-H stretching wavenumber at 2922 cm^{-1}, strong signal of C=O stretching wavenumber at 1676 cm^{-1}, medium to weak signal of C-N stretching wavenumber at 1224 cm^{-1} and strong signal of C-Cl stretching wavenumber at 670 cm^{-1}. IR spectrum can confirm main functional group of 6,7-dichloroisoquinoline-5,8-dione (**18**). IR spectrum is shown in Figure B.3. Mass spectrum are showing in Figure B.4, 6,7-dichloroisoquinoline-5,8-dione (**18**) very stable molecular.

Mass spectrum base peak show that molecular ion at 227.9533 m/z. The characterized data are confirming of the chemical structure 6,7-dichloroisoquinoline-5,8-dione (**18**) similarity previous work [46].

4.2.2 Synthesis of cyclized product 2,7-dihydrobis([1,2,4]triazino)[6,5-*f*:5',6'-*h*]isoquinoline-3,6-dithiol (19)

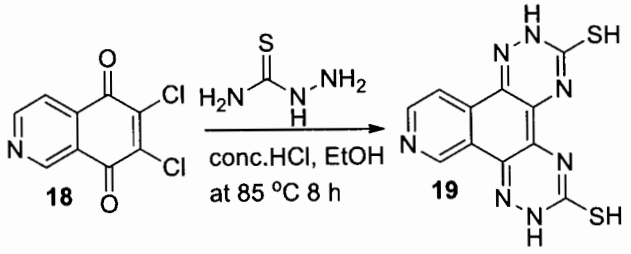

The cyclization reaction of 6,7-dichloroisoquinoline-5,8-dione (**18**) with thiosemicarbazide under acidic conditions were using hydrochloric acid as catalyst. The reaction was carried out to obtain product in moderate yield. The cyclization reaction should be carefully and without water because water attacked convert imine moiety to carbonyl moiety. The cyclized product under acidic conditions was obtain in moderate yield (40%) as brown solid.

The mechanism of cyclization reaction under acidic conditions is shown in Figure 4.8. Firstly, 6,7-dichloroisoquinoline-5,8-dione (**18**) was protonation with proton of hydrochloric at carbonyl carbon to obtaine intermediate **A**. The lone pair electrons nitrogen of thiosemicabazide attacked at carbonyl carbon of the intermediate **A** to give cation intermediate **B**. Intermediate **B** induces to hydrogen transfer to give intermediate **C**. The lone pair electrons nitrogen of thiosemicabazone moiety donates at carbon to form immine bond and loss water to obtain intermediate **D**. The lone pair electrons oxygen of water abstracted proton of intermediate **D** and loss hydronium ion to give intermediate **E**. The lone pair electrons of nitrogen in thiosemicabazone moiety attacked chloride carbon and delocalized electron to carbonyl moiety to obtain intermediate **F**. Carbanion at carbonyl delocalized electron to chloride carbon and loss chloride ion to give intermediate **G**. Chloride ion abstracted proton of intermediate **G** to give intermediate **H** and loss hydrochloric acid. The intermediate **I** to **N** was reacted with thiosemicarbazide other equivalent with the similar mechanism to give product **19**.

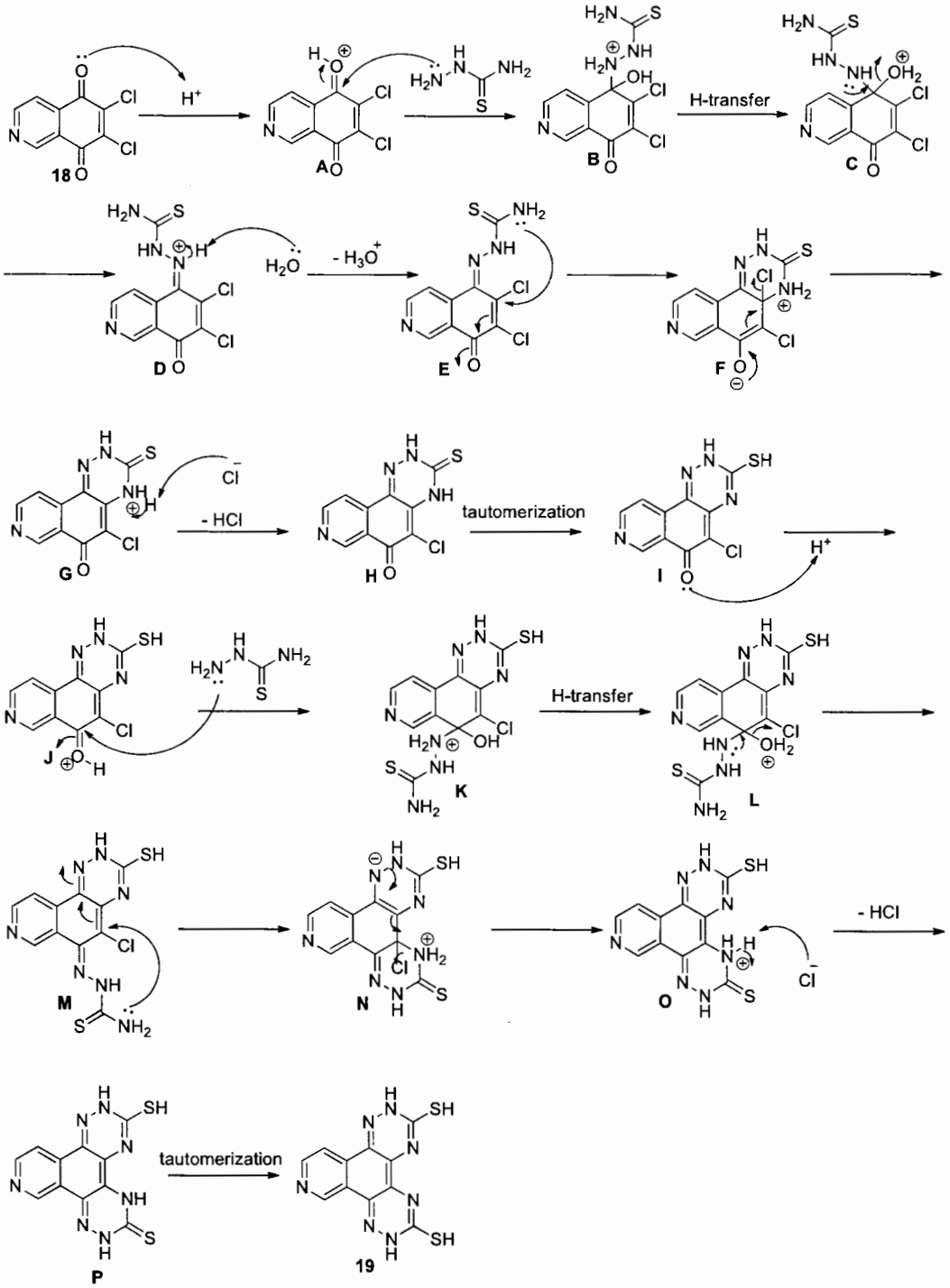

Figure 4.8 The proposed mechanism of cyclization reaction under acidic conditions 19

^{1}H-NMR spectrum of cyclized product **19** is shown in Figure 4.9. The ^{1}H-NMR proton pattern of cyclized product **19** showed shifting of signal of H-3 and H-4 in comparision with starting compound **18**. Interesting, the proton position 3 of compound **19** shift down to high field from 9.12 ppm to 8.59 ppm. Therefore the carbonyl was condensed with thiosemicarbazide. ^{1}H-NMR spectrum confirm preliminary structure of compound **19**.

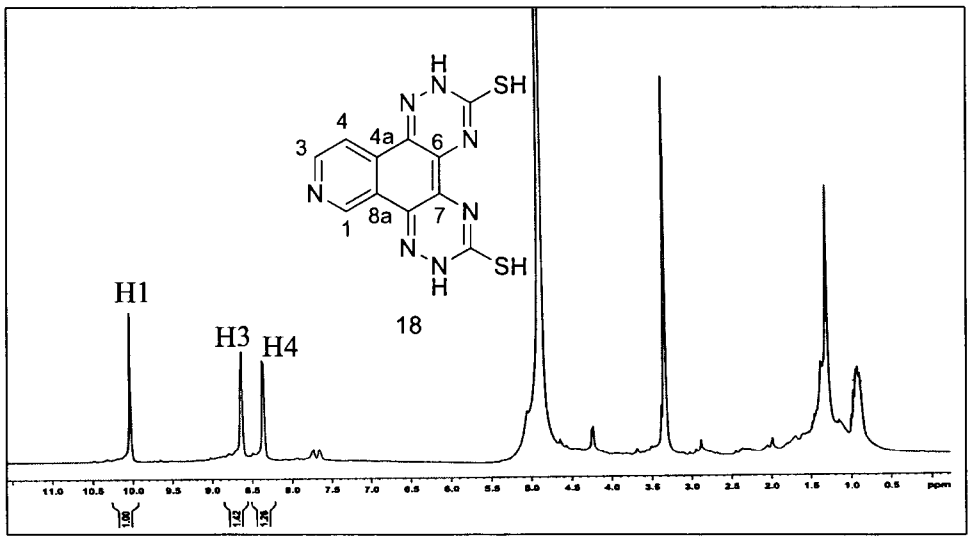

Figure 4.9 ^{1}H-NMR spectrum of cyclized product 19 in CD_3OD

^{13}C-NMR spectrum of cyclized product **19** is shown in Figure 4.10, consisting of nine aromatic carbon signals. Condensation of thiosemicarbazide at carbonyl group of 6,7-dichloroisoquinoline-5,8-dione (**18**) led to disappearing of C=O at 175.0, 173.0 ppm. The signals of C=N was detected at 162.5 and 162 ppm. The carbon signals of C-Cl in 6,7-dichloroisoquinoline-5,8-dione (**18**) at 144.0 and 143.5 ppm were shifted to 132.0 and 131.0 ppm. This indicated the cyclization reaction and structure of cyclized product **19** was confirmed. The methine carbon of isoquinoline including C1, C3 and C4 are showing chemical shift at 149.0, 146.0 and 129.0 ppm respectively. The quaternary carbons of isoquinoline including C4a, C6, C7 and C8a were found at chemical shift 125.0, 134.0, 130.0 and 138.0 ppm, respectively. ^{13}C-NMR data can confirm structure of the cyclized product **19**.

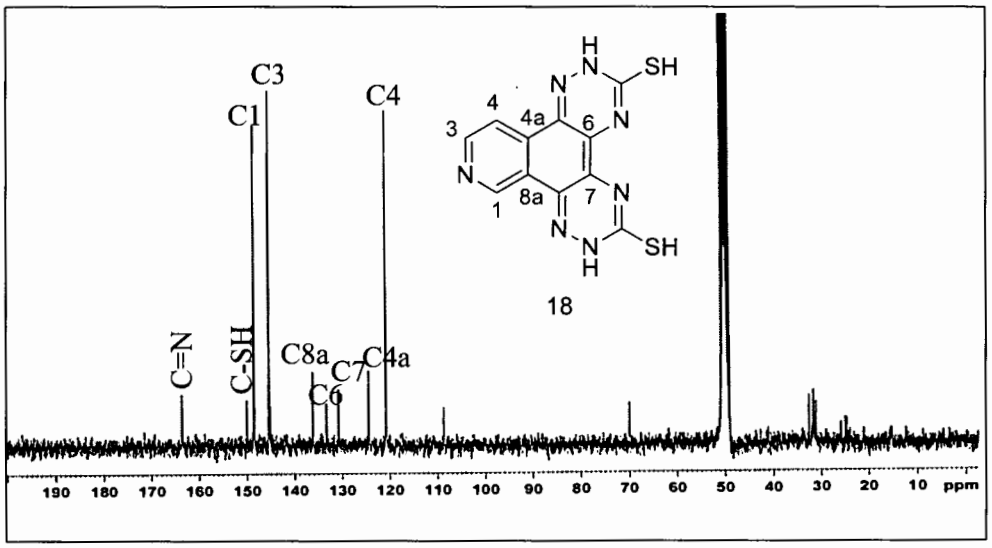

Figure 4.10 ^{13}C-NMR spectrum of cyclized product 19 in CD_3OD

IR spectrum is shown in Figure B.7. The wavenumber of functional carbonyl group at 1670-1820 cm^{-1} was disappeared can be confirmed that thiosemicarbazide was condensed at the carbonyl moiety. IR spectrum is shown that medium signal of N-H stretching at 3300 cm^{-1} secondary amine has one boarding peak. IR spectrum supported including C-H stretching medium to weak signal at 3171 cm^{-1}, N-H bending medium signal at 1610 cm^{-1} and disappeared strong signal at 600-800 of C-Cl stretching. IR spectrum data can confirm the structure of the cyclized product **19**.

Mass spectrum is showed in Figure B.8. The cyclized product **19** was unstable molecular, therefore gave fragmentations several molecular ion. The molecular ion at 299.0048 m/z was observed. Mass spectrum base peak of fragment was found at value of 257.2360 m/z and 229.1779 m/z as shown in Figure 4.11.

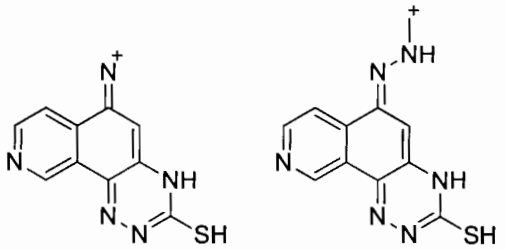

Figure 4.11 The fragment ion of cyclized product 19

4.2.3 Alkylation reaction of compound 19

The alkylation reaction was carried out using sodium hydride as base at 0 °C for 30 min. The alkyl halide was added dropwise in the reaction mixture at 0 °C then stirred at room temperature. The reaction mixture was reflux at 75 °C for 8 h under nitrogen atmosphere. Four side chains were used in the synthesis to complete four alkylated products as orange solid. Percent yield of alkylation reaction was in the range of 22-42, summarized in Table 4.2.

Table 4.2 Chemical conditions and yields of the synthesis compounds 20a-d

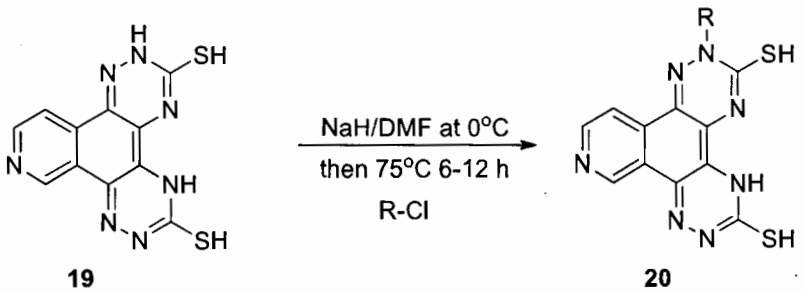

19 20

Entry	Side chain	Product	Reaction time	Yields (%)
1	a: R=$CH_2CH_2NMe_2$	**20a**	8	17
2	b: R=$CH_2CH_2CH_2NMe_2$	**20b**	8	22
3	c: R=CH_2CH_2(pyrrolidine)	**20c**	8	42
4	d: R= CH_2CH_2(piperidine)	**20d**	8	27

The mechanism of alkylation reaction is shown in Figure 4.12. The alkylation reaction occurred *via* substitution nucleophilic bimolecular reaction (S_N2)

because the alkyl halide is primary alkyl halide. Hydride ion abstracted proton of cyclized product to give intermediate **A**. Anion of intermediate **A** attacked alkyl halide and chloride ions was removed in one step to obtain product.

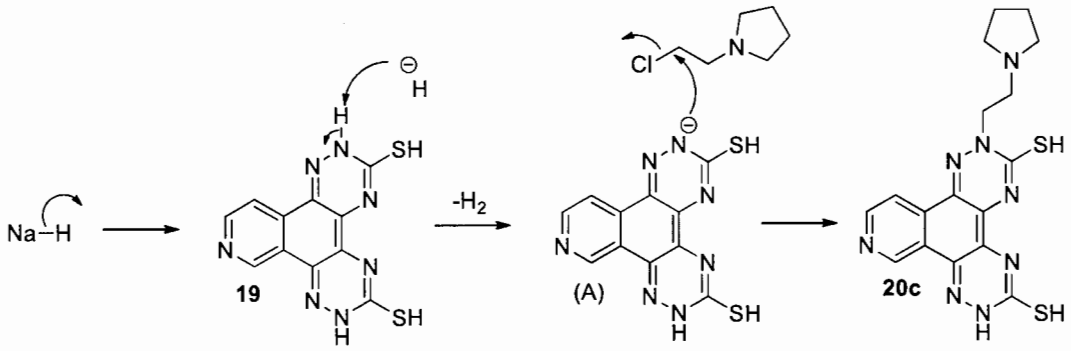

Figure 4.12 The proposed mechanism of alkylation reaction

4.2.3.1 Characterization of compound **20a**

^{1}H-NMR spectrum of alkylated product **20a** is shown in Figure B.9. The aromatic proton of core skeleton gave three signals at 9.91 (H-1), 8.99 (H-3) and 8.20 (H-4) ppm and new three aliphatic protons of side chain after alkylation with 2-chloro-*N*,*N*-dimethyl ethylamine were found at 4.64 (H-1′), 2.95 (H-2′) and 2.36 (H-3′) ppm. ^{1}H-NMR spectrum can confirm the alkyl halide or has been alkylate into core structure.

IR spectrum is shown in Figure B.10. The wavenumber of functional amine group N-H stretching gave medium to weak signal and one ban signal at 3257 cm^{-1}, C-N stretching medium to medium signal at 1101 cm^{-1}and N-H bending medium signal at 1598 cm^{-1}. The wavenumber of functional alkane group C-H stretching strong signal at 2740 cm^{-1} and C-H bending variable signal at 1488, 1451 cm^{-1}.

4.2.3.2 Characterization of compound **20b**

^{1}H-NMR spectrum of alkylated product **20b** is shown in Figure B.12. The aromatic proton of core skeleton showed three signal at 10.03 (H-1), 9.00 (H-3) and 8.22 (H-4) ppm and new pattern of four aliphatic proton of side chain after

alkylation with 2-chloro-*N*,*N*-dimethyl propylamine showing at 4.79 (H-1′), 1.25 (H-2′), 2.49 (H-3′) and 1.78 (H-4′). ^{1}H-NMR spectrum can confirm the alkyl halide or side chain formation into core structure.

^{13}C-NMR spectrum of alkylated product **20b** as shown in Figure B.13, showing nine aromatic carbon. After alkylation with 2-chloro-*N*,*N*-dimethyl propylamine indicated significant carbon of thiazole signal at chemical shift 143.0 ppm of C-SH. The important imine moiety found that chemical shift at 163.0 and 162.5 ppm for two C=N. The pattern methine carbon of isoquinoline including C1, C3 and C4 are showing chemical shift at 143.0, 134.0 and 126.0 ppm, respectively. The quaternary carbon of isoquinoline including C4a and C8a are shown at chemical shift 139.0 and 135.0 ppm, respectively. ^{13}C-NMR signals of four aliphatic carbon of side chain after alkylation with 2-chloro-*N*,*N*-dimethyl propylamine were found at 59.0 (C-1′), 29.0 (C-2′), 55.0 (C-3′) and 45.0 (C-4′). ^{13}C-NMR data can confirm chemical structure of the alkylated product **20b**.

4.2.3.3 Fully characterization of compound **20c**

^{1}H-NMR spectrum of alkylated product **20c** is shown in Figure B.16. The aromatic protons of core skeleton showed three signals at 9.69 (H-1), 8.78 (H-3) and 8.14 (H-4) ppm and new pattern of four aliphatic protons of side chain after alkylation with 1-(2-chloroethyl)pyrrolidine were found at 4.65 (H-1′), 3.11 (H-2′), 2.60 (H-3′) and 1.79 (H-4′). ^{1}H-NMR spectrum can confirm the alkyl halide or has been alkylate into core structure.

^{13}C-NMR spectrum of alkylated product **20c** as shown in Figure B.17, showing nine aromatic carbon. After cyclized product (**19**) alkylation with 1-(2-chloroethyl)pyrrolidine indicated significant carbon of thaiol thiazole ring signal chemical shift at 154.0 ppm of C-SH. The important imine moiety was found that chemical shift at 166 for two C=N. The methine carbon of isoquinoline showing three signals at chemical shift 147.0 (C-1), 135.0 (C-4) and 120.0 (C-3) ppm, respectively. The quaternary carbon of isoquinoline gave signals at chemical shift 140.0 (C-6, C-7), 133.0 (C-8a) and 124.0 (C-4a) ppm, respectively. ^{13}C-NMR new pattern four aliphatic carbon of side chain after alkylation with 1-(2-chloroethyl)pyrrolidine showing at 60.0 (C-1′), 56.0 (C-2′), 54.0 (C-3′) and 24.0 (C-4′). ^{13}C-NMR data can confirmed chemical structure of the alkylated product **20c**.

HMQC spectrum showing connection between proton and carbon is shown in Figure B.18. Firstly, 2D connection map showed that region cross peaks between ^{1}H-NMR 300 MHz δ_H and ^{13}C-NMR 75MHz δ_c the aromatic carbon and aromatic proton chemical shift at 147.0, 9.00 (C-1,H-1), 114.0, 8.91 (J = 5.4 Hz) (C-3, H-3), and 135.0, 8.25 (J = 5.7 Hz) (C-4, H-4) ppm, respectively. The aliphatic cross peaks chemical shift at 60.0, 4.44 (C-1′, H-1′), 56.0, 2.95 (C-2′, H-2′), 54.0, 2.95 (C-3′, H-3′) and 24.0, 2.60 (C-4′, H-4′) ppm, respectively. The spectrum of HMQC experiment of compound **20c** is shown in Figure B.18.

HMBC spectrum of compound **20c** showed heteronuclear correlations over longer ranges of about 2–4 bonds at Figure B.19. 2D correlations map revealed that region cross peaks at δ_H 8.25 (J = 5.7 Hz) ppm (H-3) correlations with δ_c 124.0 ppm (C-4a) two bonds and δ_c 140.0 (C-6, C-7) four bonds HMBC correlations were observed. Interestingly, at δ_H 8.25 (J = 5.7 Hz) (H-4) is showing correlations with δ_c 114.0 (C-3) one bond, 147.0 (C-1) three bonds and 60.0 (C-1′) four bonds HMBC correlations were investigated. The correlations δ_H 8.25 (J = 5.7 Hz) (H-4) and δ_c 60.0 (C-1′) can confirm the side chain was attacked into thiosemicabazone at C-5. The fully characterize can confirm the chemical structure of alkylated product **22c**.

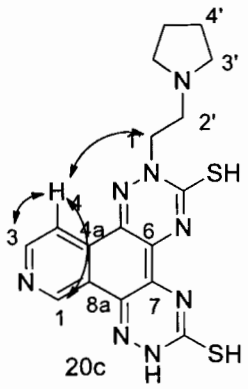

Figure 4.13 The significant position of HMBC compound 20c

IR spectrum is shown in Figure B.21. The wavenumber of functional amine group N-H stretching bonded medium to weak and one ban signal at 3358 cm^{-1}, C-N stretching medium to weak signal at 1040 cm^{-1}and N-H bending

medium signal at 1579 cm^{-1}. The wavenumber of functional alkane group C-H stretching strong signal at 2921 cm^{-1}.

4.2.3.4 Characterization of compound **20d**

^{1}H-NMR spectrum of alkylated product **20d** is shown in Figure B.22. The aromatic proton of core skeleton showed three signals at 9.90 (H-1), 8.91 (H-3) and 8.25 (H-4) ppm and new pattern six of aliphatic proton of side chain after alkylation with 1-(2-chloroethyl)piperidine showing at 4.56 (H-1′), 2.88 (H-2′), 2.44 (H-3′), 1.50-1.75 (H-5′) and 1.35-1.50 (H-6′). ^{1}H-NMR spectrum can confirm the alkyl halide or side chain formation in to core structure.

4.2.4 Synthesis of cyclized product (*E*)-2-(3-mercapto-[1,2,4]triazino[5,6-*h*]isoquinolin-6(2*H*)-ylidene)hydrazinecarbothioamide (21)

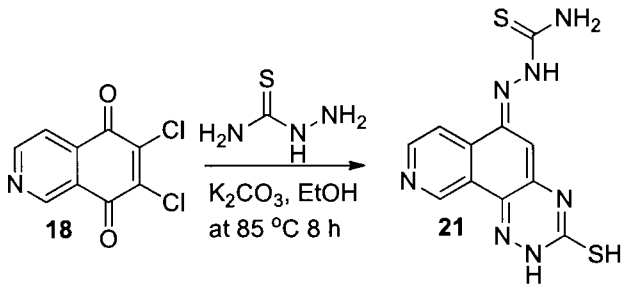

The cyclization reaction of 6,7-dichloroisoquinoline-5,8-dione (**18**) with thiosemicarbazide under basic conditions was performed by using potassium carbonate as base. The cyclized product under basic conditions **21** was obtained in moderate yield (47%) as brown solid.

The mechanism of cyclization reaction under basic conditions is shown in Figure 4.14. Firstly, The lone pair electrons of nitrogen of thiosemicarbazide attacked at carbonyl moiety of 6,7-dichloroisoquinoline-5,8-dione (**18**) to obtain intermediate **A**. The intermediate **A** induces to proton transfer to give intermediate **B.** The lone pair electrons of nitrogen in thiosemicarbazone moiety delocalized electron to (intermediate **C**) and hydroxide ion. Hydroxide ion abstract proton of intermediate **C** to give imine moiety intermediate **D** and water was removed. The lone pair electrons of nitrogen in thiosemicarbazide other equivalent attacked with intermediate **D** and the mechanism was the same as mentioned above to obtained intermediate **H**.

medium signal at 1579 cm^{-1}. The wavenumber of functional alkane group C-H stretching strong signal at 2921 cm^{-1}.

4.2.3.4 Characterization of compound **20d**

^{1}H-NMR spectrum of alkylated product **20d** is shown in Figure B.22. The aromatic proton of core skeleton showed three signals at 9.90 (H-1), 8.91 (H-3) and 8.25 (H-4) ppm and new pattern six of aliphatic proton of side chain after alkylation with 1-(2-chloroethyl)piperidine showing at 4.56 (H-1′), 2.88 (H-2′), 2.44 (H-3′), 1.50-1.75 (H-5′) and 1.35-1.50 (H-6′). ^{1}H-NMR spectrum can confirm the alkyl halide or side chain formation in to core structure.

4.2.4 Synthesis of cyclized product (*E*)-2-(3-mercapto-[1,2,4]triazino[5,6-*h*]isoquinolin-6(2*H*)-ylidene)hydrazinecarbothioamide (21)

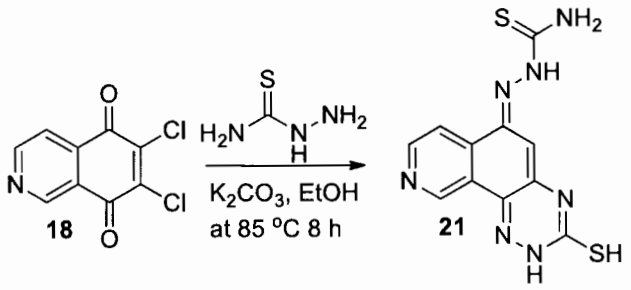

The cyclization reaction of 6,7-dichloroisoquinoline-5,8-dione (**18**) with thiosemicarbazide under basic conditions was performed by using potassium carbonate as base. The cyclized product under basic conditions **21** was obtained in moderate yield (47%) as brown solid.

The mechanism of cyclization reaction under basic conditions is shown in Figure 4.14. Firstly, The lone pair electrons of nitrogen of thiosemicarbazide attacked at carbonyl moiety of 6,7-dichloroisoquinoline-5,8-dione (**18**) to obtain intermediate **A**. The intermediate **A** induces to proton transfer to give intermediate **B.** The lone pair electrons of nitrogen in thiosemicarbazone moiety delocalized electron to (intermediate **C**) and hydroxide ion. Hydroxide ion abstract proton of intermediate **C** to give imine moiety intermediate **D** and water was removed. The lone pair electrons of nitrogen in thiosemicarbazide other equivalent attacked with intermediate **D** and the mechanism was the same as mentioned above to obtained intermediate **H**.

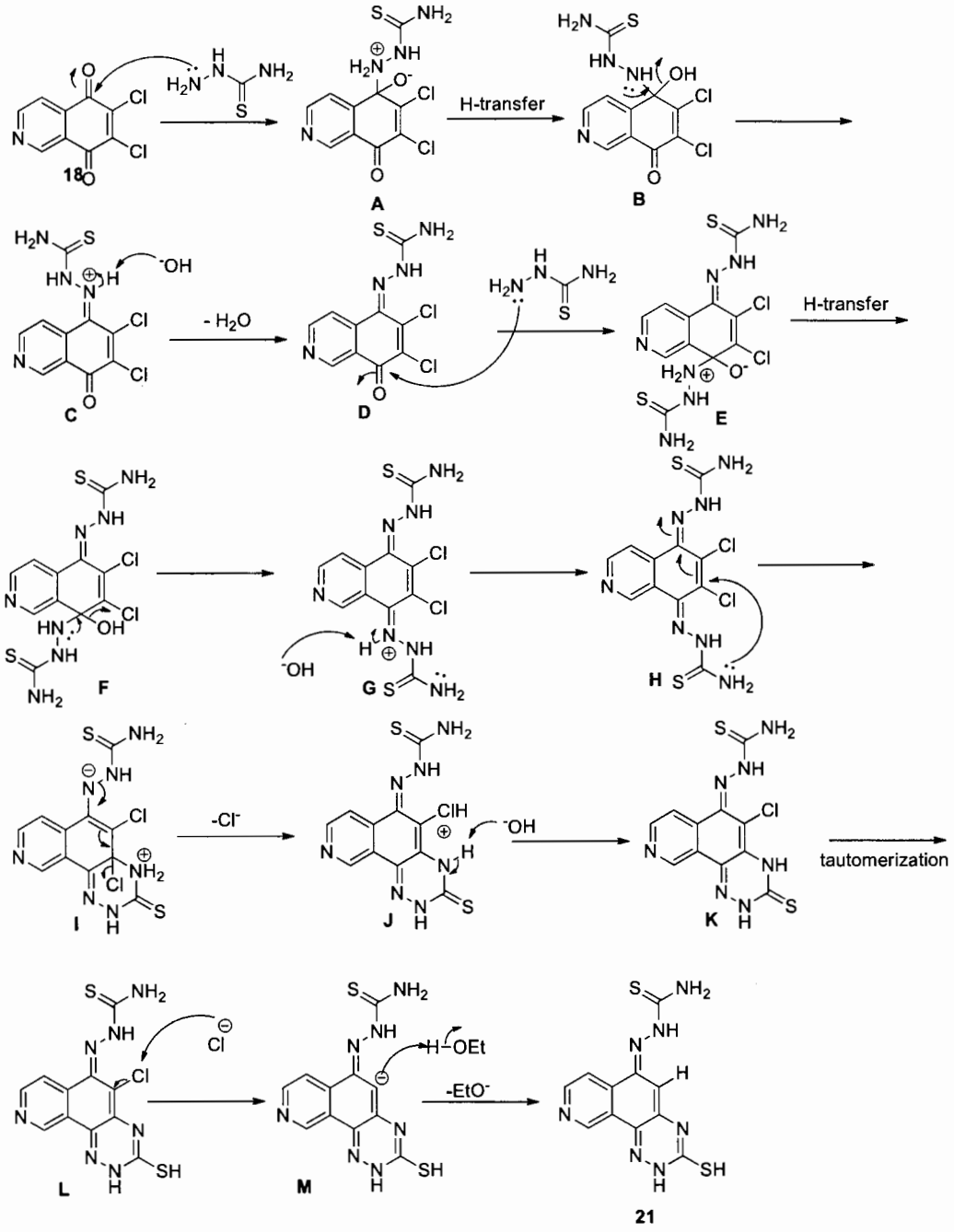

Figure 4.14 The proposed mechanism of cyclization reaction under basic conditions 21

^{1}H-NMR spectrum of cyclized product **21** is shown in Figure 4.15. The proton signal of cyclized product **21** showed different from 6,7-dichloroisoquinoline-5,8-dione (**18**). The result showed that four signals of aromatic proton at 9.97 (H-1), 9.51 (H-6), 8.76 (H-3) and 8.23 (H-4) ppm, respectively. Interestingly, after cyclization under basic conditions found that new proton (H-6). The proton position 3 of compound **21** shift down to high field from 9.12 ppm to 8.76 ppm. Therefore, the carbonyl was condensed with thiosemicarbazide. ^{1}H-NMR spectrum can confirm preliminary structure of compound **21**.

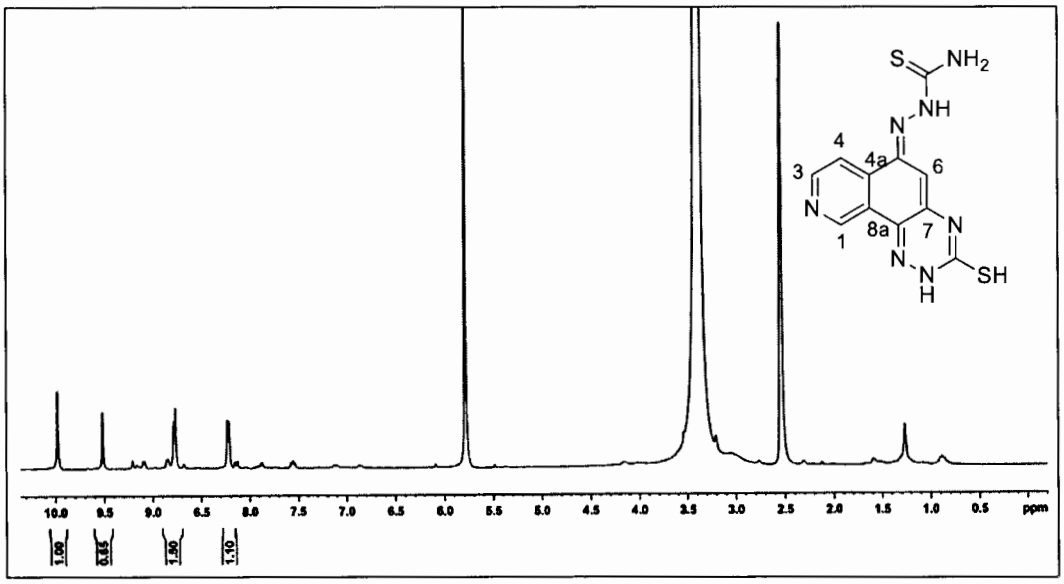

Figure 4.15 ^{1}H-NMR spectrum of cyclized product 21 in DMSO-D_6

^{13}C-NMR spectrum of cyclization under basic conditions product as shown in Figure B.26 showed nine aromatic carbon. After 6,7-dichloroisoquinoline-5,8-dione (**18**) cyclized with thiosemcarbazide, there was a signals at 158.0 ppm for C-SH. The important imine moiety found that chemical shift at 165.0 were two C=N. The methine carbon of isoquinoline is including 157.5 (C-1), 155.0 (C-3), 127.0 (C-4) and 165.0 (C-6) ppm. The quaternary carbon of isoquinoline including C4a, C7 and C8a were found at chemical shift 133.5, 147.0 and 143.0 ppm, respectively. ^{13}C-NMR data can confirm that structure of the cyclized product **21** did not cyclized at carbon position 6.

IR spectrum is shown in Figure B.27. The wavenumber of functional carbonyl group at 1670-1820 cm^{-1} was disappeared indicating the condensation at the carbonyl moiety. IR spectrum revealed that medium signal of N-H stretching at 3358 and 3066 cm^{-1} represented primary amine of thiosemicarbazone moiety. IR spectrum supported including N-H bending medium signal at 1690 cm^{-1} and disappear of strong signal at 600-800 of C-Cl stretching. IR spectrum data can support the structure of the cyclized product **21**.

Mass spectrum is shown in Figure B.28. The cyclized product **21** showed molecular ion (M^++Na) at 327.1894 m/z. Mass spectrum base peak of fragment showed fragment ion of 133.0808, 149.0182 and 195.1166 m/z as can be seen in Figure 4.16.

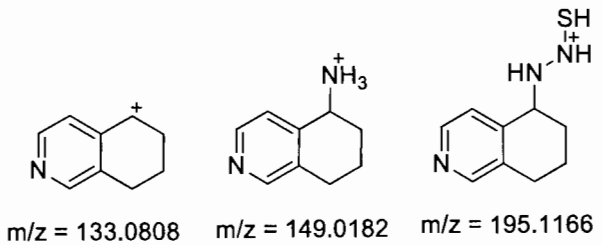

Figure 4.16 The fragment ion of cyclized product 21

4.2.4 Alkylation reaction of compound 21

The alkylation reaction was using sodium hydride in DMF as base to react with cyclized product **21** at 0 °C for 30 min. The alkyl halide was added dropwise in the reaction mixture at 0 °C then stirred at room temperature. The reaction mixture was reflux at 75 °C for 8-16 h under nitrogen atmosphere. Three side chains were used in the synthesis to complete three alkylated product as orange solid. Percent yielded of alkylation reaction was in the range of 46-59. The result was summarized in Table 4.3.

Table 4.3 Chemical conditions and yields of the synthesis compounds 20a-c

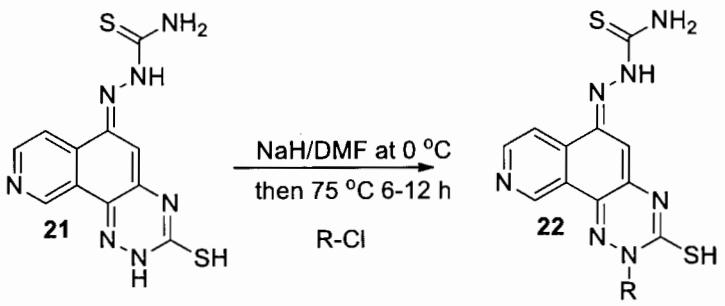

Entry	Side chain	Product	Reaction time	Yields (%)
1	a: R=$CH_2CH_2NMe_2$	**20a**	8	46
2	b: R= CH_2CH_2(pyrrolidine)	**20b**	8	47
3	c: R=CH_2CH_2(piperidine)	**20c**	8	59

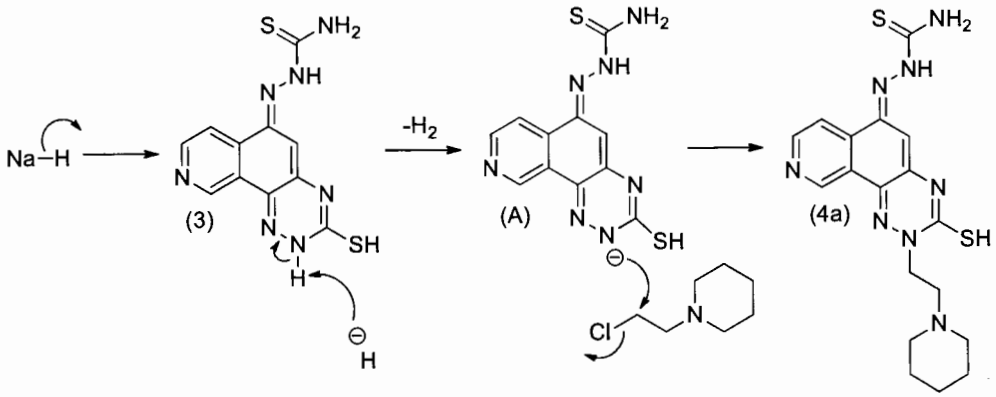

Figure 4.17 The proposed mechanism of alkylation reaction

The mechanism of alkylation reaction is shown in Figure 4.17. The alkylation reaction occurred *via* substitution nucleophilic bimolecular reaction (S_N2) because the alkyl halide is primary alkyl halide. Hydride ion abstracted proton of cyclized product to give intermediate **A**. Anion of intermediate **A** attacked alkyl halide and chloride ions was removed in one step to obtain product.

4.2.5.1 Characterization of compound **22a**

^{1}H-NMR spectrum of alkylated product **22a** is shown in Figure B.29. The aromatic proton of core skeleton showed three signals at 9.48 (H-1), 8.74 (H-3), 8.58 (H-7) and 7.98 (H-4) ppm and three aliphatic protons of side chain after alkylation with 2-chloro-*N,N*-dimethyl ethylamine showed at 4.43 (H-1′), 2.61 (H-2′) and 2.27 (H-3′) ppm. ^{1}H-NMR spectrum can confirm the alkyl halide or side chain formation into core structure.

^{13}C-NMR spectrum of alkylated product **22a** as can been seen in Figure B.30, showing nine aromatic carbons. After alkylation with 2-chloro-*N,N*-dimethyl ethylamine, ^{13}C-NMR signal showed three aliphatic carbon of side chain after alkylation with 2-chloro-*N,N*-dimethyl ethylamine at 59.0 (C-1′), 45.0 (C-2′), 29.6 (C-3′) ppm.

IR spectrum is shown in Figure B.32. The wavenumber of functional amine group N-H stretching was found at 2978 cm^{-1} represented primary amine, C-N stretching medium to weak signal at 1072 $cm^{-1}$and N-H bending medium signal at 1574 cm^{-1}. The wavenumber of functional alkane group C-H stretching strong signal at 2601 cm^{-1}.

4.2.5.2 Characterization of compound **22b**

^{1}H-NMR spectrum of alkylated product **22b** is shown in Figure B.33. The aromatic proton of core skeleton showed four signal at 9.65 (H-1), 8.90 (H-3), 8.65 (H-7) and 7.90 (H-4) ppm and new pattern four aliphatic proton of side chain after alkylation with 1-(2-chloroethyl)pyrrolidine showing at 4.75 (H-1′), 3.00 (H-2′), 2.50 (H-4′) and 1.24 (H-5′).

^{13}C-NMR spectrum of alkylated product **22b** is shown in Figure B.34, showing nine aromatic carbons. After alkylation with 1-(2-chloroethyl) pyrrolidine, ^{13}C-NMR data showed four aliphatic carbon of side chain after alkylation with 1-(2-chloroethyl)pyrrolidine at 73.0 (C-1′), 59.0 (C-2′), 28.0 (C-4′) and 26.0 (H-5′). ^{13}C-NMR data can confirm chemical structure of the alkylated product **22b**.

IR spectrum is shown in Figure B.36. The wavenumber of functional amine group N-H stretching of primary amine of Thiosemicarbazone moiety medium to weak and two ban signal at 2979 cm^{-1}, C-N stretching medium to weak signal at 1072 $cm^{-1}$and N-H bending medium signal at 1577 cm^{-1}.

4.2.5.3 Fully characterization of compound **22c**

^{1}H-NMR spectrum of alkylated product **22c** is shown in Figure B.37. The aromatic proton of core skeleton showed four signals at 10.13 (H-1), 9.16 (H-6), 8.75 (H-3) and 8.20 (H-4) ppm and new pattern five aliphatic proton of side chain after alkylation with 1-(2-chloroethyl)piperidine showed at 4.34 (H-1′), 2.93 (H-2′), 2.55 (H-3′), 1.63 (H-4′) and 1.47 (H-5′) ppm.

^{13}C-NMR spectrum of alkylated product **22c** as shown in Figure B.38, showing nine aromatic carbon of staring material. After alkylation with 1-(2-chloroethyl)piperidine, ^{13}C-NMR new pattern four aliphatic carbon of side chain after alkylation with 1-(2-chloroethyl)piperidine were found at 72.0 (C-1′), 59.0 (C-2′), 55.0 (C-3′), 27.0 (C-4′) and 25.0 (C-5′). ^{13}C-NMR data can confirm chemical structure of the alkylated product **22c**.

HMQC spectrum showed connection between proton and carbon as can be seen in Figure B.41. Firstly, 2D connection map showed that region cross peaks between ^{1}H-NMR 300 MHz δ_H and ^{13}C-NMR 75 MHz δ_c the aromatic carbon and aromatic proton chemical shift at 149.0, 10.13 (C-1, H-1), 155.0, 9.16 (C-6, H-6), 145.0, 8.75 (J = 5.7) (C-3, H-3) and 123.0, 8.20 (J = 5.7) (C-4,H-4) ppm, respectively. The aliphatic cross peaks chemical shift at 72.0, 4.34 (J = 5.1) (C-1′, H-1′), 59.0, 2.93 (J = 5.1) (C-2′, H-2′), 55.0, 2.55 (C-3′, H-3′), 27.0, 1.63 (J = 4.8) (C-4′, H-4′) and 25.0, 1.47 (C-5′, H-5′) ppm, respectively.

HMBC spectrum showed heteronuclear correlations over longer ranges of about 2–4 bonds as can seen in Figure B.42. The significant 2D correlations map shown that region cross peaks at δ_c 155.0 ppm (C-6) correlations with δ_H 8.20 (J = 5.7) ppm (H-4) four bonds can confirm that thiosemicabazide at C-5 did not cyclize to C6. These indicated the three fused ring product. δ_H 8.75 (J = 5.7) (H-3) is showing correlations with δ_c 123.0 (C-4a) two bonds and δ_c 132.0 (C-8a) three bonds. The important 2D correlations map shown that region cross peaks at δ_c 175.0 (C=N) is showing correlations with δ_H 2.93 (J = 5.1) (H-2′) four bonds can be confirm the side chain formation bond at below nitrogen group. The fully characterize can confirm the chemical structure of alkylate product under basic conditions series.

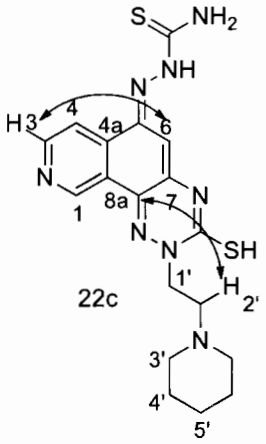

Figure 4.18 The significant position of HMBC compound 22c

IR spectrum is shown in Figure B.40. The wavenumber of functional amine group N-H stretching bonded medium to weak and two ban signal at 3179 cm^{-1}, C-N stretching medium to weak signal at 959 $cm^{-1}$and N-H bending medium signal at 1583 cm^{-1}.

4.3 Antiproliferative activity

The synthesized compound **19**, **20** and **22** (Figure 4.19) were evaluated the antiproliferative activity in comparison with the mono-substitution **71**, hydrazone **70** and thiosemicarbazone **72** and **73**. The synthesized compounds were evaluated antiproliferative activity with cancer cell human colorectal cancer cells (HT-29) and normal cell mouse subcutaneous connective tissue cells (L929). Antiproliferative testing was using doxorubicin as reference drug and incubation with cell for 24 h. The concentration of compound that inhibit 50% value (IC_{50}) was calculated and evaluated with MTT assay. The results are summarized in Table 4.4.

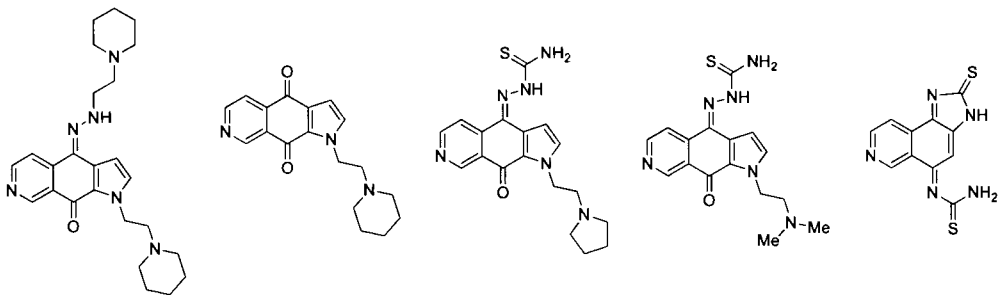

70 **71** **72** **73** **69**

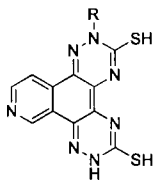

19: R = H
20a: R = $CH_2CH_2NMe_2$
20b: R = $CH_2CH_2CH_2NMe_2$
20c: R = CH_2CH_2(pyrrolidine)
20d: R = CH_2CH_2(piperidine)

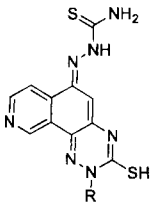

22b: R = CH_2CH_2(pyrrolidine)
22c: R = CH_2CH_2(piperidine)

Figure 4.19 Structures of azanaphthoquinone thiazole derivative were evaluated with cancer cell (HT-29) and normal cell (L929)

Table 4.4 Antiproliferative activity of synthesized compounds

Compounds	IC_{50} value (μM)	
	HT-29	L929
70	45.02 ± 1.14	95.19 ± 6.04
71	3.53 ± 0.42	5.34 ± 0.03
72	41.61 ± 2.22	100.04 ± 2.29
73	6.45 ± 0.78	54.54 ± 3.46
69	46.85 ± 1.11	32.59 ± 2.60
19 (Cytotoxicity@100 μM =34.76±2.98%)	>100	>100
20a (Cytotoxicity@100 μM =2.39±1.35%)	>100	>100
20b (Cytotoxicity@100 μM =15.21±2.03%)	>100	>100
20c (Cytotoxicity@100 μM =2.02±1.35%)	>100	>100
20d	74.88 ± 3.47	>100
22b	51.40 ± 0.78	65.37 ± 1.97
22c	62.02 ± 1.61	67.53 ± 3.27

HT-29: human colorectal cancer cells

L929: mouse subcutaneous connective tissue cells

10 μM Doxorubicin HCl (positive control), cytotoxicity = 43.32±1.80% after 24 h incubation (HT-29).

10 μM Doxorubicin HCl (positive control), cytotoxicity = 48.95±3.77% after 24 h incubation (L929 cells).

Antiproliferative activity using compound **70** represents hydrazone series, **71** represent mono-substituent series, **72** and **73** represent thiosemicarbazone series **19** and **20a-d** represent azanaphthoquinone thiazole derivative under acidic conditions, and **22c-d** represent azanaphthoquinone thiazole derivative under basic conditions. IC_{50} values of 12 compounds are shown at Table 4.2. The synthesized compound shown antiproliferative activity is moderate to good activity and selective with cancer cell because mouse subcutaneous connective tissue cells (L929) very sensitive normal cell line. Compared previous series in human colorectal cancer cells (HT-29) found that thiosemicarbazone series shown very good activity most hydrazone series, mono-substituent series. Thiosemicarbazone moiety may be key of antiproliferative activity with human colorectal cancer cells (HT-29). Thiosemicarbazone moieties are flexible, nitrogen atom sulfur atom in molecule for hydrogenbonding interaction. The result shown that basic conditions series present thiosemicarbazone moiety in core skeleton cause the basic conditions series shown activity high than acidic conditions series.

The side chain acyclic such as $CH_2CH_2NMe_2$ and $CH_2CH_2CH_2NMe_2$ chain showing antiproliferative activity lower than cyclic side chain including CH_2CH_2(pyrrolidine), CH_2CH_2(piperidine) chain. The cyclic side chain has more hydrogen atom affect to van der waals interaction and suitable solubility property for high antiproliferative activity with cancer cell.

The result shown that the three fused ring indicated antiproliferative activity high than the four fused ring. The core skeleton of four fused ring rigid and unflexible molecule cause low antiproliferative activity. However, the three fused ring showing high than antiproliferative activity. The three fused ring has thiosemicarbazone moieties in core skeleton. All the series show that side chain cyclic side chain antiproliferative activity high than acyclic side chain.

4.4 Molecular docking calculations

Molecular docking were studied on two series of synthesized compounds with DNA. Molecular docking were studied two type including minor groove binder and major groove binder.

4.4.1 Minor groove binder

Minor groove binder was using PDB ID; 2GVR Crystal structure of the berenil-D(CGCGAATTCGCG)2 complex at 1.65 Å resolution. The studied on minor groove binder used grid box 30 30 30 for optimize the synthesized structure to suitable for binding site. Binding energy and interaction between synthesized compounds and DNA is shown in Table 4.5.

Comparison of core structure with four fused ring **19**, three fused ring **21** and compound **69** found that compound **21** showed lowest binding energy (-8.43) and high H-bonding interaction. This result can explain the reason why compound **21** exhibited higher activities compare to compound **22** and **69**. Molecular docking result of minor groove binder was related to biological activity.

Table 4.5 Binding energy and interaction of minor groove binder

Compounds	Binding Energy (kcal/mol)	Mean binding energy (kcal/mol)	H-bonding	van der waals
69	-7.73	-7.73	4	3
19	-7.00	-6.96	2	4
21	-8.43	-8.13	5	5
20a	-9.06	-8.81	2	6
20b	-9.45	-8.77	3	5
20c	-10.16	-9.52	2	8
20d	-10.73	-10.54	2	5
22a	-9.92	-9.31	1	4
22b	-10.08	-9.27	6	4
22c	-10.01	-9.10	3	6
22d	-9.76	-8.94	5	5

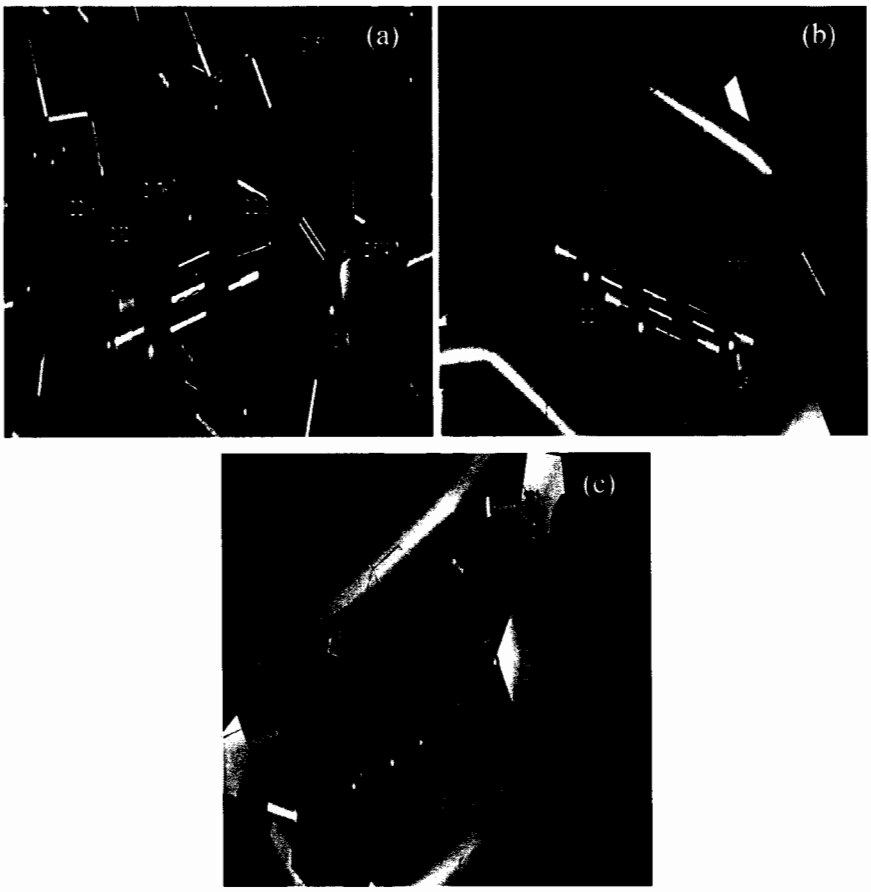

Figure 4.20 Comparison molecular docking of core structure compounds minor groove binder a) compound 69, b) four fused ring 19 and c) three fused ring 21

Molecular docking of three core skeleton are show in Figure 4.20. Molecular docking of three fused ring **21**s revealed flexible structure and more hetero atom including nitrogen atom and sulfur atom which could form hydrogen bonding interaction with DNA. Four fused ring **19** was planar, bulky and rigid molecule, this affect to low interaction with DNA and high binding energy. Comparison of side chain indicated that cyclic side chains including CH_2CH_2(pyrrolidine) and CH_2CH_2(piperidine) chains showing lowest binding energy and more intecaction with DNA. Interaction of cyclic is better than acyclic side chain indicating more van der waals interaction. Molecular docking result of minor groove binder is related to biological activity.

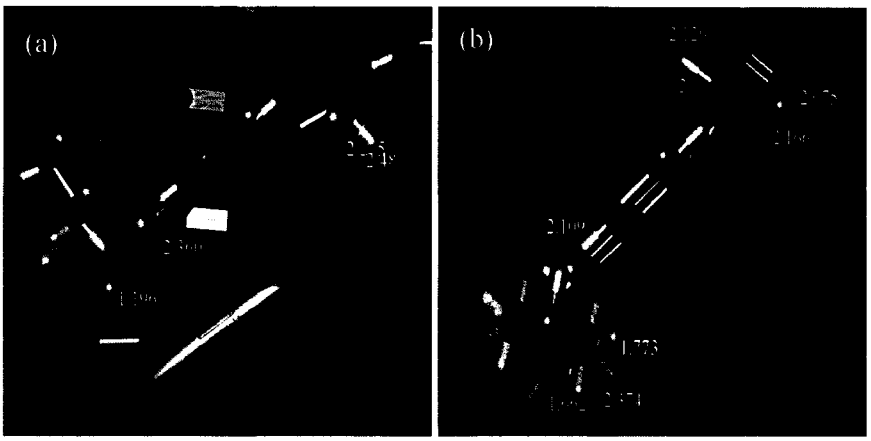

Figure 4.21 Comparison molecular docking of side chain minor groove binder a) acyclic and b) cyclic

4.4.2 Major groove binder

Major groove binder was using PDB ID; 1Z3F structure of ellipticine in complex with a 6-bp DNA at 1.50 Å resolution. Study on major groove binder used grid box 24 24 24 for optimizing the synthesized structure to suitable for binding site. Binding energy and interaction between synthesized compounds and DNA is shown in Table 4.6. Comparison of core structure with four fused ring **19**, three fused ring **21** and compound **69** found that compound **19** showed lowest binding energy (-8.39). However, compound **19** is showing weak interaction than compound **21**. Interaction of compound **21** is showed very stronger than compound **19** and compound **69** due to more possibility to form hydrogen bonding with DNA. Molecular docking result of major groove binder is related to biological activity.

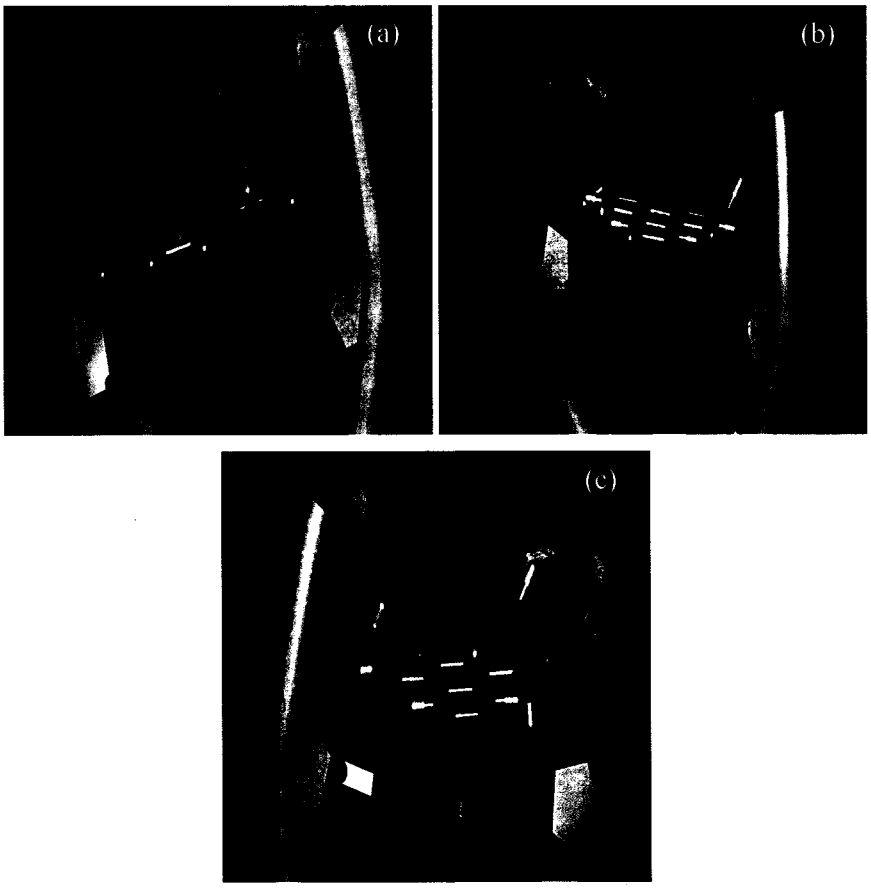

Figure 4.22 Comparison molecular docking of core structure compounds major groove binder a) compound 69, b) four fused ring 19 and c) three fused ring 21

Comparison of different side chain indicated that cyclic side chain including CH_2CH_2(pyrrolidine) and CH_2CH_2(piperidine) showed lowest binding energy and more intecaction with DNA. Interaction of cyclic was found to be better than acyclic side chain due to more H-bonding and van der waals interaction. Molecular docking result of major groove binder can support minor groove binder and result related to biological activity. Summary of molecular docking studies; we can be predicted the mechanism of action of synthesized compounds that led to minor groove binder more than major groove binder. The core structure of compound **21** is potential compound of two series. Compound three fused ring **21** showed lowest binding energy and strong interaction than the four fused rings structure. Molecular docking result

was related to antiproliferative activity. This information can explain preliminary the mechanism of action by using mode of binding.

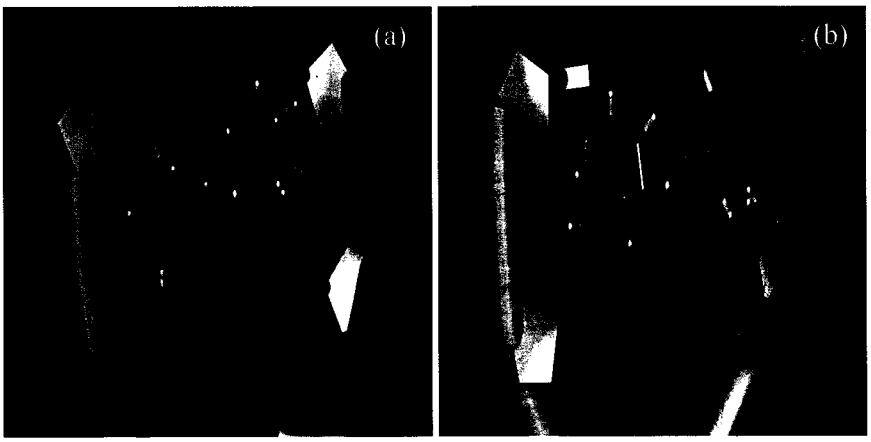

Figure 4.23 Comparison molecular docking of side chain major groove binder a) acyclic and b) cyclic

Table 4.6 Binding energy and interaction of major groove binder

Compounds	Binding Energy (kcal/mol)	Mean binding energy (kcal/mol)	H-bonding	van der waals
69	-7.18	-7.18	1	2
19	-8.39	-8.35	2	1
21	-7.48	-7.29	4	1
20a	-8.84	-8.62	2	1
20b	-8.17	-8.10	3	2
20c	-8.57	-8.45	4	3
20d	-9.08	-8.50	4	2
22a	-7.42	-7.04	4	1
22b	-7.58	-7.29	4	2
22c	-7.06	-6.25	2	4
22d	-7.34	-6.87	4	2

CHAPTER 5
CONCLUSIONS

A novel series of azanaphthoquinone annelated thiazole derivative as antiproliferative agents have been designed, synthesized, spectroscopically characterized, antiproliferative evaluated and molecular computational calculated.

The CoMSIA model based on pharmacophore alignment showed high predictive ability in evaluating the activities of azanaphthoquinone annelated pyrrole derivatives with r^2 of 0.99 and q^2 of 0.61 CoMSIA and HQSAR can be recommended to design new compounds with preliminaly combination of substituents of azanaphthoquinone annelated thiazole derivative including compounds **19** and **21** as core skeleton structure. The target molecules were designed to replace carbonyl moiety with thiosemicarbazide condensation under acidic and basic conditions to give thiazole ring in order to reduce cardiotoxic side effect. Then mono-substituted side chains were introduced into the core structure to furnish the target molecules in moderate yield.

Antiproliferative activity was evaluated on human colorectal cancer cells (HT-29) and mouse subcutaneous connective tissue cells (L929) with 12 compounds, including hydrazone **70**, mono-substituted product **71**, thiosemicabazone **72** and **73**, 5 compounds of four fused ring product **19** and **20a-d**, 2 compounds of three fused ring product **22b-c** and thiourea condensed product **69**. The results showed that compound **20a-d** and **22b-c** exhibited moderate antiproliferative activity and lower than those of mono-substituted product and thiosemicarbazone.

The acyclic side chain such as $CH_2CH_2NMe_2$ and $CH_2CH_2CH_2NMe_2$ exhibited lower antiproliferative activity than those of cyclic side chain CH_2CH_2(pyrrolidine) and CH_2CH_2(piperidine). We suggested that cyclic side chain has more van der waals interaction and high solubility in cell membrane which lead to high antiproliferative activity. Molecular docking study revealed that three fused ring product **21** could bind to minor groove of DNA better than the four fused ring product **19**. The thiosemicabazone moiety in compound **21** could form hydrogen bonding with DNA. Therefore the core structure obtained from basic cyclization is the potential anticancer compound.

REFERRENCES

REFERRENCES

[1] Adair, D. R. and Alison, R. "Synthetic metallomolecules as agents for the control of DNA structure", **Chemical Society Reviews.** 36(3): 471-483; October, 2006.

[2] Patrick L. G. **Medicinal Chemistry.** Oxford: Oxford University Press, 2005.

[3] Wikipedia. **Anthracycline.** https://en.wikipedia.org/wiki/Anthracycline. February 7, 2017.

[4] Hajihassan, Z. and Chadegani, R. A. "Interaction of mitoxantrone, as an anticancer drug, with chromatin proteins, core histones and H1, in solution", **International Journal of Biological Macromolecules.** 48(1): 87-92; October, 2011.

[5] Weiss, R. B. "The anthracyclines: will we ever find a better doxorubicin?", **Seminars in oncology.** 19(6): 670-686; December, 1992.

[6] Pongprom, N. **New anticancer compounds with an azanaphthoquinone nucleus.** Doctor's Thesis: University of Vienna, 2007.

[7] Pongprom, N. and et al. "Synthesis and Cytotoxic Activities of Azanaphthoquinone Annelated Pyrrolo Hydrazone Derivatives", **KKU Research Journal.** 17(2): 195-202; March, 2012.

[8] Somta, J. **Synthesis of thiosemicarbazone derivatives as antiproliferative agents.** Master's Thesis: Ubon Ratchathani University, 2013.

[9] Peter, C. "Cancer", **Cancer: Facts, Causes, Symptoms and Research.** http://www.medicalnewstoday.com/info/cancer-oncology. February 3, 2017.

[10] David A. W. and Thomas L. L. **Foye's principles of medicinal chemistry.** Philadelphia: Wolters Kluwer Health, 1974.

[11] Smith J. A. and Martin L. "Do cells cycle?", In **4th the National Academy of Science of the United States of America.** p.1263-1267. Washington: Kenneth R. Fulton. 1973.

[12] David O. M. **The Cell Cycle Principles of Control.** London: New Science Press, 2007.

REFERRENCES (CONTINUED)

[13] Yokota, J. "Tumor progression and metastasis", **Carcinogenesis.** 21(3): 497-503; March, 2000.

[14] National Cancer Institute. **Types of Treatment.** https://www.cancer.gov/about-cancer/treatment/types. February 7, 2017.

[15] Puyo, S. and et al. "From old alkylating agents to new minor groove binders", **Critical Reviews in Oncology/Hematology.** 89: 43-61; January, 2014.

[16] Libretexts. http://chem.libretexts.org/Core/Biological_Chemistry/Pharmaceuticals/Anti-Cancer_Drugs_II. February 7, 2017.

[17] Wang, J. C. **Untangling the double helix: DNA entanglement and the action of the DNA topoisomerases.** New York: Cold Spring Harbor Laboratory Press, 2009.

[18] Burris, H. A. and et al. "Activity of topotecan, a new topoisomerase inhibitor, against human tumor colony forming units in *vitro*", **Journal of the National Cancer Institute.** 84: 1816-1820; December, 1997.

[19] Chen, A. Y. and Liu, L. F. "DNA topoisomerases: essential enzymes and lethal targets", **Annual Review of Pharmacology and Toxicology.** 34: 191-218; April, 1994.

[20] Fayad, W. and et al. "Identification of a novel topoisomerase inhibitor effective in cells overexpressing drug efflux transporters", **Public Library of Science one.** 10(4): 38-72; October, 2009.

[21] Pommier, Y. and Kohn, K. W. "Cell cycle and checkpoints in oncology: new therapeutic targets", **Medecine Sciences.** 19: 173-186; February, 2003.

[22] Avendaño C., Carlos J. M. **Medicinal Chemistry of Anticancer Drugs.** Elsevier Science, 2008.

[23] Wikipedia. **Antimetabolite.** https://en.wikipedia.org/wiki/Antimetabolite. February 7, 2017.

[24] Pellegrini, F. and Budman, D. R. "Review: tubulin function, action of antitubulin drugs, and new drug development", **Cancer Investigation.** 23(3): 264-273, 2005.

REFERRENCES (CONTINUED)

[25] Dumontet, C. and Sikic, B. I. "Mechanisms of action of and resistance to antitubulin agents: microtubule dynamics, drug transport, and cell death", **Journal of Clinical Oncology.** 17(3): 1061-1070; March, 1999.

[26] Pearson, O. H. and et al. "Antiestrogen treatment of breast cancer: an overview", **Cancer Research.** 42(8): 3424-3429; August, 1982.

[27] Wikipedia. **Drug design**, https://en.wikipedia.org/wiki/Drug_design. February 7, 2017.

[28] Reynolds, C. H. and et al. **Drug Design: Structure and Ligand-Based Approaches.** Cambridge: Cambridge University Press, 2010.

[29] Andrew, R., **Structure-based Drug Discovery.** Berlin: Springer, 2007.

[30] Kwon, Y. and et al. "Design, Synthesis, and Biological Activity of Sulfonamide Analogues of Antofine and Cryptopleurine as Potent and Orally Active Antitumor Agents", **Journal of Medicinal Chemistry.** 58: 7749-7762; September, 2015.

[31] Jian, S. W. and et al. "Identification of Substituted Naphthotriazolediones as Novel Tryptophan 2,3-Dioxygenase (TDO) Inhibitors through StructureBased Virtual Screening", **Journal of Medicinal Chemistry.** 58: 7807-7819; September, 2015.

[33] Gach, K. and et al. "Anticancer properties of new synthetic hybrid molecules combining naphtho[2,3-*b*]furan-4,9-dione or benzo[*f*]indole-4,9-dione motif with phosphonate subunit", **European Journal of Medicinal Chemistry.** 120: 51-63; September, 2016.

[34] Afrasiabi, Z. and et al. "Appended 1,2-naphthoquinones as anticancer agents 1: synthesis, structural, spectral and antitumor activities of ortho-naphthaquinone thiosemicarbazone and its transition metal complexes", **Inorganica Chimica Acta.** 357: 271-278; January, 2004.

[35] Leite, A. C. L. and et al. "Synthesis, docking, and in vitro activity of thiosemicarbazones, aminoacyl-thiosemicarbazides and acyl-thiazolidones against Trypanosoma cruzi", **Bioorganic & Medicinal Chemistry.** 14: 3749-3757; June, 2006

REFERRENCES (CONTINUED)

[36] Rane, R. A. and et al., "Synthesis of novel 4-nitropyrrole-based semicarbazide and thiosemicarbazide hybrids with antimicrobial and anti-tubercular activity", **Bioorganic & Medicinal Chemistry.** 24: 3079-3083; May, 2014.

[37] Mahalingam, P. and et al. "Synthesis of Rigidified eIF4E/eIF4G Inhibitor-1 (4EGI-1) Mimetic and Their in Vitro Characterization as Inhibitors of Protein-Protein Interaction", **Journal of Medicinal Chemistry.** 57: 5094-5111; June, 2014.

[38] Manzano, J. I. and et al. "Arylthiosemicarbazones as antileishmanial agents", **European Journal of Medicinal Chemistry.** 123: 161-170; November, 2016.

[39] Ryu, C. K. and et al. "Synthesis and Cytotoxic Activities of 6-Chloro-7-arylamino-5,8-isoquinolinediones", **Bioorganic & Medicinal Chemistry Letters.** 9: 1075-1082; February, 1999.

[40] Kim J. S. and et al. "Synthesis and cytotoxicity of 1-substituted2-methyl-1*H*-imidazo[4,5-*g*]phthalazine-4,9-dione derivatives", **Bioorganic & Medicinal Chemistry.** 12: 3683-3686; July, 2004.

[41] Kim J. S. and et al. "Synthesis of 6-chloroisoquinoline-5,8-diones and pyrido[3,4-*b*]- phenazine-5,12-diones and evaluation of their cytotoxicity and DNA topoisomerase II inhibitory activity", **Bioorganic & Medicinal Chemistry.** 15: 451-457; January, 2007.

[42] Antonini I. and et al. "Synthesis and Antitumor Evaluation of Bis Aza-anthracene-9,10-diones and Bis Aza-anthrapyrazole-6-ones", **Journal of Medicinal Chemistry.** 51: 997-1006; February, 2008.

[43] Shanab, K. and et al. "Synthesis and biological evaluation of new cytotoxic azanaphthoquinone pyrrolo-annelated derivatives", **Bioorganic & Medicinal Chemistry Letters.** 20: 3950-3952; July, 2010.

REFERRENCES (CONTINUED)

[44] Shanab, K. and et al. "Synthesis and antiproliferative activity of new cytotoxic azanaphthoquinone pyrrolo-annelated derivatives: Part II", **Bioorganic & Medicinal Chemistry Letters.** 21: 3117-3121; June, 2011.

[45] Shahabi, M. and et al. "Synthesis and biological evaluation of new cytotoxic indazolo[4,3-*gh*]isoquinolinone derivatives", **Bioorganic & Medicinal Chemistry Letters.** 23: 1846-1852; March, 2013.

[46] Leepasert, T. and et al. "Synthesis and antiproliferative activity of new cytotoxic tri- and tetraazabenzo[3,2-*a*]fluorene-5,6-dione derivatives", **Bioorganic & Medicinal Chemistry Letters.** 23: 5264-5266; October, 2013.

[48] Shanab, K. and et al. "Synthesis and biological evaluation of novel cytotoxic azanaphthoquinone annelated pyrrolo oximes", **Bioorganic & Medicinal Chemistry Letters.** 17: 6091-6095; November, 2007.

[49] Pongprom, N. and et al. "Synthesis of new Benzo[*f*]isoindole-4,9-diones as anticancer Compounds", **Monatsh Chem.** 141: 53-62; March ,2010.

APPENDICES

APPENDIX A

Computational calculation data

Table A.1 Structure of azanaphthoquinone pyrrolo annelated derivative

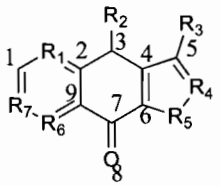

cpd	R1	R2	R3	R4	R5	R6	R7
74	C	NOH	H	C	$N(CH_2)_2N(CH_3)_2$	C	N
75	C	$NOCH_3$	H	C	$N(CH_2)_2N(CH_3)_2$	C	N
76	C	$NOCH_2COOCH_2CH_3$	H	C	$N(CH_2)_2N(CH_3)_2$	C	N
77	C	$NOCH_2CH_2OH$	H	C	$N(CH_2)_2N(CH_3)_2$	C	N
78	C	$NO(CH_2)_2N(CH_3)_2$	H	C	$N(CH_2)_2N(CH_3)_2$	C	N
79	C	$NNHCH_2CH_2N(CH_3)_2$	H	C	$N(CH_2)_2N(CH_3)_2$	C	N
80	C	piperidine-CH_3, OCH_3	H	C	$N(CH_2)_2N(CH_3)_2$	C	N
81	C	piperidine,$OCH_2CH_2N(CH_3)_2$	H	C	$N(CH_2)_2N(CH_3)_2$	C	N
82	C	piperidine-$(CH_2)_2N(CH_3)_2$, OH	H	C	$N(CH_2)_2N(CH_3)_2$	C	N
83	C	piperidine-(CH2)2OCH3, OH	H	C	$N(CH_2)_2N(CH_3)_2$	C	N
84	C	O	H	C	NCH2-epoxide	C	N
14	C	O	H	C	$N(CH_2)_2$-pyrrolidine	C	N
86	C	O	H	C	$N(CH_2)_2N(CH_3)_2$	C	N
87	C	O	H	C	$NCH_2CHOHCH2$-aziridine	C	N
88	C	O	H	C	$N(CH_2)_4$-aziridine	C	N
89	C	O	H	C	$N(CH_2)_4OH$	C	N
90	C	O	$(CH_2)_2N(CH_3)_2$	C	$N(CH_2)_2$-aziridine	C	N
91	C	O	$(CH_2)_2N(CH_3)_2$	C	$N(CH_2)_3$-aziridine	C	N
92	N	O	H	C	$N(CH_2)_2N(CH_3)_2$	C	N
93	N	O	H	C	$N(CH_2)_3N(CH_3)_2$	C	N
94	N	O	H	C	$N(CH_2)_2N(CH_3)_2$	N	C

Table A.1 Structure of azanaphthoquinone pyrrolo annelated derivative (Continued)

cpd	R1	R2	R3	R4	R5	R6	R7
95	N	$NNH(CH_2)_2N(CH_3)_2$	H	C	$N(CH_2)_2$-pyrrolidine	C	N
96	C	O	H	NCH_2-epoxide	C	C	N
97	C	O	H	$N(CH_2)_3CHOHCH_2$-epoxide	C	C	N
98	C	O	H	$N(CH_2)_4$aziridine	C	C	N
99	C	O	H	$N(CH_2)_7$-aziridine	C	C	N
100	C	O	H	$N(CH_2)_6CHOHCH_2$-aziridine	C	C	N
101	C	O	$(CH_2)_3$-aziridine	$N(CH_2)_3N(CH_3)_2$	C	C	N
102	C	$NNHCHSNH_2$	H	C	$N(CH_2)_2N(CH_3)_2$	C	N
103	C	$NNH(CH_2)_3N(CH_3)_2$	H	C	$N(CH_2)_3N(CH_3)_2$	C	N
104	C	$NNHCHSNH_2$	H	C	$N(CH2)_3N(CH_3)_3$	C	N
105	C	$NNHCHSNH_2$	H	C	$N(CH_2)_2$-pyrrolidine	C	N
106	C	O	H	C	$N(CH_2)_2$-piperidine	C	N
107	C	$NNH(CH_2)_2$-piperidine	H	C	$N(CH_2)_2$-piperidine	C	N
108	C	$NNHCHSNH_2$	H	C	$N(CH_2)_2$-piperidine	C	N
109	C	$NNHCHSNH_2$	H	C	$N(CH_2)_3$-piperidine	C	N
110	C	O	H	C	$N(CH_2)_2N(CH_3)_2$	C	N

[a]test set, [b]outlier

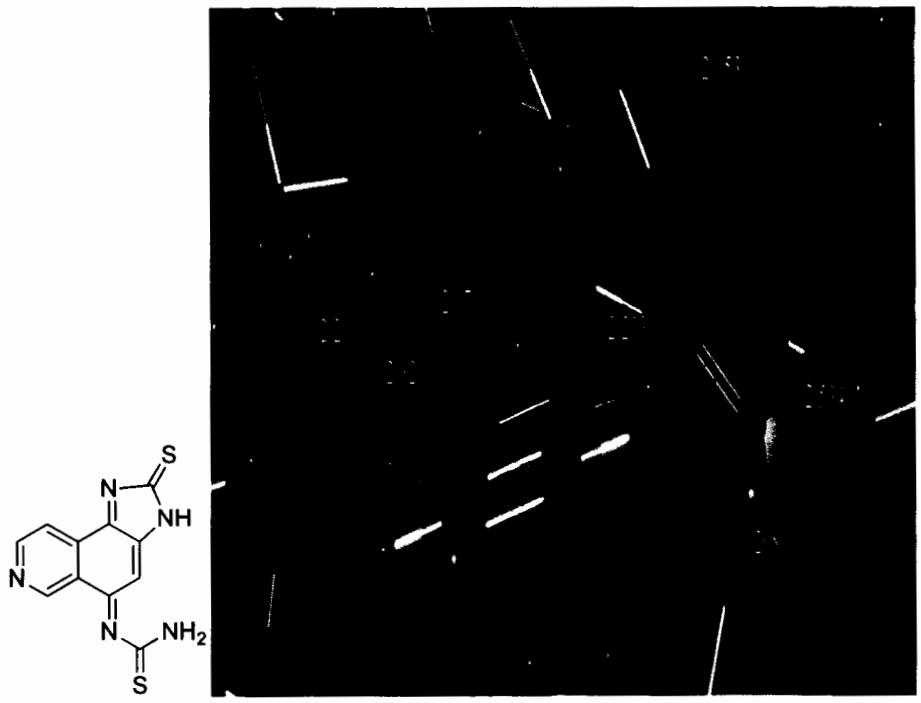

Figure A.1 Molecular docking of compound 69

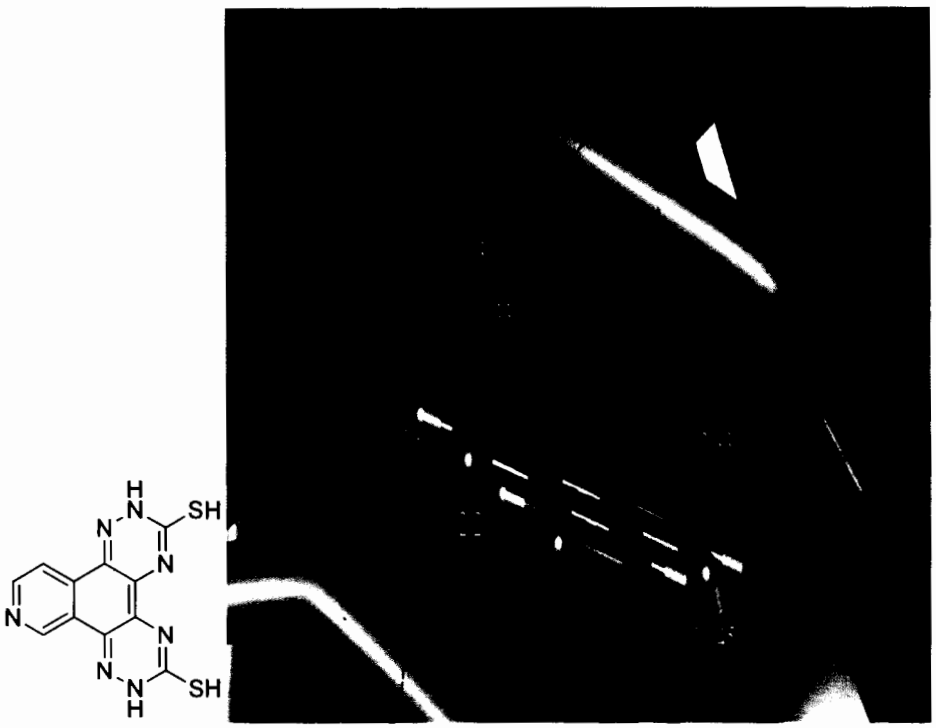

Figure A.2 Molecular docking of compound 19

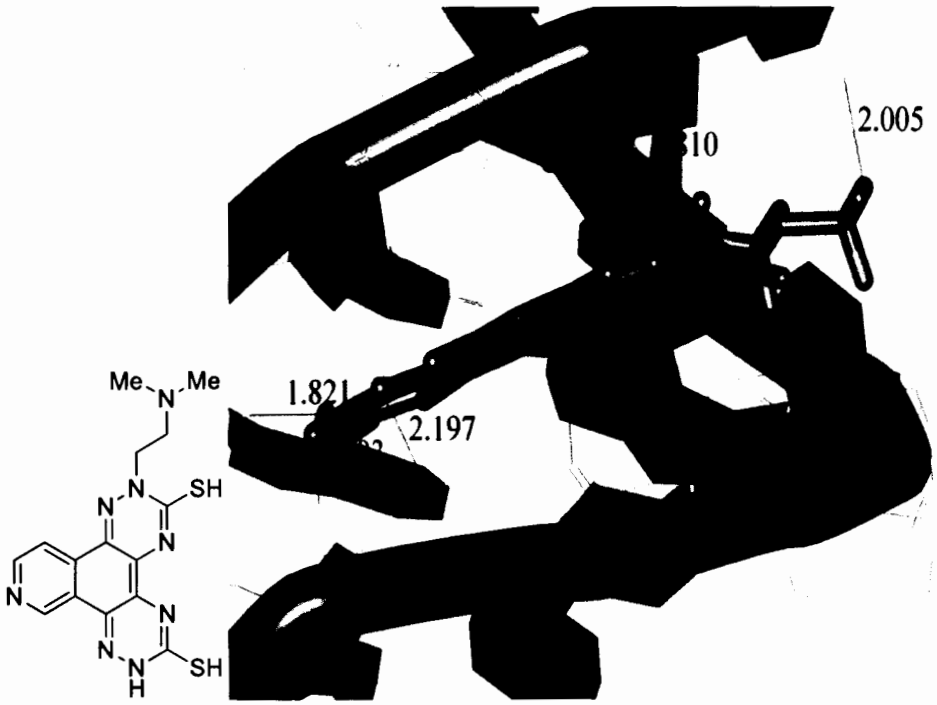

Figure A.3 Molecular docking of compound 20a

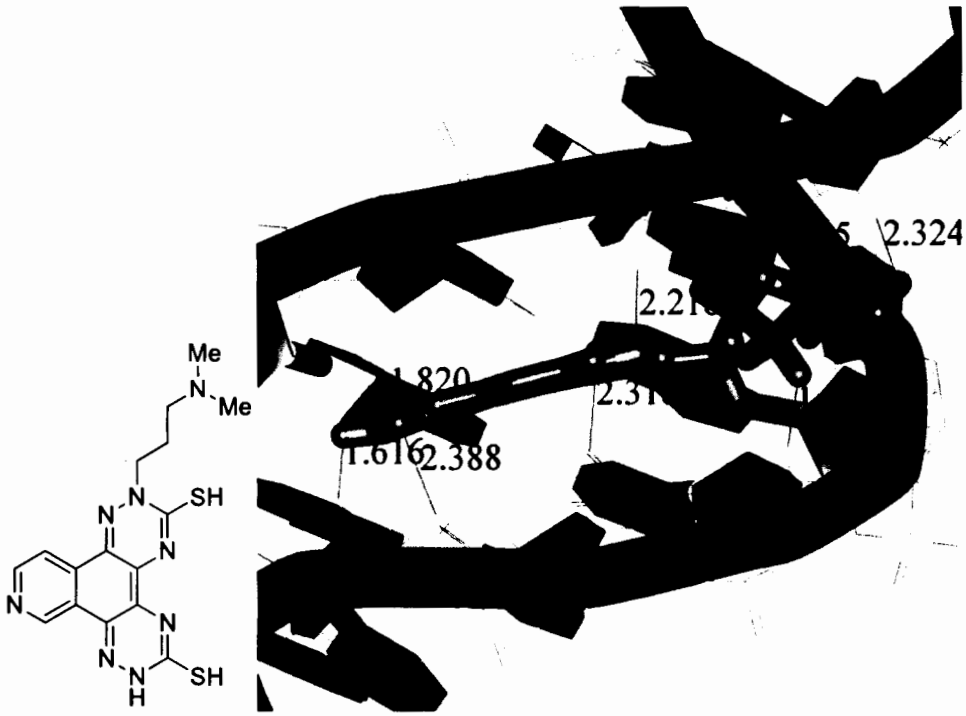

Figure A.4 Molecular docking of compound 20b

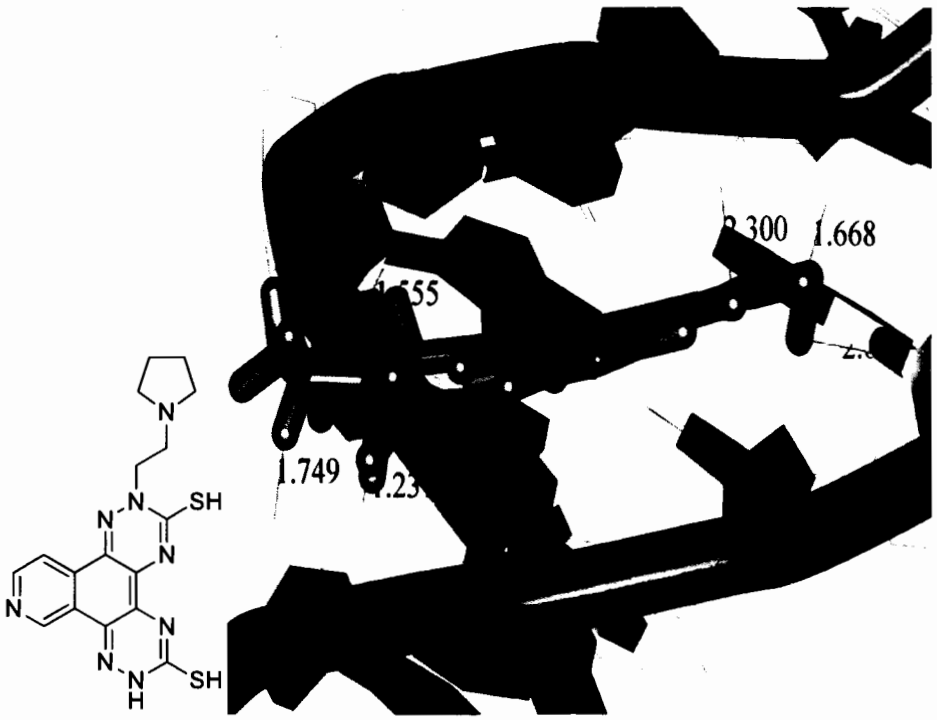

Figure A.5 Molecular docking of compound 20c

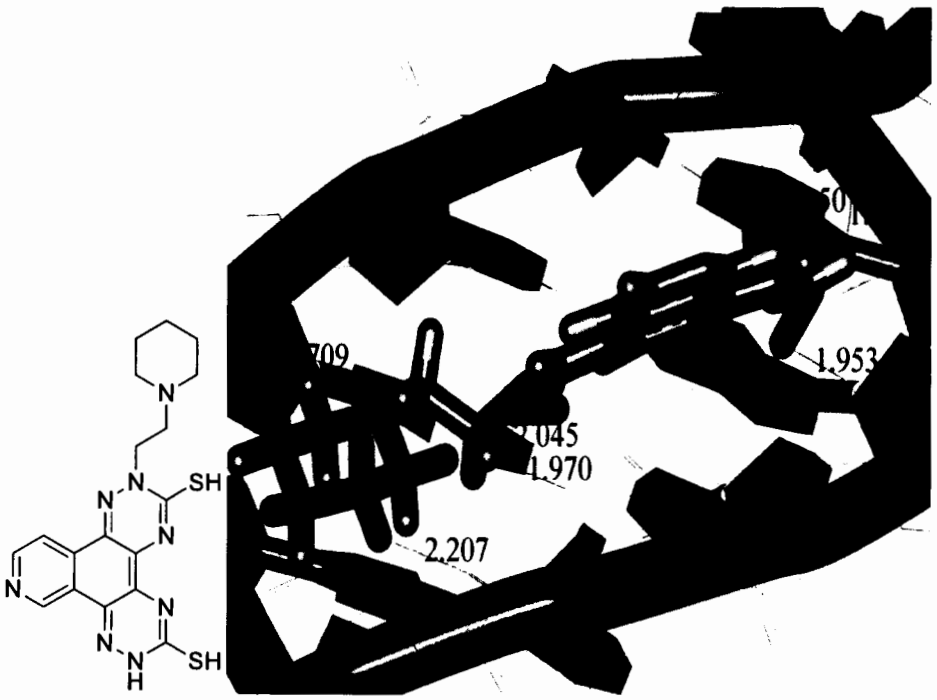

Figure A.6 Molecular docking of compound 20d

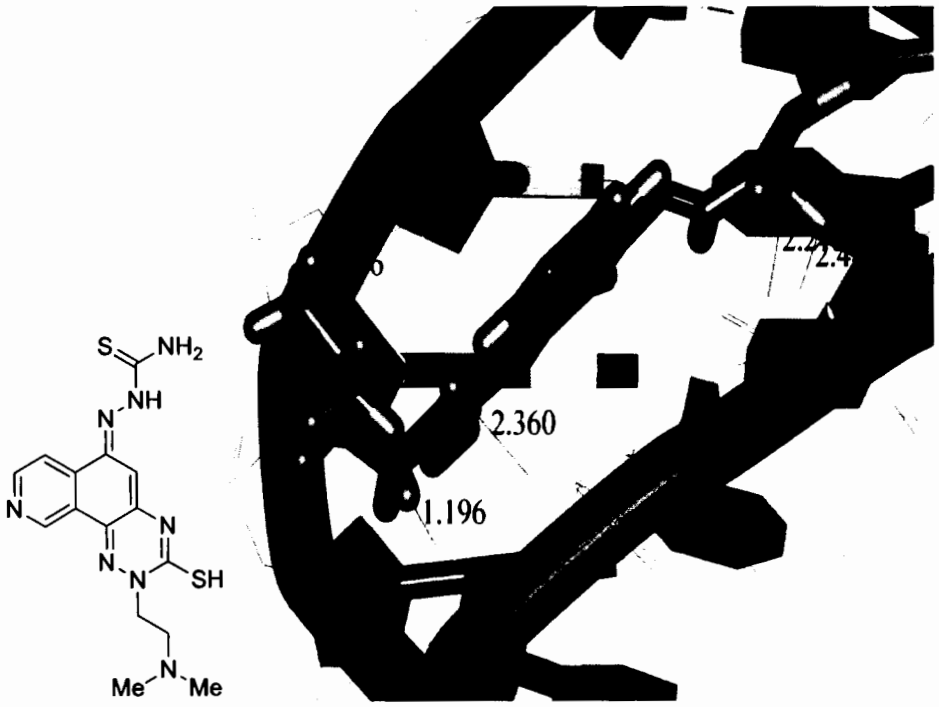

Figure A.7 Molecular docking of compound 22a

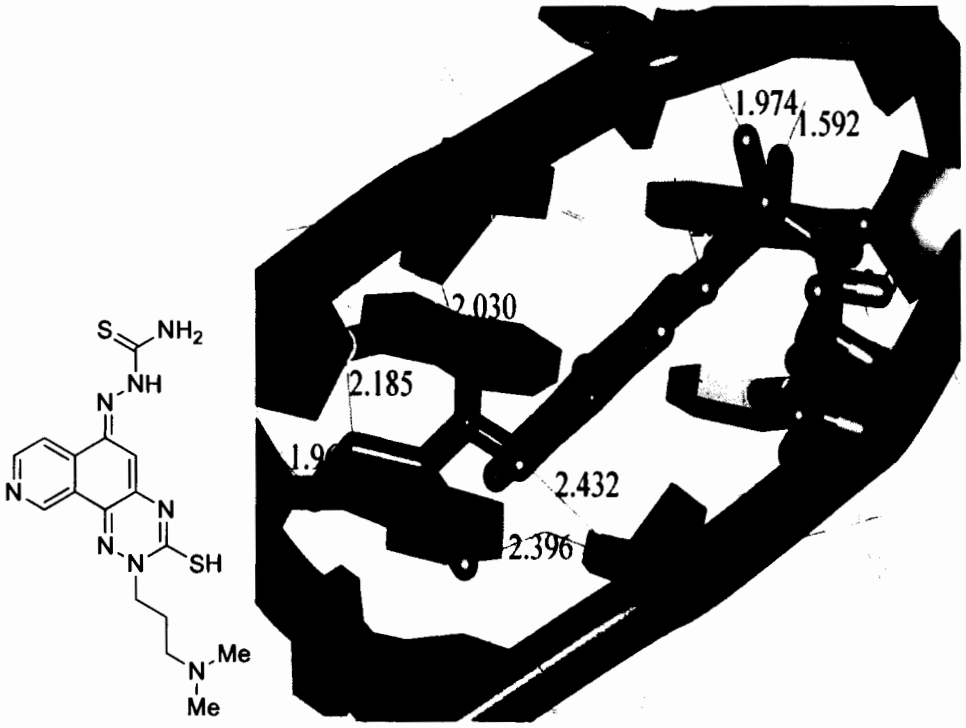

Figure A.8 Molecular docking of compound 22d

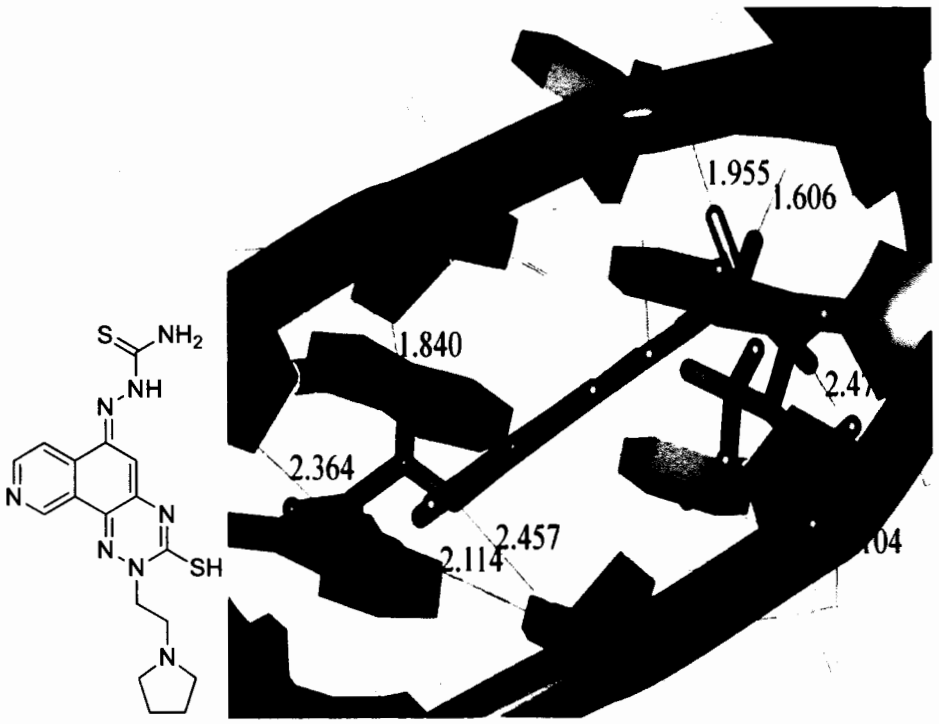

Figure A.9 Molecular docking of compound 22b

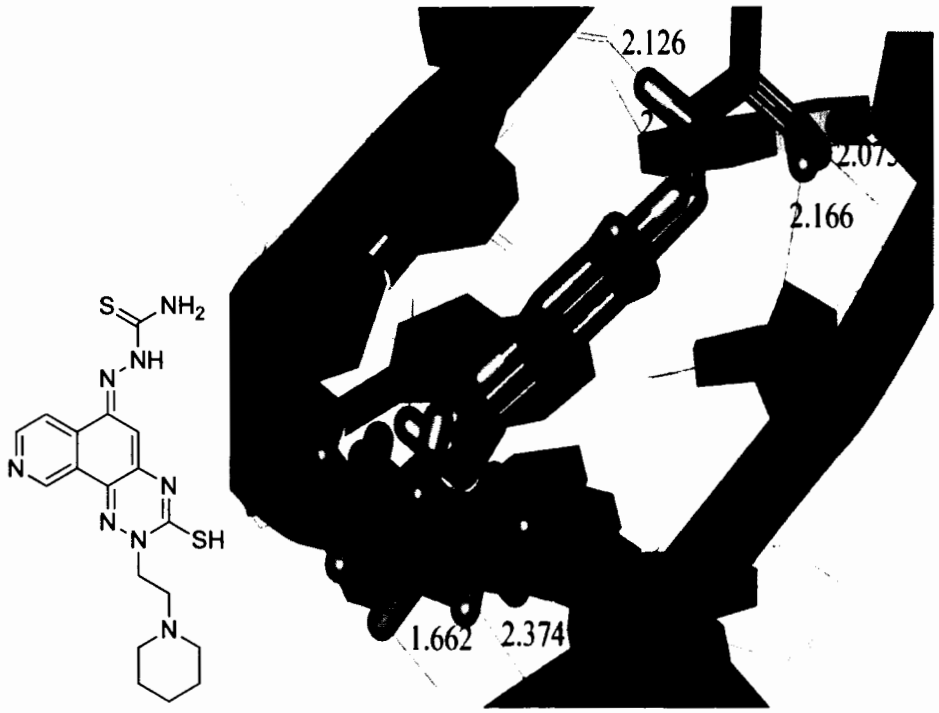

Figure A.10 Molecular docking of compound 22c

Figure A.11 Molecular docking of compound 19

Table A.2 Detail of minor groove binder

Compound	Position	Radius	Interaction
69	H′-H9	2.209	van der waals interactions
	N3-H	2.076	H-bonding interaction
	N4′-N	2.321	H-bonding interaction
	O2-H7	2.213	H-bonding interaction
	H2-H10	2.053	van der waals interactions
	H4′-N	2.534	H-bonding interaction
	H5′2-H	2.321	van der waals interactions
19	H1′-H	1.983	van der waals interactions
	H3-H	1.838	H-bonding interaction
	H4′-H	1.639	van der waals interactions
	H5′2-H8	2.261	van der waals interactions
	H2-S	2.330	H-bonding interaction
	H1′-H	1.945	van der waals interactions

Table A.2 Detail of minor groove binder (Continued)

Compound	Position	Radius	Interaction
20a	H4′-H	1.603	van der waals interactions
	H5′2-H8	2.197	van der waals interactions
	H1′-H	1.821	van der waals interactions
	O2-H	2.316	H-bonding interaction
	H4′-H16	2.005	van der waals interactions
	H4′-H15	2.447	van der waals interactions
	H2-S	2.032	H-bonding interaction
	H1′-H9	1.810	van der waals interactions
	H4′-H13	1.700	van der waals interactions
	H5′2-H12	1.415	van der waals interactions
	H4′-H15	2.324	van der waals interactions
20b	N3-H	1.820	H-bonding interaction
	H4′-H	1.616	van der waals interactions
	H5′2-H8	2.388	van der waals interactions
	O2-H	2.318	H-bonding interaction
	H4′-N	2.218	H-bonding interaction
	H1′-H	2.075	van der waals interactions
	H4′-H	1.668	van der waals interactions
	H5′2-H8	2.300	van der waals interactions
	H4′-H19	1.749	van der waals interactions
20c	H5′2-H12	1.231	van der waals interactions
	H1′-H11	1.717	van der waals interactions
	H1′-H15	1.555	van der waals interactions
	H5′2-H17	1.565	van der waals interactions
	O2-H13	2.235	H-bonding interaction

Table A.2 Detail of minor groove binder (Continued)

Compound	Position	Radius	Interaction
20d	H1′-H	1.953	van der waals interactions
	H4′-H	1.545	van der waals interactions
	H5′2-H8	2.250	van der waals interactions
	O2-H19	2.207	H-bonding interaction
	H5′2-H16	1.709	van der waals interactions
	H4′-H10	1.970	van der waals interactions
	H2-S	2.045	H-bonding interaction
22a	H1′-H	2.482	van der waals interactions
	H5′2-N	2.275	H-bonding interaction
	H4′-H12	1.196	van der waals interactions
	H5′2-H9	2.360	van der waals interactions
	H5′1-H20	1.466	van der waals interactions
	H5′1-H22	1.396	van der waals interactions
	H4′-H13	2.045	van der waals interactions
	H5′2-H11	1.592	van der waals interactions
22d	O2-H	1.974	H-bonding interaction
	H4′-H9	2.225	van der waals interactions
	O2-H	2.396	H-bonding interaction
	H5′2-S	2.185	H-bonding interaction
	H4′-H10	1.965	van der waals interactions
	O4′-H	2.030	H-bonding interaction
	H1′-N	2.432	H-bonding interaction

Table A.2 Detail of minor groove binder (Continued)

Compound	Position	Radius	Interaction
	O11′-H14	2.104	H-bonding interaction
	H5′1-H16	1.998	van der waals interactions
	H4′-H12	2.471	van der waals interactions
	H5′2-H10	1.606	van der waals interactions
	O2-H	1.955	H-bonding interaction
22b	O4′-H	2.364	H-bonding interaction
	O2-H	2.114	H-bonding interaction
	H1′-N	2.457	H-bonding interaction
	H4′-H9	2.216	van der waals interactions
	O4′-H	1.840	H-bonding interaction
22c	H1′-H	2.109	van der waals interactions
	O2-H	2.126	H-bonding interaction
	H5′2-N	2.075	H-bonding interaction
	H4′-H	2.166	van der waals interactions
	O3′-H14	2.374	H-bonding interaction
	H5′2-H13	1.662	van der waals interactions
	H4′-H15	1.773	van der waals interactions
	H5′2-H7	2.308	van der waals interactions
	H1′-H	1.205	van der waals interactions
19	N3-H	2.082	H-bonding interaction
	H2-H9	2.103	van der waals interactions
	O2-H9	2.470	H-bonding interaction
	H4′-H	1.925	van der waals interactions
	H4′-H	2.356	van der waals interactions
	O2-H	2.131	H-bonding interaction
	H5′2-S	2.301	H-bonding interaction
	H4′-H	2.395	van der waals interactions
	H1′-H	1.982	van der waals interactions

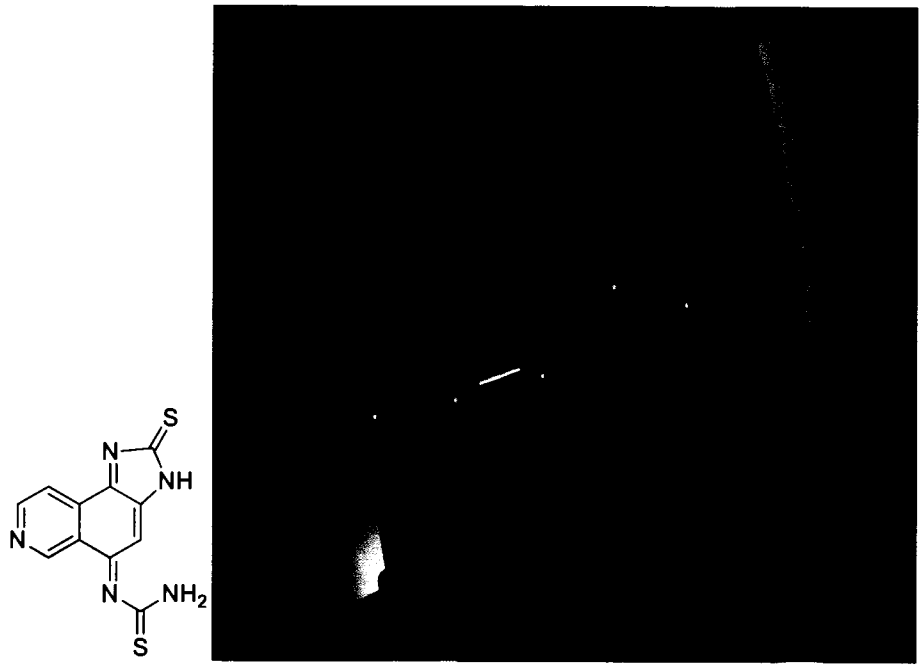

Figure A.12 Molecular docking of compound 69

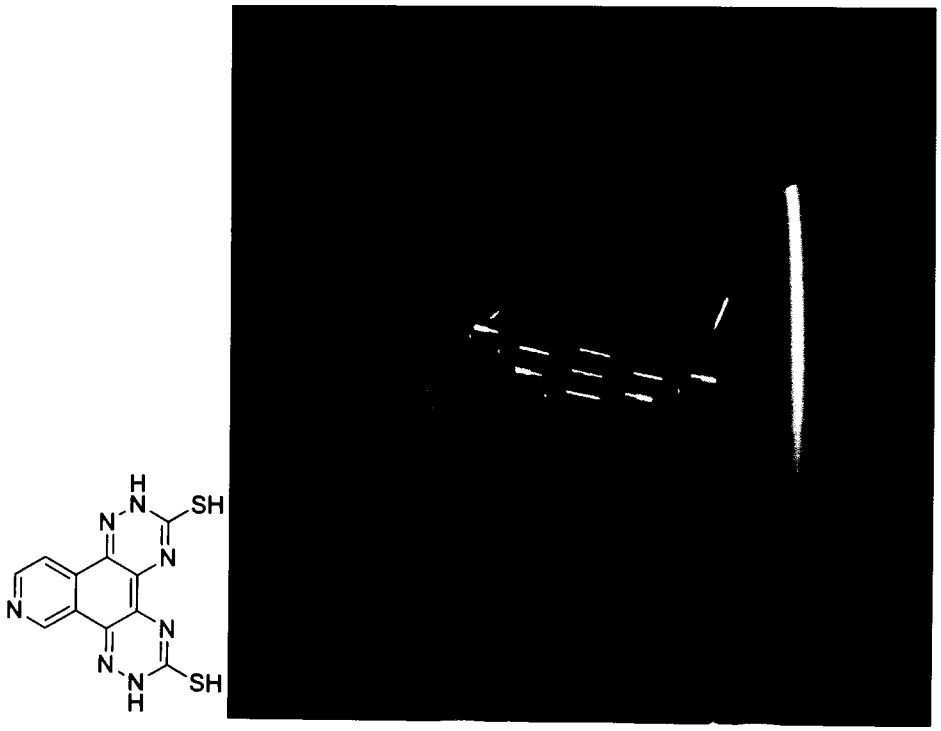

Figure A.13 Molecular docking of compound 19

Figure A.14 Molecular docking of compound 20a

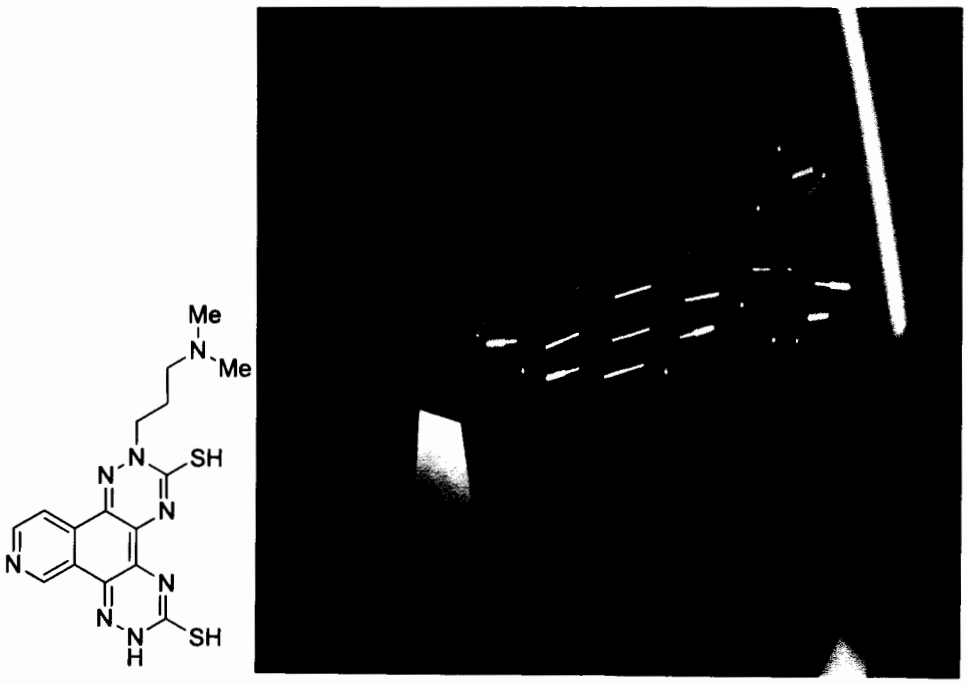

Figure A.15 Molecular docking of compound 20b

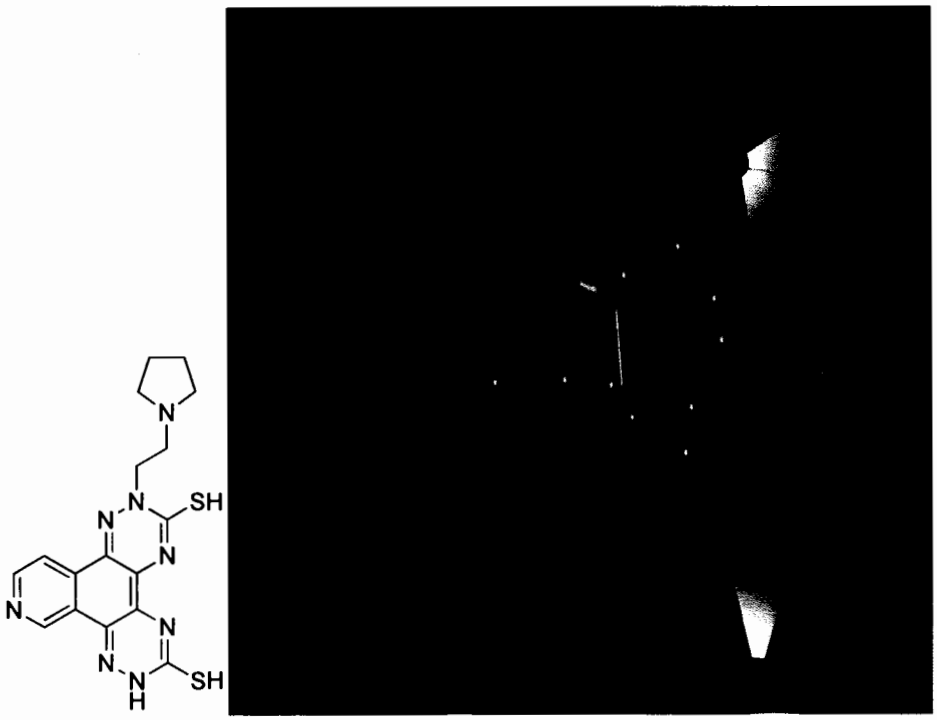

Figure A.16 Molecular docking of compound 20c

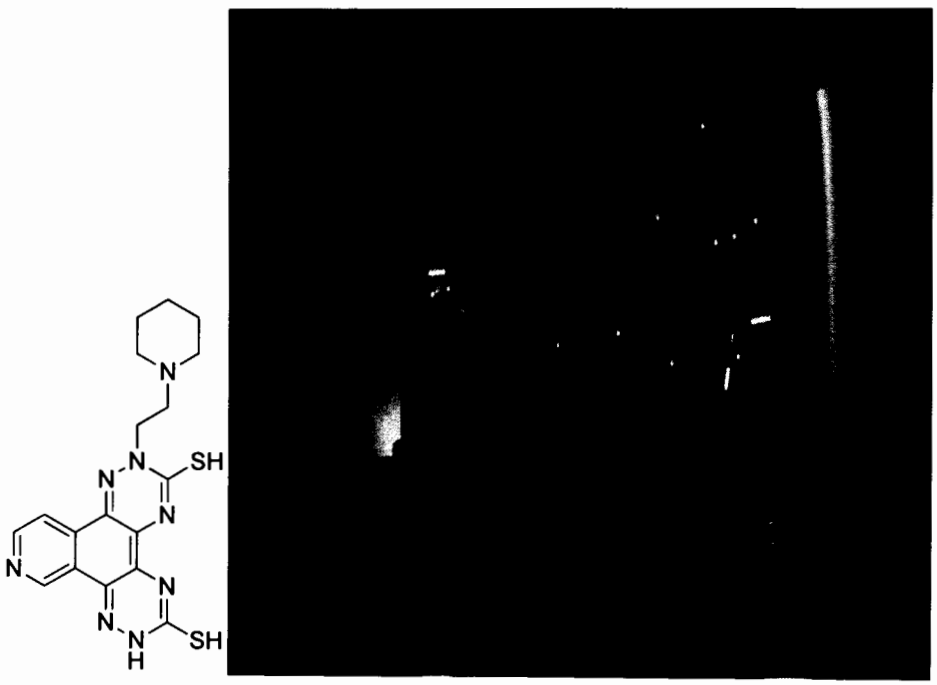

Figure A.17 Molecular docking of compound 20d

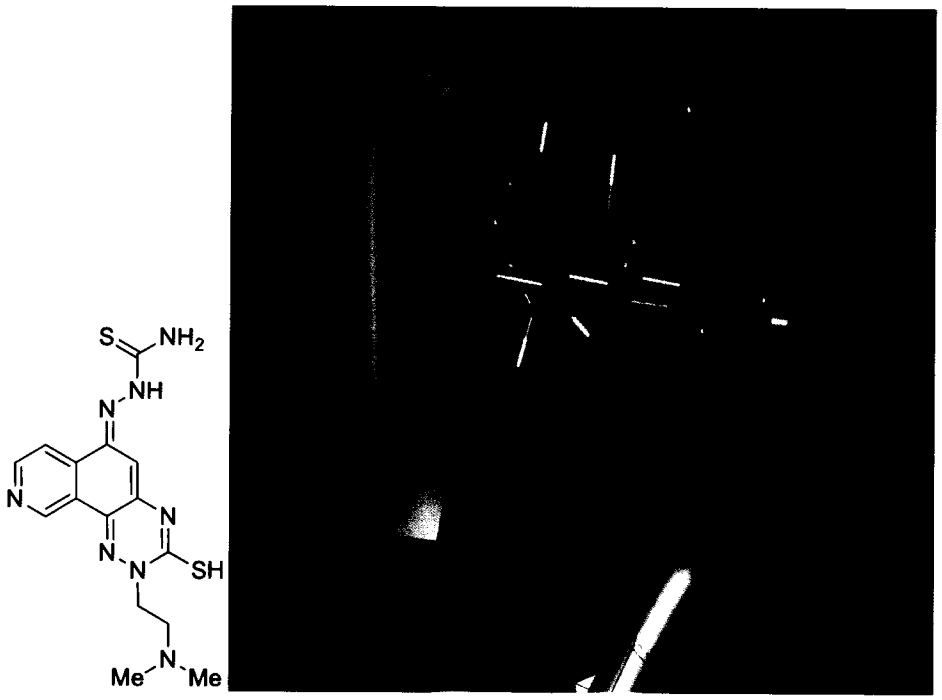

Figure A.18 Molecular docking of compound 22a

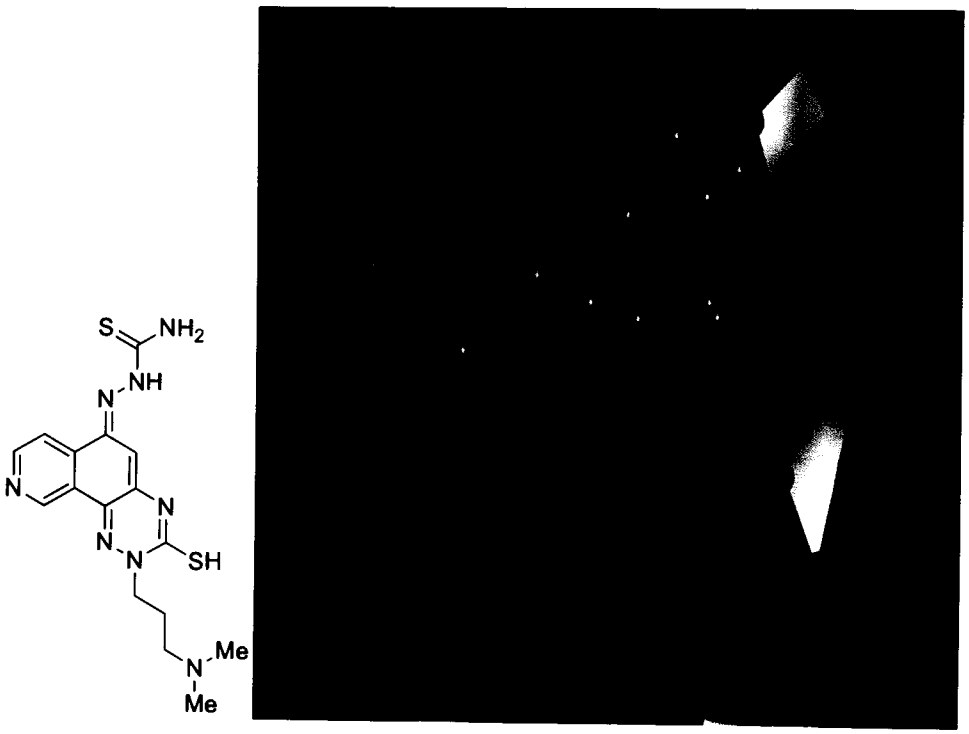

Figure A.19 Molecular docking of compound 22d

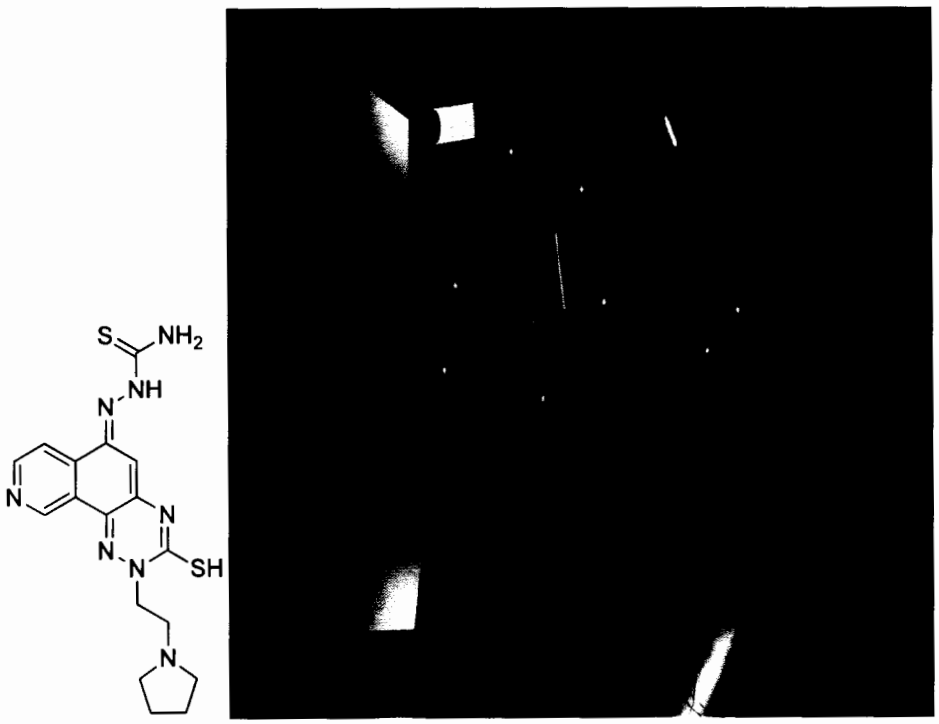

Figure A.20 Molecular docking of compound 22b

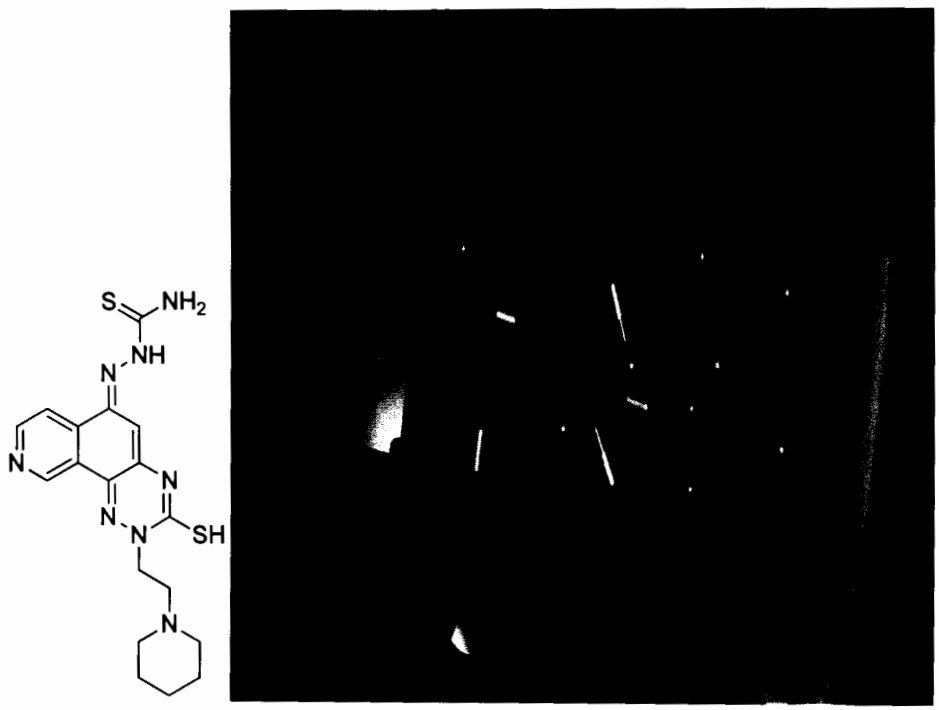

Figure A.21 Molecular docking of compound 22c

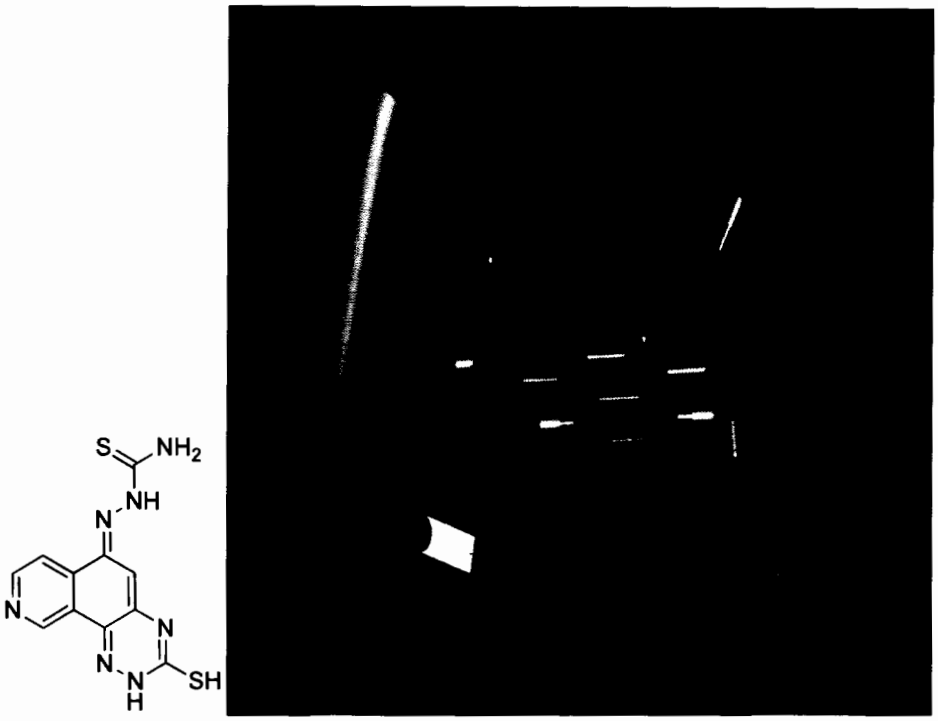

Figure A.22 Molecular docking of compound 19

Table A.3 Detail of major groove binder

Compound	Position	Radius	Interaction
	H′-H9	2.209	van der waals interactions
	N3-H	2.076	H-bonding interaction
	N4′-N	2.321	H-bonding interaction
69	O2-H7	2.213	H-bonding interaction
	H2-H10	2.053	van der waals interactions
	H4′-N	2.534	H-bonding interaction
	H5′2-H	2.321	van der waals interactions
	H1′-H	1.983	van der waals interactions
	H3-H	1.838	H-bonding interaction
19	H4′-H	1.639	van der waals interactions
	H5′2-H8	2.261	van der waals interactions
	H2-S	2.330	H-bonding interaction

Table A.3 Detail of major groove binder (Continued)

Compound	Position	Radius	Interaction
20a	H4′-H	1.603	van der waals interactions
	H5′2-H8	2.197	van der waals interactions
	H1′-H	1.821	van der waals interactions
	O2-H	2.316	H-bonding interaction
	H4′-H16	2.005	van der waals interactions
	H4′-H15	2.447	van der waals interactions
	H2-S	2.032	H-bonding interaction
	H1′-H9	1.810	van der waals interactions
	H4′-H13	1.700	van der waals interactions
	H5′2-H12	1.415	van der waals interactions
	H4′-H15	2.324	van der waals interactions
20b	N3-H	1.820	H-bonding interaction
	H4′-H	1.616	van der waals interactions
	H5′2-H8	2.388	van der waals interactions
	O2-H	2.318	H-bonding interaction
	H4′-N	2.218	H-bonding interaction
	H1′-H	2.075	van der waals interactions
20c	H4′-H	1.668	van der waals interactions
	H5′2-H8	2.300	van der waals interactions
	H4′-H19	1.749	van der waals interactions
	H5′2-H12	1.231	van der waals interactions
	H1′-H11	1.717	van der waals interactions
	H1′-H15	1.555	van der waals interactions
	H5′2-H17	1.565	van der waals interactions
	O2-H13	2.235	H-bonding interaction

Table A.3 Detail of major groove binder (Continued)

Compound	Position	Radius	Interaction
20d	H1′-H	1.953	van der waals interactions
	H4′-H	1.545	van der waals interactions
	H5′2-H8	2.250	van der waals interactions
	O2-H19	2.207	H-bonding interaction
	H5′2-H16	1.709	van der waals interactions
	H4′-H10	1.970	van der waals interactions
	H2-S	2.045	H-bonding interaction
22a	H1′-H	2.482	van der waals interactions
	H5′2-N	2.275	H-bonding interaction
	H4′-H12	1.196	van der waals interactions
	H5′2-H9	2.360	van der waals interactions
	H5′1-H20	1.466	van der waals interactions
	H5′1-H22	1.396	van der waals interactions
	H4′-H13	2.045	van der waals interactions
	H5′2-H11	1.592	van der waals interactions
22d	O2-H	1.974	H-bonding interaction
	H4′-H9	2.225	van der waals interactions
	O2-H	2.396	H-bonding interaction
	H5′2-S	2.185	H-bonding interaction
	H4′-H10	1.965	van der waals interactions
	O4′-H	2.030	H-bonding interaction
	H1′-N	2.432	H-bonding interaction

Table A.3 Detail of major groove binder (Continued)

Compound	Position	Radius	Interaction
	O11′-H14	2.104	H-bonding interaction
	H5′1-H16	1.998	van der waals interactions
	H4′-H12	2.471	van der waals interactions
	H5′2-H10	1.606	van der waals interactions
	O2-H	1.955	H-bonding interaction
22b	O4′-H	2.364	H-bonding interaction
	O2-H	2.114	H-bonding interaction
	H1′-N	2.457	H-bonding interaction
	H4′-H9	2.216	van der waals interactions
	O4′-H	1.840	H-bonding interaction
	H1′-H	2.109	van der waals interactions
	O2-H	2.126	H-bonding interaction
	H5′2-N	2.075	H-bonding interaction
	H4′-H	2.166	van der waals interactions
22c	O3′-H14	2.374	H-bonding interaction
	H5′2-H13	1.662	van der waals interactions
	H4′-H15	1.773	van der waals interactions
	H5′2-H7	2.308	van der waals interactions
	H1′-H	1.205	van der waals interactions
	N3-H	2.082	H-bonding interaction
	H2-H9	2.103	van der waals interactions
	O2-H9	2.470	H-bonding interaction
	H4′-H	1.925	van der waals interactions
19	H4′-H	2.356	van der waals interactions
	O2-H	2.131	H-bonding interaction
	H5′2-S	2.301	H-bonding interaction
	H4′-H	2.395	van der waals interactions
	H1′-H	1.982	van der waals interactions

APPENDIX B

Characterization data

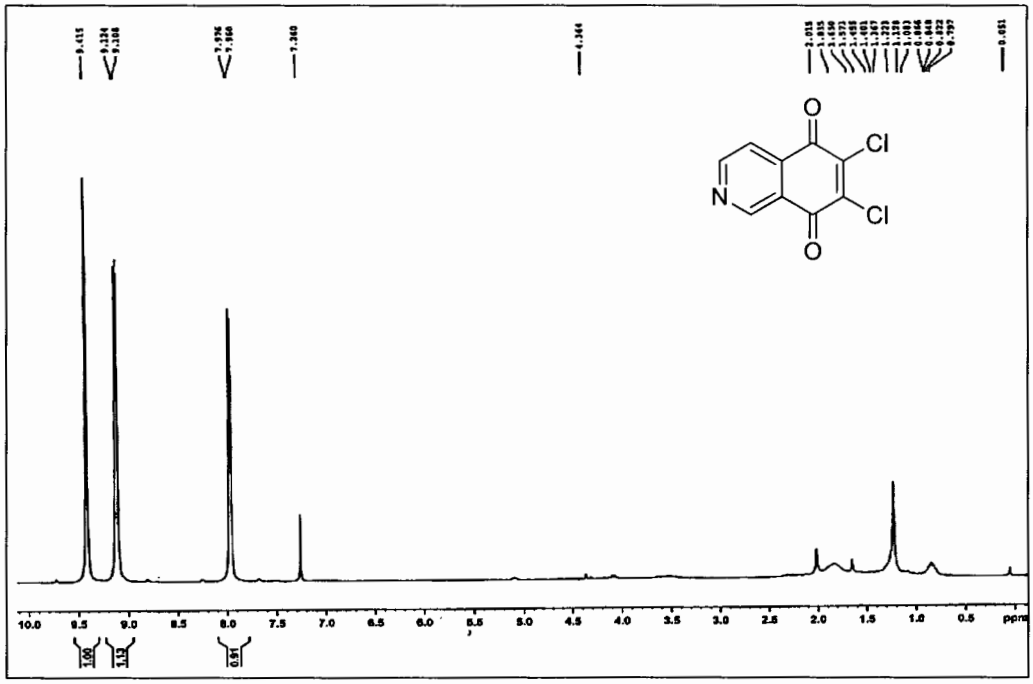

Figure B.1 ^{1}H-NMR spectrum of 6,7-dichloroisoquinoline-5,8-dione (18) in $CDCl_3$

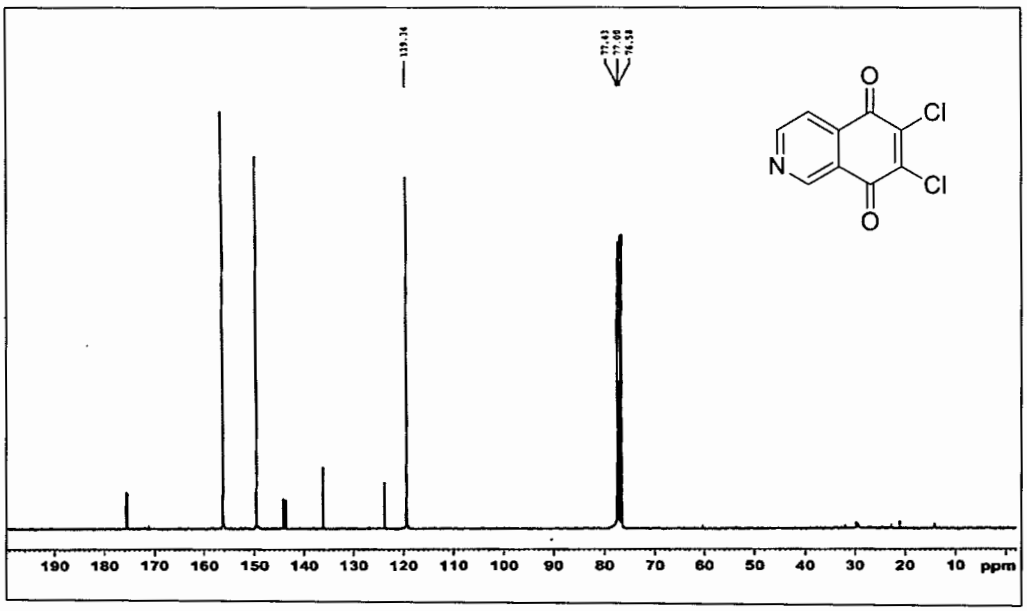

Figure B.2 ^{13}C-NMR spectrum of 6,7-dichloroisoquinoline-5,8-dione (18) in $CDCl_3$

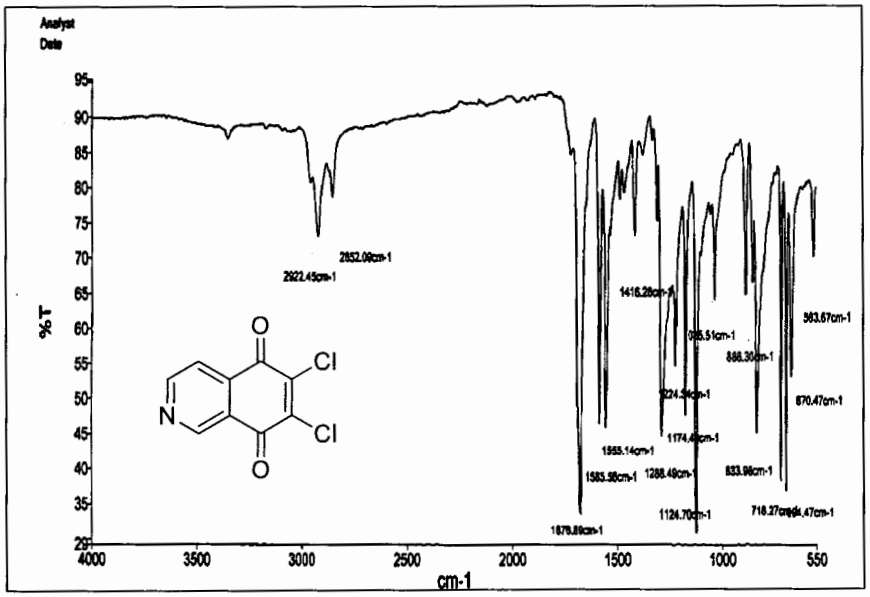

Figure B.3 IR spectrum of 6,7-dichloroisoquinoline-5,8-dione (18)

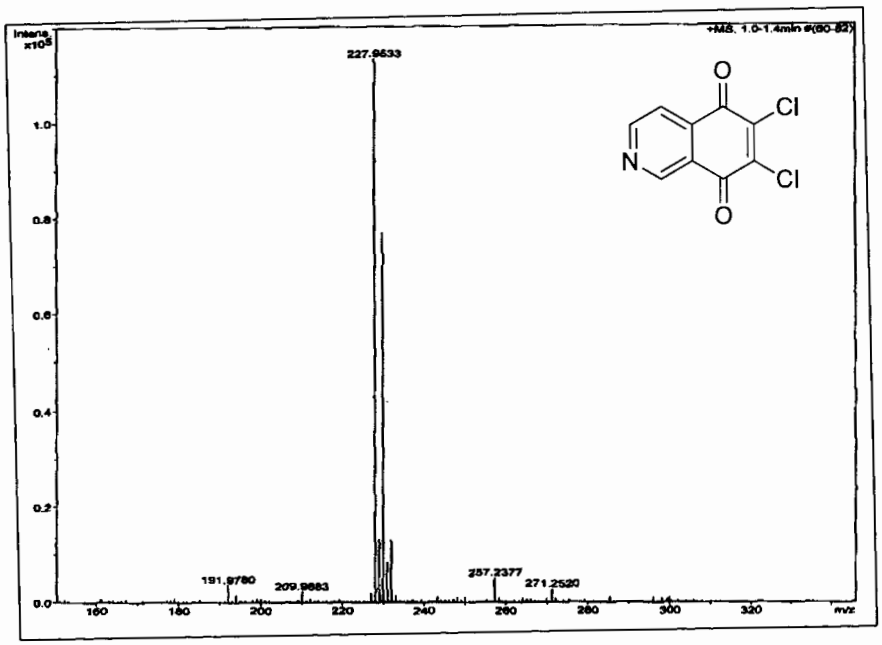

Figure B.4 Mass spectrum of 6,7-dichloroisoquinoline-5,8-dione (18)

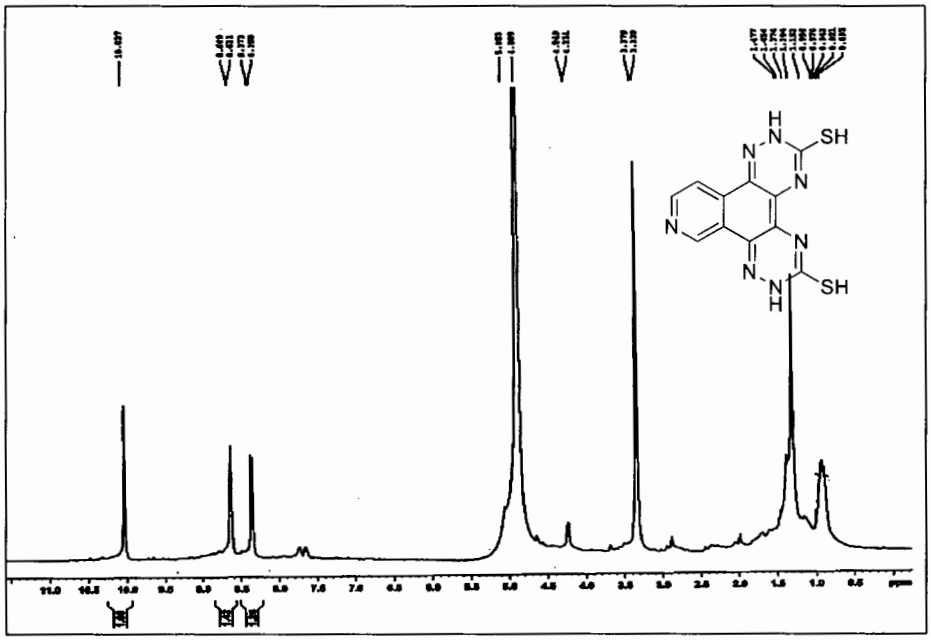

Figure B.5 ^{1}**H-NMR spectrum of cyclization under acidic condition product in CD_3OD**

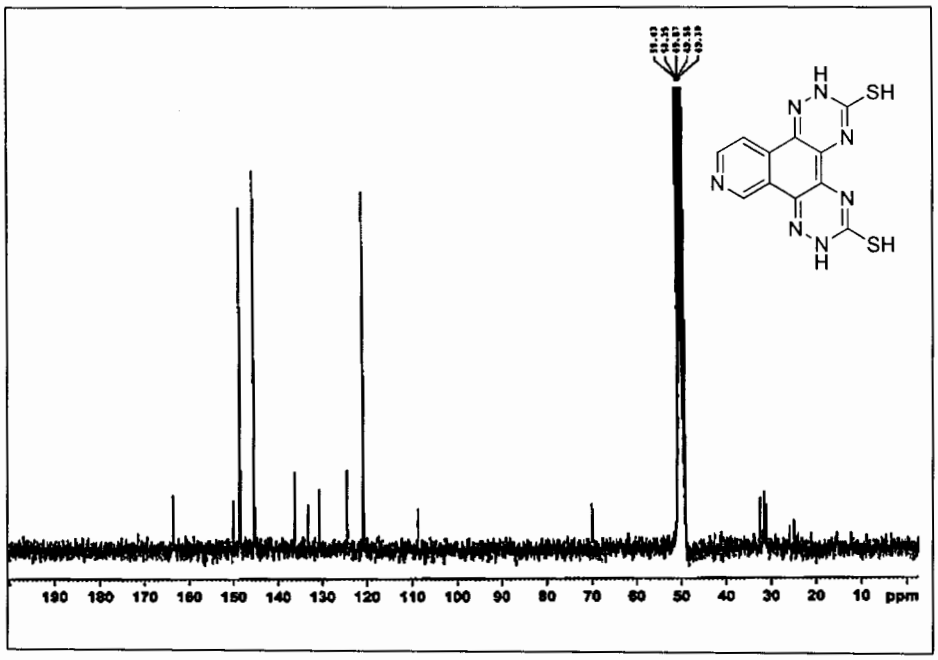

Figure B.6 ^{13}**C-NMR spectrum of cyclization under acidic condition product in CD_3OD**

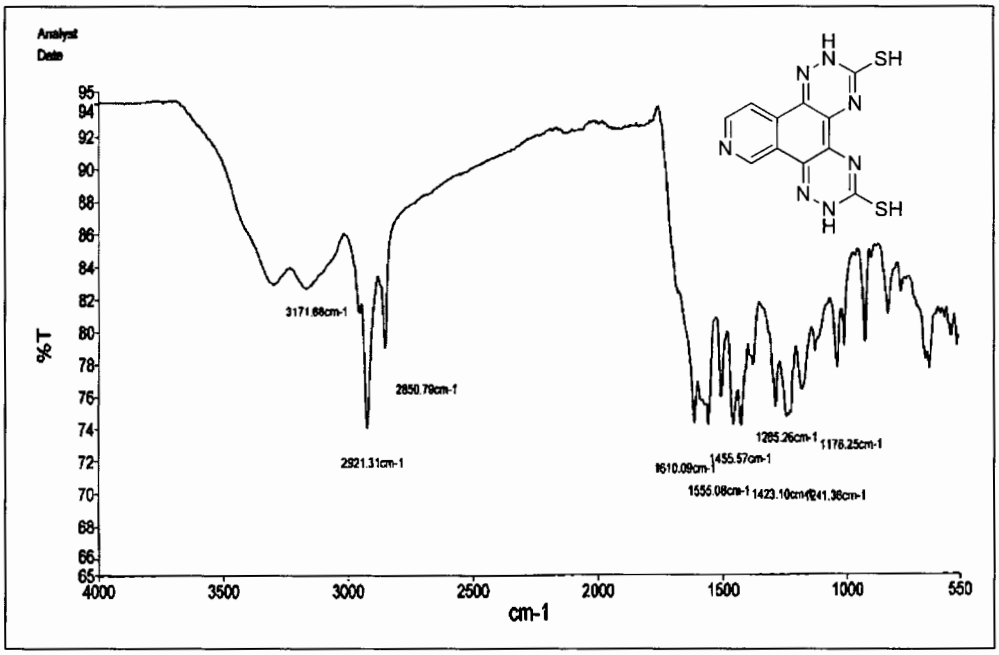

Figure B.7 IR spectrum of cyclization under acidic condition product

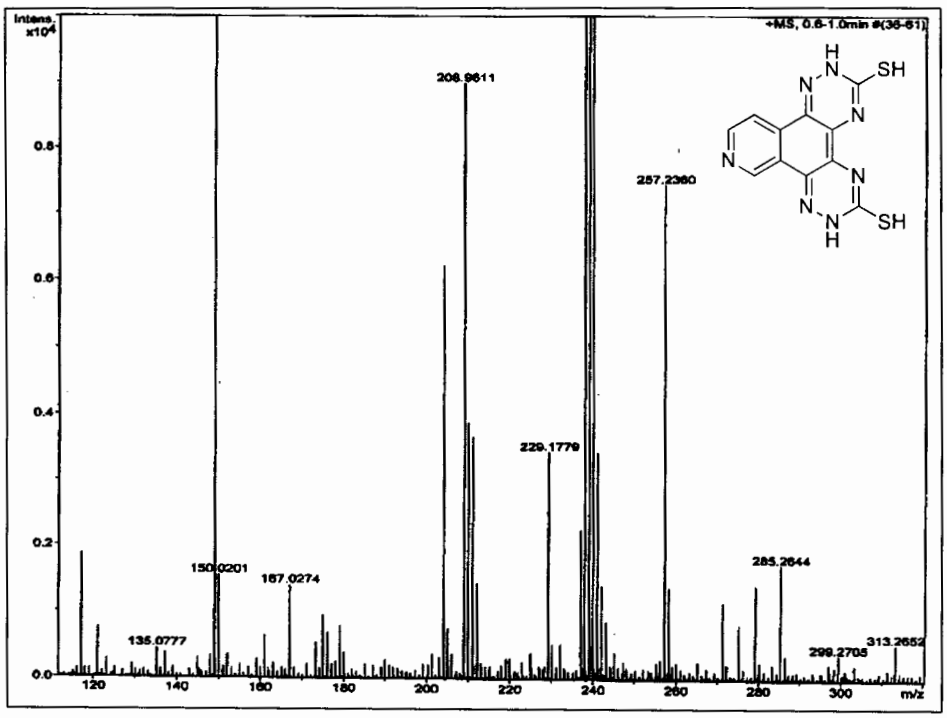

Figure B.8 Mass spectrum of cyclization under acidic condition product

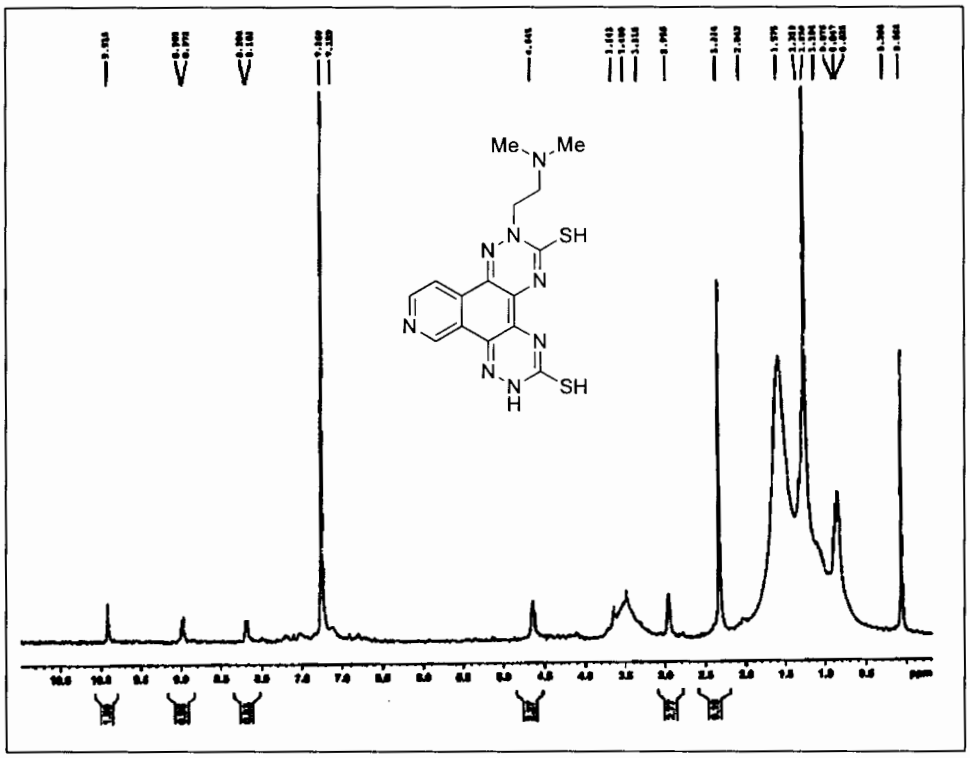

Figure B.9 ^{1}H-NMR spectrum of alkylated product 20a in acidic series in $CDCl_3$

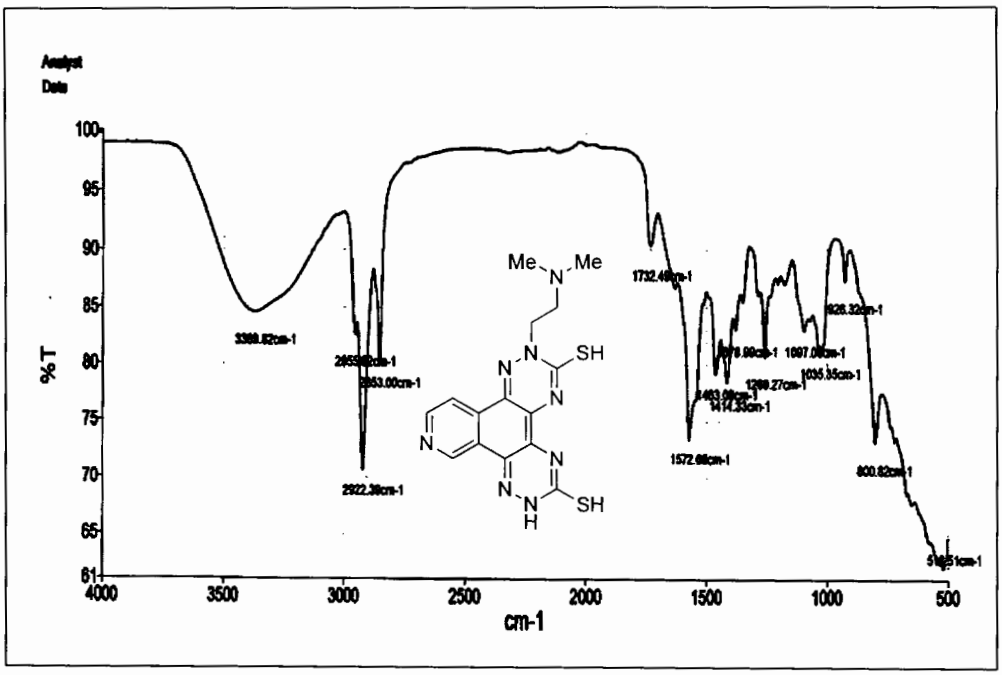

Figure B.10 IR spectrum of alkylated product 20a in acidic series

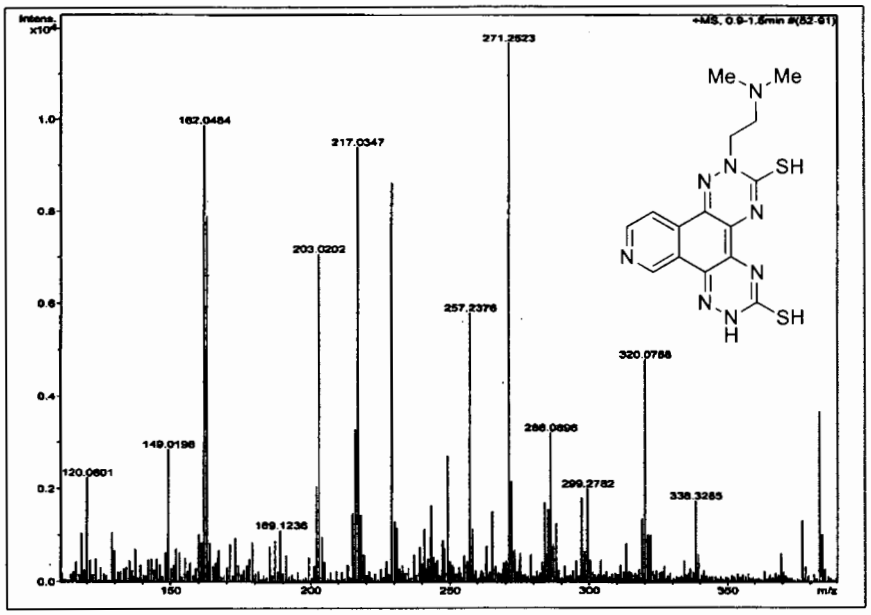

Figure B.11 Mass spectrum of alkylated product 20a in acidic series

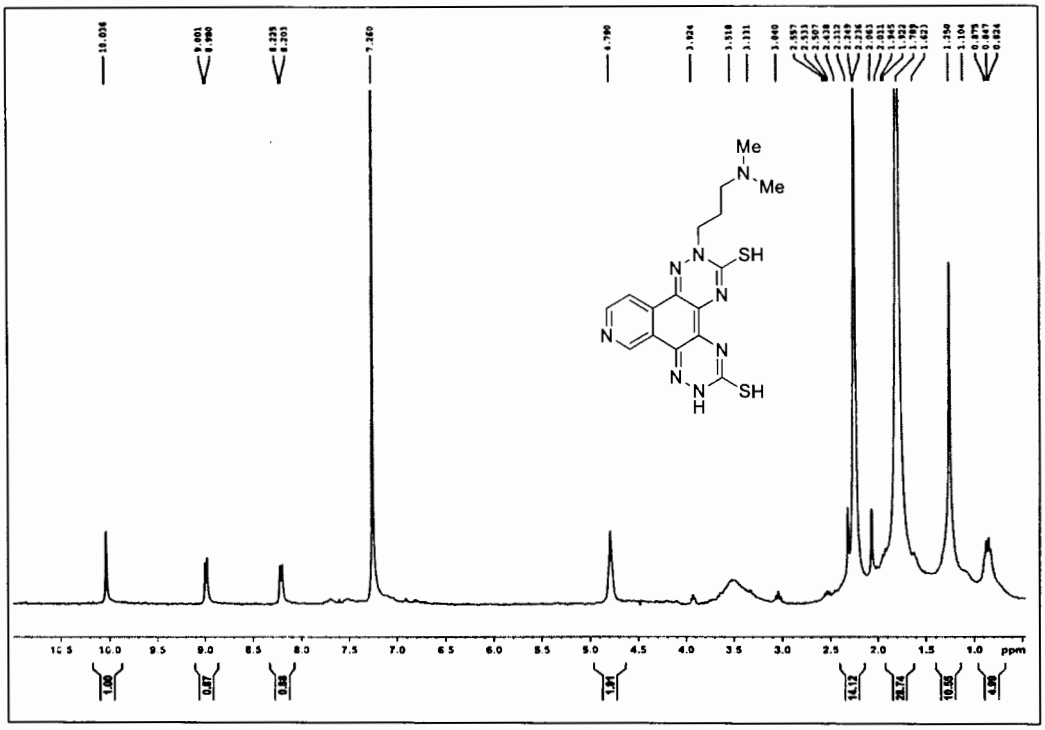

Figure B.12 ^{1}H-NMR spectrum of alkylated product 20b in acidic series in $CDCl_3$

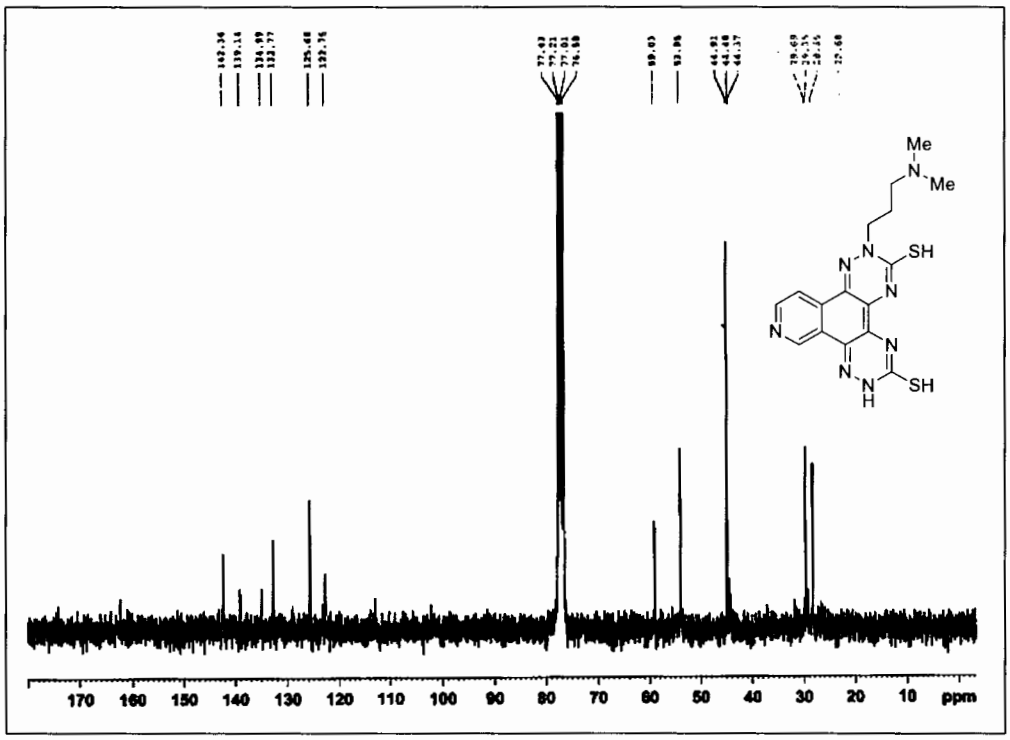

Figure B.13 ^{13}C-NMR spectrum of alkylated product 20b in acidic series in $CDCl_3$

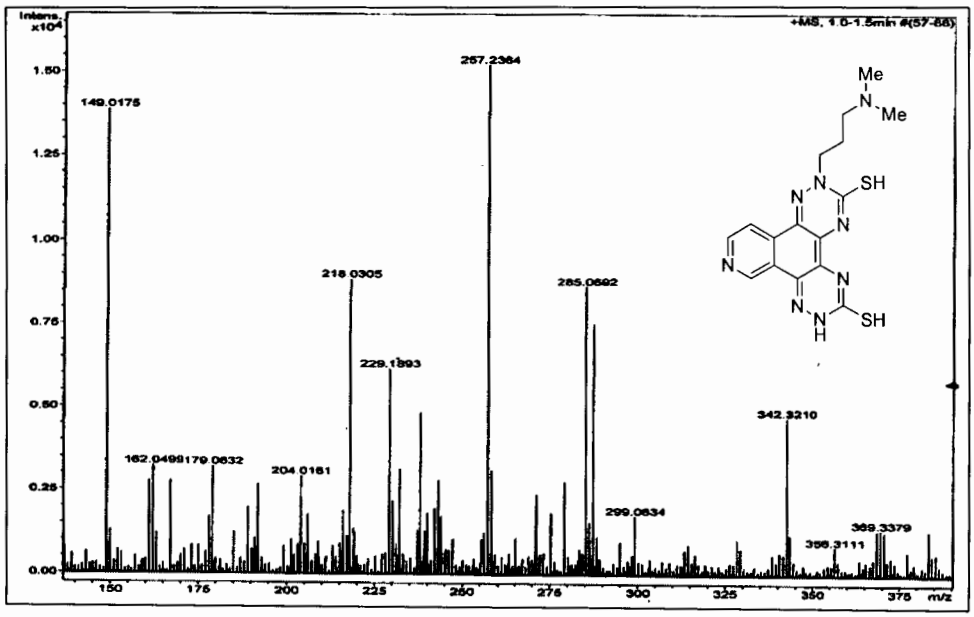

Figure B.14 Mass spectrum of alkylated product 20b in acidic series

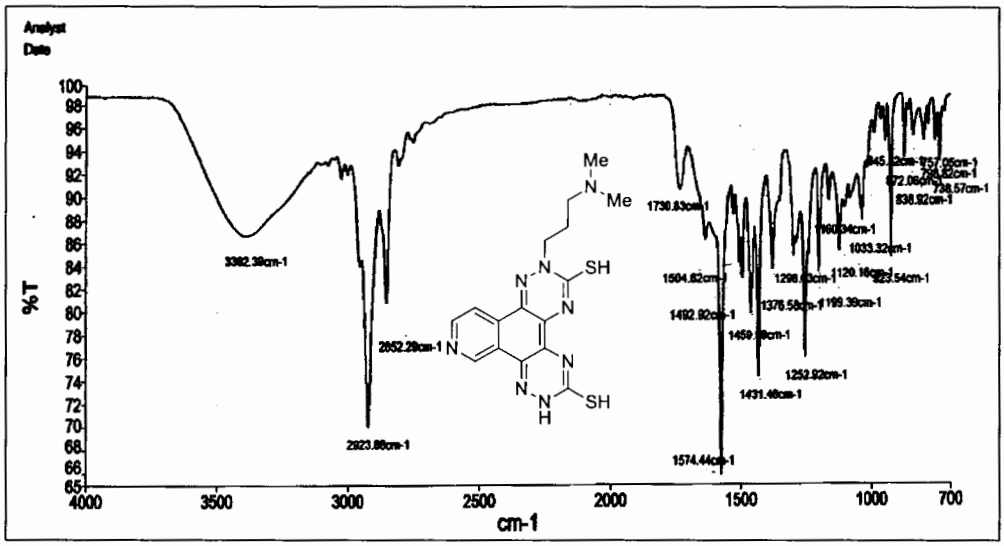

Figure B.15 IR spectrum of alkylated product 20b in acidic series

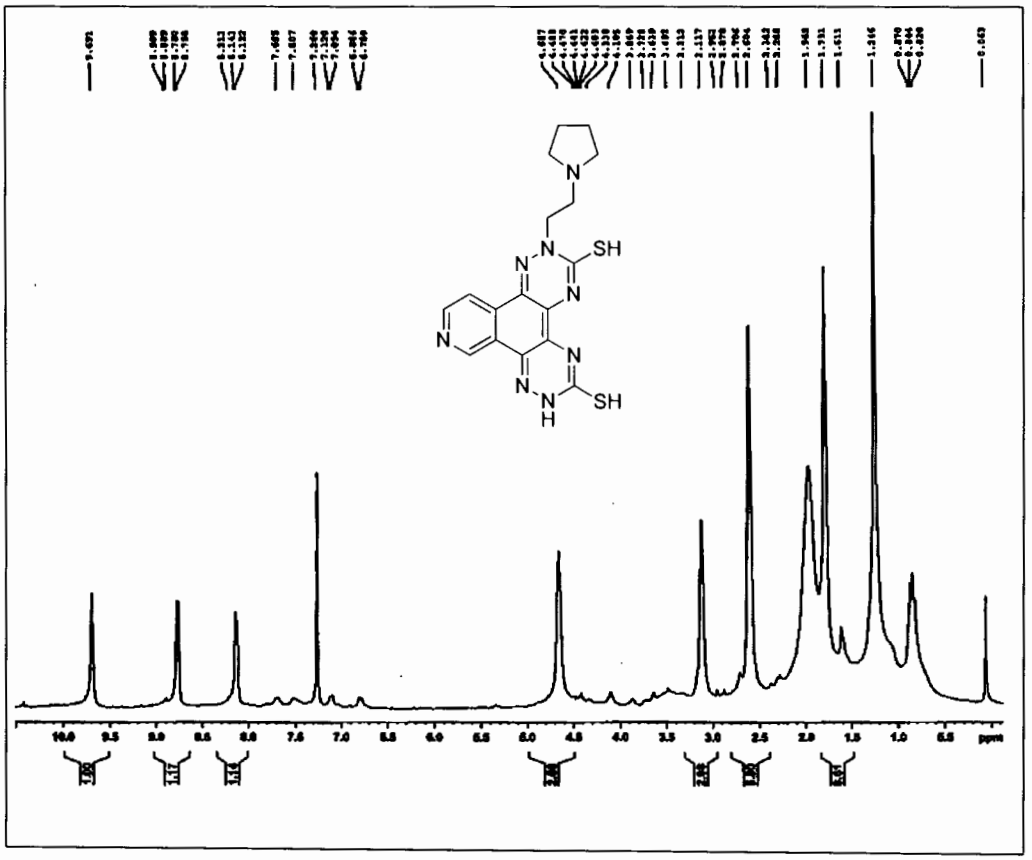

Figure B.16 ^{1}H-NMR spectrum of alkylated product 20c in acidic series in $CDCl_3$

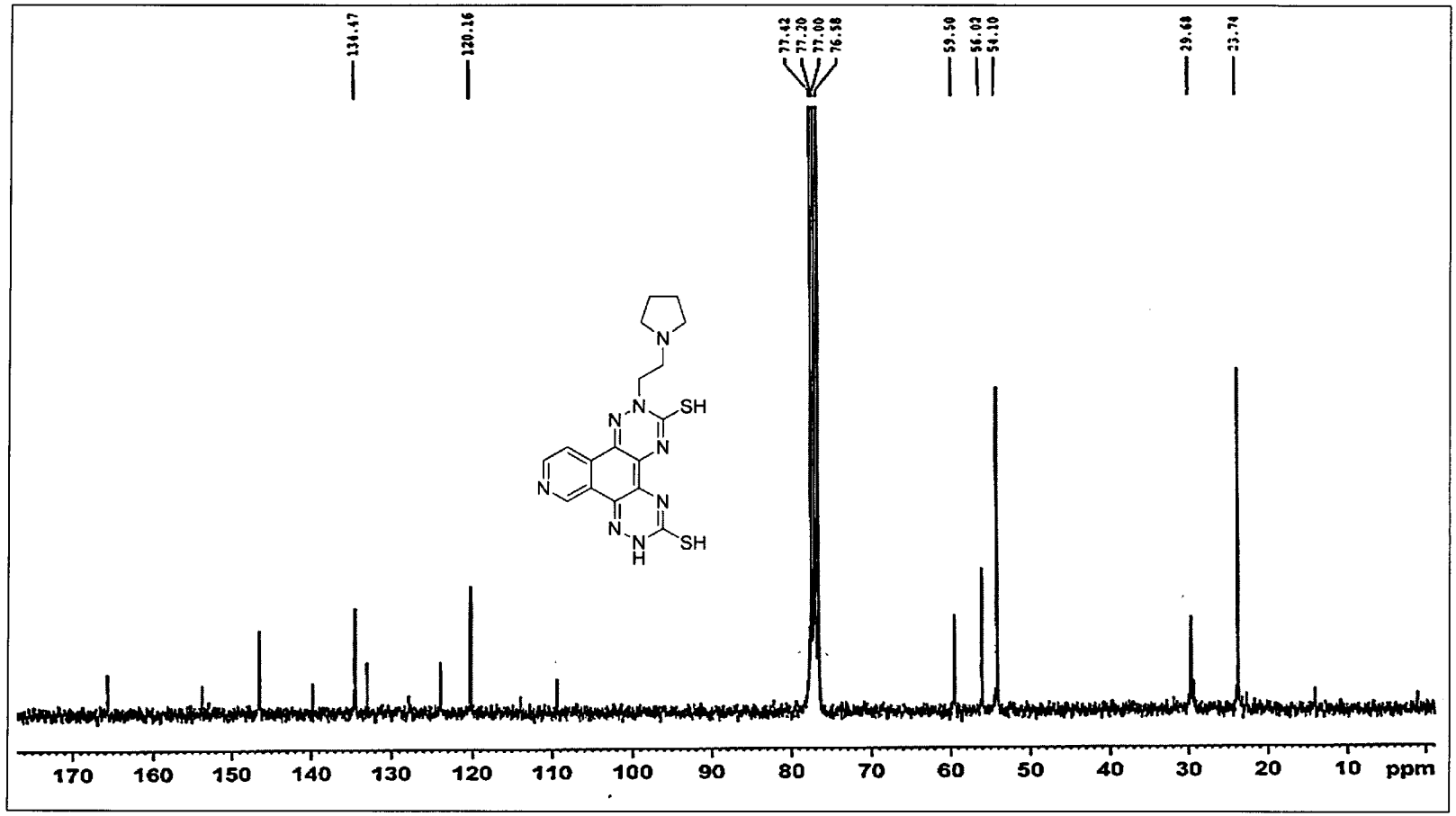

Figure B.17 ^{13}C-NMR spectrum of alkylated product 20c in acidic series in $CDCl_3$

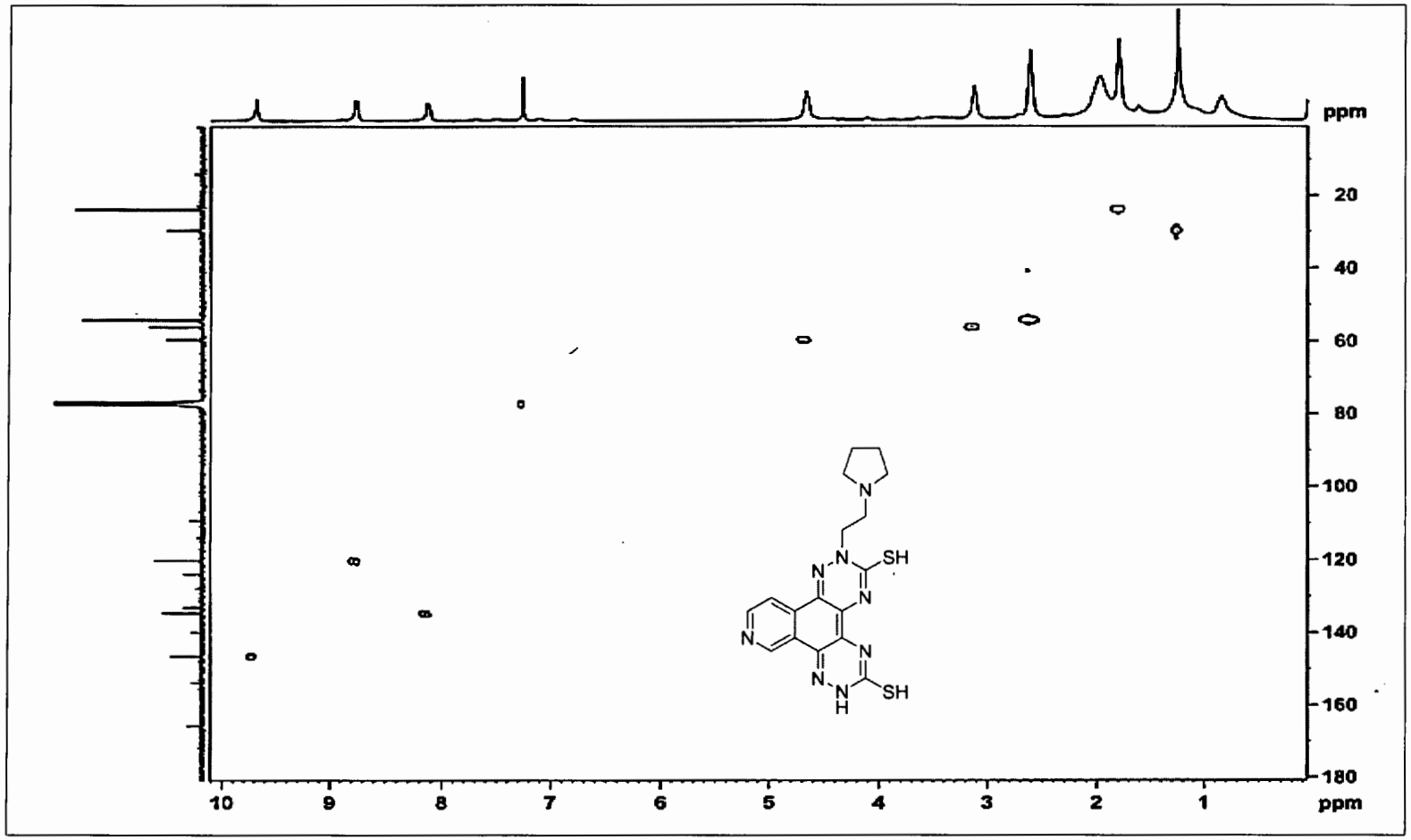

Figure B.18 HMQC spectrum of alkylated product 20c in acidic series in $CDCl_3$

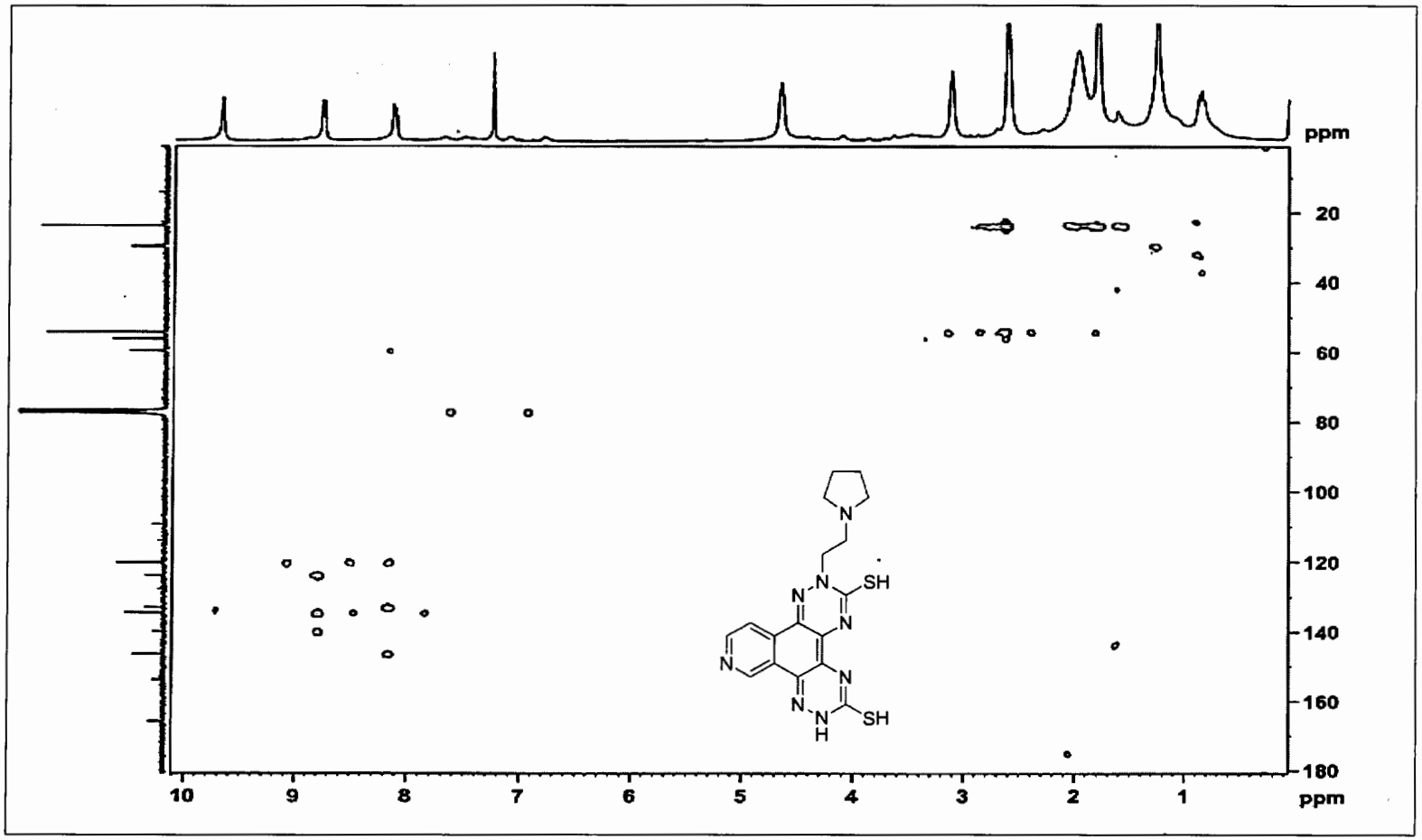

Figure B.19 HMBC spectrum of alkylated product 20c in acidic series in $CDCl_3$

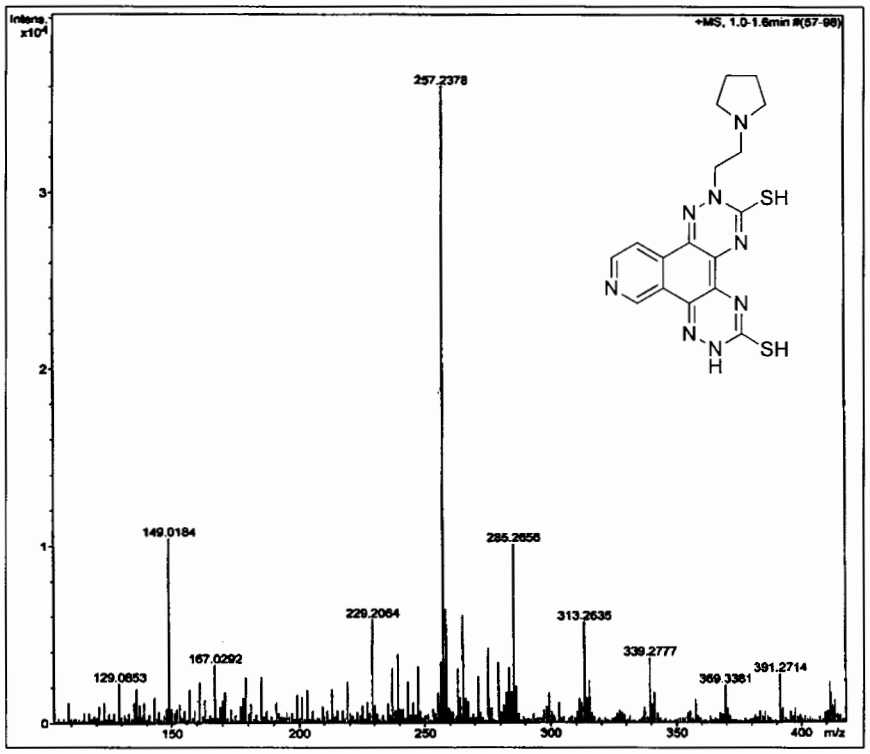

Figure B.20 Mass spectrum of alkylated product 20c in acidic series

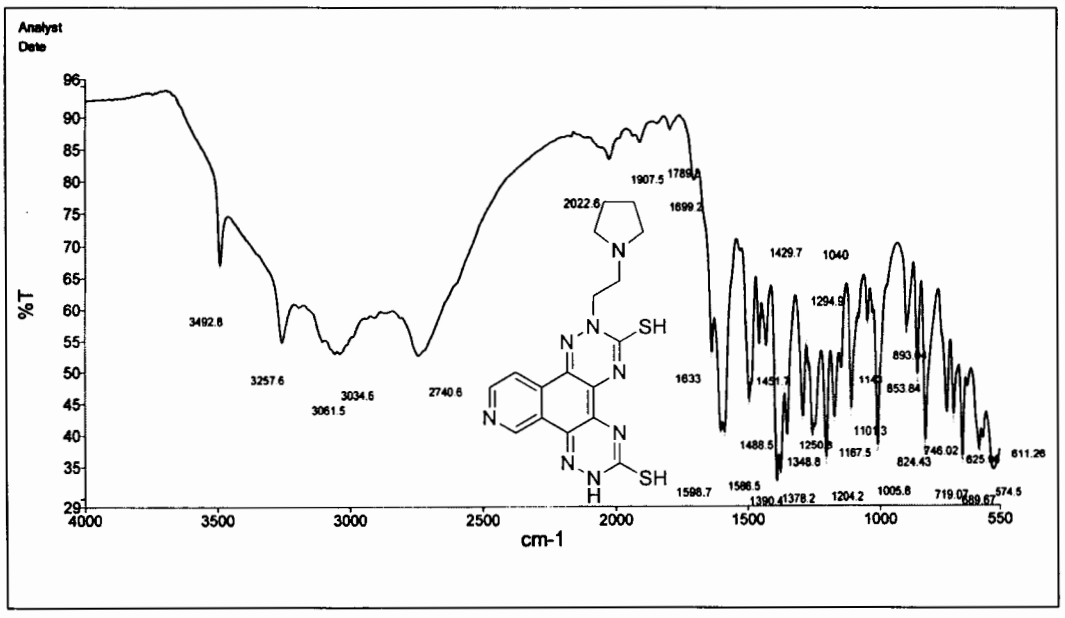

Figure B.21 IR spectrum of alkylated product 20c in acidic series

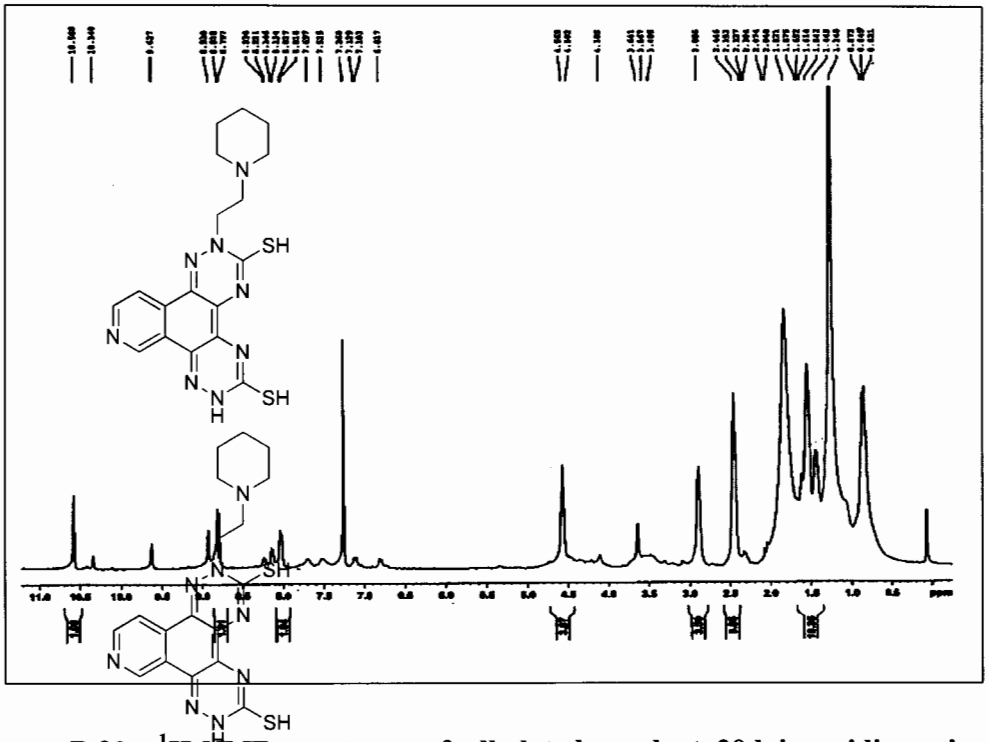

Figure B.22 ^{1}H-NMR spectrum of alkylated product 20d in acidic series in $CDCl_3$

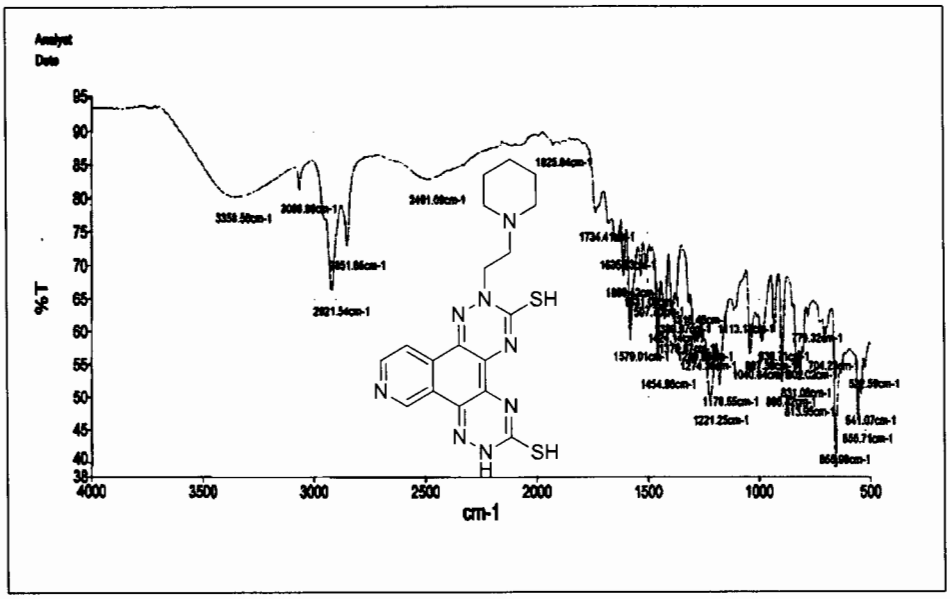

Figure B.23 IR spectrum of alkylated product 20d in acidic series

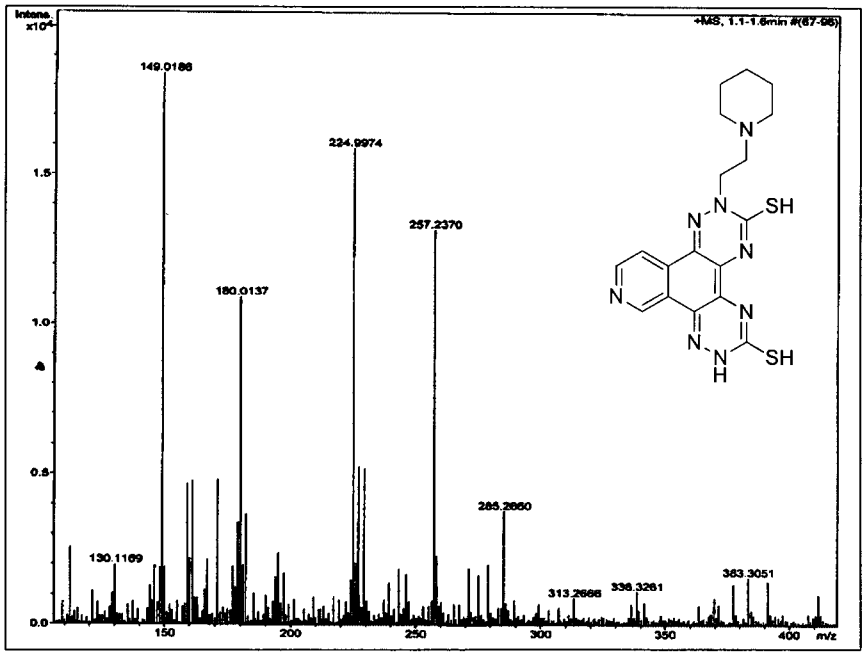

Figure B.24 Mass spectrum of alkylated product 20d in acidic series

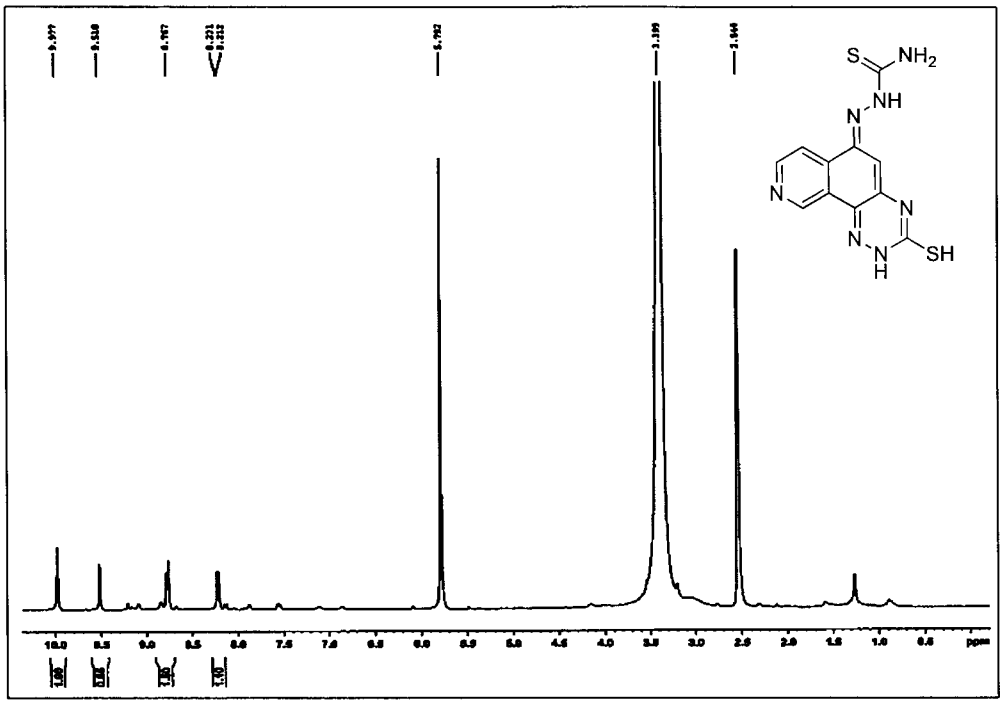

Figure B.25 ^{1}H-NMR spectrum of cyclization under basic condition product 21 in DMSO-D_6

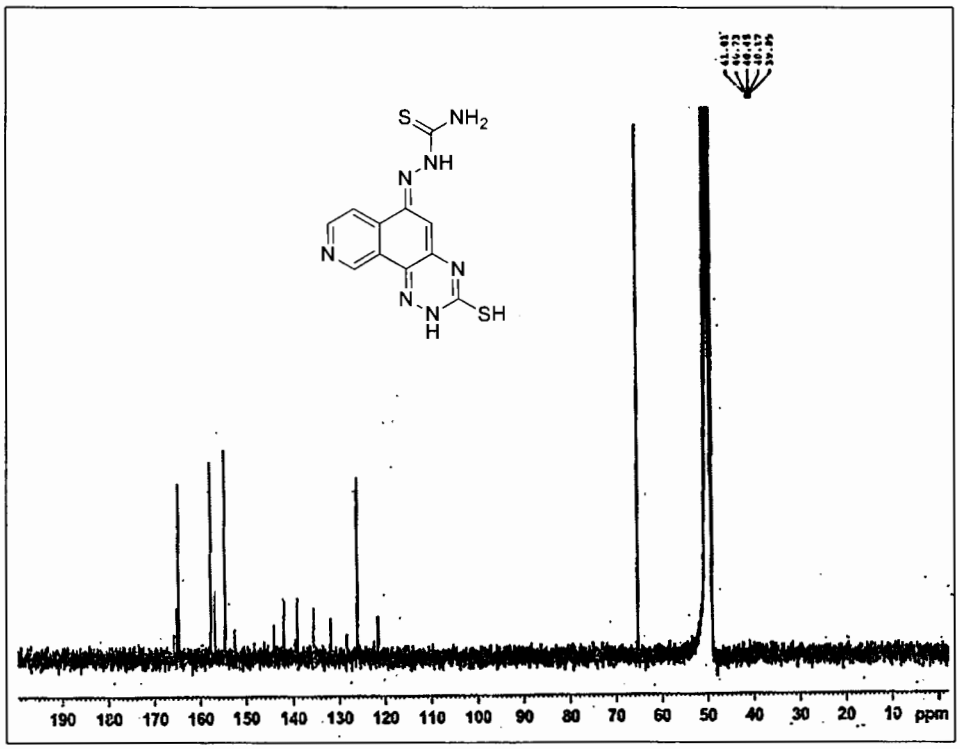

Figure B.26 ^{13}C-NMR spectrum of cyclization under basic condition product 21 in DMSO-D_6

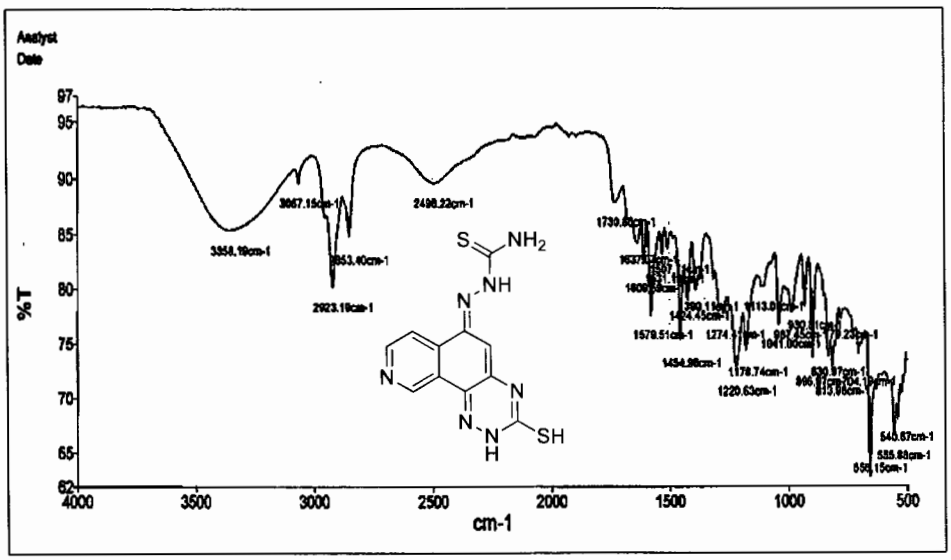

Figure B.27 IR spectrum of cyclization under basic condition product 21

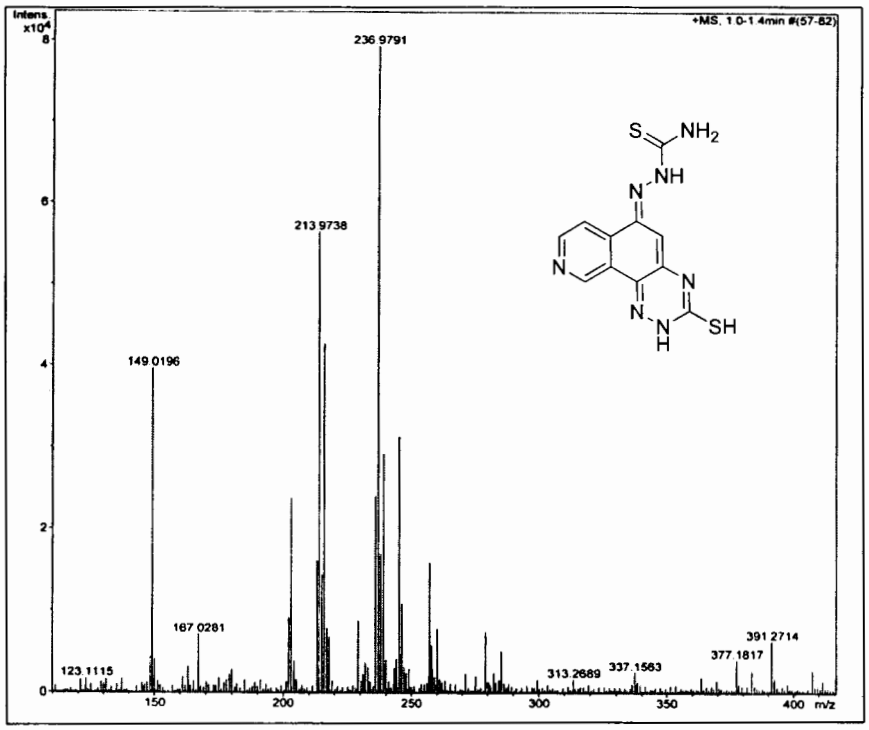

Figure B.28 Mass spectrum of cyclization under basic condition product 21

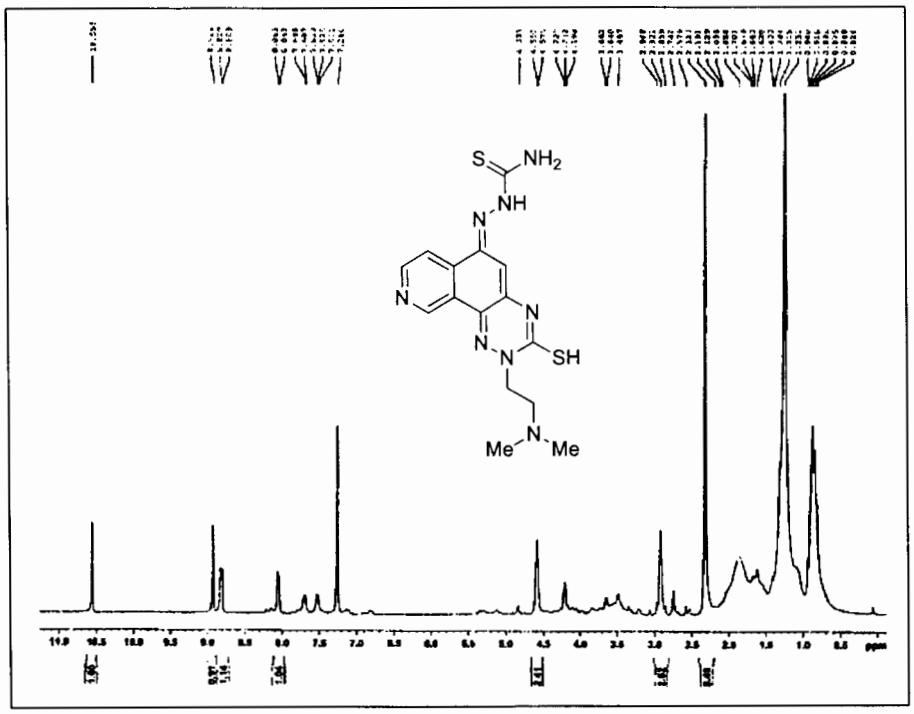

Figure B.29 ^{1}H-NMR spectrum of alkylated product 22a in basic series

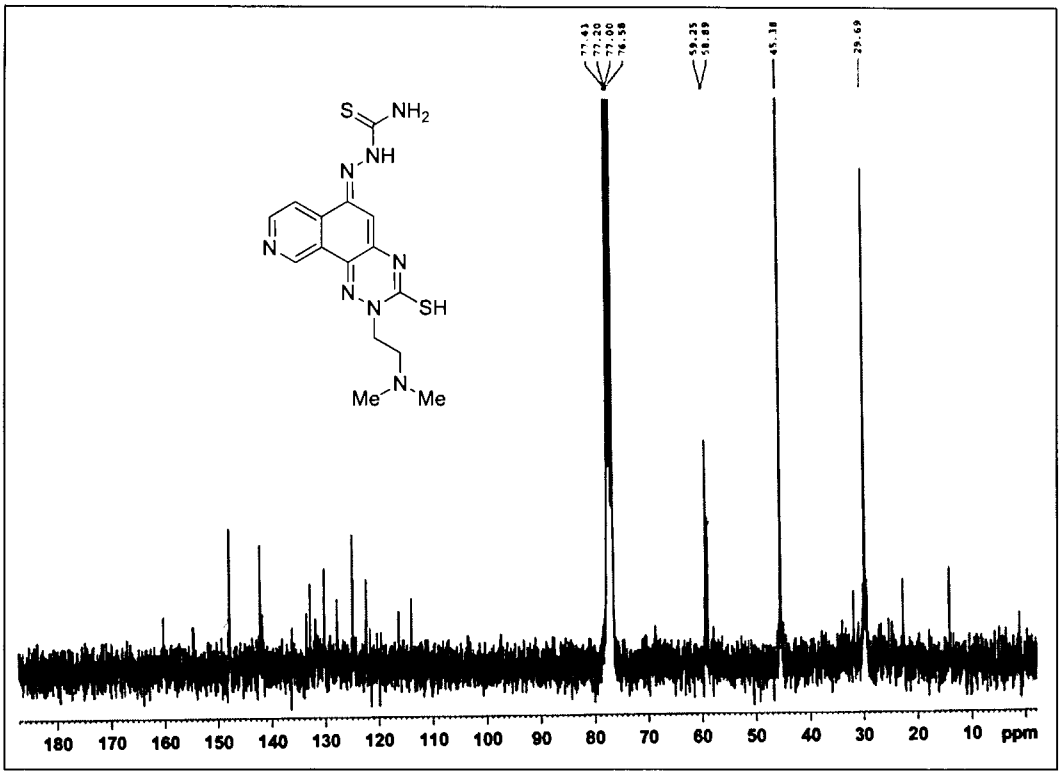

Figure B.30 ^{13}C-NMR spectrum of alkylated product 22a in basic series

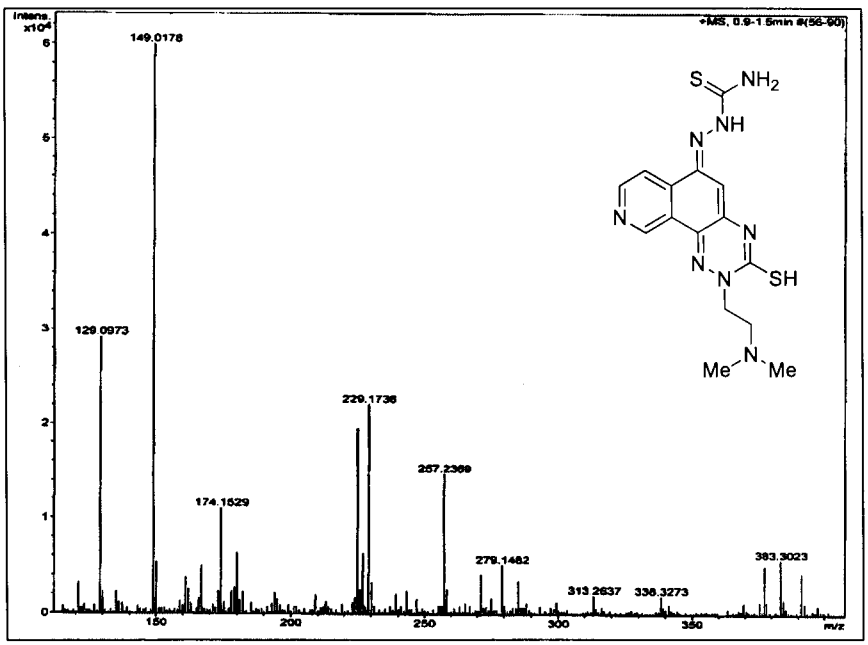

Figure B.31 Mass spectrum of alkylated product 22a in basic series

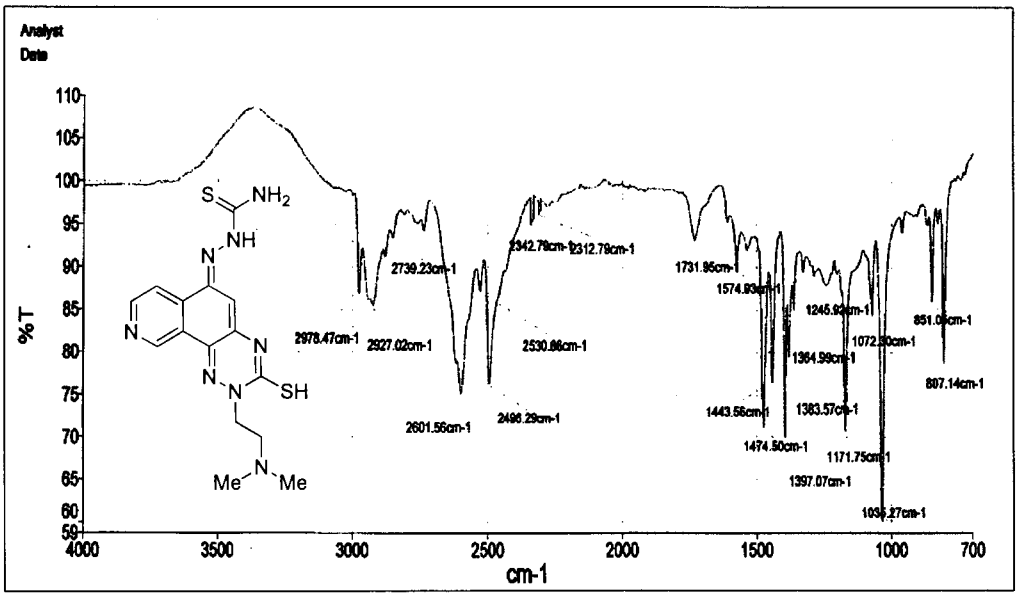

Figure B.32 IR spectrum of alkylated product 22a in acidic series

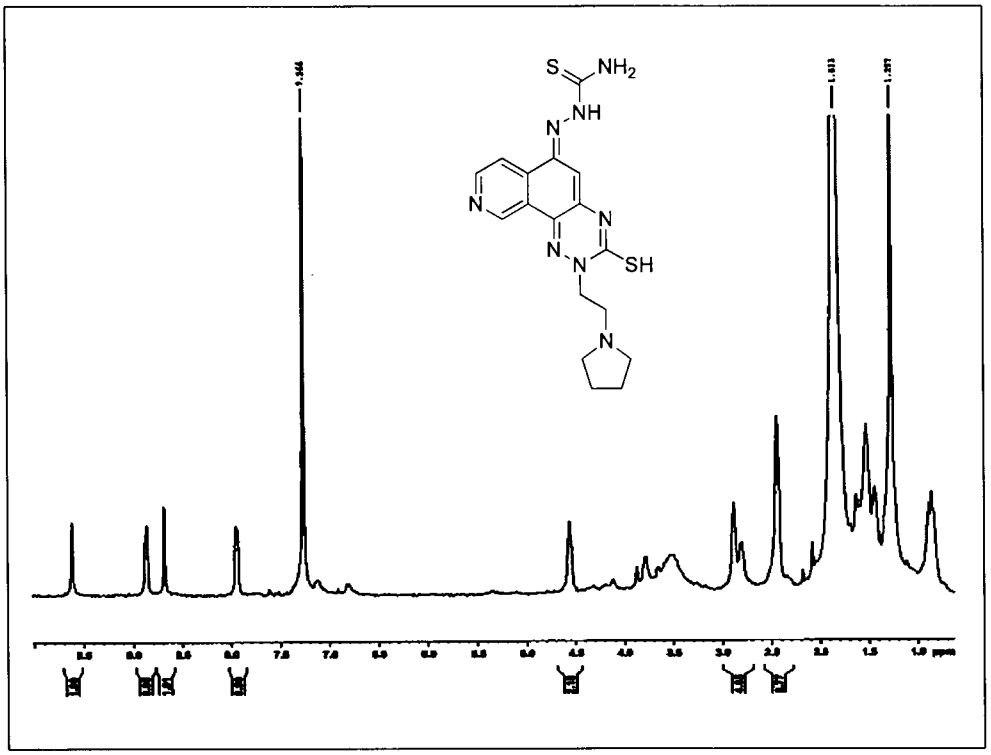

Figure B.33 ^{1}H-NMR spectrum of alkylated product 22b in basic series

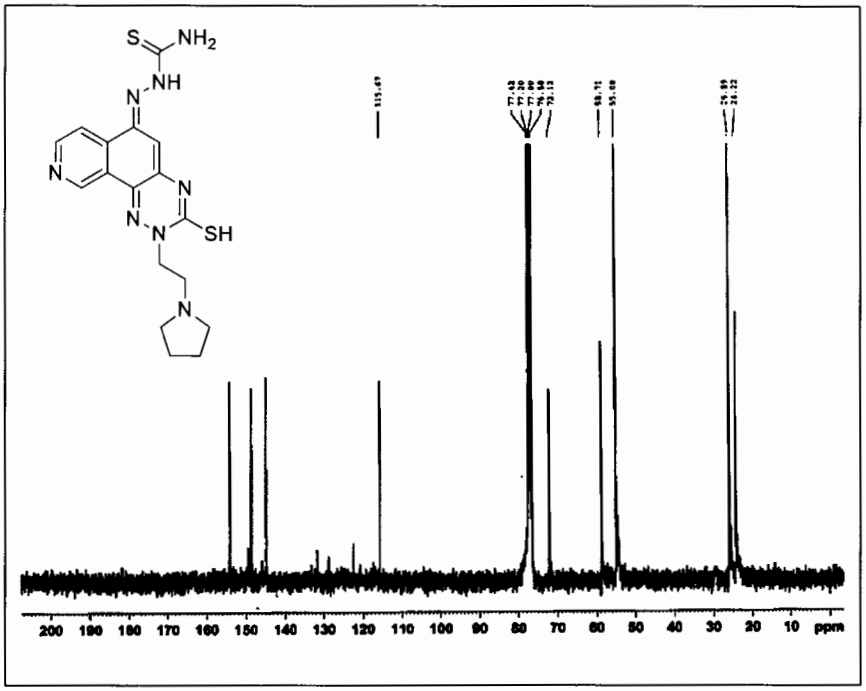

Figure B.34 ^{13}C-NMR spectrum of alkylated product 22b in basic series

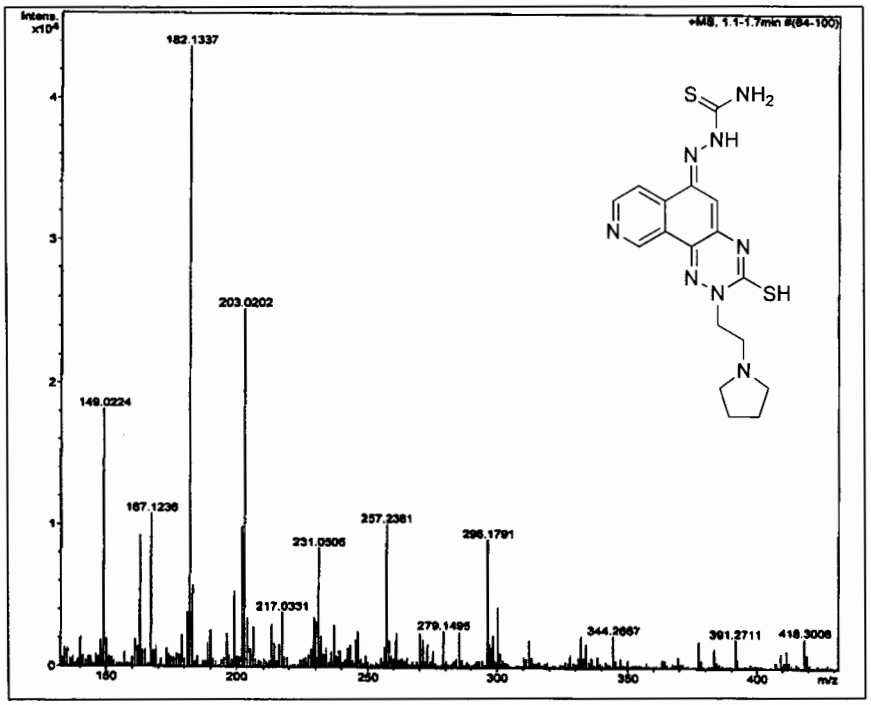

Figure B.35 Mass spectrum of alkylated product 22b in basic series

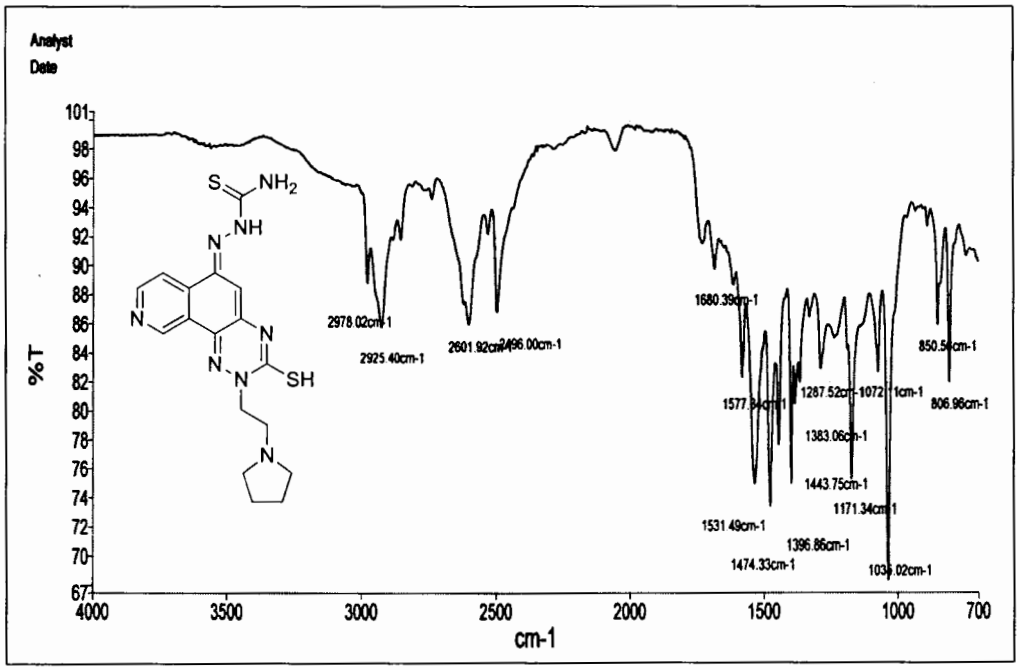

Figure B.36 IR spectrum of alkylated product 22b in acidic series

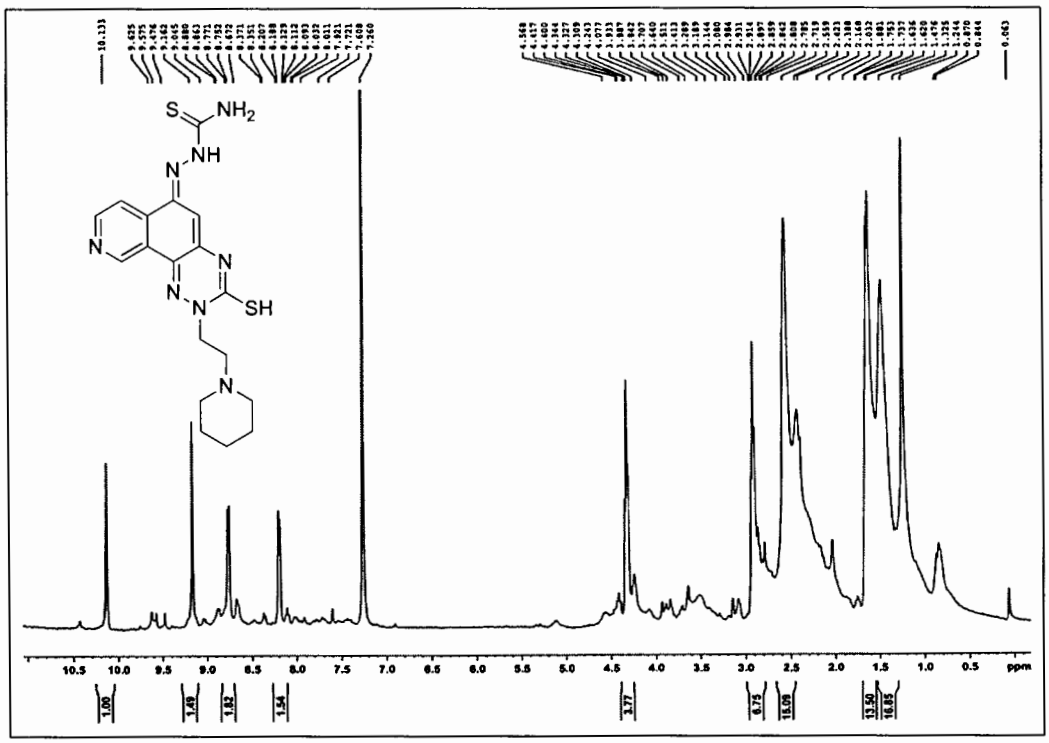

Figure B.37 ^{1}H-NMR spectrum of alkylated product 22c in basic series

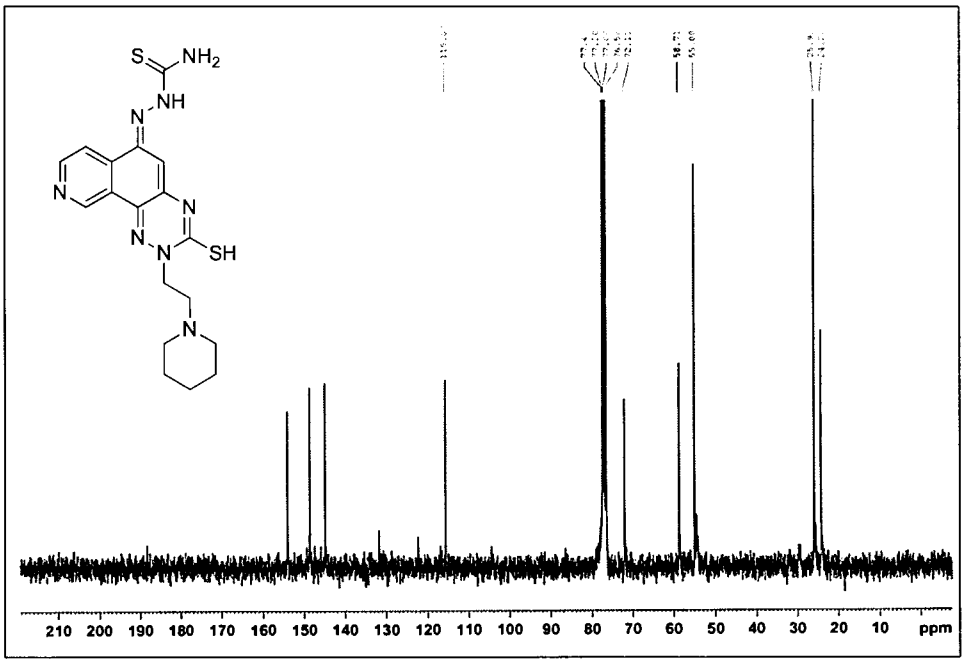

Figure B.38 ^{13}C-NMR spectrum of alkylated product 22c in basic series

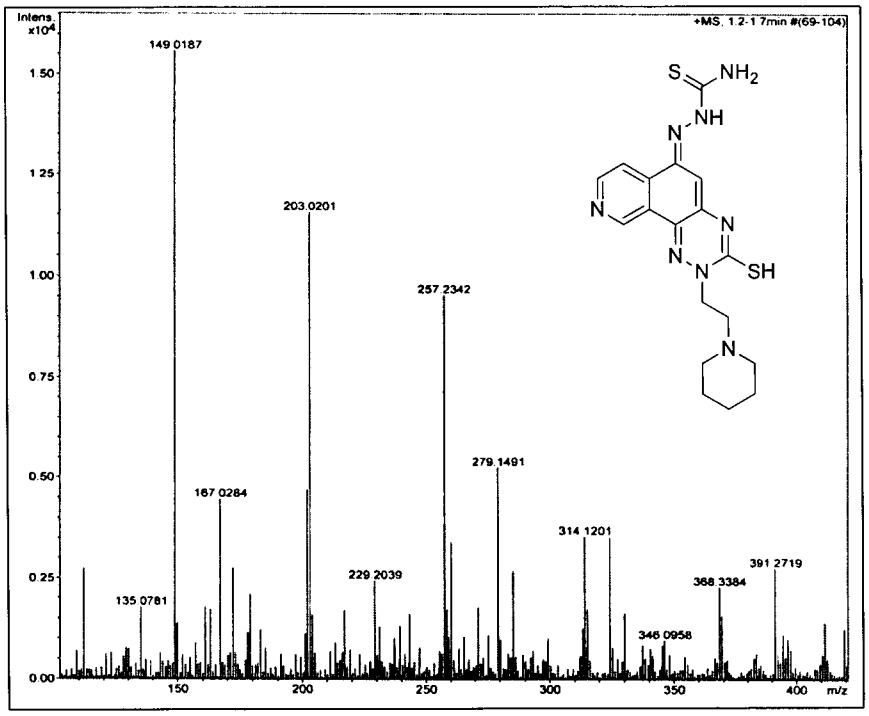

Figure B.39 Mass spectrum of alkylated product 22c in basic series

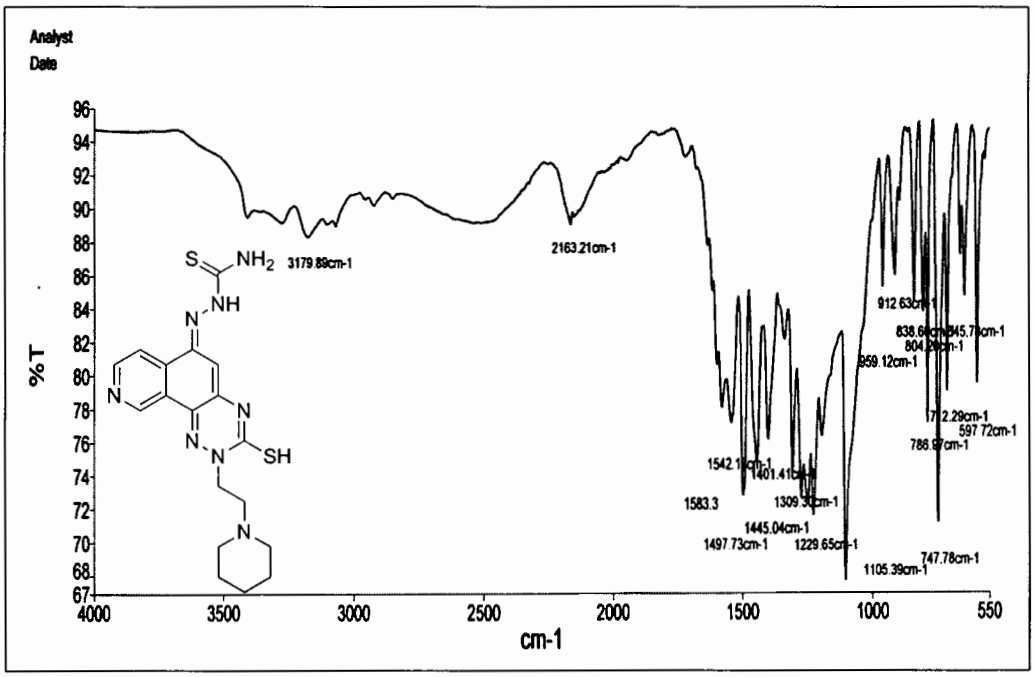

Figure B.40 IR spectrum of alkylated product 22c in acidic series

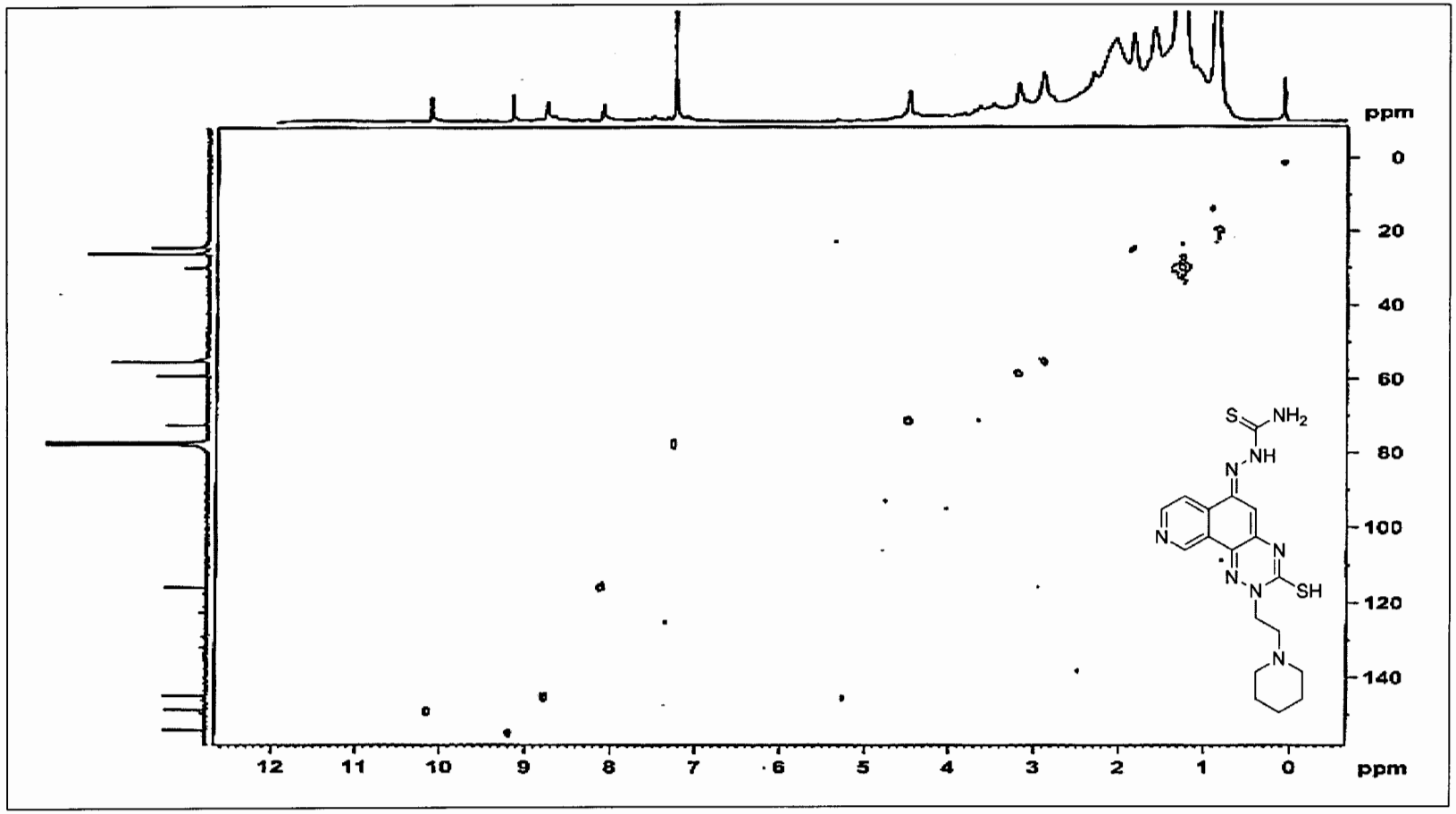

Figure B.41 HMQC spectrum of alkylated product 22c in $CDCl_3$

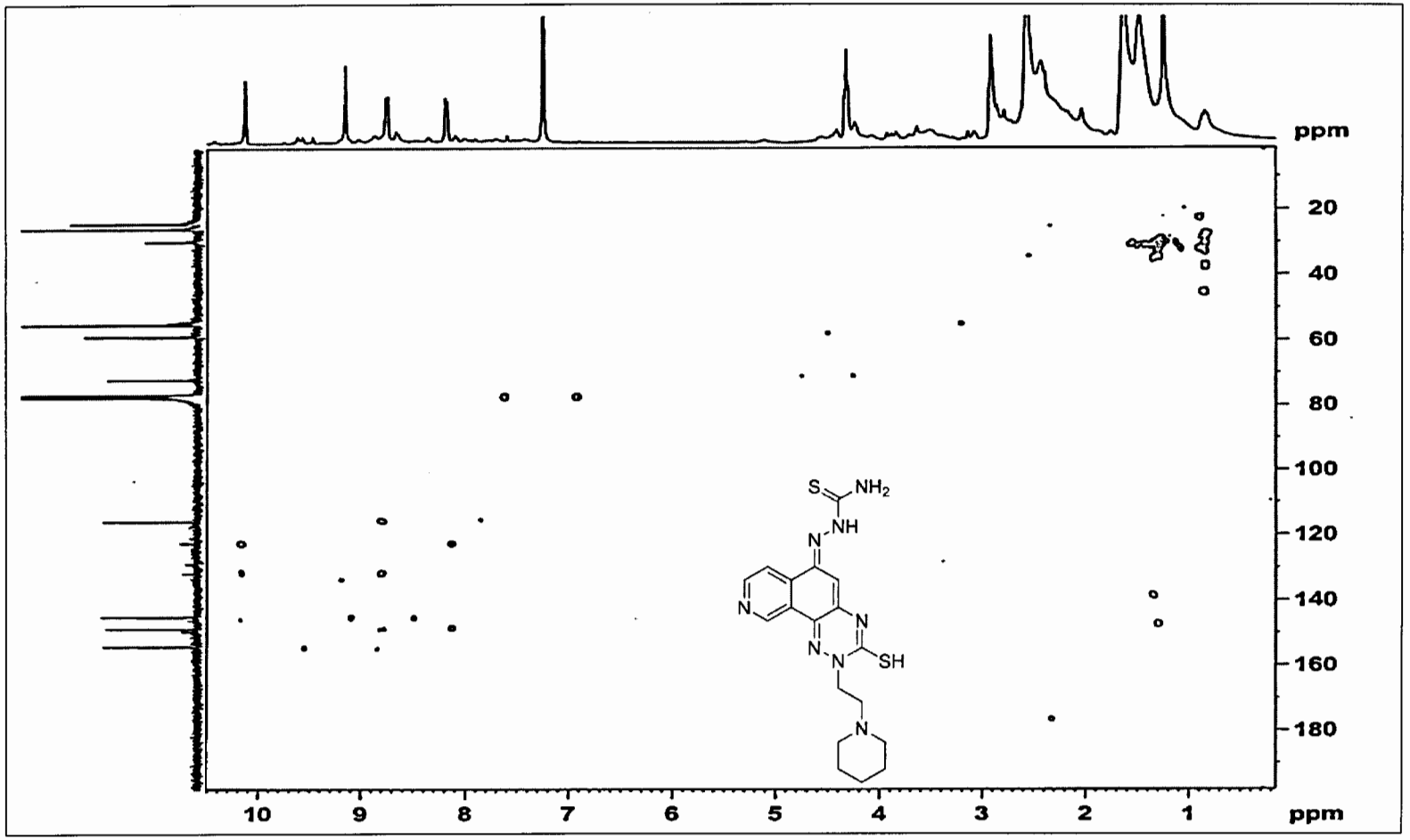

Figure B.42 HMBC spectrum of alkylated product 22c in $CDCl_3$

APPENDIX C

Publications

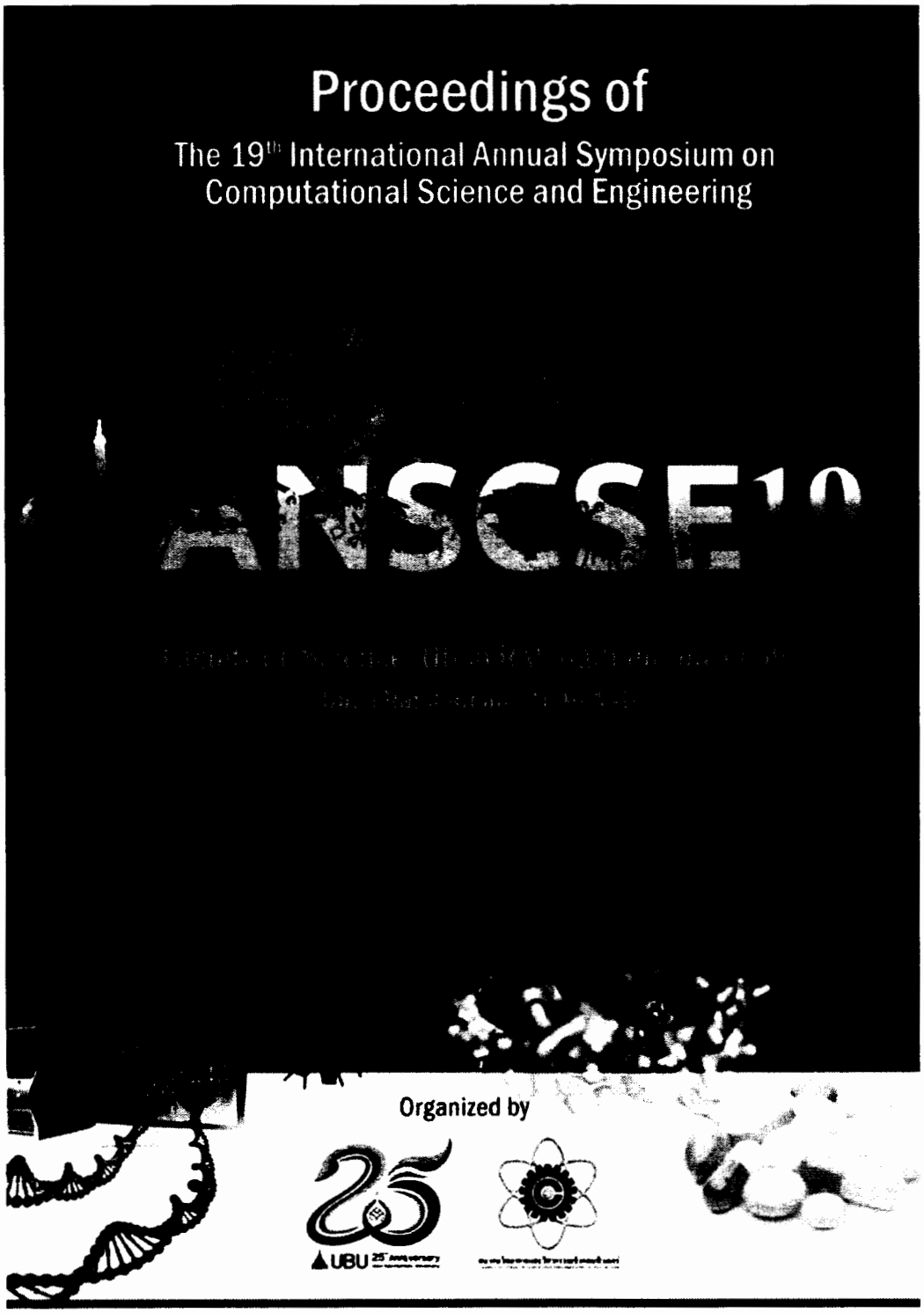
Proceedings of
The 19th International Annual Symposium on
Computational Science and Engineering
Organized by
UBU

Structural Requirement of Azanaphthoquinone Pyrrolo-annelated Derivatives against Hela Cancer Derived from 2D and 3D-QSAR Studies

Prasert Tumtong[1], Pharit Kamsri[1], Auradee Punkvang[1], Patchareenart Saparpakorn[2], Supa Hannongbua[2], Pornpan Pungpo[1*] and Nipawan Pongprom[1*]
[1]Department of Chemistry, Faculty of Science, Ubon Ratchathani University, Ubon Ratchathani, Thailand
[illegible]
Email: [illegible] Fax: [illegible]
Tel: [illegible]

INTRODUCTION

Azanaphthoquinone pyrrolo-annelated derivative were synthesized as anti-cancer agents. It is used to inhibit cancer cell types Hela Cancer cell line and the other types of mutation cancer cell line. These are effective better than paclitaxel and doxorubicin used multi-drug resistant cell lines. azanaphthoquinone pyrrolo-annelated derivative were synthesized by K. Shanab et al in 2010 [2]. It has been developed as novel anti-cancer agents and DNA intercalating agents. The mechanism of DNA intercalating agents is drug inserted between the bases of DNA. It causes twisted DNA. The body system will be eliminate the waste DNA. Which azanaphthoquinone pyrrolo-annelated derivative used to inhibit Hela Cancer cell line (wild-type (WT)) and mutation. It exhibit significantly and show better anti-proliferative effect than paclitaxel and doxorubicin on multidrug resistant cell lines. It is another important anti-cancer agents. It necessary to be studied Computational Calculation Chemistry. In this work, Studies using Quantitative structure activity relationship ; QSAR method. QSAR is mathematical models that represented quantitative relationships of the chemical structure and biological activity or toxicity. The bioactive or the toxicity of the chemical structure is based on the properties of chemicals.

THEORY AND RELATED WORKS

3D-QSAR is application in computer-aided drug design or Ligand-Based Drug Design method. It using information of drug in designing of the novel drug and increase efficient new drug. In this study, the GaussView 3.07 program and were fully optimized using the quantum chemical method (HF/6-31G*) implement in the Gaussian 09 program in the study 2D-QSAR (Conventional and HQSAR) and 3D-QSAR (CoMSIA). HQSAR and 3D-QSAR were performed using Sybyl 8.0. For obtained the results.

DATA SET AND BIOLOGICAL ACTIVITY

Structures and biological activities of azanaphthoquinone pyrrolo-annelated derivative were taken from literature [1-5] as shown in Table 1 and General structure as shown in Figure 1. The biological activities of these compounds were used The half maximal inhibitory concentration (IC_{50}) and converted to $\log(1/IC_{50})$ for simple to linear relationship and reducing the long range of biological data.

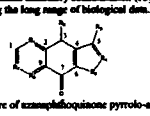

Figure 1 General structure of azanaphthoquinone pyrrolo-annelated derivative

Table 1 structure of azanaphthoquinone pyrrolo-annelated derivative

[illegible]

CoMSIA and HQSAR models

The results for HQSAR and CoMSIA model showed high correlation and predictive ability base on good statistical parameters as shown in Table 2. The best fields of CoMSIA model include the steric, electrostatic, hydrophobic and H-bond acceptor. The cross-validated correlation coefficient (q^2) is 0.61 and non- cross-validated correlation coefficient (r^2) is 0.99. The contribution of steric, electrostatic, hydrophobic and hydrogen acceptor fields is 18.5%, 27.7%, 31.5% and 22.3%, respectively. As a results show that, The electrostatic and hydrophobic fields has more influence on the activity of azanaphthoquinone pyrrolo-annelated derivative. The best HQSAR model generated based on the combination of the different fragment types, atom (At), chiral (Ch), connections (C) and bond (B) shows q^2 value of 0.62 with r^2 value of 0.86.

Table 2 Summary of statistical results of CoMSIA and HQSAR models

Models	Descriptors	Statistical parameters						Fraction
		q^2	r^2	N	S	SEE	F	
CoMSIA	S/E/H/A	0.61	0.99	6	0.84	0.11	585.36	18.5/27.7/31.5/22.3
Models	Descriptors	q^2	r^2	N	S	SEE	Bond length	
HQSAR	At/Ch/C/B	0.62	0.86	4	0.80	0.49	353	

q^2, Cross-validated correlation coefficient; r^2, Non-cross-validated correlation coefficient; N, Optimal number of components; s, standard error of prediction; SEE, standard error of estimate; F, F-test

REFERENCES
1. Shanab, K., Pongprom, N., [illegible] Med. Chem. Lett., 2007, 17, [illegible].
2. Shanab, K., [illegible] Med. Chem. Lett., 2010, 20(13), [illegible]-3952.
3. Shanab, K., [illegible] Bioorg. Med. Chem. Lett., 2011, 21(10), 3117-3121
4. Pongprom, N., Pungpo, P., [illegible] 2012, 17(2), [illegible].
5. Pongprom, N., [illegible] Chem., 2010, 141, 53-62

The data set has 37 compounds with activity range from 2.26 to 8.80 in $\log(1/IC_{50})$ units and the compound 12 show a high activity value. For evaluate the predictive ability of this CoMSIA model, the activities of the test set compounds were predicted such as compound 8, 11, 14 and 28. The relationship between experimental and predicted activities ($\log(1/IC_{50})$) of CoMSIA and HQSAR for the training set and test set are reported in Figure 2. Found that, The best model of HQSAR are not closed to the experimental biological activities. It show low correlation of the experimental and predicted biological activities. But the CoMSIA indicate linearity of the plot between the experimental biological and predicted biological activities. It has high predictive ability more than HQSAR models to predict the biological activity of azanaphthoquinone annelated pyrrole derivatives.

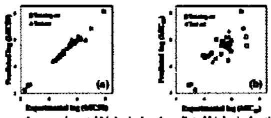

Figure 2 Plots between the experimental biological and predicted biological activities from the best CoMSIA (a) and HQSAR (b) models, respectively.

CoMSIA contour maps

In the CoMSIA contour maps as show in Figures 3. It has the influence of steric, electrostatic, hydrophobic and hydrogen acceptor fields to the activity of azanaphthoquinone annelated pyrrole derivatives. Favorable and unfavorable steric regions are represented in green and yellow contours, respectively. The electropositive and electronegative regions show in blue and red contours, respectively. The magenta and white contours imply the favorable and unfavorable hydrophobic regions. The cyan and orange contours indicate regions that favor the hydrogen donor group and unfavor hydrogen donor group, respectively. In the R1 Position founded blue, a few orange and near yellow contour refer to the small substituent, unfavor hydrogen donor and electropositive. The R1 Position should be S and N atom. The S and N atoms on the aromatic ring will be less hydrogen, small substituent and positive. The orange contour can explaining why compound 20 bearing a nitrogen atom at the R1 position exhibits lower potency than compound 13. The R2 position a large yellow and cyan, contour overlapping with a blue contour. Which R2 position is oxygen carbonyl. This confirms the results of compound 12 as well. For that reason, the oxygen carbonyl may be the best substituent in R2 position. R3, R4 and R6 position not found contour. R5 position show a large green and magent contours. The contour inserted in red contour. There corresponds to the substituent of compound 12 in R5 position. The red contour show electronegative. It confirms pyrrolidine group of compound 12 for best substituent. Which have bulky and lipophilic substituents.

Figure 3 Steric (a). Electrostatic (b). Hydrophobic (c) and Hydrogen bun acceptor (d) CoMSIA contours in combination with compound 12

HQSAR contributions

For the result of HQSAR found that the positive contribution in R1 and R7 position, the carbon near R2 and R3 position. Finally the substituent at R5 position. HQSAR model corresponds to a substituent of high activity compounds. It can confirm CoMSIA another method.

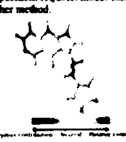

Figure 4 The HQSAR contribution map of azanaphthoquinone pyrrolo-annelated derivatives compound 12

CONCLUSIONS

The CoMSIA model based on pharmacophore alignment has high predictive ability in evaluated the activities of azanaphthoquinone annelated pyrrole derivatives with r^2 of 0.99 and q^2 of 0.61. CoMSIA and HQSAR can recommend to design molecules to compounds with the suitable combination of substituents of azanaphthoquinone annelated pyrrole derivatives. QSAR approaches aid to design new and more potent azanaphthoquinone annelated pyrrole derivatives.

ACKNOWLEDGMENTS

This work was support from Pornpan Pungpo and Nipawan Pongprom Department of Chemistry, Faculty of Science, Ubon Ratchathani University, Ubon Ratchathani, Thailand for Prasert Tumtong is gratefully acknowledged.

Proceedings of

The 19th International Annual Symposium on Computational Science and Engineering

June 17-19, 2015

Ubon Ratchathani University

Ubon Ratchathani, Thailand

The 19th International Annual Symposium on Computational Science and Engineering

ANSCSE 19

JUNE 17-19, 2015

Faculty of Science, Ubon Ratchathani University, THAILAND

Chairs and Committees

- **Steering Committee Chair:** Putchong Uthayopas (Kasetsart University and President of CSEA)
- **Scientific Committee Chair:** Vara varavithya, King Mongkut University of Technology North Bangkok
- **Computational Chemistry Chair:** Pornpan Pungpo, Ubon Ratchathani University
- **Computational Physics Chair:** Anucha Yangtaisong, Ubon Ratchathani University
- **Computational Biology and Bioinformatics:** Jeerayut Chaijaruwanich, Chiang Mai University
- **Computational Fluid Dynamics and Solid Mechanics Chair:** Vejapong Juttijudata, Kasetsart University
- **HPC and Grid computing:** Putchong Uthayopas, Kasetsart University
- **Computer Science and Engineering:** Vara varavithya, King Mongkut University of Technology North Bangkok
- **Computational Mathematics:** Somthep Vannarat, National Electronics and Computer Technology Center
- **Organizing Committee Chair:** Pornpan Pungpo, Ubon Ratchathani University

International Academic Advisory Committee

- **Prof.Ruiqin Zhang,** (City University of Hong Kong, Hong Kong)
- **Prof.Michel A. Van Hove,** (Hong Kong Baptist University, Hong Kong)
- **Prof.Weiliang Zhu** (Shanghai Institute of Materia Medica, Chinese Academy of Science, China)
- **Prof.Jun-ya Hasegawa** (Hokkaido University, Japan)
- **Prof.Philippe Bopp,** (Université Bordeaux 1, France)

Prof. Stephan Irle (Nagoya University, Japan)
Prof. Supa Hannongbua (Kasetsart University, Thailand)

Structural Requirement of Azanaphthoquinone Pyrrolo-annelated Derivatives against Hela Cancer Derived from 2D and 3D-QSAR Studies

Prasert Tumtong[1], Pharit Kamsri[1], Auradee Punkvang[2], Patchareenart Saparpakorn[2], Supa Hannonghua[2], Pornpan Pungpo[1,C] and Nipawan Pongprom[1,C]
[1] *Department of Chemistry, Faculty of Science, Ubon Ratchathani University, Ubon Ratchathani, Thailand*
[2]*Faculty of Science, Nakhon Phanom University, Nakhon Phanom, Thailand*
[3]*Department of Chemistry, Faculty of Science, Kasetsart University, Bangkok, Thailand*
[C] ***E-mail**: pornpan_ubu@yahoo.com, nippongprom@yahoo.com ; **Fax**: +66(45) 288 379; **Tel**. +66(45) 353401-4 Ext.4124*

ABSTRACT

Azanaphthoquinone pyrrolo-annelated derivative were synthesized as anti-cancer agents. It is used to inhibit cancer cell types Hela Cancer cell line and the other types of mutation cancer cell line. There are effective better than paclitaxel and doxorubicin used multi-drug resistant cell lines. The study of computational calculation chemistry of Azanaphthoquinone pyrrolo-annelated derivative is relatively few. In this work, we studied the computational calculation chemistry using QSAR methods, including 2D-QSAR (Conventional and HQSAR) and 3D-QSAR (CoMSIA). For conventional 2D-QSAR study, two charges, mulliken charges and RESP charges, were compared. The QSAR model of mulliken charges is as follows: (model I ; Log $1/IC_{50}$ = -0.098(±0.026)POL – 1.475(±1.977)C2 + 8.853(±0.955)). The results obtained from RESP charges are as follows: (model II ; Log $1/IC_{50}$ = -0.094(±0.027)POL + 2.373(±1.413)C5 + 1.456(±1.626)C6 + 6.473(±6.761)O8 +12.884(±3.347)). The predictive ability of models I and II shows lower than 0.6. In HQSAR study, leave-one out cross-validation correlation coefficients (q^2) is 0.62. For 3D-QSAR (CoMSIA), the leave-one out cross-validation correlation coefficients (q^2) of CoMSIA was 0.61. The results of HQSAR and 3D-QSAR CoMSIA show high correlation and predictive ability. The information obtained from our QSAR models can be beneficial for designing novel inhibitors with higher potency.

Keywords: Azanaphthoquinone pyrrolo-annelated derivatives, 2D-QSAR, 3D-QSAR, Anti-cancer agents.

1. INTRODUCTION

Azanaphthoquinone pyrrolo-annelated derivative were synthesized by K. Shanab et al in 2010 [2]. It has been developed as novel anti-cancer agents and DNA intercalating agents. The mechanism of DNA intercalating agents is drug inserted between the bases of DNA. It causes twisted DNA. The body system will be eliminate the waste DNA. Which azanaphthoquinone pyrrolo-annelated derivative used to inhibit Hela Cancer cell line (wild-type (WT)) and mutation. It exhibit significantly and show better anti-proliferative effect than paclitaxel and doxorubicin on multidrug resistant cell lines. It is another important anti-cancer agents. It necessary to be studied Computational Calculation Chemistry. In this work, Studies using Quantitative structure activity relationship ; QSAR method. QSAR is mathematical models that represented quantitative relationships of the chemical structure and biological activity or toxicity. The bioactive or the toxicity of the chemical structure is based on the properties of chemicals.

2. THEORY AND RELATED WORKS

3D-QSAR is application in computer-aided drug design or Ligand-Based Drug Design method. It using information of drug in designing of the novel drug and increase efficient new drug. In this study, the GaussView 3.07 program and were fully optimized using the quantum chemical method

(HF/6-31G*) implement in the Gaussian 09 program in the study 2D-QSAR (Conventional and HQSAR) and 3D-QSAR (CoMSIA). HQSAR and 3D-QSAR were performed using Sybyl 8.0. For obtained the results.

3. EXPERIMENTAL or COMPUTATIONAL DETAILS

3.1 Data set and Biological Activity

Structures and biological activities of azanaphthoquinone pyrrolo-annelated derivative were taken from literature [1-5] as shown in Table 1 and General structure as shown in Figure 1. The biological activities of these compounds were used The half maximal inhibitory concentration (IC_{50}) and converted to $\log(1/IC_{50})$ for simple to linear relationship and reducing the long range of biological data.

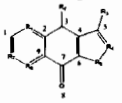

Figure 1 General structure of azanaphthoquinone pyrrolo-annelated derivative

Table 1 Structure and biological activity of azanaphthoquinone pyrrolo-annelated derivative

No	Structure	Log ($1/IC_{50}$)	No	Structure	Log ($1/IC_{50}$)
1[b]	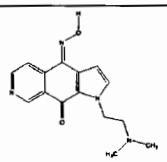	4.92	5	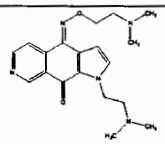	6.17
2	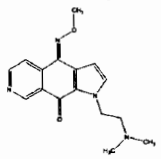	5.92	6[b]	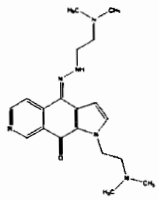	6.55
3	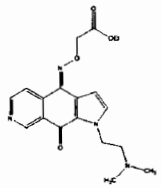	4.92	7	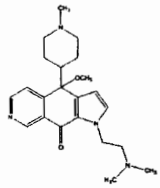	4.45
4	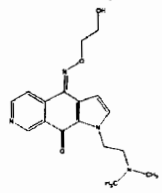	6.18	8[a]	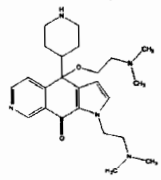	5.05

No	Structure	Log ($1/IC_{50}$)	No	Structure	Log ($1/IC_{50}$)
9	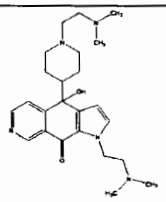	4.75	16	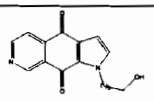	5.13
10	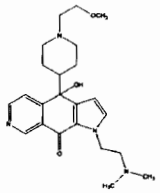	4.67	17	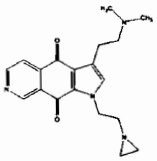	5.54
11[a]	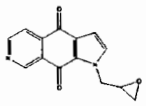	6.61	18	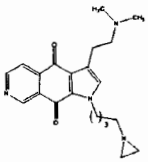	5.85
12	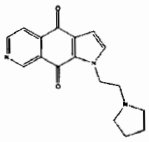	8.10	19	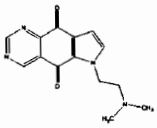	6.19
13	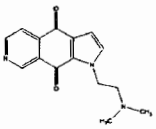	6.85	21	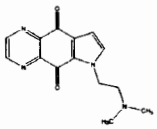	5.66
14[a]	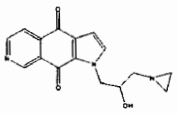	5.60	22	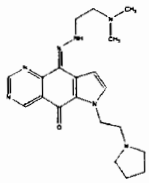	5.55
15	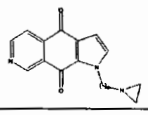	4.75	23	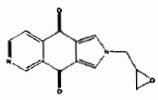	5.68

No	Structure	Log (1/IC50)	No	Structure	Log (1/IC50)
24	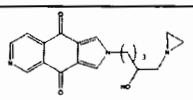	5.66	30	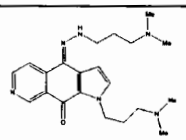	2.60
25	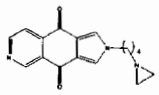	5.55	31	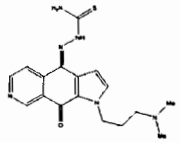	2.67
26	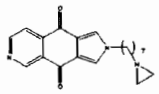	5.68	32	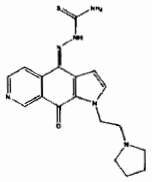	4.96
27	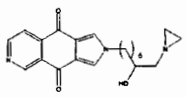	5.55	33[b]	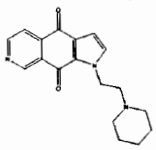	4.38
28	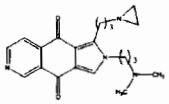	5.56	34[b]	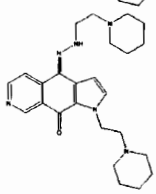	2.68
29	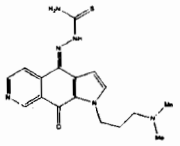	2.67	35[a]	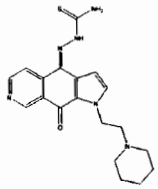	4.28
30	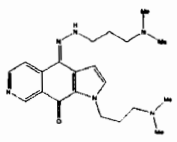	2.60	36	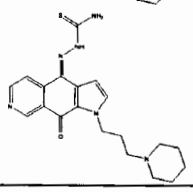	2.26

No	Structure	Log (1/IC50)
37[b]	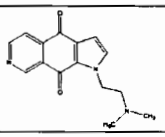	4.96

[a]test set, [b]outlier

3.2 2D and 3D-QSAR Technique

2D-QSAR were using HQSAR (Hologram Quantitative Structure Relationship) and 3D-QSAR were using CoMSIA (Comparative Molecular Similarity Indices Analysis) performed by Sybyl 8.0. Molecular alignment was used pharmacophore alignment GALAHAD (genetic algorithm with a linear assignment for the hypermolecular alignment of datasets module). There used to be explained the relationship between the structures and the biological activities of azanaphthoquinone annelated pyrrole derivatives. The descriptors of HQSAR, including atom (At), bond (B), connections (C), chiral (Ch) hydrogen atom (H) and donor and acceptor (DA) fields were calculated. Five CoMSIA similarity index descriptors including steric (S), electrostatic (E), hydrophobic (H), hydrogen donor (D) and hydrogen acceptor (A) fields were derived with the grid spacing of 2 Å. The statistical method partial least square (PLS) analysis was performed the relationship between molecular descriptors and activities. The cross-validation was performed using the leave-one-out method with a 2.0 kcal/mol column filter to minimize the influence of noisy columns. A final non cross-validated analysis with the optimal number of components was sequentially performed and was then employed to analyze the results. The predictive ability of CoMSIA models used evaluate by r^2 and q^2 values.

4. RESULTS AND DISCUSSION

4.1 CoMSIA and HQSAR models

The results for HQSAR and CoMSIA model showed high correlation and predictive ability base on good statistical parameters as shown in Table 2. The best fields of CoMSIA model include the steric, electrostatic, hydrophobic and H-bond acceptor. The cross-validated correlation coefficient (q^2) is 0.61 and non- cross-validated correlation coefficient (r^2) is 0.99. The contribution of steric, electrostatic, hydrophobic and hydrogen acceptor fields is 18.5%, 27.7%, 31.5% and 22.3%, respectively. As a results show that, The electrostatic and hydrophobic fields has more influence on the activity of azanaphthoquinone pyrrolo-annelated derivative. The best HQSAR model generated based on the combination of the different fragment types, atom (At), chiral (Ch), connections (C) and bond (B) shows q^2 value of 0.62 with r^2 value of 0.86.

Table 2 Summary of statistical results of CoMSIA and HQSAR models

Models	**Descriptors**	**Statistical parameters**						**Fraction**
		q^2	r^2	N	S	SEE	F	
CoMSIA	S/E/H/A	0.61	0.99	6	0.84	0.11	585.36	18.5/27.7/31.5/22.3
Models	**Descriptors**	q^2	r^2	N	S	SEE	**Bond length**	
HQSAR	At/Ch/C/B	0.62	0.86	4	0.80	0.49	353	

q^2, Cross-validated correlation coefficient; r^2, Non-cross-validated correlation coefficient; N, Optimal number of components; s, standard error of prediction; SEE, standard error of estimate; F, F-test

The data set has 37 compounds with activity range from 2.26 to 8.10 in $\log(1/IC_{50})$ units and the compound **12** show a high activity value. For evaluate the predictive ability of this CoMSIA model, the activities of the test set compounds were predicted such as compound **8**, **11**, **14** and **35**. The relationship between experimental and predicted activities ($\log(1/IC_{50})$ of CoMSIA and HQSAR for the training set and test set are reported in Figure 2. Found that, The best model of HQSAR are not

closed to the experimental biological activities. It show low correlation of the experimental and predicted biological activities. But the CoMSIA indicate linearity of the plot between the experimental biological and predicted biological activities. It has high predictive ability more than HQSAR models to predict the biological activity of azanaphthoquinone annelated pyrrole derivatives.

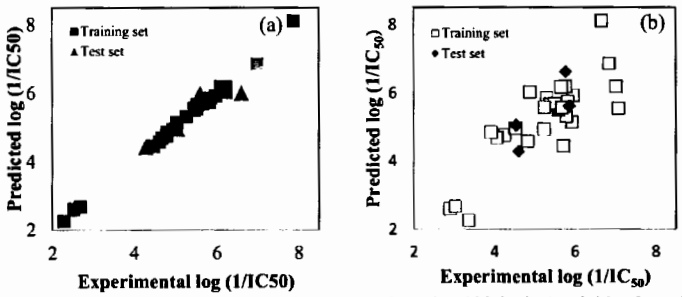

Figure 2 Plots between the experimental biological and predicted biological activities from the best CoMSIA **(a)** and HQSAR **(b)** models, respectively.

4.2 CoMSIA contour maps

In the CoMSIA contour maps as show in Figures 3. It has the influence of steric, electrostatic, hydrophobic and hydrogen acceptor fields to the activity of azanaphthoquinone annelated pyrrole derivatives. Favorable and unfavorable steric regions are represented in green and yellow contours, respectively. The electropositive and electronegative regions show in blue and red contours, respectively. The magenta and white contours imply the favorable and unfavorable hydrophobic regions, The cyan and orange contours indicate regions that favor the hydrogen donor group and unfavor hydrogen donor group, respectively. In the R1 Position founded blue, a few orange and near yellow contour refer to the small substituent, unfavor hydrogen donor and electropositive. The R1 Position should be S and N atom. The S and N atoms on the aromatic ring will be less hydrogen, small substituent and positive. The orange contour can explaining why compound **20** bearing a nitrogen atom at the R1 position exhibits lower potency than compound **13**. The R2 position a large yellow and cyan, contour overlapping with a blue contour. Which R2 position is oxygen carbonyl. This confirms the results of compound **12** as well. For that reason, the oxygen carbonyl may be the best substituent in R2 position. R3, R4 and R6 position not found contour. R5 position show a large green and magent contours. The contour inserted is red contour. There corresponds to the substituent of compound **12** in R5 position. The red contour show electronegative. It confirms pyrrolidine group of compound **12** for best substituent. Which have bulky and lipophilic substituents.

Figure 3 Steric (a), Electrostatic (b), Hydrophobic (c) and Hydrogen bon acceptor (d) CoMSIA contours in combination with compound **12**

4.3 HQSAR contributions

For the result of HQSAR found that the positive contribution in R1 and R7 position, the carbon near R2 and R3 position, Finally the substituent at R5 position. HQSAR model corresponds to a substituent of high activity compounds. It can confirm CoMSIA another method.

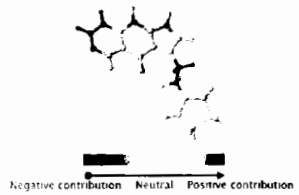

Figure 4 The HQSAR contribution map of azanaphthoquinone pyrrolo-annelated derivatives compound **12**

5. CONCLUSIONS

The CoMSIA model based on pharmacophore alignment shows high predictive ability in evaluating the activities of azanaphthoquinone annelated pyrrole derivatives with r^2 of 0.99 and q^2 of 0.61. CoMSIA and HQSAR can be recommended to design new compounds with suitable combination of substituents of azanaphthoquinone annelated pyrrole derivatives. Based on the obtained results, QSAR approaches are fruitful tools to design new and more potent azanaphthoquinone annelated pyrrole derivatives.

REFERENCES

1. Shanab, K., Pongprom, N., Wulz, E., Holzer, W., Spreitzer, H., Schmidt, P., Aicher, B., Müller, G., Günther, E., *Bioorg. Med. Chem. Lett.*, 2007, **17**, 6091-6095.
2. Shanab, K., Schirmer, E., Knafl, H., Wulz, E., Holzer, W., Spreitzer, H., Schmidt, P., Aicher, B., Müller, G., Günther, E., *Bioorg. Med. Chem. Lett.*, 2010, **20**(13), 3950-3952.
3. Shanab, K., Schirmer, E., Wulz, E., Weissenbacher, B., Lassnig, S., Slanz, R., Fösleitner, G., Holzer, W., Spreitzer, H., Schmidt, P., Aicher, B., Müller, G., Günther, E., *Bioorg. Med. Chem. Lett.*, 2011, **21**(10), 3117-3121.
4. Pongprom, N, Pungpo, P., *KKU Res. J.*, 2012, **17**(2), 195-202.
5. Pongprom, N, Bachitsch, H., Bauchinger, A., Ettefagh, H., Haider, T., Hofer, M., Knafl, H., Slanz, R., Waismeyer, M., Wieser, F., Spreitzer, H., *Monatsh. Chem.*, 2010, **141**, 53–62

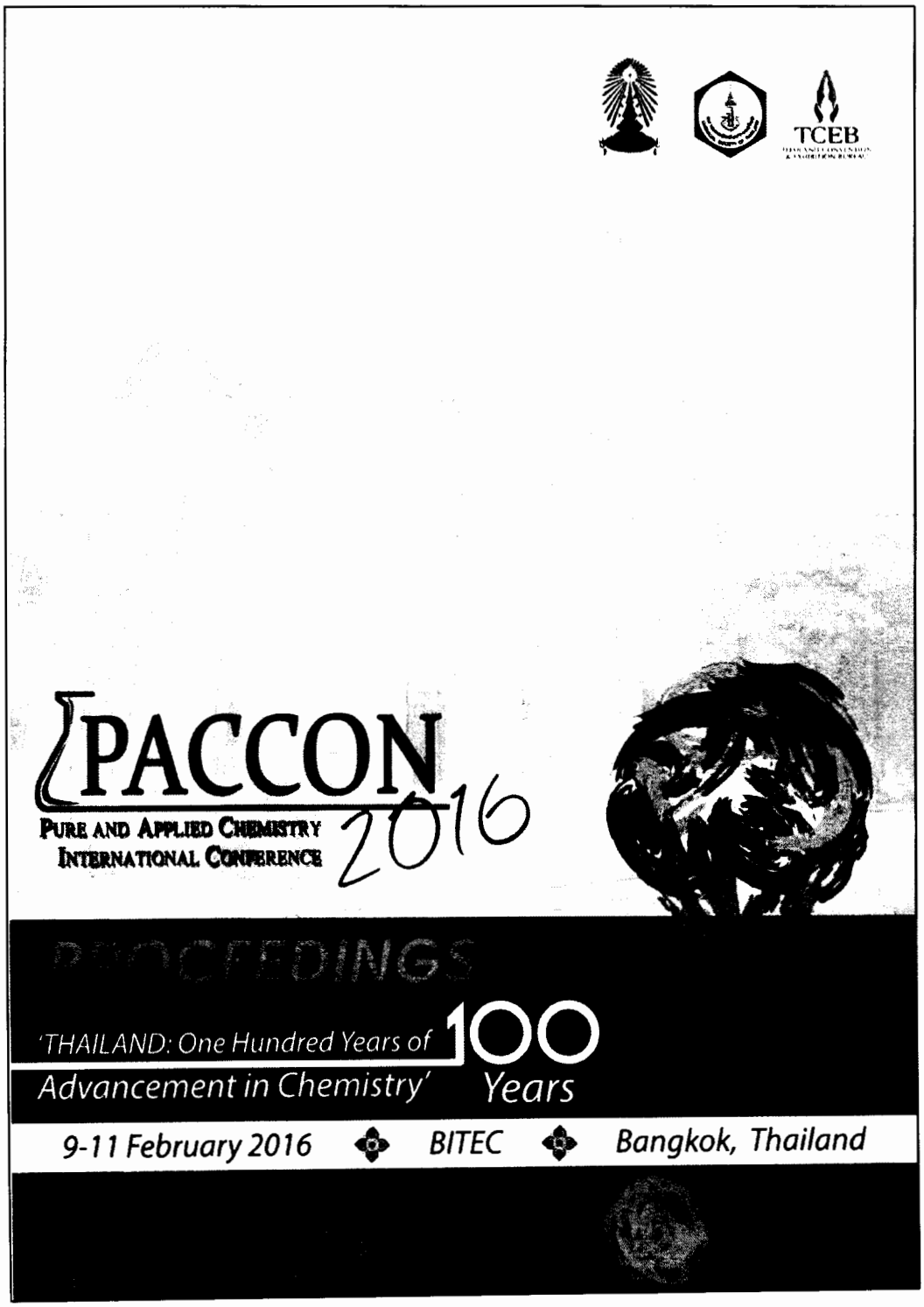
TCEB
PACCON 2016
PURE AND APPLIED CHEMISTRY INTERNATIONAL CONFERENCE
PROCEEDINGS
'THAILAND: One Hundred Years of Advancement in Chemistry'
100 Years
9-11 February 2016
BITEC
Bangkok, Thailand

Proceedings

The Pure and Applied Chemistry International Conference 2016 (PACCON2016)

"THAILAND: One Hundred Years of Advancement in Chemistry"

February 9 –11, 2016

at

Bangkok International Trade and Exhibition Centre (BITEC)

Bangkok, Thailand

Organized by

The Chemical Society of Thailand under the

Patronage of Professor Dr. HRH Princess Chulabhorn

In association with

Department of Chemistry, Faculty of Science

Chulalongkorn University

PDF version of this book

Update/correction note

Proceedings of the Pure and Applied Chemistry International Conference 2016 (PACCON2016)

Editor-in-Chief Tirayut Vilaivan

ISBN (e-book) 978-616-407-033-2

Prepared by Department of Chemistry, Faculty of Science
Chulalongkorn University

1st edition May 2016 (available in PDF version only)

Committees

Chairperson
Associate Professor Dr. Vudhichai Parasuk

Secretary General
Assistant Professor Dr. Warinthorn Chavasiri
Assistant Professor Dr. Worawan Bhanthumnavin
Associate Professor Dr. Voravee Hoven

Honorary Advisory Committee
Associate Professor Dr. Surin Laosooksathit
(President of the Chemical Society of Thailand under the Patronage of Professor Dr. HRH Princess Chulabhorn)

Associate Professor Dr. Polkit Sangvanich
Dean of the Faculty of Science, Chulalongkorn University

Associate Professor Dr. Supawan Tantayanon
(Immediate Past President of the Chemical Society of Thailand the Patronage of Professor Dr. HRH Princess Chulabhorn)

Professor Dr. Supot Hannongbua
(President of the Science Society of Thailand under the Patronage of His Majesty the King)

International Advisory Committee

Professor Dr. Kurt Kalcher	Austria
Professor Dr. Niyazi Serdar Sariciftci	Austria
Professor Dr. Ian D. Williams	HKSAR
Professor Dr. Tomatsu Takahashi	Japan
Professor Dr. Ken-ichi Sugiura	Japan
Professor Dr. Stephan Irle	Japan
Professor Dr.Yasushi Nishihara	Japan
Datuk Dr. Ting-Kueh Soon	Malaysia
Professor Dr. Roderick W. Bates	Singapore
Professor Dr. John H. K. Yip	Singapore
Professor Dr. Andy Hor Tzi Sum	Singapore
Professor Dr. Jin-Ho Choy	South Korea
Professor Dr. Harm-Anton Klok	Switzerland
Professor Dr. Charles Henry	USA
Professor Dr. Richard W. Vachet	USA
Dr. Santi Kulprathipanja	USA

Scientific Committee

Professor Dr. Tirayut Vilaivan (Chairperson)
Professor Dr. Harm-Anton Klok
Professor Dr. Ian D. Williams
Professor Dr. Jin-Ho Choy
Professor Dr. John H. K. Yip
Professor Dr. Niyazi Serdar Sariciftci
Professor Dr. Roderick W. Bates
Professor Dr. Stephan Irle
Professor Dr. Suttichai Assabumrungrat
Professor Dr. Orawon Chailapakul
Professor Dr. Richard W. Vachet
Professor Dr. Thawatchai Tuntulani
Professor Dr. Vatcharin Rukachaisirikul
Associate Professor Dr. Bhinyo Panijpan
Associate Professor Dr. Mongkol Sukwattanasinitt
Associate Professor Dr. Paitoon Rashatasakhon
Associate Professor Dr. Patchanita Thamyongkit
Associate Professor Dr. Pornthep Sompornpisut
Associate Professor Dr. Pramoch Rangsunvigit
Associate Professor Dr. Sirirat Kokpol
Associate Professor Dr. Supason Wanichwecharungruang
Associate Professor Dr. Suwimol Asavapisit
Associate Professor Dr. Vinich Promarak
Associate Professor Dr. Voravee Hoven
Associate Professor Dr. Weena Siangproh
Assistant Professor Dr. Anawat Ajavakom
Assistant Professor Dr. Apichat Imyim
Assistant Professor Dr. Khanitha Pudhom
Assistant Professor Dr. Kittipong Chainok
Assistant Professor Dr. Pattara Thiraphibundet
Assistant Professor Dr. Sumrit Wacharasindhu
Dr. Kwanruthai Tadpetch
Dr. Panadda Silva
Dr. Santi Kulprathipanja

Local Organizing Committee

Professor Dr. Orawan Chailapakul
Professor Dr. Supa Hannongbua
Associate Professor Dr. Amorn Petsom
Associate Professor Dr. Kitti Amornraksa
Associate Professor Dr. Ladda Meesuk
Associate Professor Narumol Kreua-ongarjnukool
Associate Professor Dr. Noppavan Chanunpanich
Associate Professor Dr. On-uma Kheowan
Associate Professor Dr. Paitoon Rashatasakhon
Associate Professor Dr. Patchanita Thamyongkit
Associate Professor Sutha Poosittisak
Associate Professor Dr. Thanuttkhul Mongkolaussavarat
Assistant Professor Dr. Amarawan Intasiri
Assistant Professor Dr. Apichat Imyim
Assistant Professor Dr. Aroonsiri Shitangkoon
Assistant Professor Dr. Boonyaras Sookkheo
Assistant Professor Dr. Boosayarat Tomapatanaget
Assistant Professor Dr. Chanatip Samart
Assistant Professor Dr. Fuengfa Unob
Assistant Professor Dr. Kanet Wongravee
Assistant Professor Dr. Khanitha Pudhom
Assistant Professor Dr. Narong Praphairaksit
Assistant Professor Dr. Pakorn Varanusupakul
Assistant Professor Dr. Pattara Thiraphibundet
Assistant Professor Dr. Pornpan Pungpo
Assistant Professor Dr. Rojrit Rojanathanes
Assistant Professor Dr. Saowarux Fuangswasdi
Assistant Professor Dr. Soamwadee Chalanansutcharit
Assistant Professor Dr. Somsak Pianwanit
Assistant Professor Dr. Suchada Chuanuwatanakul
Assistant Professor Dr. Supakorn Boonyuen
Assistant Professor Dr. Wanlapa Aeungmaitrepirom
Assistant Professor Dr. Yongsak Sritana-anant
Dr. Boonnak Sukhummek
Dr. Charoenkwan Kraiya
Dr. Duangruthai Sridaeng
Dr. Janjira Panchompoo
Dr. Nipaka Sukpirom
Dr. Nattapong Paiboonvorachat
Dr. Nawaporn Vinayavekhin
Dr. Numpon Insin
Dr. Pannee Leeladee
Dr. Panuwat Padungros
Dr. Passapol Ngamukot
Dr. Prompong Pienpinijtham
Dr. Puttaruksa Varanusupakul
Dr. Sakulsuk Unarunotai
Dr. Thanit Praneenararat
Dr. Uthai Wichai
Dr. Wipark Anutrasakda

PACCON Proceedings 2016: Article Content

PACCON Proceedings 2016: Analytical Chemistry (ANC)

PACCON Proceedings 2016: Synthetic Organic, Medicinal and Process Chemistry (SYN-1463)

Synthesis of azanaphthoquinone annelated triazine thiones as antiproliferative agents

Praseat Tumtong, Apisara Chansook, Supreeya Chaladdee, Thiraprapa Srilawan, Nipawan Pongprom*
Department of Chemistry, Faculty of Science, Ubon Ratchathani University, Ubon Ratchathani 34190, Thailand
*e-mail: nippongprom@yahoo.com

Abstract:
A novel series of azanaphthoquinone annelated triazine thione derivative as antiproliferative agents have been synthesized and spectroscopically characterized. The target molecules were designed to replace carbonyl moiety with thiosemicarbazone condensation in acidic condition to give triazine thione ring in order to reduce cardiotoxic and then mono-substituted side chains were introduced into the core structure to furnished the target molecules.

1. Introduction

The azanaphthoquinone annelated pyrrole and its oxime derivatives (**1**) were synthesized and found to be promising anticancer agents.[1] The oxime series was designed to replace carbonyl moiety of azanaphthoquinone annelated pyrrole by carbon-nitrogen double bond expecting to reduce bioreductive effect of the quinone moiety. It has been found that oxime series showed better anticancer activity than the azanaphthoquinone annelated pyrrole. Therefore, we have synthesized hydrazone derivatives (**2**) and thiosemicarbazone derivatives (**3**) which exhibited remarkable activity on cervical carcinoma cell line (HeLa cell).[2–3]

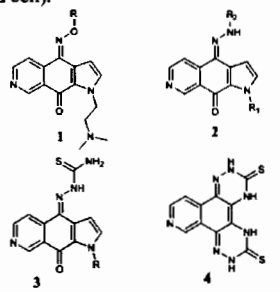

Figure 1. Structure of oximes (**1**), hydrazones (**2**), thiosemicarbazones (**3**) and triazine thiones (**4**).

Moreover, the azanaphthoquinone annelated pyrrole derivatives were investigated on structure-activity relationship by using quantitative structure activity relationship (QSAR) and molecular dynamics simulations (MD). The results showed that the key of enhance biological activity is side chain. The recommended side chain should be bulky, hydrophobic favor and hydrogen donor group.[4–6]

In this work, we study the synthesis of azanaphthoquinone annelated triazine thione (**4**) as antiproliferative agents. The target molecules were designed to replace carbonyl moiety with thiosemicarbazone moiety. We modify core skcleton by condensation with thiosemicarbazide to give triazine thione ring. We added nitrogen atom and sulfur atom in molecule for hydrogen bonding interaction, increase hydrogen donor at the side chain position and reduce cardiotoxic from quinone moiety. Finally, mono-substituted side chains will be introduced into core skeleton. Side chains with 2-carbon linker with amino group (**a–c**) will be used to give final compounds.

2. Materials and Methods

2.1 Materials

^{1}H NMR spectra were recorded on a Bruker AVANCE (300 MHz) spectrometer. The residue of the non-deuterated solvent was used as internal standard which was relate to tetramethylsilane with δ = 7.26 ppm for $CDCl_3$. ^{13}C NMR spectra were recorded on a Bruker AVANCE (75 MHz) with the residue of the non-deuterated solvent peak as the internal standard, δ = 77.0 ppm for $CDCl_3$. The IR spectra were recorded on Perkin-Elmer FT-IR spectroscopy Spectrum RXI.

Thin layer chromatography (TLC) was performed with Merck silica gel 60 PF254 plate (Merck-Nr 1.05554: 0.2 mm, 20×20 cm) or Merck aluminium oxide plate (Merck-Nr 1.05550 : 0.2 mm, 20×20 cm). Chromatography was performed using Merck silica gel 60, 70–230 mesh ASTM, Nr 1.07734.

2.2 Materials and Methods

2.2.1 The preparation of 6,7-dichloroisoquinoline-5,8-dione (6)[7]

5-Hydroxyisoquinoline (**5**) (1.116 g, 7.65 mmol) was dissolved in hydrochloric acid (19 ml) and then nitric acid (1 ml) was slowly added. The mixture was stirring 1 h at 80 – 90 °C under nitrogen atmosphere. The mixture was extracted with DCM (5x100 ml). The organic layers were dried over anh. $MgSO_4$. The solvent was removed in rotary evaporator. The residue of **6** was purified by column chromatography (silica gel) eluting with Hexane/EtOAc; 7:3 to give product **6** (0.0918 g, 5.26 %) as bright yellow solid.

^{1}H NMR (300 MHz, $CDCl_3$): δ = 9.42 (s, 1H, H-1), 9.12 (d, J = 4.8 Hz, 1H, H-3), 7.97 (d, J = 4.8 Hz, 1H, H-4) ppm. ^{13}C NMR (75 MHz, $CDCl_3$): δ = 175.5 (C-5), 175.3 (C-8), 156.0 (C-3), 149.5 (C-1), 144.0 (C-6), 143.5 (C-7), 136.0 (C-4a), 124.0(C-8a), 119.5 (C-4) ppm. IR (Neat): V_{max} = 2919, 1675, 1224, 670 cm^{-1}.

2.2.2 The preparation of 5,7-dihydrobis ([1,2,4]triazino)[6,5-f:5',6'-h]isoquino-line-3,6(2H,4H)-dithione (4)

The mixture of compound **6** (0.2540 g, 1.06 mmol) and thiosemicarbazide (0.1218 g, 1.27 mmol) was dissolved in EtOH. After that, 10 drops of hydrochloric acid were added at room temperature into the mixture and then reaction mixture was refluxed at 85 °C for 8 h under nitrogen atmosphere. The crude reaction **4** was removed solvent by rotary evaporator. The crude reaction of **4** was purified by column chromatography (silica gel) eluting with gradient EtOAc to EtOAc/MeOH; 8:2 to give product **4** (0.3285 g, 97.86 %), as dark brown solid.

^{1}H NMR (300 MHz, MeOD): δ = 9.98 (s, 1H, H-1), 8.59 (d, J = 5.4 Hz, 1H, H-3), 8.34 (d, J = 5.7 Hz, 1H, H-4) ppm. ^{13}C NMR (75 MHz, $CDCl_3$): δ = 180.0 (C=S), 180.0 (C=S), 162.5 (C=N), 162.0 (C=N), 155.5 (C-7), 147.0 (C-6), 146.5 (C-6), 143.0 (C-1), 134.5 (C-4a), 122.5 (C-8a), 119.0 (C-4) ppm. IR (Neat): V_{max} = 3307, 2920, 1608, 1558, 1289, 1242 cm^{-1}.

2.2.3 The synthesis of mono-substituted azanaphthoquinone annelated triazine thione derivative

General procedure

60% NaH (2.6 equiv.) was dissolved in DMF stirring and cooled at 0 °C and then the compound **6** (1 equiv.) in DMF added dropwise stirring for 30 min under nitrogen atmosphere. The side chain (1.5 equiv.) in DMF was added in the mixture and refluxed at 75 °C for 8 h. After that, water was added to quench the reaction. The mixture was removed solvent by rotary evaporator. The crude product was purified by column chromatography (silica gel) eluting with gradient EtOAc to EtOAc/MeOH 7:3 to give alkylated product.

Synthesis of 7-(2-(dimethylamino)ethyl)-5,7-dihydrobis([1,2,4]triazino)[6,5-f:5', 6'h]isoquinoline-3,6(2H,4H)-dithione (7a)

The mixture of NaH (0.0299 g, 1.25 mmol), compound **4** (0.0620 g, 0.21 mmol) and 1-chloro-2-dimethylamino-ethane (0.0593 g, 0.55 mmol) in DMF was refluxed at 75 °C for 8 h under nitrogen

atmosphere. The crude reaction of **7a** was purified by column chromatography (silica gel) eluting with gradient EtOAc to EtOAc/MeOH; 7:3 to give product **7a** (0.0547 g, 71.38 %), as orange solid. ^{1}H NMR (300 MHz, $CDCl_3$): δ = 9.93 (s, 1H, H-1, 9.03 (d, *J* = 5.4 Hz, 1H, H-3), 8.18 (d, *J* = 5.7 Hz, 1H, H-4), 4.63 (t, *J* = 6.5 Hz, 2H, triazine-$\underline{CH_2}$), 3.0 (t, *J* = 6.5 Hz, 2H, $\underline{CH_2}$-$N(CH_3)_2$), 2.35 (s, 6H, $N(CH_3)_2$) ppm.

Synthesis of 7-(2-(pyrrolidin-1-yl)ethyl)-5,7-dihydrobis([1,2,4]triazino)[6,5-f:5',6'-h]-isoquinoline-3,6(2H,4H)-dithione (7b)

The mixture of NaH (0.0441 g, 1.84 mmol), compound **4** (0.0918 g, 0.30 mmol) and *N*-(2-chloroethyl)prrolidine (0.1038 g, 0.61 mmol) in DMF was refluxed at 75 °C for 8 h under nitrogen atmosphere. The crude reaction of **7b** was purified by column chromatography (silica gel) eluting with gradient EtOAc to EtOAc/MeOH; 7:3 to give product **7b** (0.0690 g, 56.84 %) as orange solid. ^{1}H NMR (300 MHz, $CDCl_3$): δ = 9.90 (s, 1H, H-1), 8.91 (d, *J* = 5.4 Hz, 1H, H-3), 8.25 (d, *J* = 5.7 Hz, 1H, H-4), 4.50-4.90 (m, 2H, H-1'), 2.55-2.70 (m, 4H, H-4'), 2.31 (t, *J* = 6.6 Hz, 2H, H-2'), 1.50-1.65 (m, 4H, H-5') ppm.

Synthesis of 7-(2-(piperidin-1-yl)ethyl)-5,7-dihydrobis([1,2,4]triazino)[6,5-f:5',6'-h]-isoquinoline-3,6(2H,4H)-dithione (7c)

The mixture of NaH (0.0772 g, 0.52 mmol), compound **4** (0.1608 g, 0.53 mmol) and 1-(2-chloroethyl)piperidine (0.1610 g, 1.07 mmol) in DMF was refluxed at 75 °C for 12 h under nitrogen atmosphere. The crude reaction of **(7c)** was purified by column chromatography (silica gel) eluting with gradient EtOAc to EtOAc/MeOH; 7:3 to give product **7c** (0.0422 g, 19.17 %) as orange solid. ^{1}H NMR (300 MHz, $CDCl_3$): δ = 9.90 (s, 1H, H-1), 8.91 (d, *J* = 5.4 Hz, 1H, H-3), 8.25 (d, *J* = 5.7 Hz, 1H, H-4), 4.60-4.9 (m, 2H, H-1'), 2.40-2.65 (m, 2H, H-4'), 2.25-2.40 (m, 2H, H-2'), 1.50-1.75 (m, 2H, H-5'), 1.35-1.50 (m, 2H, H-6') ppm.

3. Results & Discussion

The azanaphthoquinone annelated triazine thione derivatives **7a–c** were synthesized by three step as show in scheme 1. The first, 5-hydroxyisoquinoline **(5)** was oxidized with hydrochloric acid and nitric acid at 80 – 90 °C (1 h) to give 6,7-dichloroisoquinoline-5,8-dione **(6)** in 5.26% as bright yellow solid. The second, 6,7-dichloroisoquinoline-5,8-dione **(6)** was cyclized under acid conditions (hydrochloric acid) with thiosemicarbazide at 85 °C (8 h) to obtained compound **4** 97.86 % in as dark brown solid. We found that, the carbonyl moiety of 6,7-dichloroisoquinoline-5,8-dione **(6)** were condensed with thiosemicarbazide to give triazine thione ring. ^{13}C NMR signal of C=N at 162.5 and 162.0 of the compound **4** and disappearing of carbonyl signal in IR spectrum confirmed that thiosemicarbazide was condensed with the carbonyl moiety. Finally, the alkylation reaction of compound **4** with side chain **a–c** under basic condition at 75 °C (8–12 h) gave mono-substituted product **7a-c**. In further studies, synthesis of target molecules with 3-carbon linker side chain will be carried on. The structure characterization of all synthesized compounds by mass

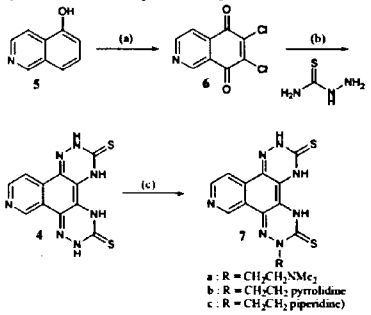

Scheme 1. The synthetic pathway of azanaphthoquinone annelated triazine thione derivative by three step reaction. Reagents and conditions: (a) conc. HCl, conc. HNO_3 at 80–90 °C 1 h, (b) conc. HCl, EtOH at 85 °C 8 h, (c) NaH/DMF, then 70 °C, 8–12 h.

spectrometry and biological evaluation of synthesized compounds are on going.

4. Conclusion

The novel series of azanaphthoquinone annelated triazine thione derivative were successfully synthesized under acid condition. The three products with 2-carbon linker were primarily investigated. However, the over all yield was quite low. Therefore, the optimal conditions were needed to be investigated in order to complete the series of target molecules with other side chains with 3-carbon linker. The biological activity of target molecules will be evaluated in the further.

Acknowledgements

We would like to thank Faculty of Science, Ubon Ratchathani University for facility.

References:

1. Shanab, K.; Pongprom, N.; Wulz, E.; Holzer, W.; Spreitzer, H.; Schmidt, P.; Aicher, B.; Mueller, G.; Guenther, E. *Bioorg. Med. Chem. Lett.* **2007**, *17*, 6091–6095.
2. Pongprom, N.; Pungpo, P. *KKU Res. J.* **2012**, *17*, 195–202.
3. Somta, J.; Panomket, P.; Pongprom, N. *Proceeding of Pure and Applied Chemistry International Conference*, January 8–10, 2014, Khon Kaen. 132–136.
4. Punkvang, A.; Pungpo, P.; Kamsri, P.; Kasamsri, D.; Srisupan, A.; Saparpakorn, P.; Hannongbua, S.; Wolschann, P.; Prueksaaroon, S.; Pongprom, N. *Int. J. Quantum Chem.* **2013**, *113*, 555–562.
5. Kamsri, P.; Punkvang, A.; Pongprom, N.; Srisupan, A.; Saparpakorn, P.; Hannongbua, S.; Wolschann, P.; Pungpo, P. *Mol. Inf.* **2013**, *32*, 541–554.
6. Tumtong, P.; Kamsri, P.; Punkvang, A.; Saparpakorn, P.; Hannongbua, P.; Pungpo, P.; Pongprom, N. *The 19th International Annual Symposium on Computational Science and Engineering*, June 17–19, **2015**, Ubon Ratchathani. 249–255.
7. Leepasert, P.; Shahabi, M.; Shanab, K.; Schirmer, E.; Holzer, W.; Spreitzer, H.; Aicher, B.; Müller, G.; Günther, E. *Bioorg. Med. Chem. Lett.* **2013**, *23*, 5264–5266.

VITAE

NAME	Praseat Tumtong
BORN	March, 16, 1989, Ubon Ratchathani, Thailand
ADDRESS	333/1 Satonramark Rd. Warin chamrab District, Ubon Ratchathani, 34190
EDUCATION	2007-2011 B.Sc. (Chemistry), Ubon Ratchathani University, Ubon Ratchathani, Thailand
EXPERIENCE	April, 19, 2012 - August, 4, 2014 Chemical laboratory section, Production Control Division, Military Explosives Factory, Defence Industry Department, Defence Industry and Energy Centre
SCHOLARSHIP AND AWARDS	Domestic scholarships for government officials of Office of the Secretary of Defense
SCIENTIFIC CONTRIBUTIONS	(1) Tumtong P., Kamsri P., Punkvang A., Saparpakorn P., Hannongbua P., Pungpo P. and Pongprom N., "Structural Requirement of Azanaphthoquinone Pyrroloannelated Derivatives against Hela Cancer Derived from 2D and 3D-QSAR Studies", **The 19th International Annual Symposium on Computational Science and Engineering**, June 17-19, 2015, Ubon Ratchathani. Thailand. 249-255. (poster presentation with proceeding) (2) Tumtong P., Chansook A., Chaladdee S., Srilawan T.and Pongprom N., "Synthesis of azanaphthoquinone annelated triazine thiones as antiproliferative agents", **The Pure and Applied Chemistry International Conference 2016**, February 9 -11, 2016, Bangkok, Thailand. 1532 - 1535. (poster presentation with proceeding)
POSITION	2012 - 2014, Second lieutenant at Military Explosives Factory, Nakhon Sawan, Thailand 2014 - Present, Lieutenant at Defence Industry Department, Bangkok, Thailand